



**EFFECT OF MINERAL FILLERS ON AGEING OF  
BITUMINOUS MIXTURES**

**M.Sc. Thesis**

**Filippos Mastoras**

**2019, Delft, The Netherlands**



# **EFFECT OF MINERAL FILLERS ON AGEING OF BITUMINOUS MIXTURES**

Thesis

for the degree Master of Science (M.Sc.) in Structural Engineering,  
Faculty of Civil Engineering,  
Delft University of Technology,  
to be defended publicly on the 27<sup>th</sup> of February 2019

by

Filippos Mastoras  
born in Kozani, Greece

Graduation Committee:

Dr. ir. A. Varveri	TU Delft, Chair
Prof. dr. ir. S.M.J.G Erkens	TU Delft
Dr. M.M. van Tooren	TU Delft
Ing. W. Verwaal	TU Delft
Ir. L.J.M. Houben	TU Delft

An electronic version of this thesis is available at <http://repository.tudelft.nl/>.



## Preface

This thesis is submitted as a partial fulfilment of the requirements for the acquisition of the Master of Science degree in Structural Engineering, with specialization in Road & Railway Engineering. At this point, I would like to express my sincere gratitude to the people who contributed to the realization and completion of this research.

First and foremost, I would like to express my gratitude to my supervisor Dr. Aikaterini Varveri for trusting me and providing me with the opportunity to get involved in such an interesting and challenging research, as well as for her continuous support and guidance throughout the whole duration of this study. Moreover, I would like to express my gratitude to Dr. Ruxin Jing for his assistance in the laboratory of the Pavement Engineering Section of TU Delft and for bringing-in his exceptional knowledge on the ageing of bituminous mixtures during our discussions.

Furthermore, I would like to express my appreciation to the members of my assessment committee: Prof. Sandra Erkens, who supported, by every means, the realization of the proposed research methodology, Dr. Maaike van Tooren and Ing. Wim Verwaal, from the Geosciences Department of TU Delft, who joined this research and, by virtue of their expertise, provided valuable insight with respect to the mineral fillers and, last but not least, the coordinator of the Structural Engineering Master's Program Ir. Lambert Houben for always being extremely helpful with the program's students.

Special thanks to Sibelco Winterswijk and Sibelco Dessel for providing the majority of the utilized mineral fillers and for making their facilities available for the testing of the mineral matters. More specifically, my acknowledgements are dedicated to Bart Renssen and Joris de Gooijer, from Sibelco Winterswijk, and Hellen Hamaekers and Sofie Hollanders, from Sibelco Dessel. Your contribution was vital for the execution of the experimental plan and your involvement, undoubtedly, increased the quality of this research.

I am very thankful to Ing. Michele van Aggelen and Ing. Marco Poot for always being there to provide technical support, during the experiments in the Pavement Engineering laboratory of TU Delft.

In addition, I would like to thank my dear friends and colleagues Georgios, Giannis and Marios. Our mutual support and collaboration during the Master's Program were exceptionally effective in achieving our goals.

Last but certainly not least, I express my immense gratitude to my parents Athanasios and Despina and my sisters Zoe and Chrysanthi, for without their support, at so many levels, nothing of these would be possible.



*Filippos Mastoras  
Delft, February 2019*



## Abstract

Ageing of bitumen has been long-recognized as one of the major reasons responsible for the gradual deterioration of asphalt pavements. Age-hardening of the binder leads to the embrittlement of the overall asphalt mixture, which entails its increased susceptibility to traffic and environmental induced damage. As a result, high maintenance efforts as well as increased expenses are required to allow for an asphalt pavement to reach its expected service-life.

Past research efforts have established a solid background with respect to the implications of bitumen ageing on the overall response of an asphalt mixture as well as on the binder's physico-chemical properties. In the same framework, studies have demonstrated that the ageing process of bitumen in the field is not solely a function of the bitumen type itself, but rather, added effects have been identified attributed to the mineral matter and the asphalt mixture design parameters.

This thesis attempts to provide a deeper understanding of the effect of mineral aggregates on the ageing of bitumen, and more specifically, the effect of a special fraction of the solid phase in asphalt mixtures, the mineral fillers. Six different mineral fillers were employed in this research, covering a wide range of physical and composition-related (i.e. elemental/mineralogical) properties. Bitumen-mineral filler blends were prepared, according to a single design protocol, and the resulting mastics along with neat bitumen were subjected to accelerated laboratory ageing by means of the Pressure Ageing Vessel.

The rheological (i.e. Dynamic Shear Rheometer) evaluation of the resulting materials and the derivation of ageing indices revealed the overall ability of the mineral fillers, regardless of their individual properties, to mitigate the ageing of bitumen incorporated in the mastics. The chemical (i.e. Fourier Transform-Infrared Spectroscopy) investigation of the materials showed that, in fact, the chemically active mineral fillers catalysed the oxidation of bitumen incorporated in the mastics. These results allowed for the identification of two mechanisms through which the effect of the mineral fillers on the ageing of bitumen occurs. The first one is related to the physical presence of the mineral matter in the mastics, whereas the second one to the developed physico-chemical interactions between the mineral fillers' particles and the bitumen. Basic mineral fillers were found to be more efficient in reducing the age-hardening of mastics, compared to acidic ones, by allowing for more intensive interactions between the mastics' constituent materials. Moreover, there are indications that the mineral fillers' specific surface area also has a primary role to the developed interactions, and, by extension, to the ageing behavior of the mastics.

Finally, in addition to the aforementioned main findings, binders were extracted and recovered from the aged mastics, in an effort to derive further information on the effect of mineral fillers on ageing of bituminous mixtures by investigating the aged mastics' constituent materials on their individual level. The rheological and chemical examination of the recovered materials did not lead to any further insight regarding the research questions of this study. Instead, features were revealed which manifest that the extraction and recovery of bitumen may not be a suitable approach for the investigation of the research problem addressed in this thesis.





## **Table of contents**

<b>List of figures.....</b>	<b>i</b>
<b>List of tables .....</b>	<b>vi</b>
<b>1 Introduction.....</b>	<b>1</b>
1.1 General introduction.....	2
1.2 Porous asphalt pavements .....	3
1.2.1 General .....	3
1.2.2 Bitumen ageing in porous asphalt pavements.....	5
1.3 Problem statement .....	7
1.4 Thesis outline.....	8
<b>2 Literature review.....</b>	<b>9</b>
2.1 Chemical composition of bitumen.....	10
2.1.1 Elemental analysis.....	10
2.1.2 Molecular structure of bitumen.....	10
2.1.3 SARA fractionation .....	11
2.1.4 Chemical functional groups .....	14
2.2 Ageing of bitumen .....	14
2.2.1 General .....	14
2.2.2 Effect of oxidation on the chemical composition of bitumen .....	17
2.2.2.1 Fractional changes .....	17
2.2.2.2 Molecular changes.....	18
2.2.3 Bituminous binders ageing assessment .....	19
2.2.3.1 Changes on physical properties of bitumen .....	19
2.2.3.2 Changes on chemical properties of bitumen.....	20
2.2.4 Bituminous binders' laboratory ageing tests .....	23
2.2.4.1 Thin film oven test (TFOT).....	23
2.2.4.2 Rolling thin film oven test (RTFOT).....	25
2.2.4.3 Pressure ageing vessel (PAV).....	26
2.3 Mineral aggregates .....	26
2.3.1 Mineral fillers .....	27
2.3.1.1 Definition of mineral fillers .....	27
2.3.1.2 Properties of mineral fillers .....	28
2.3.2 Mineral aggregates surface characteristics.....	29
2.3.2.1 Surface charge.....	29

2.3.2.2 Surface interaction with bitumen components .....	30
2.4 Mineral aggregates and ageing of bituminous binders.....	32
2.4.1 General .....	32
2.4.2 Effect of mineral fillers on ageing of bitumen .....	32
2.4.2.1 Effect of hydrated lime on ageing of bitumen.....	44
2.5 Conclusions on literature review.....	51
2.6 Research objectives.....	53
2.7 Research methodology.....	54
<b>3 Materials and methods .....</b>	<b>55</b>
3.1 Bitumen.....	56
3.1.1 Penetration grade .....	56
3.1.2 Softening point.....	56
3.2 Mineral fillers.....	57
3.2.1 Types of mineral fillers considered in the study.....	57
3.2.2 Density of fine particles.....	59
3.3 Materials preparation.....	60
3.3.1 Mastics preparation.....	60
3.3.2 Bitumen preparation.....	61
3.4 Ageing of bitumen and mastics.....	62
3.4.1 Ageing protocol.....	62
3.4.2 Materials' film thickness during ageing.....	63
3.5 Mineral fillers characterization methods .....	64
3.5.1 Laser diffraction .....	64
3.5.2 Environmental scanning electron microscope (ESEM) imaging.....	67
3.5.3 Rigden voids.....	67
3.5.4 Braunauer-Emmett-Teller (BET) method .....	68
3.5.5 Swelling test.....	71
3.5.6 Methylene blue.....	72
3.5.7 X-ray fluorescence (XRF) spectroscopy.....	73
3.5.8 X-ray diffraction (XRD).....	73
3.6 Bitumen and mastics test methods.....	74
3.6.1 Dynamic shear rheometer (DSR) .....	74
3.6.1.1 Preliminary study on DSR configuration.....	78
3.6.1.2 Amplitude sweep test - materials' linear visco-elastic (LVE) region .....	80
3.6.1.3 Frequency Sweep Test .....	82
3.6.1.4 Construction of complex shear modulus and phase angle master-curves	84

---

3.6.2 Fourier transform infrared (FTIR) spectroscopy .....	88
3.6.2.1 Attenuated total reflectance (ATR) spectrometer .....	89
3.6.2.2 FTIR/ATR spectrometer test method .....	90
3.6.2.3 Analysis method of infrared spectra .....	91
<b>4 Mineral fillers tests results and discussion .....</b>	<b>93</b>
4.1 Particles' size distribution and specific surface area.....	94
4.2 Microscopic imaging .....	96
4.3 Fractional voids.....	100
4.4 Specific surface area – BET method.....	102
4.5 Swelling percentage .....	104
4.6 Harmful fines – methylene blue value .....	105
4.7 Elemental and mineralogical analysis .....	105
<b>5 Bitumen and mastics tests results and discussion .....</b>	<b>109</b>
5.1 Rheological evaluation .....	110
5.1.1 Complex shear modulus and phase angle master-curves analysis .....	110
5.1.2 Complex shear modulus ageing indices.....	114
5.1.3 Relation between mastics' rheological ageing indices and properties of mineral fillers.....	117
5.2 Chemical evaluation .....	121
5.2.1 Infrared spectra.....	121
5.2.2 Carbonyls index.....	123
<b>6 Bitumen extraction and recovery from aged mastics.....</b>	<b>127</b>
6.1 Preliminary information.....	128
6.1.1 "Fresh" bitumen.....	128
6.1.2 Materials preparation and ageing protocol .....	128
6.2 Bitumen extraction and recovery process .....	129
6.3 Neat aged bitumen conditioning.....	132
6.4 Assessment of extraction and recovery process .....	134
6.4.1 Mineral filler contamination and solvent residual.....	134
6.4.2 Recovery of bitumen components .....	137
6.5 Rheological evaluation of recovered and neat bitumen – results and discussion	139
6.5.1 Complex shear modulus and phase angle master-curves analysis .....	140
6.5.2 Complex shear modulus ageing indices.....	141
6.6 Chemical evaluation of recovered and neat bitumen – results and discussion....	143
6.6.1 Infrared spectra.....	143

6.6.2 Carbonyls and sulfoxides indices .....	144
6.7 Reflection on extraction and recovery of bitumen from aged mastics .....	146
<b>7 Conclusions and recommendations .....</b>	<b>149</b>
7.1 Conclusions .....	150
7.2 Recommendations .....	152
<b>References.....</b>	<b>155</b>
<b>Appendix A Mineral fillers isothermal curves and BET plots .....</b>	<b>163</b>
<b>Appendix B Amplitude sweep test results.....</b>	<b>169</b>
<b>Appendix C WLF master-curves .....</b>	<b>179</b>
<b>Appendix D Modified CAM model fitting parameters .....</b>	<b>203</b>

## List of figures

Figure 1.1: Average annual precipitation in the Netherlands. 1981-2010 (Varveri 2017). .....	3
Figure 1.2: TLPA cross-section (Hagos 2008). .....	4
Figure 1.3: PA service-life and bitumen properties in time (Verra et al. 2003, Voskuilen et al. 2004). .....	4
Figure 1.4: Comparison of DAC and PA cross-sections (Hagos 2008). .....	5
Figure 1.5: Ravelling in PA pavement (Hagos 2008). .....	6
Figure 2.1: Principal types of molecules in bitumen microstructure (Wu 2009). .....	11
Figure 2.2: Schematic representation of the Corbett fractionation procedure (Van Lent 2013). .....	12
Figure 2.3: Chemical model of saturates in bitumen (Hunter et al. 2015). .....	12
Figure 2.4: Chemical model of aromatics in bitumen (Hunter et al. 2015). .....	13
Figure 2.5: Chemical model of asphaltenes in bitumen (Hunter et al. 2015). .....	13
Figure 2.6: Chemical functionalities naturally present in bitumen (Petersen 2009). .....	14
Figure 2.7: Effect of STA and LTA on bitumen’s rheology (Hunter et al. 2015). .....	15
Figure 2.8: Mechanisms of bitumen ageing (Traxler 1963). .....	15
Figure 2.9: SARA fractional changes upon oxidation as a function of ageing time (Wu 2009). .....	17
Figure 2.10: Schematic illustration of the movement of bitumen components from non-polar to more polar fractions (Hagos 2008). .....	18
Figure 2.11: Chemical functionalities formed upon oxidative ageing (Petersen 2009). ..	18
Figure 2.12: Benzylic carbon (Petersen 2009). .....	19
Figure 2.13: Ketone formation at benzylic carbon position (Petersen 2009). .....	19
Figure 2.14: Infrared spectrum, carbonyls and sulfoxides peaks. ....	21
Figure 2.15: Various approaches for infrared spectra analysis (Hofko et al. 2017). .....	21
Figure 2.16: (a) TFOT (Wu 2009). (b) TFOT pan. ....	23
Figure 2.17: The RTFOT and apparatus (Hagos 2008). .....	25
Figure 2.18: (a) PAV. (b) PAV pan. ....	26
Figure 2.19: Aggregates classification as acidic or basic based on their surface charge (Mertens & Wright 1959). .....	29
Figure 2.20: Percentage of strongly adsorbed bitumen fraction on aggregates surface against aggregates specific surface area (Plancher et al. 1977). .....	31
Figure 2.21: Oxygen diffusion path simulation (Moraes & Bahia 2015a). .....	32
Figure 2.22: Bitumen’s and mastic’s glass transition temperature for various ageing times (Moraes & Bahia 2015a). .....	34
Figure 2.23: Complex shear modulus master-curves. Anti-clockwise rotation of aged mastic (Moraes & Bahia 2015a). .....	35
Figure 2.24: Ageing indices of neat bitumen, limestone and granite mastics (Moraes & Bahia 2015a). .....	35
Figure 2.25: Ageing indices of “inert” and granite mastics (Moraes & Bahia 2015a). ....	36
Figure 2.26: Schematic representation of the GPC test (Moraes & Bahia 2015b). .....	37
Figure 2.27: Example of GPC chromatogram with three elution time fractions (Moraes & Bahia 2015b). .....	37

Figure 2.28: Molecular size areas ageing indices for neat bitumen Flint Hills PG 64-22 and mastics. 48 hours-aged materials. (a) 3.15 mm film thickness. (b) 1.00 mm film thickness (Moraes & Bahia 2015b). .....	38
Figure 2.29: Molecular size areas ageing indices for neat bitumen Valero PG 64-16 and mastics. 48 hours-aged materials. (a) 3.15 mm film thickness. (b) 1.00 mm film thickness (Moraes & Bahia 2015b). .....	38
Figure 2.30: Molecular size areas ageing indices. 24 hours-aged materials. (a) Flint Hills PG 64-22. (b) Valero PG 64-16 and mastics (Moraes & Bahia 2015b). .....	39
Figure 2.31: Molecular weights ageing indices. 24 hours-aged materials. (a) Flint Hills PG 64-22. (b) Valero PG 64-16 and mastics (Moraes & Bahia 2015b). .....	39
Figure 2.32: Ageing indices of neat bitumen, gritstone, limestone and ordinary Portland cement mastics (Wu 2009). .....	41
Figure 2.33: Complex shear modulus master-curves of Reference “fresh” and aged bitumen and recovered bitumen from 5-hours-aged mastics (Wu 2009). .....	41
Figure 2.34: Complex shear modulus master-curves of gritstone mastics at various ageing times (Wu 2009). .....	42
Figure 2.35: Complex shear modulus master-curves of limestone mastics at various ageing times (Wu 2009). .....	42
Figure 2.36: Ageing indices of neat bitumen, gritstone and limestone mastics at various ageing times (Wu 2009). .....	43
Figure 2.37: Ageing indices of neat bitumen and recovered bitumen from gritstone and limestone mastics at various ageing times (Wu 2009). .....	43
Figure 2.38: FTIR analyses on bitumen recovered from the 3-hour aged gritstone and limestone mastics (Wu 2009). .....	44
Figure 2.39: Complex shear modulus master-curves. (a) “Fresh” and aged bitumen. (b) “Fresh” and aged granite mastics. (c) “Fresh” and aged limestone mastics (Alfaqawi et al. 2017). .....	46
Figure 2.40: Phase angle master-curves. (a) “Fresh” and aged neat bitumen and granite mastics. (b) “Fresh” and aged neat bitumen and limestone mastics (Alfaqawi et al. 2017). .....	47
Figure 2.41: Ageing indices of granite and limestone mastics (Alfaqawi et al. 2017). .....	48
Figure 2.42: Carbonyl index of recovered bitumen from granite mastics (Alfaqawi et al., 2017). .....	48
Figure 2.43: Ageing indices for neat bitumen and mastics at 10 rad/s (Gundla et al. 2015). .....	49
Figure 2.44: Ageing indices for neat bitumen and recovered bitumen from hydrated lime and Portland cement mastics (Gundla et al. 2015). .....	50
Figure 2.45: Ageing indices for control, hydrated lime and Portland cement mixtures (Gundla et al. 2015). .....	51
Figure 2.46: Predicted fatigue life for “fresh” and aged mixtures (Gundla et al. 2015). ..	51
Figure 2.47: Research approach flow diagram. .....	54
Figure 3.1: Ring & Ball test. (a) Rings. (b) Overall apparatus. (c) Bitumen after test completion. ....	57
Figure 3.2: Schematic representation of batch type asphalt production unit including a dust collector. ....	58
Figure 3.3: Materials in the PAV pans prior to ageing. ....	63
Figure 3.4: Laser diffraction operating principles (Michel & Courard 2014). .....	65

Figure 3.5: Laser diffraction test. Particles' geometry and texture assumptions (Taylor 2007).....	65
Figure 3.6: Laser diffraction equipment used in this study.....	66
Figure 3.7: Laser diffraction analysis. Example of exported gradation curve.....	66
Figure 3.8: The ESEM utilized in this study. ....	67
Figure 3.9: Concepts of "fixed" and "free" binder (Aburkaba & Muniandy 2016). ....	68
Figure 3.10: Solid particle in gas sorption measurement (Taylor 2007). ....	68
Figure 3.11: Example of a typical BET plot. ....	70
Figure 3.12: Completed swelling test. Volumetric tubes with methanol (left) and water (right).....	71
Figure 3.13: Methylene blue test setup. ....	72
Figure 3.14: Principal of XRF (Nageswaran 2016).....	73
Figure 3.15: Example of an XRD spectrum (Gupta 2011).....	74
Figure 3.16: (a) 8 mm-diameter oscillating plate. (b) 25 mm-diameter oscillating plate. ....	75
Figure 3.17: DSR operating principal (Woldekidan 2011).....	75
Figure 3.18: (a) Maximum shear stress location. (b) Maximum shear strain location (Woldekidan 2011).....	75
Figure 3.19: Phase lag between loading and response (Van den Bergh 2011).....	76
Figure 3.20: Phase angle as a function of material's behavior (Apostolidis 2015). ....	76
Figure 3.21: Relationship between complex shear modulus, storage modulus, loss modulus and phase angle (Van den Bergh 2011).....	77
Figure 3.22: DSR CP configuration (Woldekidan 2011). ....	78
Figure 3.23: DSR mastic column configuration. (a) FEM model. (b) Real specimen. (c) Specimen cross-section (Woldekidan 2011).....	78
Figure 3.24: (a) PP configuration. (b) MC configuration. ....	79
Figure 3.25: (a) Mastic column silicon mold. (b) Mastic column specimens. ....	79
Figure 3.26: Complex shear modulus master-curves PP and MC configurations.....	80
Figure 3.27: Example of the determination of the LVE limit. Stress amplitude sweep... ..	81
Figure 3.28: LVE region stress limit as a function of temperature and frequency for aged 40/60 Pen bitumen (Rahimzadeh 2002). ....	81
Figure 3.29: Example of average isothermal plots. (a) Complex shear modulus. (b) Phase angle.....	83
Figure 3.30: Example of the generation of master-curve (Van den Bergh 2011).....	85
Figure 3.31: Example of plotting the $\log(aT)$ against temperature with reference temperature of 20°C. ....	85
Figure 3.32: Fitting potential of the modified CAM model. Example of an aged mastic... ..	87
Figure 3.33: Fitting potential of the modified CAM model. Example of "fresh" bitumen. ....	87
Figure 3.34: Various regions of the electromagnetic spectrum (Van den Bergh 2011)... ..	88
Figure 3.35: Different types of stretching and bending vibrations (Van Lent 2013). ....	89
Figure 3.36: FTIR/ATR spectrometer. (a) Multiple FTIR/ATR. (b) Single point FTIR/ATR (Van den Bergh 2011). ....	90
Figure 3.37: Spectrum 100 FTIR spectrometer Perkin Elmer with a single-point-ATR fixture.....	91
Figure 4.1: Mineral fillers gradation curves.....	94
Figure 4.2: Mineral fillers fineness modulus.....	95
Figure 4.3: Mineral fillers estimated specific surface area. ....	96

Figure 4.4: Mineral fillers fineness modulus and estimated specific surface area correlation.....	96
Figure 4.5: Microscopic imaging of WG60K.....	97
Figure 4.6: Microscopic imaging of WG.....	97
Figure 4.7: Microscopic imaging of BD.....	98
Figure 4.8: Microscopic imaging of GR.....	98
Figure 4.9: Microscopic imaging of QZ.....	99
Figure 4.10: Microscopic imaging of BE.....	99
Figure 4.11: Mineral fillers Rigden voids.....	101
Figure 4.12: Mineral fillers BET specific surface area.....	102
Figure 4.13: Mineral fillers laser diffraction estimated specific surface area and BET specific surface area correlation.....	103
Figure 4.14: Mineral fillers swelling percentage.....	104
Figure 4.15: Mineral fillers methylene blue value.....	105
Figure 4.16: Classification of mineral matter based on its silicon content (Nageswaran 2016).....	107
Figure 5.1: Bitumen and mastics complex shear modulus master-curves at “fresh” and aged state.....	110
Figure 5.2: Bitumen and mastics phase angle master-curves at “fresh” and aged state.....	110
Figure 5.3: “Fresh” mastics complex shear modulus at various frequencies and temperature of 20°C.....	111
Figure 5.4: “Fresh” bitumen, aged bitumen and aged mastics complex shear modulus master-curves.....	113
Figure 5.5: Change of the phase angle upon ageing at various frequencies and temperature of 20°C.....	114
Figure 5.6: Complex shear modulus ageing indices as a function of the reduced frequency at 20°C.....	115
Figure 5.7: Crossing point of 40/60_WG60K and 40/60_WG AI curves at ~0.049 Hz and 20°C.....	116
Figure 5.8: Complex shear modulus ageing indices at 20°C and 0.001 Hz.....	117
Figure 5.9: Relationship between mineral fillers’ CaO content and mastics’ AI at 20°C and 0.001 Hz.....	118
Figure 5.10: “Fresh” and aged bitumen and mastics infrared spectra. (a) Total spectra. (b) Carbonyls close-up. (c) Sulfoxides close-up.....	122
Figure 5.11: Example of infrared spectra of mineral filler, bitumen and resulting mastic.....	122
Figure 5.12: Aged bitumen and mastics carbonyls’ index.....	123
Figure 6.1: Complex shear modulus and phase angle master-curves of “fresh” bitumen utilized at mastics evaluation phase and bitumen extraction phase.....	128
Figure 6.2: Aged mastic-dichloromethane solution.....	129
Figure 6.3: Removal of mineral filler particles larger than 63 µm.....	129
Figure 6.4: Centrifuge of the asphaltanalysator.....	130
Figure 6.5: Glass filter of pores’ size equal to 10 µm.....	130
Figure 6.6: Rotary evaporator set-up.....	131
Figure 6.7: Complex shear modulus and phase angle master-curves of unconditioned and conditioned neat aged bitumen.....	132



Figure 6.8: Infrared spectra of “fresh”, unconditioned and conditioned neat aged bitumen. .... 133

Figure 6.9: Carbonyls’ index of “fresh”, unconditioned and conditioned neat aged bitumen. .... 133

Figure 6.10: Sulfoxides’ index of “fresh”, unconditioned and conditioned neat aged bitumen..... 133

Figure 6.11: Mineral filler WG60K, recovered bitumen RB\_40/60\_WG60K\_Aged and neat aged bitumen 40/60\_Aged\_ExPh\_Cond infrared spectra. .... 134

Figure 6.12: Mineral filler WG, recovered bitumen RB\_40/60\_WG\_Aged and neat aged bitumen 40/60\_Aged\_ExPh\_Cond infrared spectra. .... 135

Figure 6.13: Mineral filler BD, recovered bitumen RB\_40/60\_BD\_Aged and neat aged bitumen 40/60\_Aged\_ExPh\_Cond infrared spectra. .... 135

Figure 6.14: Mineral filler GR, recovered bitumen RB\_40/60\_GR\_Aged and neat aged bitumen 40/60\_Aged\_ExPh\_Cond infrared spectra. .... 135

Figure 6.15: Mineral filler QZ, recovered bitumen RB\_40/60\_QZ\_Aged and neat aged bitumen 40/60\_Aged\_ExPh\_Cond infrared spectra. .... 136

Figure 6.16: Mineral filler BE, recovered bitumen RB\_40/60\_BE\_Aged and neat aged bitumen 40/60\_Aged\_ExPh\_Cond infrared spectra. .... 136

Figure 6.17: Original and recovered mineral filler WG60K infrared spectra..... 137

Figure 6.18: Original and recovered mineral filler WG infrared spectra. .... 137

Figure 6.19: Original and recovered mineral filler BD infrared spectra. .... 138

Figure 6.20: Original and recovered mineral filler GR infrared spectra..... 138

Figure 6.21: Original and recovered mineral filler QZ infrared spectra..... 138

Figure 6.22: Original and recovered mineral filler BE infrared spectra..... 139

Figure 6.23: “Fresh”, neat aged and recovered bitumen complex shear modulus master-curves..... 139

Figure 6.24: “Fresh”, neat aged and recovered bitumen phase angle master-curves. ... 140

Figure 6.25: Recovered and neat aged bitumen complex shear modulus ageing indices as a function of the reduced frequency at 20°C..... 141

Figure 6.26: Recovered and neat aged bitumen complex modulus ageing indices at 20°C and 0.001 Hz..... 141

Figure 6.27: “Fresh”, neat aged and recovered bitumen infrared spectra. (a) Total spectra. (b) Carbonyls close-up. (c) Sulfoxides close-up..... 144

Figure 6.28: “Fresh”, neat aged and recovered bitumen carbonyls’ index..... 145

Figure 6.29: “Fresh”, neat aged and recovered bitumen sulfoxides’ index. .... 145

Figure 6.30: “Fresh”, neat aged and recovered bitumen carbonyls’ + sulfoxides’ index.145



## List of tables

Table 2.1: Elemental composition of bitumen (Hunter et al. 2015).....	10
Table 2.2: FTIR areas integration boundaries (Van den Bergh 2011).....	22
Table 2.3: Bitumen ageing tests (Airey 2003).....	24
Table 2.4: Mineral fillers gradation requirements according to NEN-EN 13043. ....	27
Table 2.5: Mineral filler properties according to NCHRP 9-45 (2010).....	28
Table 2.6: Mineral filler geometrical properties, means of measurement and corresponding standards (Aburkaba & Muniandy 2016). ....	28
Table 2.7: Mineral filler physical and mechanical properties, means of measurement and corresponding standards (Aburkaba & Muniandy 2016). ....	28
Table 2.8: Mineral filler stiffening properties, means of measurement and corresponding standards (Aburkaba & Muniandy 2016). ....	28
Table 2.9: Mineral filler chemical properties, means of measurement and corresponding standards (Aburkaba & Muniandy 2016). ....	29
Table 2.10: Bitumen components relative affinity to aggregate surface (Plancher et al. 1977).....	31
Table 3.1: Needle penetration test results.....	56
Table 3.2: Ring & Ball test results.....	57
Table 3.3: 40/60 penetration grade bitumen conventional properties. ....	57
Table 3.4: Mineral fillers abbreviations. ....	59
Table 3.5: Mineral fillers particles' densities.....	60
Table 3.6: Mastics abbreviations. ....	61
Table 3.7: PAV pan dimensions.....	63
Table 3.8: Mastics densities.....	64
Table 3.9: Mass of mastics in the PAV pan that yields a film thickness of 0.315 cm. ....	64
Table 3.10: Amplitude sweep test conditions.....	82
Table 3.11: Chosen stress levels applied in the frequency sweep tests. ....	82
Table 3.12: Frequency sweep test conditions. ....	84
Table 3.13: Area integration boundary-wave numbers (Hofko et al. 2017).....	91
Table 4.1: Mineral fillers cumulative percentage passing. ....	94
Table 4.2: Mineral fillers particles type ranking.....	100
Table 4.3: Mineral fillers particles surface texture ranking. ....	100
Table 4.4: Mineral fillers Rigden voids measurements.....	101
Table 4.5: Mineral fillers laser diffraction estimated specific surface area ranking. ....	103
Table 4.6: Mineral fillers BET specific surface area ranking. ....	103
Table 4.7: Mineral fillers swelling test measurements. ....	104
Table 4.8: Mineral fillers methylene blue measurements. ....	105
Table 4.9: Mineral fillers elemental composition.....	106
Table 4.10: Mineral fillers loss on ignition.....	106
Table 4.11: Mineral fillers mineralogical composition. ....	106
Table 4.12: Mineral fillers classification as acidic or basic.....	107
Table 5.1: Bitumen and mastics ranking based on the complex shear modulus ageing indices at 20°C and 0.001 Hz.....	117
Table 5.2: Aged bitumen and mastics ranking based on the carbonyls' indices.....	124

Table 6.1: Bitumen recovery process conditions. .... 131  
Table 6.2: Recovered bitumen abbreviations. .... 131  
Table 6.3: Reclaimed mineral fillers abbreviations..... 131  
Table 6.4: Recovered and neat aged bitumen ranking based on the complex shear modulus ageing indices at 20°C and 0.001 Hz..... 142

# 1

## Introduction

## 1.1 General introduction

Highway infrastructures constitute one of the most important assets of modern society that contribute to its economic growth and overall prosperity. Considering the ever-increasing public mobility and transfer of goods, it is of immense importance that road networks ensure a safe, fast and continuous flow of every-day-transportations, while, at the same time, their development and required maintenance impose the minimum possible financial burden to society.

Important characteristics that are closely related to the sustainability of highway infrastructures are the adequate design and enhanced durability of the applied asphalt mixture. If fulfilled, the aforementioned aspects lead to the proper performance of the asphalt pavement which, by extension, implies minimum maintenance efforts and expenses to reach its expected life-time. However, the latter constitutes a very challenging task. From the very beginning and throughout its service-life, an asphalt pavement is exposed to severe conditions, both environmental and traffic-related. As a result, gradual deterioration of its constituent materials occurs, which is usually translated, in time, to damage of the overall asphalt pavement. It is thus vital that deep understanding is obtained with respect to the influence of such environmental and traffic-related factors on the performance of asphalt pavements that will allow the development of adequate design guidelines and durable constituent materials.

An inevitable process that highly affects the behavior of an asphalt pavement is the ageing, also referred to as age-hardening, of bitumen. The aged-hardening of bitumen is initiated from the very beginning at the production of the asphalt mixture and construction of the asphalt pavement and continuously develops during its service-life in the field. Oxygen, moisture, extreme temperatures and ultraviolet (UV) radiation, are some factors that greatly promote the ageing of bitumen (Erkens et al. 2016). A direct outcome of the process is the gradual change of the physico-chemical properties of bitumen in time, leading to a stiff and brittle material. Consequently, the overall stiffness of the asphalt mixture increases. Even though this may be beneficial with respect to the resistance to certain failure modes (e.g. rutting), the resulting embrittlement implies high susceptibility to fatigue failure, thermal induced cracking, moisture damage and loss of stones, or ravelling (Francken 1997, Leech & Nunn 1997, Woo et al. 2008, King et al. 2012). It is commonly accepted that ageing of bitumen constitutes one of the major reasons that negatively affect the performance of an asphalt pavement in the long-run, which establishes it as one of the most interesting and attractive topics for continuous scientific research.

Over the years, substantial research has been conducted to gain insight regarding the effect of bitumen ageing both on the global response of an asphalt pavement as well as on the bitumen micro-structure itself. These efforts have borne fruits and a solid background has been set with respect to the implications of the ageing process at various levels (i.e. macro- and micro-level). Nevertheless, little attention has been given to the interaction of the constituent materials of a conventional asphalt mixture (i.e. bitumen and mineral matter) and how these interactions may affect the ageing process of bitumen. The present thesis, based on the well-established knowledge on bitumen ageing and materials interaction, attempts to couple the aforementioned features and reveal potential inter-relations.

## 1.2 Porous asphalt pavements

### 1.2.1 General

In the Netherlands, the most commonly type of asphalt mixture applied on wearing courses is Porous Asphalt (PA), or in Dutch Zeer Open Asphalt Beton (ZOAB). Currently, more than 90% of the country's road network is surfaced with this type of asphalt mixture and its wider application only increases. The extensive use of PA stems, mainly, from its excellent traffic-induced-noise reduction capability. In a densely populated country, as the Netherlands, the highway network inevitably crosses inhabited regions. In such cases, traffic noise may disturb the welfare of the public and proper practices should be followed to ensure that this phenomenon is reduced to the minimum possible level. The implementation of PA surface courses on motorways constitute a cost-effective and efficient method for the mitigation of traffic noise, compared to other possible solutions, such as the application of noise barriers (Hagos 2008). It is worth mentioning, that the noise tolerance caused by traffic is controlled by governmental regulations, which undoubtedly assists in establishing PA as the prevalent type of mixture applied on surface courses and promote its widespread use along the country.

However, the evidently great noise reduction capability of PA is not the only reason for this type of mixture to be selected above other types. The term "porous" witnesses the ability of this open-graded mixture to allow water drain through its structure with an increased rate. Direct benefits of the latter are the prevention of aquaplaning, reduction of "splash and spray" effect and improved head-light glare (Hagos 2008, Varveri 2017). Hence, such type of mixture can be extremely beneficial when applied to regions with high precipitation rate, such as the Netherlands (*Fig. 1.1*).

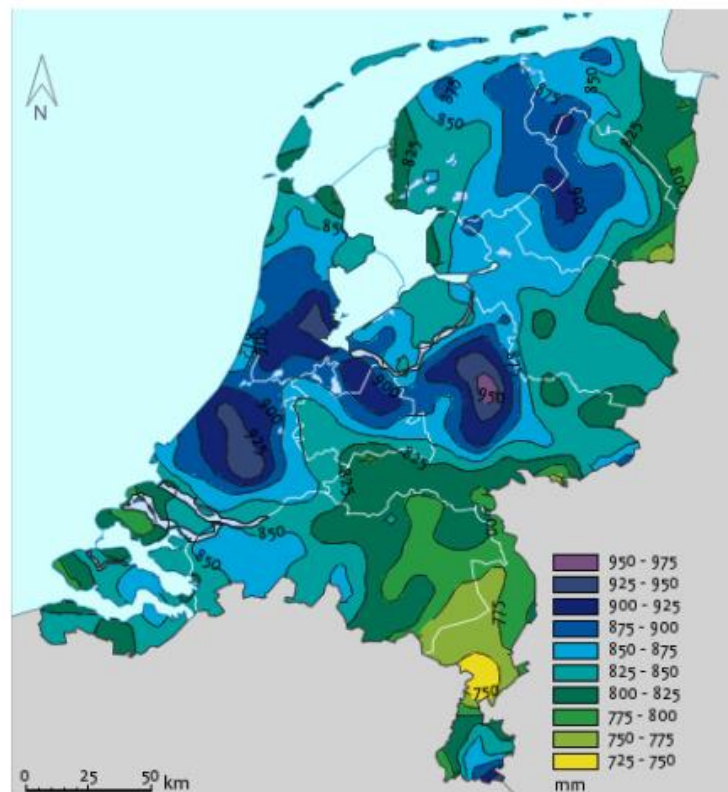


**Figure 1.1:** Average annual precipitation in the Netherlands. 1981-2010 (Varveri 2017).

From the very first applications and up till now, PA mixtures were applied on the Dutch highways in a Single Layer Porous Asphalt (SLPA) of thickness, typically, 50 mm and gradation 0/16 mm (Van der Zwan et al. 1990, Hagos 2008). In the early nineties, the Two Layer Porous Asphalt (TLPA) was introduced to the Dutch motorways. The latter consists of a bottom layer of thickness 40-50 mm and gradation 0/16 mm and a top layer of thickness 20-30 mm with 0/8 mm chipping size (Goubert et al. 2005, Hagos 2008). In *Fig. 1.2*, a typical cross-section of a TLPA is presented. The primary advantage of TLPA over SLPA lies in its ability to reduce traffic noise over 4-6 dB(A) compared to the latter that yields a traffic-noise reduction equal to 2-3 dB(A) (Hagos 2008).

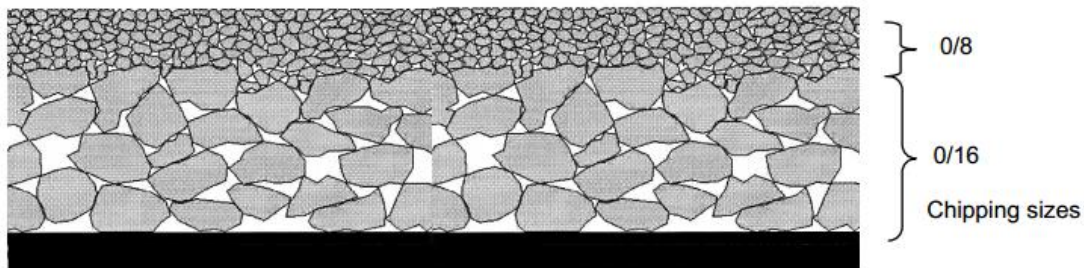


**Figure 1.2:** TLPA cross-section (Hagos 2008).

The average lifetime of PA on highways fluctuates between 11 and 12 years for the right-hand driving lane whereas higher lifetimes were observed for the rest of the lanes (Hagos 2008, Varveri 2017). Provided that the applied mixture and pavement construction are of high quality, the service-life of PA may reach 16 years, however lifetimes of, as low as, 4 years were also observed. In general, the average lifetime of PA wearing courses is substantially lower, approximately 5 years less, than the minimum expected lifetime of Dense Asphalt Concrete (DAC) surface courses (Hagos 2008). In *Fig. 1.3*, the service-life of PA pavements is graphically represented (Verra et al. 2003, Voskuilen et al. 2004). In the very same figure, the change, in time, of the conventional bitumen properties are depicted as well.

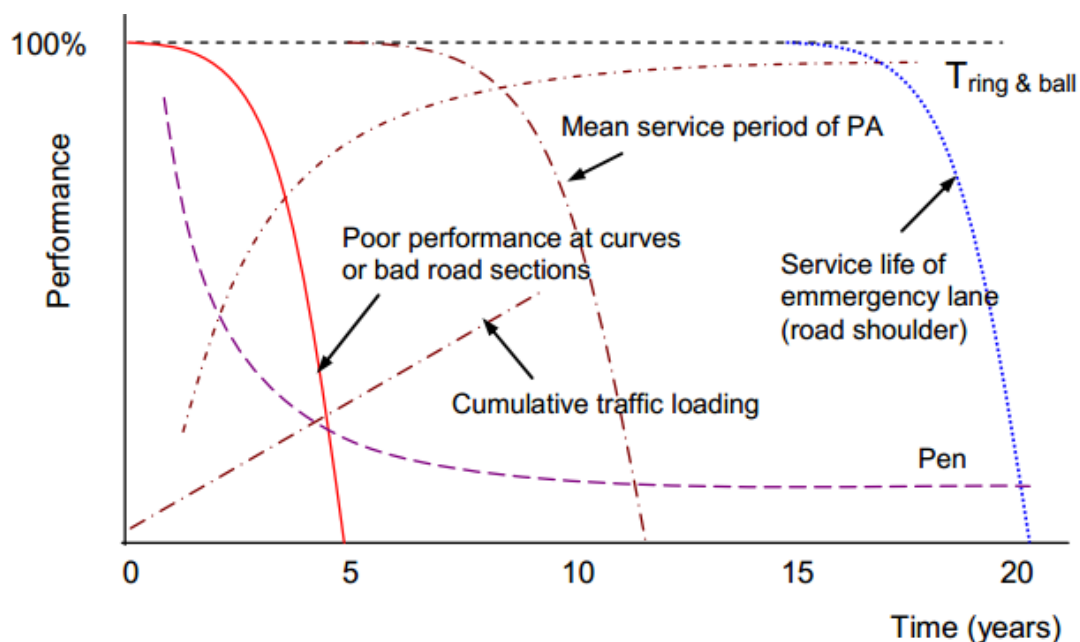


**Figure 1.3:** PA service-life and bitumen properties in time (Verra et al. 2003, Voskuilen et al. 2004).



PA mixtures are designed with a high voids content (20-25%) to fulfil their traffic noise reduction and drainage purposes. DAC mixtures, which are designed with a voids content of 3-5%, have longer service-life, it is readily conceivable that several performance-related issues, which manifest the need for early maintenance and/or the end of the service-life of PA, are closely associated to its permeable structure. In *Fig. 1.4*, the difference in the voids content between DAC and PA mixtures as captured by X-Ray CT-Scan analyses is demonstrated.

Disadvantages of PA mixtures, that are related to its open structure, include, among others, pollution of the open-graded surface layer with matter (clogging), of several origins, that decreases its noise absorbance capability and increased susceptibility to environmental deteriorating factors. The latter has been proven to be decisive with respect to the service-life of PA wearing courses (Hagos 2008).

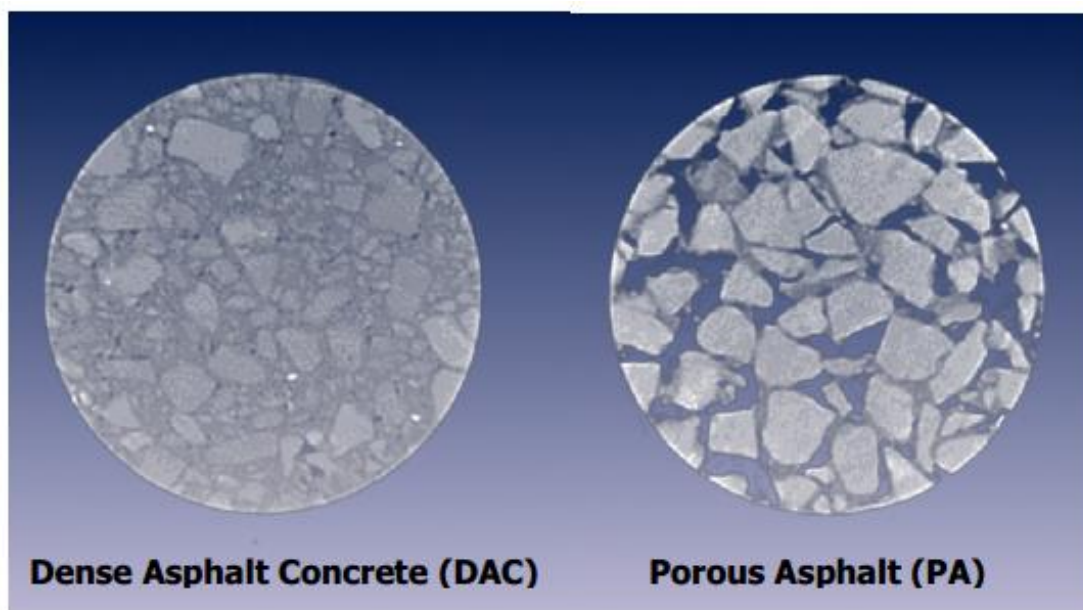


**Figure 1.4:** Comparison of DAC and PA cross-sections (Hagos 2008).

### 1.2.2 Bitumen ageing in porous asphalt pavements

One of the major concerns regarding PA mixtures is the rapid ageing that the bituminous binder undergoes in the field. Excessive age-hardening of the binder occurs due to two primary reasons: the high content of interconnected voids in the PA mixture and the relatively thin binder film that coats the aggregates (Kandhal & Chakraborty 1996). Mo et al. (2007) reported an estimated mineral filler-bitumen mixture, hereafter designated as mastic, thickness that coats the aggregates equal to 0.45 mm. Environmental factors that promote bitumen ageing, such as oxygen, water and UV radiation can easily access the internal structure of PA and impose modifications on the properties of the binding material (Francken 1997). As a result, oxidation of the binder is observed throughout the whole thickness of the PA layer (Hagos 2008).

On the contrary, in DAC mixtures the effect of ageing on the properties of the binder is mostly limited on the top part of the pavement layer. Influencing environmental factors cannot easily affect the internal structure of the mixture by virtue of its relatively impermeable nature. Choquet & Verhasselt (1994) recovered and tested bitumen from the top and bottom part of DAC pavements. The researchers observed that the bitumen

coming from the top part (within 5 mm thickness) was heavily aged whereas the properties of the bitumen originating from the bottom part were almost unchanged. These observations were also corroborated by the findings of other studies. Fonseca & Witczak (1996) reported that the viscosity of the binder as a function of the DAC pavement thickness (from top to bottom) follows a decreasing trend.

It is thus evident that the major drawback of PA mixtures is a durability issue (Hagos 2008). The increased rate of ageing causes the binding material to alter its favourable properties, with respect to deformability and relaxation of stresses, in relatively short time (*Fig. 1.3*). This opens the way to the early occurrence of ravelling (*Fig. 1.5*), the main distress type of PA pavements. Considering that ageing is an inevitable process and that the design of PA mixtures serves, more than well, its overall purpose, the research efforts towards minimizing the ageing rate of the bituminous binder are focused in the mixture's constituent materials and the interaction between them, in terms of gaining insight and, subsequently, developing anti-ageing technologies.

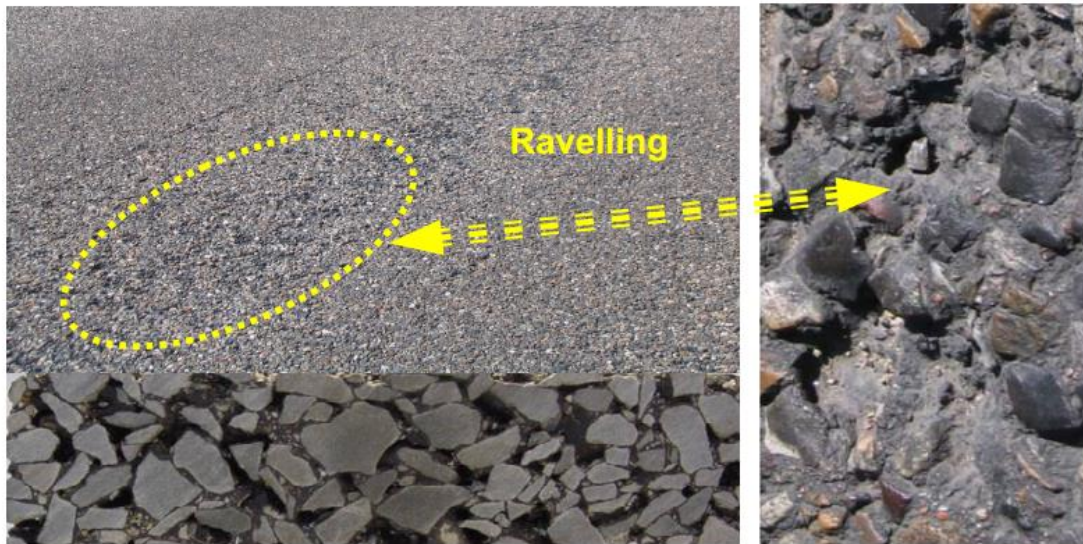


**Figure 1.5:** Ravelling in PA pavement (Hagos 2008).

### 1.3 Problem statement

Over the years, in-depth investigations have been conducted with respect to the response of different bituminous binders, in terms of source, properties and modification level, upon ageing. In addition, the effect that several mixture design parameters (e.g. voids content) and various field conditions have on bitumen ageing have been well-identified and reported. However, it is still unclear whether mineral fillers have an effect on bitumen ageing, and if they do so, how do they affect this process.

The primary function of mineral fillers is to increase the stiffness of an asphalt mixture and improve its behavior with respect to fatigue performance and permanent deformation resistance. Nevertheless, they constitute an integral part of the binding material in an asphalt mixture. In the field, bitumen undergoes ageing in the form of bitumen-filler-sand (i.e. mortar) system. This establishes mineral fillers as a participating material in the ageing process. It is, thus, plausible to expect that the mineral matter might influence this process, and it may do so in a variety of ways, depending on the physico-chemical properties of the considered materials (i.e. bitumen and mineral filler).

Two major ways can be distinguished through which mineral fillers may affect ageing: The first can be attributed to the physico-chemical interactions that take place between the bitumen and the mineral matter. Depending on the nature of these interactions, mineral fillers may act as catalysts, by enhancing bitumen ageing, or act as inhibitors of the ageing process or even act as “inert” and thus having no effect on it. The second can be related to the physical presence of the mineral matter in the mastic. A sound hypothesis would be that the presence of the solid and impermeable to oxygen particles within the mastic, could lead to the hindrance of the oxygen diffusion process and, thus, decelerating the rate of bitumen ageing. The latter is strongly dependent on the concentration and the spatial distribution of the mineral filler in the mastic as well as on its gradation.

Provided that there is an effect of the mineral matter on ageing, it is reasonable to expect that different mineral fillers with different properties may affect the bitumen's ageing to a different extend and in a different way (i.e. positively or negatively). Hence, it is of high importance to identify which mineral fillers' properties prevail in this influence and what are the mechanisms through which this influence occurs. The latter could lead to a deep understanding of the role of the mineral fillers in the ageing process and possibly to subsequent development of manufactured mineral materials with favourable properties with regards to bitumen ageing.

## 1.4 Thesis outline

The present report is organized in seven chapters:

- *Chapter 1* constitutes a general introduction to the present research, where a brief description of the asphalt pavements in the Netherlands is provided. The latter is followed by the effect of the major physico-chemical process concerned in this study, ageing of bitumen, on the performance of the PA pavements. The chapter is concluded with the statement of the research problem addressed in this report.
- *Chapter 2* consists of an extensive literature review, where basic information about bitumen's chemistry, the process of ageing and the effect of ageing on the binder's chemical structure are provided. Moreover, reference is made to the developed ageing assessment techniques, and laboratory ageing methods as well as to the main properties and relevant-to-the present-study-characteristics of the mineral fillers. The literature review is concluded through the citation of studies directly related to the topic of this research i.e. the effect of mineral fillers on bitumen ageing. The chapter is completed with the determination of the objectives of this study and the description of the applied research methodology.
- *Chapter 3* includes the description of the considered raw materials, the materials and various blends preparation and the utilized ageing protocol. In addition, it provides an overview of the testing methods and equipment along with the description of the results post-processing techniques. Preliminary studies with respect to the selection of the conditions of the main experiments are also presented in this chapter.
- *Chapter 4* consists of the results of the mineral fillers' characterization. The outcomes of the various measurements are reported and discussed.
- *Chapter 5* provides the rheological and chemical evaluation of mastics and neat bitumen. The results are presented and discussed. Moreover, the ageing ranking of the various materials and the correlation to the relevant mineral filler properties are carried out in this chapter. Finally, the various mechanisms through which the effect of the mineral matters on the ageing of bituminous mixtures occurs are established.
- *Chapter 6* refers to the extraction and recovery of binders from aged mastics and their rheological and chemical evaluation. The ageing assessment of the recovered materials as well as the correlation of the results on bitumen level and mastic level are examined in this very chapter.
- *Chapter 7* constitutes the conclusion of this report, where the main conclusions derived from the research and recommendations are cited.

# 2

## Literature review

## 2.1 Chemical composition of bitumen

### 2.1.1 Elemental analysis

The chemical composition of bitumen is regarded as extremely complex. It is highly dependent on the source of the crude oil, from which bitumen originates, and the refinery process (Hunter et al. 2015). Studies within the framework of the Strategic Highway Research Program (SHRP) had shown that bitumen originating and utilized in the United States and Canada presented quite different compositions (Mortazavi & Moulthrop 1993). As a general rule, bitumen is predominantly composed of hydrocarbon molecules, as well as some heterocyclic species and functional groups (heteroatoms) containing sulfur, nitrogen and oxygen atoms. In addition, traces of metals such as nickel, vanadium, iron, calcium and magnesium, in the form of metallic salts, oxides or in porphyrin structures, can be found in its chemical structure (Hunter et al. 2015).

*Table 2.1* presents the elemental composition of bitumen. The results are derived by elemental analyses performed on different bitumen, originating from a variety of sources, and reflect the actual state for the majority of the tested bitumen (Hunter et al. 2015).

**Table 2.1:** Elemental composition of bitumen (Hunter et al. 2015).

Element	Wt (%)
Carbon	82-88
Hydrogen	8-11
Sulfur	0-6
Oxygen	0-1.5
Nitrogen	0-1

Even though it is useful to identify the elements present in bitumen, the elemental analyses are average values of bitumen manufactured from different crude oil sources and provide little information with respect to the arrangement of the various atoms, forming the molecules, or the type of the molecular structure. The latter are extremely important in drawing correlations between the composition and the physical properties and chemical reactivity of bitumen (Petersen 1984).

### 2.1.2 Molecular structure of bitumen

Apart from the total amount of each element present in bitumen's microstructure, what is of greater importance is the way in which these elements are incorporated in the molecules as well as the apparent existing molecular structure. *Fig 2.1* illustrates the three main types of molecules observed in bitumen's microstructure. In the aliphatic structures, the carbon atoms are linked in straight or branched chains, whereas in the naphthenics (or cyclics) they are linked in simple or complex saturated rings. The term "saturated" refers to the fact that all electron bonds of the carbon atoms are occupied by hydrogen. Finally, aromatics are molecules comprised by very stable six-atoms rings (Wu 2009).

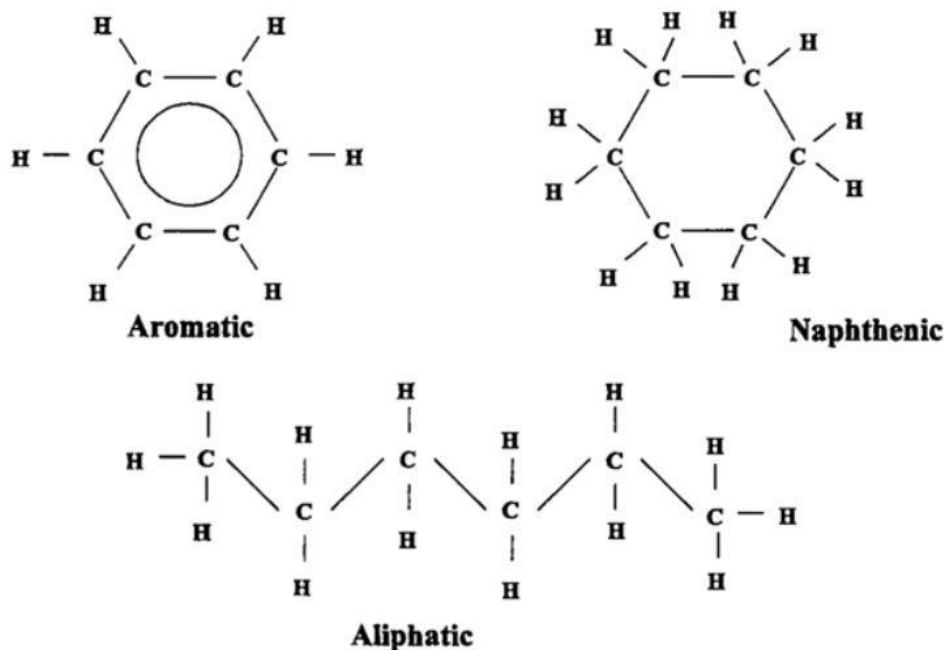


**Figure 2.1:** Principal types of molecules in bitumen microstructure (Wu 2009).

Considering that in a single type of bitumen a vast number of different molecules with various chemical structures exist and that the chemical composition of bitumen is greatly affected by its origin and the implemented refinery process, it is impossible to completely separate and identify every single molecule present in its micro-structure. Even if it was possible, handling the obtained information and correlating them to physical properties would be at least impractical (Hunter et al. 2015). For that reason, researchers had put efforts to separate bitumen into less complex and more homogeneous (generic) fractions and/or identify the chemical composition of bitumen by means of chemical functional groups, for research purposes.

### 2.1.3 SARA fractionation

Amongst different proposed fractionation schemes, the procedure developed by Corbett (1969) is perhaps the scheme most widely used to describe bitumen's chemical composition. The four bitumen fractions resulting from the Corbett procedure are (in increasing molecular polarity order): Saturates, (naphthene) Aromatics, Resins (polar aromatics) and Asphaltenes (Petersen 2009). In literature, usually the acronym SARA is used to describe the aforementioned bitumen fractions. The first three fractions are also reported as the maltene phase of bitumen (Hunter et al. 2015). In *Fig. 2.2*, a schematic representation of the procedure proposed by Corbett is presented.

According to this method, initially, the asphaltene fraction is separated based on their insolubility in n-heptane. The precipitation of asphaltenes is followed by chromatographic separation of the remaining fractions (Hunter et al. 2015). In the following paragraphs, the main characteristics of the four resulting fractions are briefly discussed.

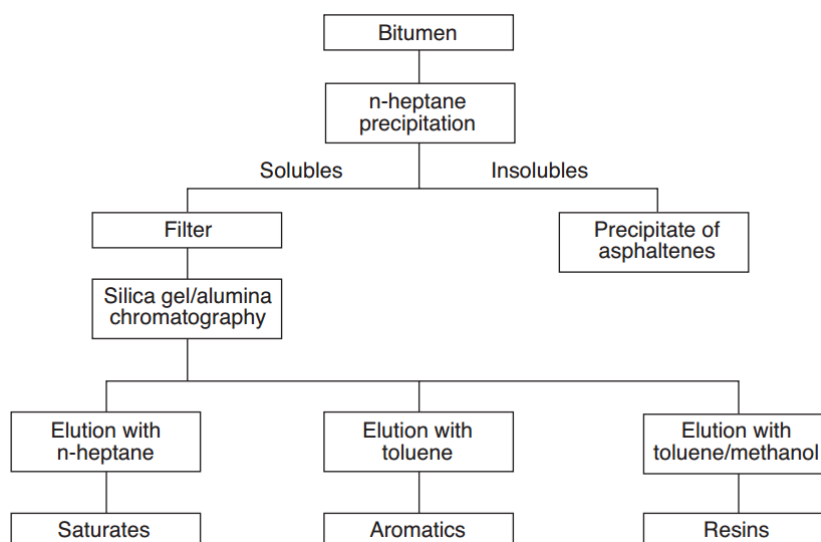


**Figure 2.2:** Schematic representation of the Corbett fractionation procedure (Van Lent 2013).

### Saturates

Saturates are characterized as non-polar, viscous oils (Hunter et al. 2015). They may consist of straight and branched-chain hydrocarbons, saturated cyclic hydrocarbons (naphthenic hydrocarbons) and sometimes a small quantity of mono-ring aromatic hydrocarbons. The latter are dominated by attached saturated hydrocarbon side chains (Fig. 2.3). In addition, sulphur can be found in the saturate fraction (Petersen 1984). Lesueur (2009) reported that, in this fraction, the ratio of hydrogen over carbon is approximately equal to 2. In general, this fraction constitutes 5-20% of the total bitumen (Hunter et al. 2015).

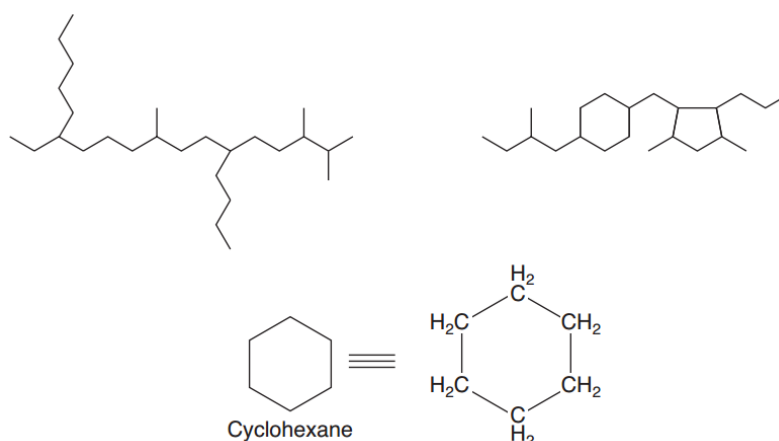


**Figure 2.3:** Chemical model of saturates in bitumen (Hunter et al. 2015).

### Aromatics

Aromatics are viscous liquids and consist of non-polar carbon chains attached to unsaturated ring systems (Fig. 2.4) (Hunter et al. 2015). The heteroatoms sulphur, oxygen and nitrogen may also be part of the molecules (Petersen 1984). Aromatics constitute the major component of the bitumen's maltene phase, the dispersion medium for the peptized asphaltenes. In general terms, they account for 40-65% of the total bitumen. The hydrogen-to-carbon ratio fluctuates between 1.4 and 1.6 (Lesueur 2009).



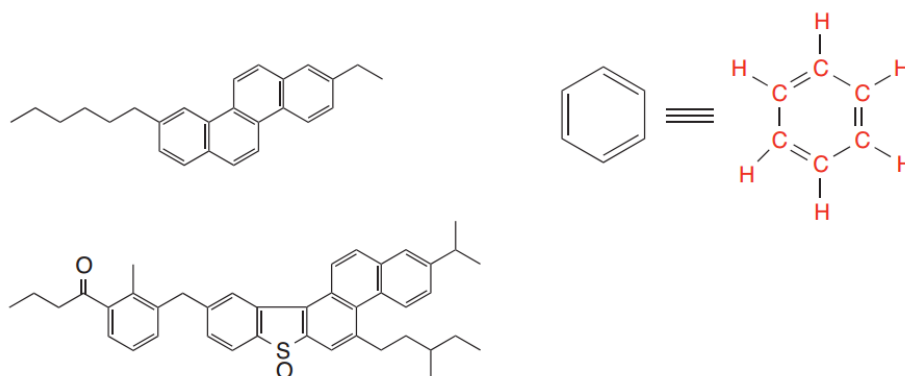


**Figure 2.4:** Chemical model of aromatics in bitumen (Hunter et al. 2015).

### Resins

Resins are primarily composed of hydrogen and carbon. The hydrogen-to-carbon ratio is estimated in-between 1.4 and 1.7. Moreover, atoms of sulphur, oxygen and nitrogen can be found in this fraction. Unlike the previous two fractions, resins are solid or semi-solid and very polar, leading to enhanced adhesive ability. By virtue of their role as dispersive agents for the asphaltene fraction, the ratio of the resins to asphaltenes determines, to an extent, the solution (SOL) or gelatinous (GEL) character of the bitumen (Hunter et al. 2015).

### Asphaltenes

Asphaltenes are n-heptane insoluble solids, which, except for hydrogen and carbon, also contain sulphur, oxygen and nitrogen atoms. They are chemically similar to the resinous fraction. However, the prevalence of molecules with highly condensed planar and polarized aromatic ring systems along with a high concentration of polar heteroatomic functional groups is a unique characteristic of this fraction. The latter features, lead to strong interactions of the fraction's molecules which establishes their dispersion difficult to achieve, even with polar solvents (Petersen 1984). Asphaltenes account for 5-25% of the total bitumen. The effect of this fraction on the rheological properties of bitumen is of high importance. An increased content of asphaltene leads to a harder more viscous bitumen, with higher softening point and lower penetration (Hunter et al. 2015). In *Fig.2.5*, a schematic representation of an asphaltene is presented.

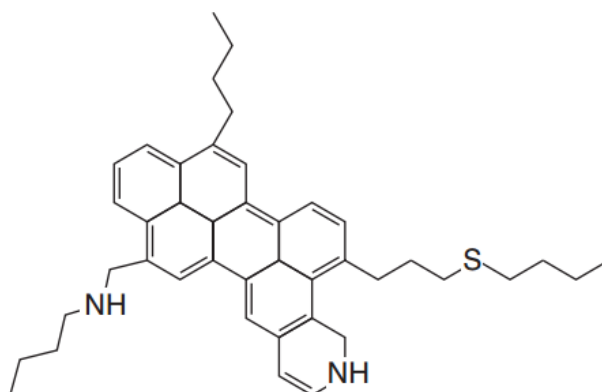


**Figure 2.5:** Chemical model of asphaltene in bitumen (Hunter et al. 2015).

As mentioned before, the Corbett fractionation scheme is the most widely used amongst other proposed separation schemes. Petersen (2009) stated that fractions from other fractionation schemes can be related, in terms of chemistry, to the fractions produced by Corbett. This is because, in all proposed schemes, fractions are generally separated based on increasing molecular polarity, aromaticity and heteroatoms content. The reader is directed to Petersen (1984) for more information with respect to the interrelations between various separation schemes.

### 2.1.4 Chemical functional groups

The elements presented in *Table 2.1* may appear in different chemical functionalities, that are integral parts of large bitumen molecules. Molecules with different chemical structure may incorporate similar chemical functional groups, which, by extension, yield similar effects on the bitumen's physical properties. This implies that when the dominating, in terms of properties of molecules, functional groups are considered, the number of types of chemical functionalities that need to be taken into account is significantly reduced (Petersen 2009). In *Fig. 2.6*, examples of naturally occurring chemical functional groups in the molecular structure of bitumen are illustrated.

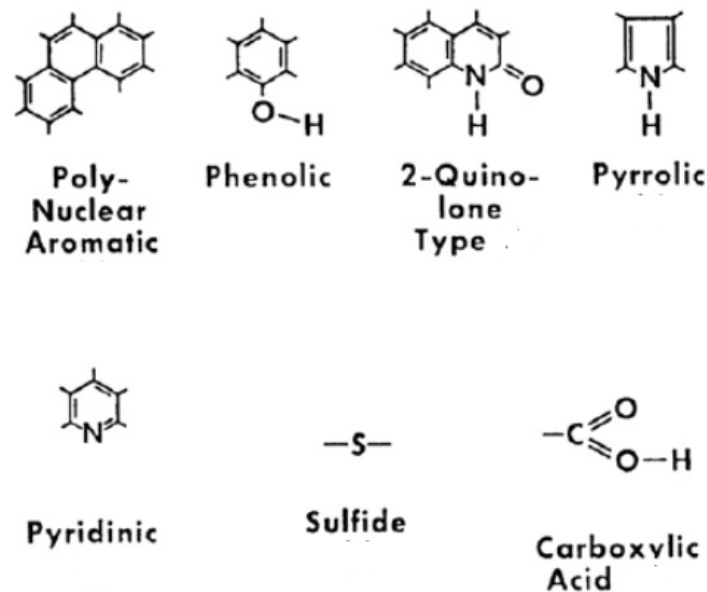


**Figure 2.6:** Chemical functionalities naturally present in bitumen (Petersen 2009).

## 2.2 Ageing of bitumen

### 2.2.1 General

Bitumen, being an organic material, is susceptible to the effect of atmospheric oxygen, ultraviolet radiation and (extreme) temperature fluctuations. The ageing that bitumen undergoes both in the production/construction phase and within its service life in the field, has been long-recognized as one of the most important features that lead to the gradual deterioration of an asphalt pavement.

Ageing of bitumen is usually classified into two major categories, based on its occurrence in the time scale: The Short-Term Ageing (STA) and the Long-Term Ageing (LTA). STA refers to the ageing that bitumen undergoes in the asphalt plant during production of Hot Mix Asphalt (HMA), where (super-) heated aggregates are brought in contact with bitumen, enabling the loss of volatile components and initial oxidation of the

binder. Ageing of bitumen, at this initial stage, continues to occur during storage, transport, laying and compaction of the asphalt mixture, however, in a slower rate than in the mixing of its constituents. LTA refers to the gradual oxidation that bitumen undergoes in the field, under the influence of environmental and/or traffic factors (Roberts et al. 1996). In Fig. 2.7, the effect of STA and LTA on bitumen's rheology is presented through the ratio of its viscosity in the aged state over the fresh state.

Traxler (1963) identified 15 different mechanisms (Fig. 2.8) that promote bitumen ageing (Hunter et al. 2015). It should be noted, that some of them were proved through experimental research, performed by Traxler, whereas others had not been given experimental support (Wu 2009).

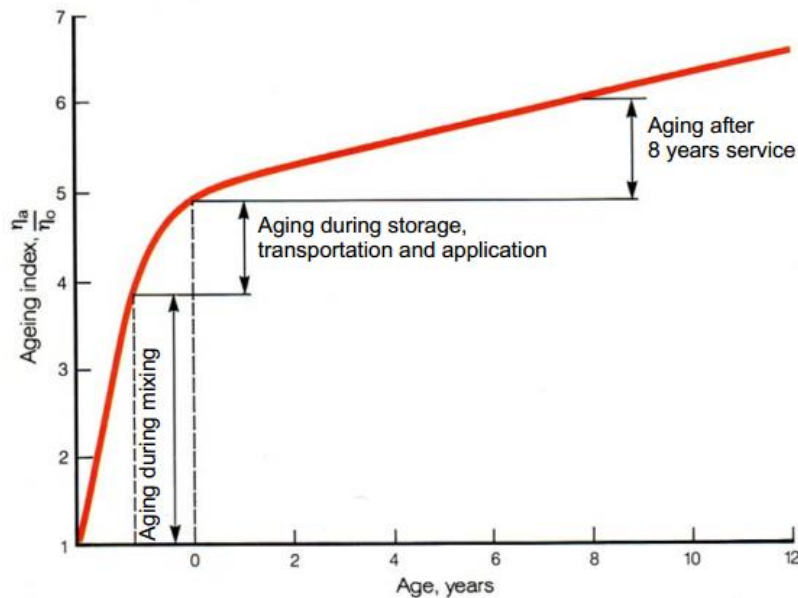


Figure 2.7: Effect of STA and LTA on bitumen's rheology (Hunter et al. 2015).

Factors that influence bitumen ageing	Influenced by					Occurring	
	Time	Heat	Oxygen	Sunlight	Beta and gamma rays	At the surface	In the mixture
Oxidation (in dark)	✓	✓	✓			✓	
Photo-oxidation (direct light)	✓	✓	✓	✓		✓	
Volatilisation	✓	✓				✓	✓
Photo-oxidation (reflected light)	✓	✓	✓	✓		✓	
Photochemical (direct light)	✓	✓		✓		✓	
Photochemical (reflected light)	✓	✓		✓		✓	✓
Polymerisation	✓	✓				✓	✓
Steric or physical	✓					✓	✓
Exudation of oils	✓	✓				✓	
Changes by nuclear energy	✓	✓			✓	✓	✓
Action by water	✓	✓	✓	✓		✓	
Absorption by solid	✓	✓				✓	✓
Absorption of components at a solid surface	✓	✓				✓	
Chemical reactions	✓	✓				✓	✓
Microbiological deterioration	✓	✓	✓			✓	✓

Figure 2.8: Mechanisms of bitumen ageing (Traxler 1963).

Among the various mechanisms the following have been reported to have the most pronounced effect on bitumen ageing:

#### *Oxidation*

Oxidation refers to the reaction of atmospheric oxygen with bitumen, leading to irreversible hardening of the material. The oxidation rate is a function of the composition of bitumen, temperature and time of exposure. Hardening of bitumen due to oxidation has been identified as the major cause of ageing. The latter resulted in limited attention to other, less important but still measurable, factors affecting ageing of bitumen (Moraes & Bahia 2015a, Hunter et al. 2015). As mentioned before, oxidation is a mechanism responsible for both the STA and LTA of the binder. Regarding LTA, oxidation is the prevalent ageing mechanism.

#### *Volatilization*

Volatilization refers to the evaporation of the volatile components of bitumen and is mainly dependent on temperature and exposure conditions. The lighter fractions of bitumen tend to evaporate above their boiling temperature, approximately 150°C. Volatilization is a mechanism that is more significant during the mixing process of the asphalt mixture's constituents, where high temperatures are involved. Its contribution to the LTA of bitumen is usually regarded as negligible (Moraes & Bahia 2015a, Hunter et al. 2015).

#### *Polymerization*

Polymerization describes the process according to which similar molecules form associations, leading to the configuration of large molecules. As a result, the molecular weight increases which is translated into progressive hardening of the material. At low temperatures, where the viscosity of bitumen is high, the rate of polymerization is considered low (Moraes & Bahia 2015a).

#### *Steric Hardening (Thixotropy)*

In 1944, Traxler observed and reported that bitumen stored in 25°C showed an increase in viscosity. This physical hardening, called steric hardening, is the result of the reorientation/restructuring of the molecules in the bitumen and the gradual crystallisation of waxes over a period of time. These changes in the inner-structure of bitumen are reversible, to an extent, through the application of heat (Moraes & Bahia 2015a, Hunter et al. 2015).

#### *Syneresis*

Syneresis refers to the separation of thin oily, less viscous, liquids from the more viscous components of bitumen. In the absence of the oily components, the inner-structure of bitumen undergoes shrinkage and/or rearrangements (physical or chemical changes), resulting in hardening of the material (Hagos 2008, Moraes & Bahia 2015a).

#### *Separation*

Separation describes the hardening of the binder that results from the movement (absorption) of the oily components, released from bitumen, into the pores of the aggregates. It is a function of both the exudative tendency of bitumen and the porosity of the mineral matter (Moraes & Bahia 2015a, Hunter et al. 2015).

### 2.2.2 Effect of oxidation on the chemical composition of bitumen

The mechanism of bitumen oxidation, being widely recognized as the main source of bitumen age-hardening and, by extension, the deterioration of the asphalt pavements (Petersen 2009), has been given substantial attention by the scientific community over the years. Generally, studies that investigate bitumen oxidation deal with: a) Fractional changes (i.e. changes on SARA components) and b) molecular changes in the bitumen micro-structure (Wu 2009).

#### 2.2.2.1 Fractional changes

According to Petersen (2009), compositional changes in bitumen during oxidative ageing can be described by the movement of components from the non-polar fractions to the more polar fractions, due to the formation of oxygen-containing functional groups in bitumen molecules. The level of reactivity of the different SARA fractions with oxygen varies and, as a result, usually, a decrease of the naphthene aromatics and resins with a corresponding increase of the asphaltenes fraction is observed upon oxidation. The saturates fraction, by virtue of their low chemical reactivity, show a rather inert behavior. *Fig 2.9* graphically represents the fractional changes as a function of ageing time. The apparent small decrease of the saturates fraction can be attributed to the volatilization of saturate components (Wu 2009).

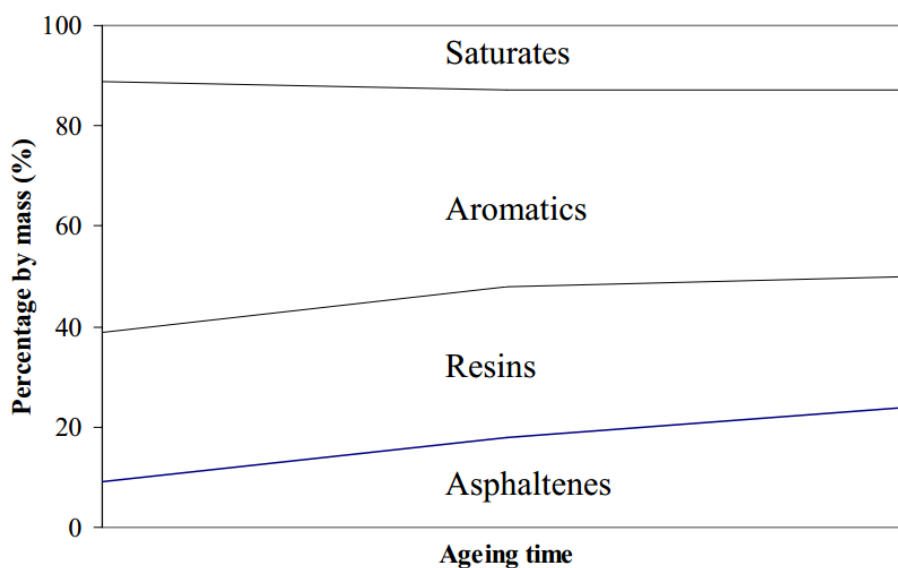


**Figure 2.9:** SARA fractional changes upon oxidation as a function of ageing time (Wu 2009).

The aforementioned fractional changes during oxidative ageing were also observed in a study performed by Domke et al. (1999). The researchers reported that oxidative ageing of bitumen led the non-polar naphthene aromatics to form polar aromatics (resins), which in turn formed asphaltenes (*Fig. 2.10*). The saturates fraction was considered to be chemically inert.

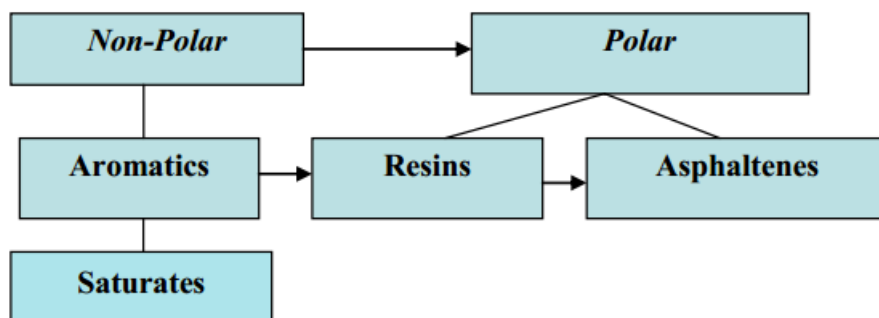


**Figure 2.10:** Schematic illustration of the movement of bitumen components from non-polar to more polar fractions (Hagos 2008).

However, the relative changes in the mass percentages of the Corbett (SARA) fractions, when the different fractions are aged as a whole, provide little information with respect to the chemical reactions that occur within the fractions themselves and/or the susceptibility of the different fractions to oxidation (Petersen 2009). In an effort to gain additional chemical insight, Petersen et al. (1974) oxidized separately, at 130°C, the SARA fractions from a Wilmington (California) bitumen and determined the formation of oxygenated products in each of them. Based on the obtained results, they were able to rank the relative reactivity with atmospheric oxygen of saturates, naphthene aromatics, polar aromatics (resins) and asphaltenes as 1:7:32:40, respectively. This result demonstrates that reactivity with oxygen increases with increasing fraction polarity.

Even though some researchers (Rostler & White 1959) argue that the asphaltenes fraction is chemically inert, the analysis presented above clearly shows that asphaltenes are very reactive with oxygen. Petersen (2009) provides an explanation for the contradicting opinions: Asphaltenes are brittle solids at ambient temperatures and, thus, quite unreactive with oxygen. Their resistance to air oxidation is attribute to their highly structured state which hinders the molecular mobility. This is not the case when the asphaltenes are separated and oxidised at high temperatures (e.g. 130°C), where molecular mobility increases and so does their chemical reactivity.

### 2.2.2.2 Molecular changes

Changes on molecular level, that occur during oxidation of bitumen, are usually studied from the aspect of the formation of chemical functional groups in bitumen molecules. Upon oxidation the main occurring chemical functionalities are ketones and sulfoxides whereas dicarboxylic anhydrides and carboxylic acids are also formed, but in substantially lower amounts (Plancher & Petersen 1976). Ketones, dicarboxylic anhydrides and carboxylic acids are usually referred to as the carbonyls functional group (Wu 2009). In Fig 2.11, the structural formulas of the functional groups formed during oxidative ageing are presented.

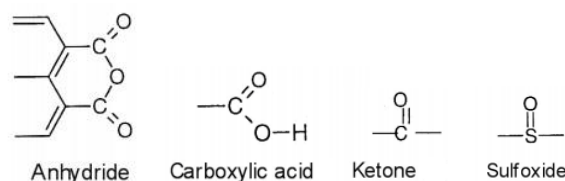


**Figure 2.11:** Chemical functionalities formed upon oxidative ageing (Petersen 2009).

Dorrence et al. (1974) reported that ketones are formed at the benzylic carbon position (Fig. 2.12). The hydrogen attached to this position is highly reactive and can be readily removed upon oxidation. This leads to a free radical on the carbon where the ketone is formed (Fig. 2.13) (Petersen 1984).

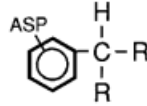


Figure 2.12: Benzylic carbon (Petersen 2009).

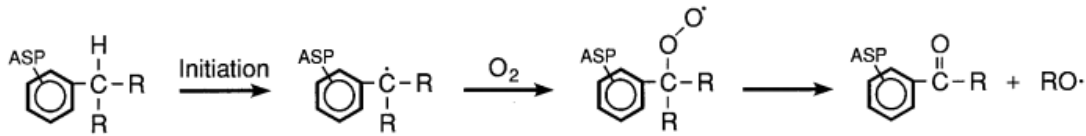


Figure 2.13: Ketone formation at benzylic carbon position (Petersen 2009).

Sulfoxides, the second major oxidation product, result from the oxidation of the sulphides present in the bitumen's molecules. At the initial oxidation spurt, the rate of formation of sulfoxides is much higher than the one of ketones. At this initial stage, oxygen reacts with hydrocarbons to form hydroperoxides. There is a rapid reaction, characterized by the scavenger action of sulphides, according to which the latter react with hydroperoxides to form sulfoxides. However, when high temperatures are involved during oxidation, the hydroperoxides may decompose, due to their thermal instability, and free radicals are formed which favour the formation of ketones. As a result, more ketones are formed at the expense of sulfoxides. The rate of sulfoxides formation over ketones is also highly dependent on the sulphur content of bitumen (Petersen 2009).

Petersen (2009) stressed an important issue. By comparing the oxidation products formed in four different bitumen and their oxidative hardening, as determined by the ratio of their viscosity after and prior to ageing, the following observations were made: Bitumen in which approximately the same amounts of ketones and sulfoxides were formed, exhibited quite different age-hardening. On the other hand, bitumen which showed similar oxidative hardening, contained fairly different amounts of oxygenated products. These observations suggest that, the susceptibility of different bitumen to oxidative hardening may be more accurately described by the effect of the formation of oxygenated products on its components' compatibility rather than the actual amounts of ketones and sulfoxides formed. For instance, a highly oxidised bitumen may show a small change in viscosity if the capacity of the non-polar components, to effectively disperse the polar functional groups formed upon ageing, is high (Wu 2009).

### 2.2.3 Bituminous binders ageing assessment

#### 2.2.3.1 Changes on physical properties of bitumen

The extent of ageing of bitumen and/or bituminous mixtures is usually assessed by the degree of change of one or more physical properties upon ageing, expressed through the so-called Ageing Indices (AI). In Eq. 2.1, the generic form of an AI is presented. The utilized physical property can vary between viscosity ( $\eta$ ), or more fundamental properties such as the complex shear modulus ( $G^*$ ).

$$AI = \frac{X_{\text{Aged}}}{X_{\text{Unaged}}} \quad (2.1)$$

where,

$X_{\text{Aged}}$  = Physical property after ageing

$X_{\text{Unaged}}$  = Physical property prior to ageing

Moreover, the degree of ageing can be determined through the Retained Penetration (RP) (Eq. 2.2), the difference in the Softening Point ( $\Delta T_{\text{R\&B}}$ ) (Eq. 2.3) and the Mass Loss/Gain (ML/G) (Eq. 2.4) of bitumen after ageing (Roberts et al. 1996).

$$RP = \frac{P_{\text{Aged}}}{P_{\text{Unaged}}} \cdot 100\% \quad (2.2)$$

where,

$P_{\text{Aged}}$  = The penetration of the aged binder ([L])

$P_{\text{Unaged}}$  = The penetration of the binder prior to ageing ([L])

$$\Delta T_{\text{R\&B}} = T_{\text{R\&B,Aged}} - T_{\text{R\&B,Unaged}} \quad (2.3)$$

where,

$T_{\text{R\&B,Aged}}$  = The softening point of the aged binder ([T])

$T_{\text{R\&B,Unaged}}$  = The softening point of the binder prior to ageing ([T])

$$ML/G = M_{\text{Aged}} - M_{\text{Unaged}} \quad (2.4)$$

where,

$M_{\text{Aged}}$  = The mass of the aged binder ([M])

$M_{\text{Unaged}}$  = The mass of the binder prior to ageing ([M])

### 2.2.3.2 Changes on chemical properties of bitumen

As pointed out in *Sub-Section 2.2.2.1* oxidative ageing of bitumen leads to an increase of its polar functional groups (i.e. asphaltenes) with a simultaneous decrease of the naphthene aromatics and resins, while saturates show negligible chemical reactivity (Fig. 2.9). The extent of ageing of the binder, by means of chemical changes, can be expressed through the Gaestel Index (IC), which constitutes a description of the chemical configuration of the binder that explains its internal colloidal structure. More severe ageing is captured through an increase of the IC (Ishai 1996). The IC is given in Eq. 2.5.

$$IC = \frac{\text{Asphaltenes} + \text{Saturates}}{\text{Aromatics} + \text{Resins}} \quad (2.5)$$

#### *Fourier transform infrared spectroscopy*

Fourier Transform Infrared (FTIR) spectroscopy is a technique that has been gaining ground, the past few years, in identifying changes in the chemical structure of bituminous binders upon oxidative ageing. A detailed description of the basic principles of this method is provided in *Sub-Section 3.6.2*. As mentioned previously, sulfoxides (S=O) and carbonyls (i.e. ketones, dicarboxylic anhydrides and carboxylic acids) (C=O) are the main products formed in bitumen's microstructure upon oxidative ageing. The formation of these functional groups is traceable, through visible peaks, in the infrared spectrum



obtained by FTIR, at specific wave numbers, i.e. sulfoxides at  $\sim 1030\text{ cm}^{-1}$  and carbonyls (ketones) at  $\sim 1700\text{ cm}^{-1}$  (Fig. 2.14). From the analysis of the band areas around the aforementioned wave numbers, indices for the carbonyls (CI) and sulfoxides (SI) may be derived that can describe the degree of oxidative ageing of the examined bitumen.

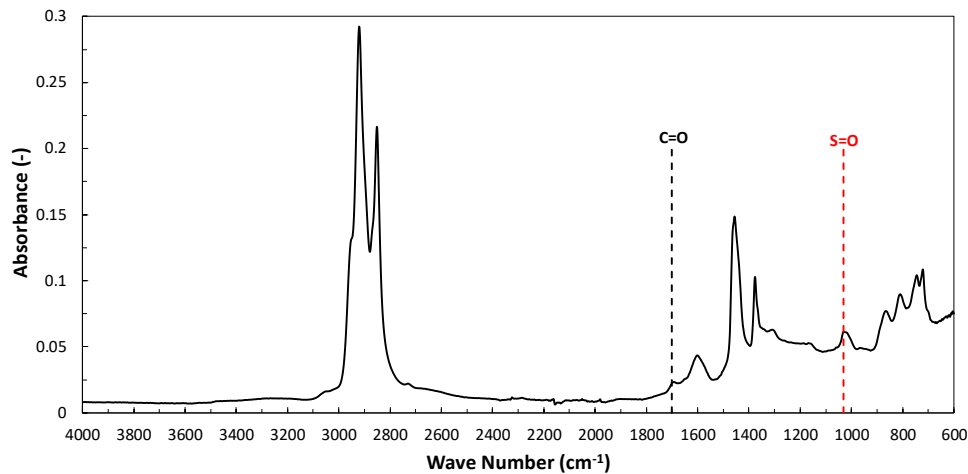


Figure 2.14: Infrared spectrum, carbonyls and sulfoxides peaks.

There are several approaches according to which analysis of the obtained spectra may be performed. It may be performed on original or normalized spectra. Quantitative analyses of certain functional groups may be carried out by obtaining directly the value of the respective peak (maximum absorbance value) or by integrating the area, determined by pre-defined boundary-wave numbers, below the absorbance spectrum and around the peak of interest. Finally, the aforementioned values can be obtained by considering an absolute or tangential base line (Hofko et al. 2017). Fig. 2.15 schematically illustrates all of the above-mentioned approaches.

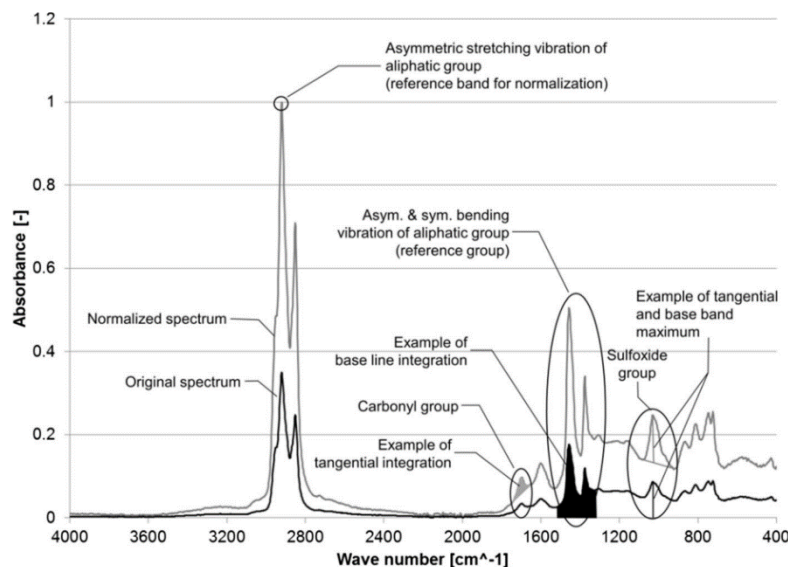


Figure 2.15: Various approaches for infrared spectra analysis (Hofko et al. 2017).

Hofko et al. (2017) performed an ageing study on one conventional and one polymer modified Performance Grade (PG) bitumen. The two materials were laboratory-aged, simulating both short and long-term ageing. For the latter various ageing times were applied. The control and aged materials were then investigated by means of FTIR. Defined indices were calculated for the oxygenated functional groups (carbonyls and sulfoxides)

by analysing the obtained spectra based on all possible combinations of the various previously-discussed approaches. The ultimate goal of the research was to provide recommendation on which of the different approaches should be utilized for infrared spectra analysis. The final suggestion was based on adequate repeatability of the results and on the ability of the different methods to detect small changes in the chemical structure of bitumen upon ageing (sensitivity of results). The researchers concluded that the derivation of the CI and SI should be performed on normalized spectra, by using integration of areas and the absolute baseline approach. The asymmetric stretching vibration of the aliphatic group is taken as the basis for spectra normalization (reference band) (Fig. 2.15).

Van den Bergh (2011) investigated five different methods for the semi-quantitative analysis of infrared spectra. Based on experimental research and statistical evaluation of the results, the researcher concluded and recommended that the method proposed by Lamontagne et al. (2001) should be used for the spectra analyses, due to the fact that it presented low coefficient of variation and provided more information about the chemical composition of bituminous binders. The boundary-wave numbers for the areas' integration are shown in Table 2.2. The CI and SI are calculated according to Eq. 2.6 and 2.7, respectively.

**Table 2.2:** FTIR areas integration boundaries (Van den Bergh 2011).

Area	Upper boundary (cm <sup>-1</sup> )	Lower boundary (cm <sup>-1</sup> )
A <sub>2953</sub>	2990	2880
A <sub>2862</sub>	2880	2820
A <sub>1700</sub>	1753	1660
A <sub>1600</sub>	1670	1535
A <sub>1460</sub>	1525	1395
A <sub>1376</sub>	1390	1350
A <sub>1030</sub>	1047	995
A <sub>864</sub>	912	838
A <sub>814</sub>	838	783
A <sub>743</sub>	783	734
A <sub>724</sub>	734	710

$$CI = \frac{A_{1700}}{\sum A} \quad (2.6)$$

$$SI = \frac{A_{1030}}{\sum A} \quad (2.7)$$

where,

A<sub>1700</sub> = The area beneath the spectrum around the wave number 1700 cm<sup>-1</sup>

A<sub>1030</sub> = The area beneath the spectrum around the wave number 1030 cm<sup>-1</sup>

$$\sum A = A_{2953} + A_{2862} + A_{1700} + A_{1600} + A_{1460} + A_{1376} + A_{1030} + A_{864} + A_{814} + A_{743} + A_{724}$$

### 2.2.4 Bituminous binders' laboratory ageing tests

Over the years many investigations have been performed by researchers in an effort to develop accelerated laboratory ageing techniques that would simulate, accurately enough, the ageing that bitumen undergoes both during production/construction (STA) and in the field (LTA). Airey (2003) provided an extensive list of the various existing bitumen ageing methods, which is presented in *Table 2.3*. Among the different ageing techniques, the Thin Film Oven Test (TFOT), Rolling Thin Film Oven Test and Rotating Flask Test (RFT) are widely used to simulate STA of bitumen, while the Rotating Cylinder Ageing Test (RCAT) and the Pressure Ageing Vessel (PAV) are regarded as the most appropriate in simulating LTA of bitumen (Wu 2009).

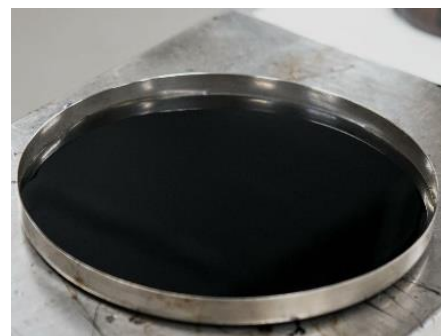
#### 2.2.4.1 Thin film oven test (TFOT)

The TFOT (*Fig. 2.16a*) is conducted in accordance with NEN-EN 12607-2. 50 grams of bitumen are poured in the TFOT pan (*Fig. 2.16b*), of 140 mm diameter, to form a film thickness of approximately 3.2 mm. It should be noted that when this method is used for ageing of a bituminous mixture (e.g. mastic) the effect of the density of the material on the resulting film thickness should be taken into consideration. If, for instance, in ageing of mastics the same film thickness as in bitumen is about to be achieved (i.e. ~3.2 mm) the quantity of the material placed in the TFOT pan should be adjusted accordingly. The norm specifies that the test is conducted at 163°C for a duration of 5 hours. TFOT is, primarily, used to simulate the ageing that the bitumen undergoes during production in the asphalt plant (Wu 2009). Airey (2003) stretched out that, due to the static state of the sample (i.e. no agitation or rotation) during the test, age-hardening is likely to be limited at the top part of material. The latter is far from reality and constitutes the main reason for subsequent developed modifications of the test.

Wu (2009) reported that ageing of mastics with TFOT had caused the mineral filler to settle at the bottom of the TFOT pan, under the effect of gravity. This was attributed to the relative high testing temperature (i.e. 165°C), since the testing duration was kept within reasonable limits (maximum ageing time 20 hours). It is easily conceivable that such an effect is undesirable by virtue of the potential hindrance of the effect of the mineral filler on ageing of bitumen. The experience of Wu dictates that ageing of mastics should be performed with a test that allows the utilization of lower temperatures, always in accordance with the respective norm.



(a)



(b)

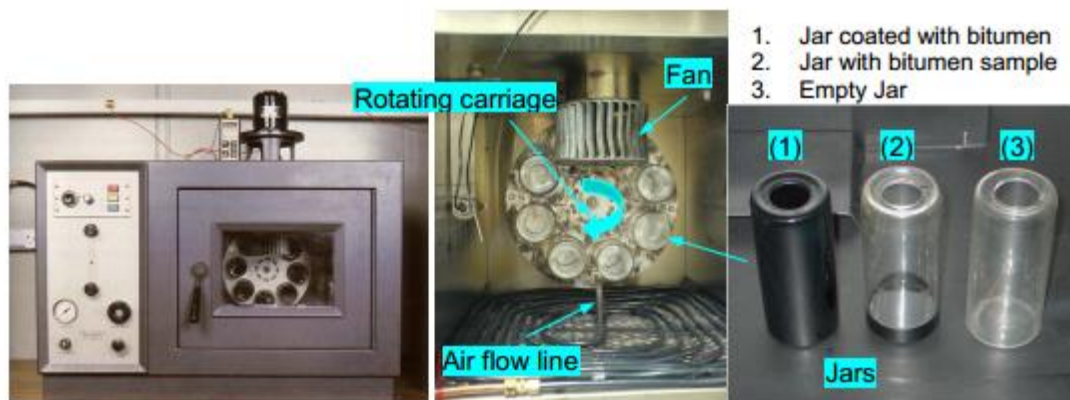
**Figure 2.16:** (a) TFOT (Wu 2009). (b) TFOT pan.

Table 2.3: Bitumen ageing tests (Airey 2003).

Ageing test	Temp (°C)	Time (hrs)	Sample size (gr)	Film thickness (mm)	Feature
Thin Film Oven Test (TFOT)	163	5	50	3.2	-
Modified Thin Film Oven Test (MTFOT)	163	24	-	0.1	-
Rolling Thin Film Oven Test (RTFOT)	163	1.25	35	1.25	Air Flow 4000 ml/min
Extended Rolling Thin Film Oven Test (ERTFOT)	163	8	35	1.25	Air Flow 4000 ml/min
Nitrogen Rolling Thin Film Oven Test (NRTFOT)	163	1.25	35	1.25	N <sub>2</sub> Flow 4000 ml/min
Rotating Flask Test (RFT)	165	2.5	100	-	Flask Rotation 20 rpm
Shell Microfilm Test	107	2	-	0.005	-
Modified Shell Microfilm Test 1963	99	24	-	0.02	-
Modified Shell Microfilm Test 1961	107	2	-	0.015	-
Rolling Microfilm Oven Test (RMFOT)	99	24	0.5	0.02	Benzene Solvent
Modified Rolling Microfilm Oven Test (MRMFOT)	99	48	0.5	0.02	Opening ∅ 1.04 mm
Tilt-Oven Durability Test (TODT)	113	168	35	1.25	-
Alternative Tilt-Oven Durability Test (ATODT)	115	100	35	1.25	-
Thin Film Accelerated Ageing Test (TFAAT)	130/113	24/72	4	0.16	Opening ∅ 3 mm
Modified Rolling Thin Film Oven Test (MRTFOT)	163	1.25	35	1.25	Steel Rods
Iowa Durability Test (IDT)	65	1000	50	3.2	Pure Oxygen 2.07 MPa
Pressure Oxidation Bomb (POB)	65	96	-	0.03	Pure Oxygen 2.07 MPa
Accelerated Ageing Test Device/Rotating Cylinder Ageing Test (RCAT)	70-100	144	500	2	Pure Oxygen 4~5 lit/hr
Pressure Ageing Vessel (PAV)	90-100	20	50	3.2	Air 2.07 MPa
High Pressure Ageing Test (HiPAT)	85	65	50	3.2	Air 2.07 MPa

### 2.2.4.2 Rolling thin film oven test (RTFOT)

The RTFOT (*Fig. 2.17*) was developed in the early 60's, by the State of California Department of Public Works, Division of Highways (Hveem et al. 1963), and constitutes perhaps the most important modified version of the TFOT (Wu 2009). The test is performed in accordance with NEN-EN 12607-1. The RTFOT apparatus consists of 8 glass bottles which are placed horizontally in a rotating shelf. In each bottle 35 grams of bitumen are placed, as specified in the norm. The test is conducted at 163°C for 75 minutes. During the test, due to the rotation of the shelf, the bitumen is able to flow in the bottle forming a thin film (*Table 2.3*), while hot air is supplied in each bottle. A direct advantage of RTFOT over TFOT is that all bitumen is exposed to the hot air, leading to a relatively homogeneous age-hardening. Even though the ageing conditions in the RTFOT differ with the respective ones found in asphalt mixture production, the age-hardening achieved in the laboratory seems to correlate well enough with that observed in a conventional batch mixer (Hunter et al. 2015).



**Figure 2.17:** The RTFOT and apparatus (Hagos 2008).

However, RTFOT is an ageing method in which the viscosity of the tested material plays an important role to the final outcome, due to the fact that the material forms a rotating film whose thickness is highly dependent on the material's ability to flow, as reported by Lesueur et al. (2016). The latter is corroborated by the difficulties encountered when polymer-modified bitumen (thick binders) were tested with the RTFOT (Vassilyev et al. 2001). This could be an important issue when bitumen and mastics are to be compared after ageing by means of the RTFOT. It is well known that the mineral fillers (significantly) increase the viscosity of bitumen when blended together. As a consequence, when mastic is tested with the RTFOT it is expected that its exposure to the hot air will be substantially less compared to neat bitumen, because of the different formed film thicknesses, which, in-turn, are controlled by the different viscosities of the materials. In a subsequent comparison of mastic and bitumen, the former would appear to be less aged, which could be incorrectly interpreted as a mitigating effect of the mineral filler on ageing of bitumen (Lesueur et al. 2016). Under the same considerations, uncertainty for the obtained outcome may also exist when mastics incorporating different types of mineral fillers are tested with the RTFOT and then are evaluated for age-hardening in comparison with each other. In this case, a potential different stiffening effect of the various mineral fillers could be the main reason behind observed differences.

### 2.2.4.3 Pressure ageing vessel (PAV)

The PAV (*Fig. 2.18a*) is an ageing method developed by the SHRP-A-002A research team, with the purpose to provide accelerated laboratory ageing similar to the LTA that bitumen undergoes in the field (Christensen & Anderson 1992). The test is conducted in accordance with NEN-EN 14769. PAV oxidative ageing is usually conducted on TFOT or RTFOT bitumen residue, 50 grams of which are poured into metallic trays (PAV pans) (*Fig. 2.18b*), resulting in approximately 3.15 mm binder film. The same considerations apply as in TFOT, regarding the material's film thickness in the pan, when ageing of mastics is to be performed, which were discussed previously. The test is performed for 20 hours under the effect of pressurized air, at 2.10 MPa, and temperatures ranging between 90 and 110°C.

To the authors knowledge, there are no relevant issues reported in literature with respect to the ageing of mastics by means of PAV. Given the similarities that exist, regarding the test set-up, between the TFOT and PAV, one could argue that settlement of the mineral filler may also occur in the PAV. This is not excluded. However, by strictly following the norms, ageing in the PAV provides the opportunity to utilize temperatures as low as 90°C, instead of the 163°C specified in the TFOT. For equivalent test duration, mineral fillers' settlement is more likely to occur in the case of the TFOT rather in the PAV.

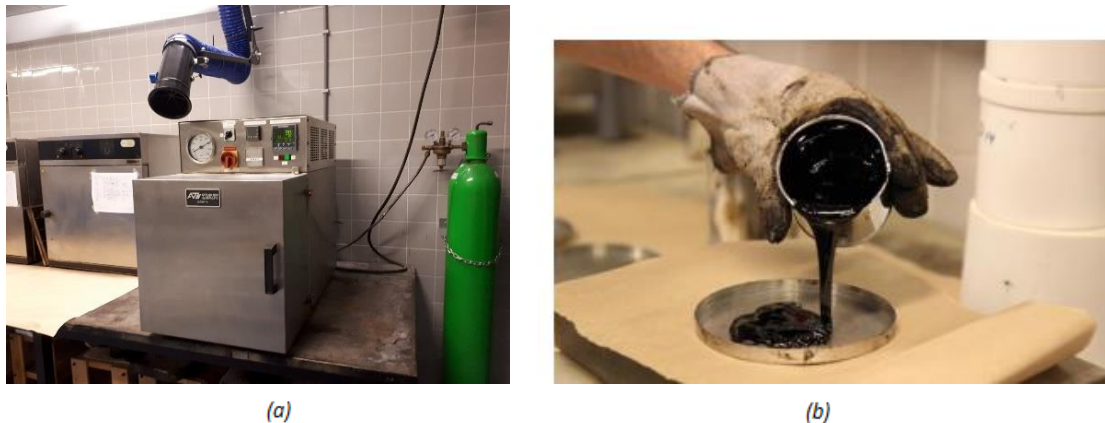


**Figure 2.18:** (a) PAV. (b) PAV pan.

## 2.3 Mineral aggregates

Mineral aggregates are the major component, in terms of proportions, in an asphalt mixture. Hence, their properties are of immense importance for the performance of a bituminous mixture. Particles' size distribution, shape, roughness, strength etc. are some of the most commonly properties studied and reported in literature that are related to the performance of an asphalt mixture (Wu 2009).

Mineral aggregates, as a whole, and their influencing properties are out of the scope of this study. Nevertheless, in this literature review, attention is paid to a special fraction of the aggregates system, the mineral filler, and on the aggregate particles' surface characteristics which are relevant to the objectives of the present thesis.

### 2.3.1 Mineral fillers

#### 2.3.1.1 Definition of mineral fillers

Mineral fillers were initially considered as the fraction of the aggregate's system whose sole purpose was to fill the voids in the mixture and satisfy the gradation requirements. However, subsequent studies showed that the function of mineral fillers, in an asphalt mixture, is much more than a simple void-filling material. The filler particles smaller than the binder film thickness form a mastic when blended with bitumen, leading to increased stiffness of the overall mixture. The larger particles behave as mineral aggregate and, thus, contributing to the contact points between individual aggregate particles (Aburkaba & Muniandy 2016).

According to NEN-EN 13043, the term mineral filler refers to the aggregate's fraction, most or all of which passes a 63  $\mu\text{m}$  mesh sieve. In the American specifications, a 75  $\mu\text{m}$  mesh (#200) sieve is used as the defining one for the definition of mineral fillers. Table 2.4 shows the mineral filler gradation requirements as specified in the Dutch (European) norm (NEN-EN 13043).

**Table 2.4:** Mineral fillers gradation requirements according to NEN-EN 13043.

Sieve size ( $\mu\text{m}$ )	Cumulative percentage passing by mass (%)
2000	100
125	85 to 100
63	70 to 100

Tunncliff (1962) attempted to provide a definition of the mineral fillers based on their void-filling ability and its resulting effect: "*Filler is the portion of the mineral aggregate generally passing #200 sieve and occupying void spaces between the coarser aggregate particles in order to reduce the size of these voids and increase the density and stability of the mass*". Another definition was given by Tunncliff, based on the effect of filler on bitumen: "*Filler is the mineral material that is in colloidal suspension in the asphalt cement and results in cement with a stiffer consistency*".

According to the definition provided by Puzinauskas (1969): "*Mineral fillers play a dual role in paving mixtures. First, they are part of the mineral aggregate. They fill the interstices and provide contact points between larger aggregate particles and thereby strengthen the mixture. Second, when mixed with the asphalt, mineral fillers form a high-consistency binder or matrix which cements larger particles together*". This definition incorporates both definitions which were separately cited by Tunncliff (1962) (Aburkaba & Muniandy 2016).

Wypych (1999) provided yet another definition for the very fine fraction: "*Mineral filler can be defined as solid material capable of changing the physical and chemical properties of materials by surface interaction or its lack thereof and by its own physical characteristics*". This definition stresses two aspects of the effect of the mineral filler on the mastic system. For one, the effect that its physical properties (i.e. particles' size, shape, distribution etc.) have on the end product, when the bitumen phase is filled with solid particles. For another, the effect that the physico-chemical interactions between the mineral fillers' particles and the liquid phase have on the properties of the resulting material. The latter may vary from strong physico-chemical bonds to almost no

interactions at all, leading to a variable reinforcing effect in the end product (Aburkaba & Muniandy 2016).

### 2.3.1.2 Properties of mineral fillers

In a literature review performed within the framework of the National Cooperative Highway Research Program (NCHRP) Project 9-45 (2010), it was concluded that the most commonly measured mineral filler properties for the characterization of the mineral matter can be classified in two major categories: a) Geometrical (or physical) and b) chemical properties. Within each category a number of properties (*Table 2.5*) were found to have the most predominant effect on the performance of mastics and/or asphalt mixtures.

**Table 2.5:** Mineral filler properties according to NCHRP 9-45 (2010).

<b>Geometrical/physical property</b>	<b>Chemical property</b>
Particles' Size and Size Distribution	Plasticity Index
Specific Gravity	Clay Content-Methylene Blue Test
Surface Area	pH Value of Diluted Suspension
Fractional Voids-Rigden Voids	Water Solubility/Susceptibility
Shape, Angularity and Texture	Elemental Analysis

Aburkaba & Muniandy (2016) provided a more extensive summary of the mineral fillers' key properties, their means of measurement and the corresponding standards, as shown in *Tables 2.6 to 2.9*.

**Table 2.6:** Mineral filler geometrical properties, means of measurement and corresponding standards (Aburkaba & Muniandy 2016).

<b>Geometrical property</b>	<b>Means of measurement</b>	<b>Standard</b>
Particles' Size Distribution	Air-Jet, Sedimentation, Laser Diffraction	EN 993-10/ BS ISO13320-1:1999
Particles' Morphology	Scanning Electron Microscopy (SEM)	-
Surface Area	Blaine test	EN 196-6

**Table 2.7:** Mineral filler physical and mechanical properties, means of measurement and corresponding standards (Aburkaba & Muniandy 2016).

<b>Physical/mechanical property</b>	<b>Means of measurement</b>	<b>Standard</b>
Water Content	-	EN 1097
Particles' Density	-	EN 1097-7

**Table 2.8:** Mineral filler stiffening properties, means of measurement and corresponding standards (Aburkaba & Muniandy 2016).

<b>Stiffening property</b>	<b>Means of measurement</b>	<b>Standard</b>
Fractional Voids	Rigden Voids	EN 1097-4:1998
Delta Ring and Ball	-	EN 13179-1
Absorption	Bitumen Number	EN 13179-2
Loose Bulk Density in Kerosene	-	EN 1097-3



**Table 2.9:** Mineral filler chemical properties, means of measurement and corresponding standards (Aburkaba & Muniandy 2016).

Chemical property	Means of measurement	Standard
Water Solubility	-	EN 1744-1:1998
Water Susceptibility	-	EN 1744-4:2001
Calcium Carbonate Content	X-Ray Fluorescence Spectroscopy	EN 196-21/EN 495-2
Calcium Hydroxide Content	-	EN 495-2
Organic Content	Loss on Ignition of Coal Fly Ash	EN 1744-1:1998
Organic Content	Loss on Ignition of Blast-Furnace Slags	EN 196-2:1994
Mineral Composition	Energy-Dispersive X-Ray (EDX) Spectroscopy	-
Harmful Fines	Methylene Blue Test	EN 933-9
Plasticity Index	-	BS1377:1990

### 2.3.2 Mineral aggregates surface characteristics

#### 2.3.2.1 Surface charge

The surface of the mineral aggregates is characterized by an electrical charge, by virtue of the ionization of their minerals (Bagampadde et al. 2005). Different aggregates with different mineralogy may be charged differently (i.e. positively or negatively). Based on the sign of the charge, aggregates are classified as acidic or basic. According to Su (1996), acidic are the aggregates rich in silicates (e.g. quartzite, granite etc.) which are negatively charged by forming  $\text{SiO}_3^{2-}$  ions. On the other hand, basic aggregates, such as limestone (rich in calcium), form positively charged  $\text{Ca}^{2+}$  ions. The classification of aggregates by surface charge is illustrated in *Fig 2.19*.

Due to such different chemical charges, the aggregate surfaces may result in variable polarity and, by extension, variable affinity towards the polar components of bitumen, when they are brought in contact (Wu 2009). In general, it has been shown in bitumen-aggregate adhesion (stripping) studies, that basic aggregates form stronger chemical bonds with bitumen components than the acidic ones (Van Lent 2013).

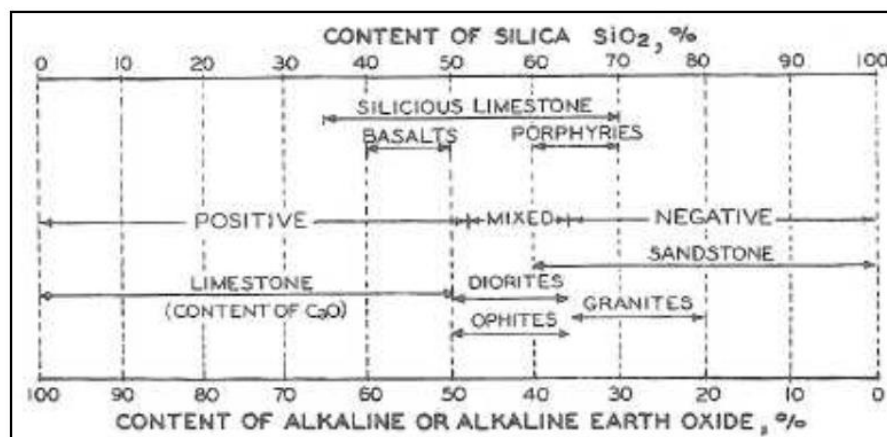


**Figure 2.19:** Aggregates classification as acidic or basic based on their surface charge (Mertens & Wright 1959).

### 2.3.2.2 Surface interaction with bitumen components

Two major mechanisms are distinguished regarding the interaction of mineral matter and bitumen when the two materials are mixed together: a) Absorption of bitumen components into the mineral aggregates structure and b) adsorption of bitumen components on the mineral aggregates surface.

#### *Absorption*

Absorption refers to the phenomenon according to which, the oily components of bitumen migrate into the porous structure of aggregates. Hence, the action of absorption is not a phenomenon limited on the interface of bitumen and aggregates but, rather, free space and volume, in the internal structure of aggregates, are required to accommodate the absorbed material (Osman 2004). The absorption of bitumen oily components can lead to hardening of the material. This was classified, in *Sub-Section 2.2.1*, under the name *Separation*, as one of the main reasons that could lead to bitumen hardening. Unlike the adsorption mechanism, absorption has received limited attention, in terms of research (Scott 1978).

In a literature review conducted by Van Lent (2013) it was reported that less viscous fractions of bitumen were preferentially absorbed into aggregate particles and that the left-behind heavier fraction of asphaltenes established the bitumen as more susceptible to premature age-hardening.

On the same grounds, Wu (2009) observed in his research that recovered bitumen from aged mastics were characteristically softer than the pure aged bitumen, aged under identical conditions. According to the researcher, a possible explanation for the latter is that oily and/or less polar components of bitumen were absorbed into the mineral filler particles. These components, being protected from oxidation and evaporation, are easily reclaimed upon extraction, by virtue of their weak bonds with the aggregate surface, and give the recovered bitumen a softer nature.

#### *Adsorption*

Adsorption is a surface phenomenon and refers to the bonding of bitumen components onto the aggregates surface through the development of molecular forces (Wu 2009).

Plancher et al. (1977) identified the strongly adsorbed bitumen components on the aggregates surface. Five different aggregates were used in their study, namely quartzite 15, Hol limestone, Riverton limestone, granite and granite P-6 and four different bitumen. The coated with bitumen aggregates were washed with benzene until the benzene extract was colourless. The material residue on the aggregates surface was considered to be the strongly adsorbed bitumen fraction. The residue material was removed by the aggregate surface through an 8-hour extraction process with pyridine.

The researchers identified that the amount of the strongly adsorbed material, for all bitumen-aggregate combinations, was less than 1% with an average value of 0.4%. A very important observation was that the percentage of the amount of the adsorbed material was dependent on the specific surface area of the each-time tested aggregate (*Fig. 2.20*). This implies that the adsorption intensity of bitumen components onto the aggregates surface, apart from other factors (i.e. aggregate mineralogy), is (highly) affected by the available interfacial area for interactions.

The chemical analysis of the strongly adsorbed material revealed that the residual material on the aggregate surface was composed of all five oxygenated functional groups present in the bitumen micro-structure (i.e. ketones, carboxylic acids, dicarboxylic anhydrides, 2-quinolone types and sulfoxides) as well as nitrogen. Based on their relative affinity to the aggregates surface the various components were ranked as shown in *Table 2.10*.

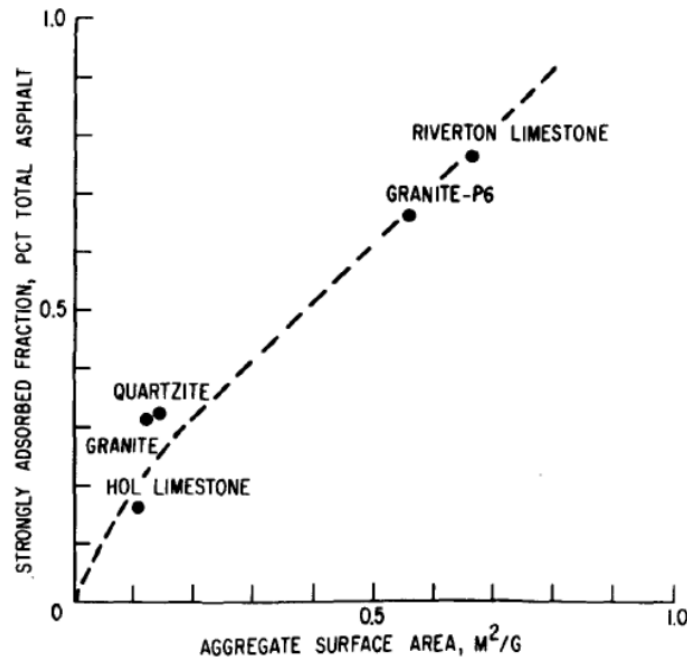


**Figure 2.20:** Percentage of strongly adsorbed bitumen fraction on aggregates surface against aggregates specific surface area (Plancher et al. 1977).

**Table 2.10:** Bitumen components relative affinity to aggregate surface (Plancher et al. 1977).

Bitumen component	Relative affinity
Carboxylic Acids	High
Dicarboxylic Anhydrides	↑ ↓
2-Quinolone Types	
Sulfoxides	
Nitrogen	
Ketones	

The research conducted by Plancher et al. (1977) highlights two very important aspects. For one the importance of the aggregate particles' specific surface area in the adsorption mechanism and, for another, the tendency of the chemical functional groups of bitumen, formed upon oxidation, to strongly adsorb on the surface of the mineral matter. As it is discussed in *Section 2.4*, these two aspects, in most of the cases, constitute the major ways through which the results are interpreted when the effect of mineral fillers on ageing of bituminous mixtures is considered.

In a similar study performed by Scott (1978) it was shown that polar molecules of bitumen, and in particular the oxygen containing functional groups from the asphaltene fraction, are strongly adsorbed onto the surface of the mineral aggregates. The researcher concluded that the adsorption process is influenced by the properties of bitumen and aggregates as well as by the adsorption conditions.

## 2.4 Mineral aggregates and ageing of bituminous binders

### 2.4.1 General

In practice, during the service life of an asphalt pavement, ageing of bitumen occurs while the bitumen is in contact with mineral aggregates. However, most of the ageing studies do not account for the presence of the mineral matter (aggregates, sand and filler) and the effect it may have on the ageing process of bitumen. Instead, neat bitumen is subjected to ageing and further evaluated as an independent material (Moraes & Bahia 2015a). The latter can lead to either underestimation or overestimation of the ageing level of the examined bitumen by virtue of the apparent catalytic or mitigating effect of the mineral matter on ageing.

Anderson et al. (1992) stated that the properties of fine aggregates and, in particular those of the mineral fillers, govern the physico-chemical interactions between bitumen and mineral aggregates. The latter stems from the fact that fines, which have substantially larger surface area compared to coarse aggregates, are embedded in the bitumen and as a result the majority of the bitumen-aggregate interface area is generated by them. Hence, some benefits of conducting ageing studies on mastic level, can be derived: For one, the very fine fraction provides the largest surface area for physico-chemical interactions with bitumen, so any potential, catalytic or mitigating, effect of mineral matter on ageing can be captured. For another, unlike ageing studies on mixture level, factors that evidently affect the bitumen ageing process and are of great variability among different studies, such as air voids content in the mixture and binder film thickness, are eliminated since the mineral filler can be viewed as being embedded in bitumen (Alfaqawi et al. 2017).

### 2.4.2 Effect of mineral fillers on ageing of bitumen

Han (2011) reported that the presence of mineral filler in mastics may mitigate the oxidation of bitumen in two possible ways. The mineral matter, being less permeable to air, compels the oxygen molecules to follow a spiral path (*Fig. 2.21*) through the diffusion medium, thus lengthening the diffusion path and reducing the rate of oxidative ageing of bitumen (Charles et al. 2009). Furthermore, the viscosity of the bitumen is increased, upon addition of mineral filler, which may lead to further hindrance of the oxygen diffusion process. Both of the above statements do not take into account any possible chemical interactions that are induced by the mineral matter, but rather, are based on the physical presence of the mineral filler in the mastics and its primary stiffening effect.

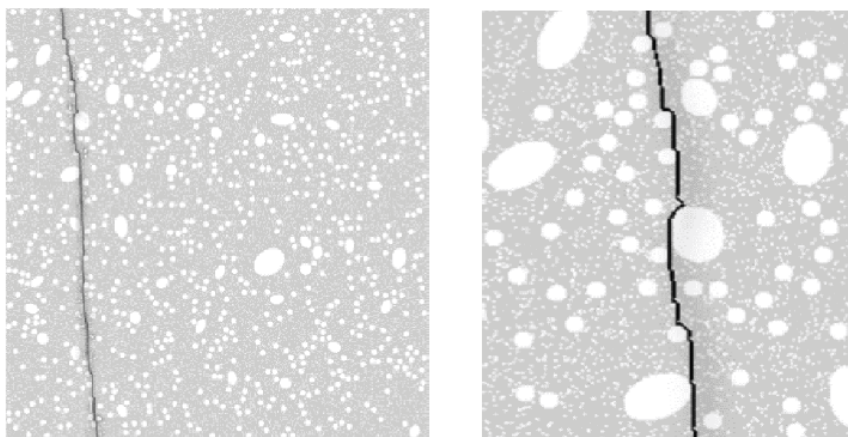


**Figure 2.21:** Oxygen diffusion path simulation (Moraes & Bahia 2015a).

Mineral fillers may affect the ageing of bitumen in two ways, when potential chemical interactions come to the foreground. Firstly, the existence of certain mineral components on their surface may catalyse the oxidation of bitumen (Petersen et al. 1974). Secondly, an adsorption mechanism may occur according to which polar functional groups, either naturally existing ones in the bitumen's chemical structure or oxidation products, are adsorbed and immobilized at the mineral matter's surface, decelerating the ageing process (Wu 2009).

Gubler et al. (1999) conducted research on mastic level, considering two types of bitumen and three types of mineral fillers, namely limestone, granite and siliceous limestone. The mastics were prepared with varying volumes of free bitumen (Rigden 1954). The Dynamic Shear Rheometer (DSR) and the Bending Beam Rheometer (BBR) tests were employed to evaluate the effect of the mineral fillers on bitumen's ageing. The obtained data demonstrated that different mineral fillers and different types of bitumen behave differently upon ageing. Nevertheless, all utilized fillers appeared to promote the oxidation and hardening of bitumen during the ageing simulation. On the contrary, Curtis et al. (1993), with reference in two other SHRP studies (Kennedy et al. 1990, Petersen et al. 1994), suggested that the presence of mineral matter decreases the rate of the binder's viscosity build-up when compared to neat bitumen, under the same ageing conditions. The latter was attributed to the adsorption mechanism of polar functional groups. According to the authors, the difference in the viscosities was the result of the aggregates adsorbing some of the highly polar oxygenated products, which did not contribute to the binder's viscosity build-up. Nevertheless, in their very study, Curtis et al. (1993) showed that the, distinct, chemistry of granite and limestone had no effect on the formation of carbonyls and sulfoxides in bitumen when the latter was aged while in contact with the mineral aggregates.

Moraes & Bahia (2015a) performed research on the effect of mineral fillers on the oxidative ageing of mastics. Two PG bitumen and three mineral fillers were included in the study, namely hard limestone, hard granite and soft dolomite. The aforementioned mineral materials present quite different specific surface area, which constitutes an important variable that greatly affects the adsorption process of bitumen fractions (Plancher et al., 1977). In addition, a fourth type of filler, which contained zirconia and silica was considered. The latter was designated as "inert" since it was expected that bitumen would not interact with its components and it was used, in particular, to demonstrate any potential interactions between the bitumen and the filler particles when compared to the other products. Mastics were prepared at concentrations of mineral filler of 10% and 40% by volume. Neat bitumen as well as resulting mastics were then artificially aged by means of PAV for several ageing times.

The low-temperature performance of the materials was evaluated by recording and plotting the change of the glass transition temperature ( $T_g$ ) as a function of the ageing time (Fig. 2.22). Mastics with limestone and granite, at the two concentrations mentioned above, were compared with the neat bitumen, as well as with each other, at equivalent ageing times. The results indicated that even though the utilization of mineral filler (any type at any concentration) led to an initial decrease of the  $T_g$ , due to the adsorption of asphaltenes on the filler particle's surface, the overall curves of the mastics were shifted towards higher temperatures, compared to the neat bitumen curve, as ageing time increased. Moreover, with respect to the mineral filler concentration and the specific surface area, the increase of either, or both, of the aforementioned parameters led to a decrease of the  $T_g$ . The latter implies that when the contact area of the mineral fillers'

particles and bitumen increases, by either a higher specific surface area or increased mineral filler volume fraction, the asphaltene adsorption on the mineral matter's surface becomes more intense which, in extension, leads to an overall softening of the bulk material (Moraes & Bahia 2015a).

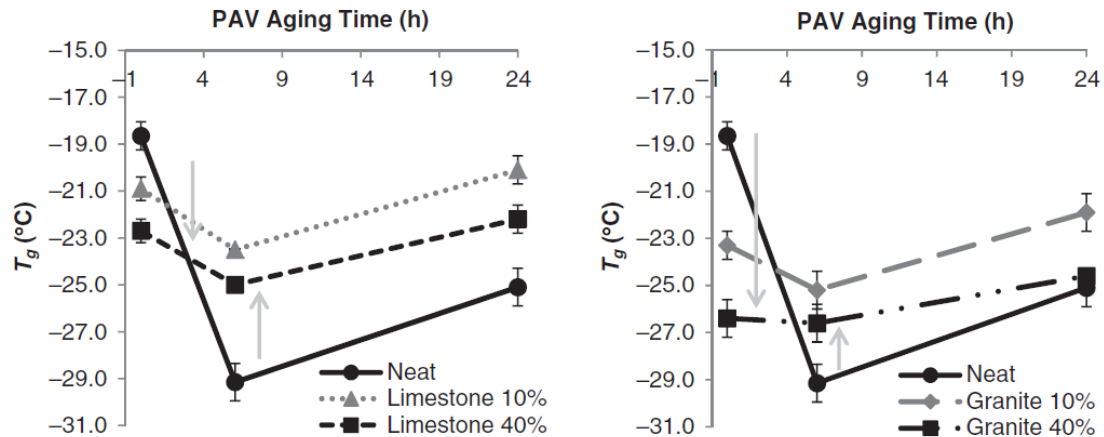


**Figure 2.22:** Bitumen's and mastic's glass transition temperature for various ageing times (Moraes & Bahia 2015a).

$G^*$  master-curves were constructed for the neat bitumen, before and after ageing for 24 hours in the PAV, and mastics with the various types of mineral fillers at a concentration of 40% by volume, after ageing for 24 hours in the PAV. According to the results, the master-curves of the aged bitumen were shifted towards higher values of the complex shear modulus, as it was very well expected, which was accompanied by a clockwise rotation of the very same master-curves. This outcome indicates a decrease of the time-dependency of the material's response over the tested frequencies. The addition of any type of mineral filler led to the shift of the master-curves towards higher frequencies, implying a more elastic response. However, the most important observation derived by the rheological analysis, was that the aged mastic master-curves did not show the clockwise rotation, with respect to the unaged bitumen, as observed for the aged bitumen master-curves (Fig. 2.23). This observation constitutes a strong statement according to which, when the mastic phase is considered, there is a possible counter-effect of the filler to the changes that ageing of bitumen, alone, imposes to the binder's mechanical properties (Moraes & Bahia 2015a). Alfaqawi et al. (2017) observed the same trend through the evaluation of  $G^*$  master-curves.

The effect of ageing on the properties of the neat bitumen and mastics was evaluated by calculating and comparing ageing indices based on the value of the complex shear modulus, at specific temperature and frequency, before and after ageing in the PAV for 24 hours (Fig. 2.24). The results indicated that the addition of mineral filler decelerated the age stiffening of mastics compared to the reference bitumen, showing lower values of the ageing index. This is in line with the observations of other researchers (Curtis et al. 1993, Wu 2009) in the context that mineral fillers have a mitigating effect on bitumen's age-hardening. It was stated that the mechanism of the adsorption of the bitumen's asphaltene on the mineral filler surface led to this outcome. Moreover, a comparison between the mastics with limestone and granite, at equal mineral filler concentration, revealed the capability of granite to more effectively decelerate the ageing process. The latter was attributed to the larger specific surface area of the granite particles leading to a more pronounced asphaltene adsorption effect.

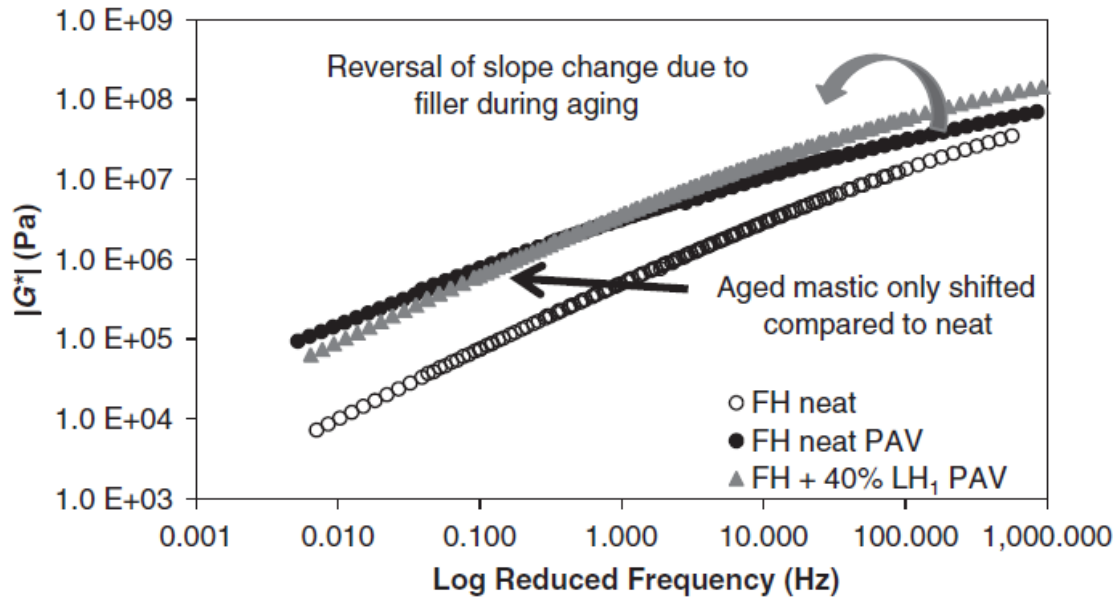


**Figure 2.23:** Complex shear modulus master-curves. Anti-clockwise rotation of aged mastic (Moraes & Bahia 2015a).

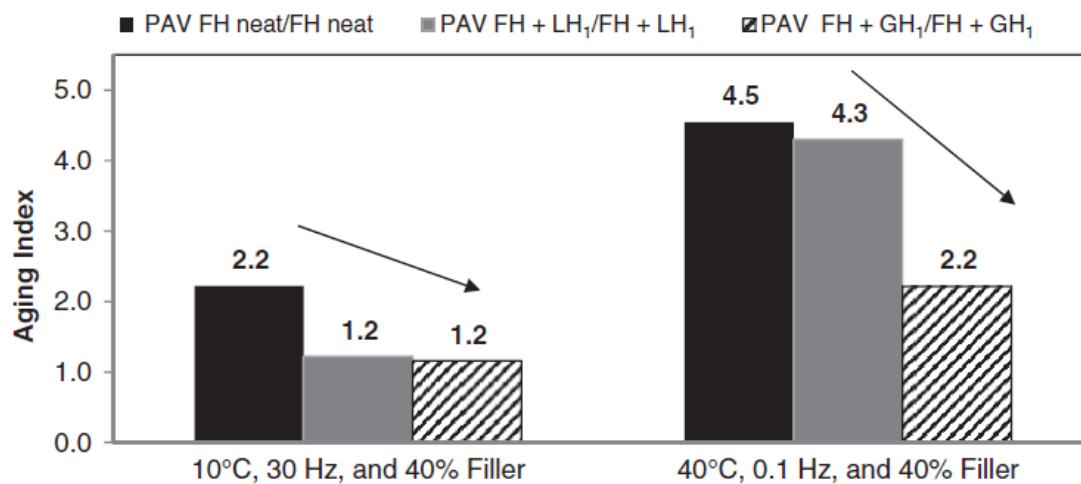


**Figure 2.24:** Aging indices of neat bitumen, limestone and granite mastics (Moraes & Bahia 2015a).

The researchers, in order to prove that, indeed, an adsorption mechanism exists upon ageing of mastics, prepared and aged mastics with “inert” and granite mineral filler. The two mineral matters had similar particles’ size and were added at the same concentration to the base bitumen. Both above features ensured that any effect of the solids on the oxygen diffusion path, caused by the mineral filler’s particles’ size and spatial distribution within the diffusion medium, was eliminated, as it was considered equal. Hence, any difference in the ageing indices would reveal the interactions between the granite particles and bitumen, keeping in mind that the “inert” mineral filler was supposed not to interact with the bitumen. The outcome, indeed, verified the presence of surface interactions, on top of any effect that the mineral fillers may had on the oxygen diffusion path, when granite was used, which was captured through the granite mastic’s lower ageing index compared to the one of the mastic prepared with the “inert” mineral filler (*Fig. 2.25*).

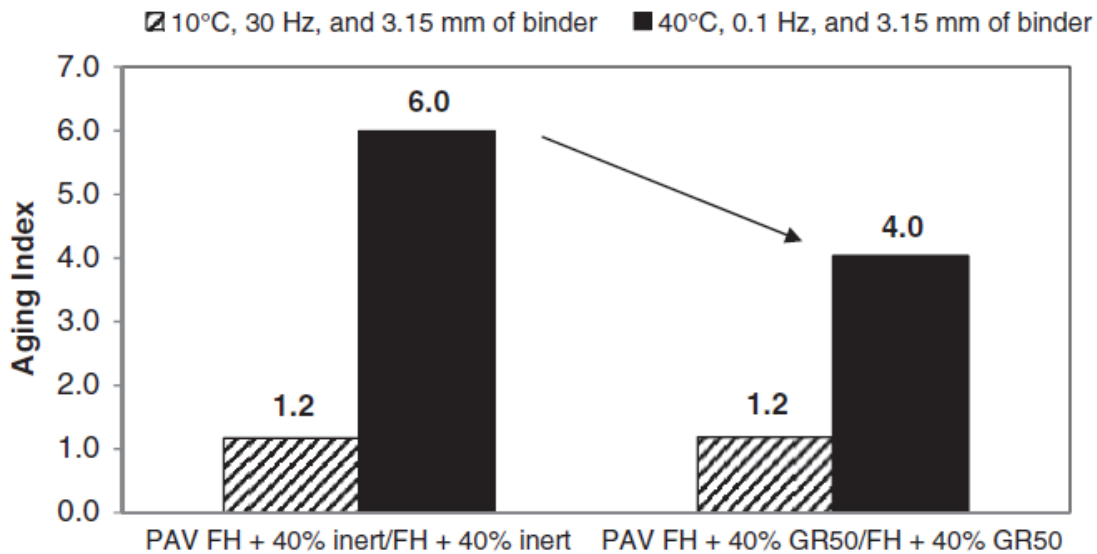


**Figure 2.25:** Ageing indices of “inert” and granite mastics (Moraes & Bahia 2015a).

With respect to the effect of the mineral fillers on the oxygen diffusion path during ageing, the authors referred to another study (Bahia et al. 2014) which demonstrated the analytical calculation of the increase of the length of the diffusion path due to the presence of the mineral filler with the assistance of software. They concluded that, even though there is an effect of the mineral fillers on the oxygen diffusion mechanism, the major contribution to the decrease of the ageing index stems from the adsorption of bitumen components to the surface of the mineral particles.

Moraes & Bahia (2015b) extended their research by evaluating the effect of mineral fillers on changes in the Molecular Size Distribution (MSD) of bitumen due to ageing. The Gel Permeation Chromatography (GPC) method was utilized (*Fig. 2.26*). With this method, which allows the separation of molecules according to their size, the MSD of an asphalt binder can be obtained, which is graphically presented in a chromatogram (*Fig. 2.27*). The chromatogram may provide information regarding the effect of oxidative ageing on different fractions of bitumen: Large Molecular Size (LMS), Medium Molecular Size (MMS) and Small Molecular Size (SMS). Ageing, typically, leads to the increase of the LMS molecules (Glover et al. 1988).

Three types of mineral fillers with different specific surface areas and chemical compositions, namely hard limestone, hard granite and soft dolomite, and two PG bitumen were considered in the research. The mastics were prepared with a mineral filler concentration of 40% by volume. The resulting materials as well as neat bitumen were artificially aged by means of the PAV test for 24 and 48 hours with film thicknesses 3.15 and 1.00 mm. In addition, control (unaged) samples were prepared and tested for the calculation of ageing indices. The ageing indices were calculated based on three distinct molecular size areas (*Fig. 2.27*) after and prior to ageing.



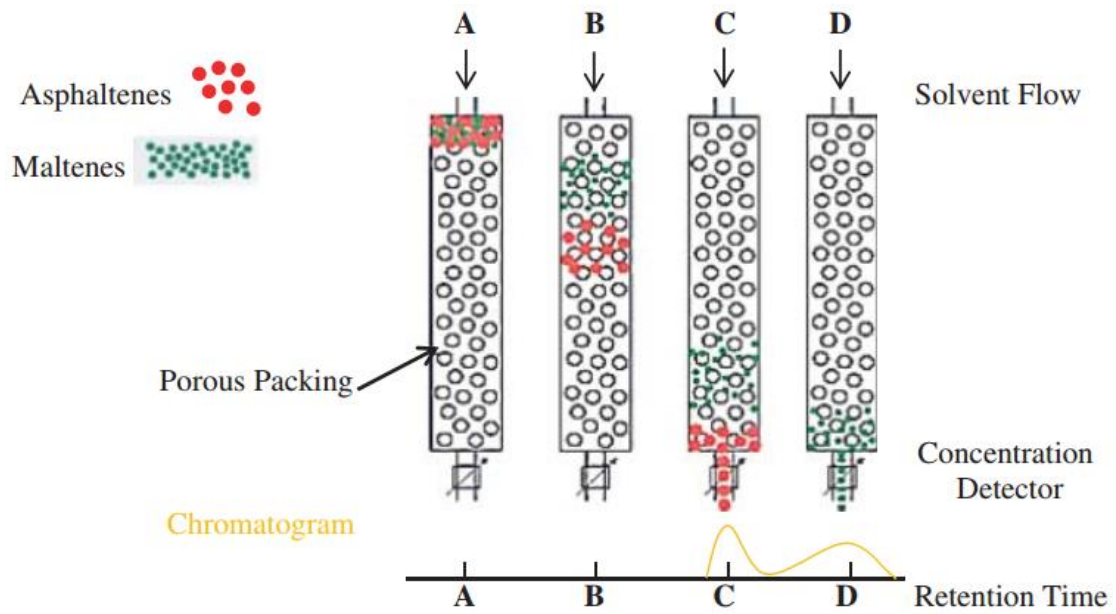
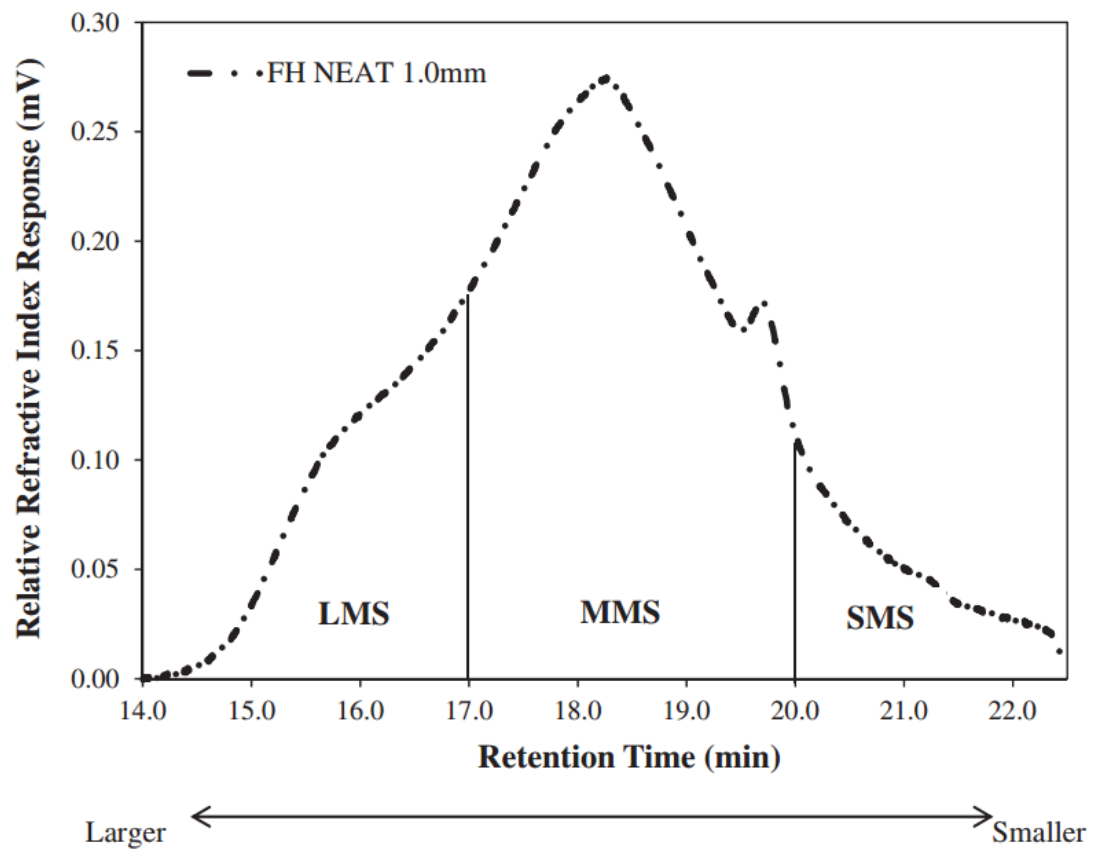


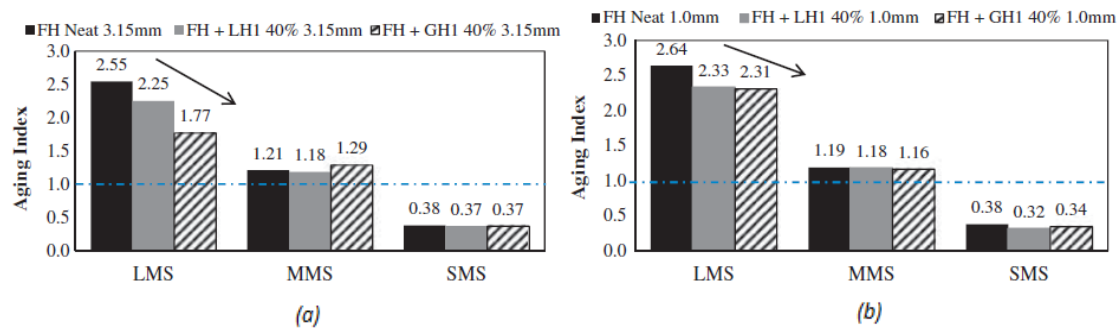
Figure 2.26: Schematic representation of the GPC test (Moraes & Bahia 2015b).



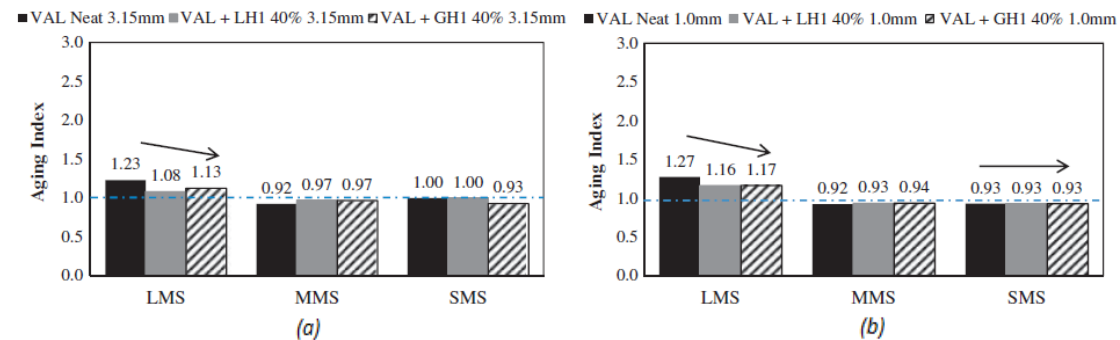
LMS = large molecular size; MMS = medium molecular size; SMS = small molecular size

Figure 2.27: Example of GPC chromatogram with three elution time fractions (Moraes & Bahia 2015b).

For the 48 hours-aged materials, the results indicated, first and foremost, that the addition of mineral filler in the bitumen phase affects its response to ageing and its resulting molecular distribution and, secondly, the ability of the mineral fillers to mitigate the increase of LMS molecules in the mastics' binders compared to the neat bitumen, upon ageing (*Fig. 2.28 and 2.29*). This holds true for every type of mineral filler used and every considered film thickness. More specifically, granite performed better than limestone by demonstrating the lowest ageing index. The latter was attributed to the highest specific surface area of granite, which led to a more intense surface adsorption of large molecular size polar components from bitumen on the mineral matter's particles. The information obtained by the GPC analysis are in good agreement with the results obtained by the rheological analysis presented in the research by Moraes & Bahia (2015a).



**Figure 2.28:** Molecular size areas ageing indices for neat bitumen Flint Hills PG 64-22 and mastics. 48 hours-aged materials. (a) 3.15 mm film thickness. (b) 1.00 mm film thickness (Moraes & Bahia 2015b).



**Figure 2.29:** Molecular size areas ageing indices for neat bitumen Valero PG 64-16 and mastics. 48 hours-aged materials. (a) 3.15 mm film thickness. (b) 1.00 mm film thickness (Moraes & Bahia 2015b).

Regarding the 24 hours-aged materials, the results (i.e. ageing indices) (*Fig. 2.30*) showed a similar trend to the ones obtained from the 48 hours-aged materials, that is, the addition of mineral filler (any type) decreased the rate of formation of LMS molecules. However, in this case, the MMS and SMS regions remained almost intact. For the Flint Hills PG 64-22 bitumen, granite appeared to perform better than limestone which is depicted through the lower LMS ageing index. On the other hand, when the Valero PG 64-16 bitumen is considered the behavior of the materials originating from the granite and limestone mastics was identical.

By comparing the results obtained from the two ageing times one may observe that, even though the generic trend is similar, the changes in molecular size distribution differ. This implies that longer ageing times are possibly necessary to obtain the full picture regarding the response of bitumen and mastics to oxidative ageing, on molecular level. For instance, the increase of LMS molecules in the case of Flint Hills PG 64-22 bitumen and mastics, aged for 48 hours in the PAV, is accompanied by a considerable

decrease of SMS molecules (Fig. 2.28). This feature is not observed, for the very same bitumen, when the materials are aged for 24 hours (Fig. 2.30a).

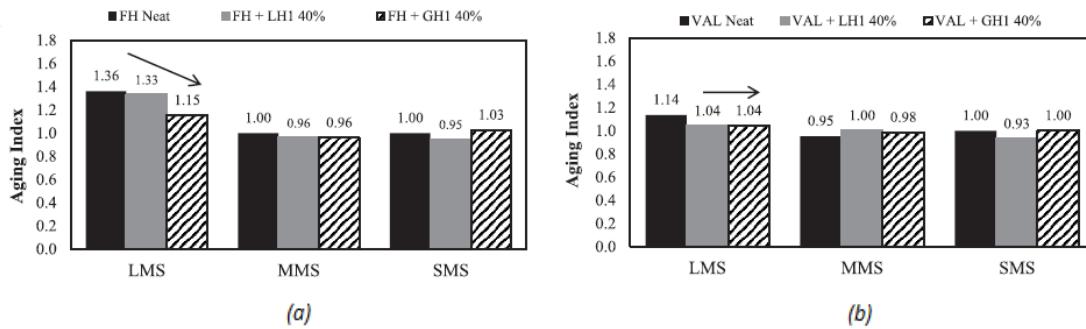


Figure 2.30: Molecular size areas ageing indices. 24 hours-aged materials. (a) Flint Hills PG 64-22. (b) Valero PG 64-16 and mastics (Moraes & Bahia 2015b).

In addition to the ageing indices calculated based on molecular size areas, ageing indices derived by quantitative data (molecular weights) of the GPC chromatogram were also reported. Hagos (2008) stated that oxidative ageing of bitumen leads to the formation of more polar molecules (high molecular weight molecules) at the expense of the lower weight molecules. Thus, it is meaningful to examine the effect of mineral fillers on ageing of bitumen from the aspect of molecular weights.

In Fig. 2.31, the ageing indices, as calculated by the numerical values of the molecular weights, are presented, for both considered bitumen and recovered binders from mastics, aged for 24 hours in the PAV. Almost in all cases, the ageing indices corresponding to mastics are lower than the base bitumen, implying the effectiveness of mineral fillers to decelerate the formation of highly polar molecules. As previously, also in this type of evaluation, granite appeared to be at least equally effective, and in some cases way more effective, to limestone. The more significant effect is observed for the  $M_z$  index (average molecular size), which roughly corresponds to the LMS. Having mentioned that, the previously presented results, that showed a decreased rate of production of LMS oxidation products in the bitumen phase, when mineral filler is present, are fully corroborated by the molecular weights analysis.

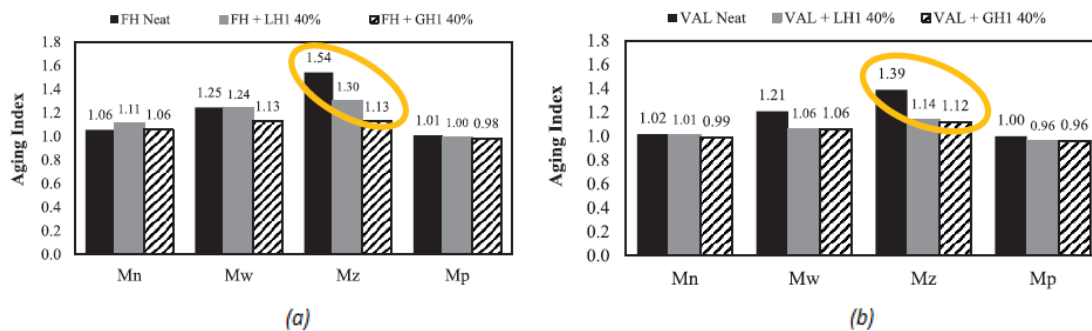


Figure 2.31: Molecular weights ageing indices. 24 hours-aged materials. (a) Flint Hills PG 64-22. (b) Valero PG 64-16 and mastics (Moraes & Bahia 2015b).

Overall, in this study, the researchers demonstrated that the GPC method constitutes a reliable and effective way to evaluate the molecular state of bitumen before and after oxidative ageing. Through this method, parameters sensitive to ageing (e.g. LMS molecules) can be determined and the effect of different mineral fillers on the rate of ageing of bitumen may be clearly illustrated, compared and evaluated.

Wu (2009) carried out an ageing study on mastics. The DSR and the FTIR tests were employed to evaluate the properties of the mastic as well as of the recovered bitumen at different ageing levels. Three types of mineral fillers were used in the research, limestone and ordinary Portland cement, which are basic fillers, and gritstone, which is an acidic one. A Penetration Grade 70/100 bitumen was utilized to produce the various mastics. All mastics were prepared with the same filler concentration, 40% by volume and were aged in the Thin Film Oven Test (TFOT) at 165°C for 5 hours. Neat bitumen 70/100 was also aged under identical conditions for comparison reasons.

G\* master-curves were constructed for the tested mastics, as well as for the neat bitumen, before and after ageing. The comparison of the various master-curves, both before and after ageing, did not reveal any obvious differences. Therefore, to assess the effect of the fillers on ageing in a quantitatively way, ageing indices were calculated based on the value of the complex shear modulus at 35°C and 0.4 Hz, for all mastics and the base bitumen, before and after ageing (*Fig. 2.32*). The results indicated that all mineral fillers were capable in decelerating the ageing process compared to pure bitumen by demonstrating lower values of the ageing index. Among the considered mineral matters, limestone appeared as the most effective, whereas the performance of the gritstone and Portland cement was almost identical. The author concluded that the basic limestone has a greater ability to adsorb and hold polar functional groups from bitumen on its surface compared to acidic mineral fillers, such as granite and gritstone. This observation is opposite to the conclusion drawn by Moraes & Bahia (2015a) and Moraes & Bahia (2015b) who showed that granite, being an acidic material, had a superior effect on reducing ageing compared to the basic limestone. In this very study the acidic mineral filler had, almost two times, higher specific surface area than the basic one. In the research of Wu (2009) no information is given regarding the specific surface area of the utilized mineral fillers. However, it is speculated that the considered materials (limestone and gritstone) had a less pronounced difference in their specific surface area values and, consequently, the results were dominated by the mineralogy (acidic or basic) of the mineral fillers.

Bitumen of the 5-hours-aged mastics were recovered and their rheology was evaluated by means of DSR. G\* master-curves were constructed and plotted together with the ones corresponding to neat bitumen before and after 5-hours-ageing (*Fig. 2.33*). A comparative analysis of the master-curves revealed that most of the recovered bitumen were softer than the pure aged bitumen and even softer than the “fresh” neat bitumen. The latter was the case for the bitumen recovered from the limestone mastic. These findings further corroborated the statements of previous researchers that the presence of mineral filler may delay the age-stiffening of the bitumen by adsorbing the polar functional groups on its surface (Curtis et al. 1993) and that upon extraction and recovery of bitumen a substantial portion of these adsorbed components cannot be recovered (Petersen et al. 1974).

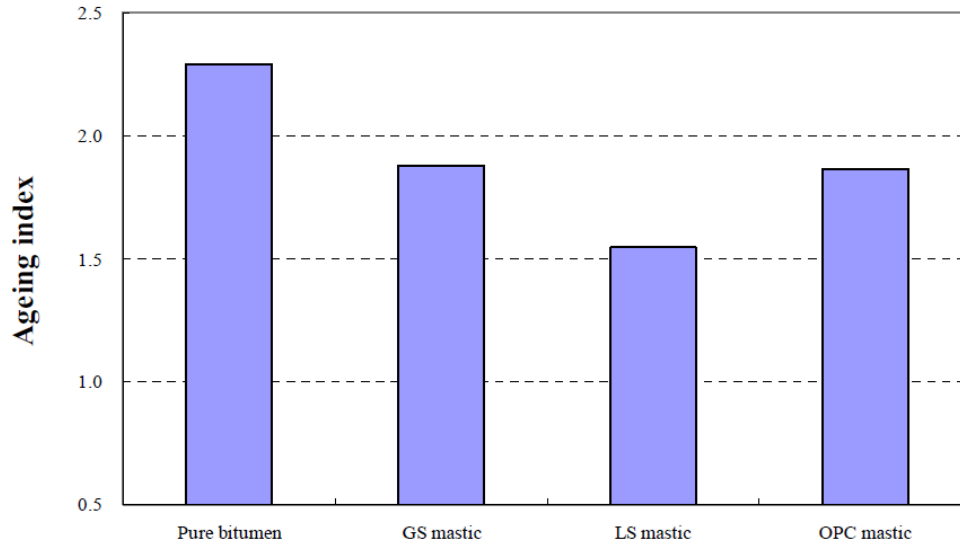


**Figure 2.32:** Ageing indices of neat bitumen, gritstone, limestone and ordinary Portland cement mastics (Wu 2009).

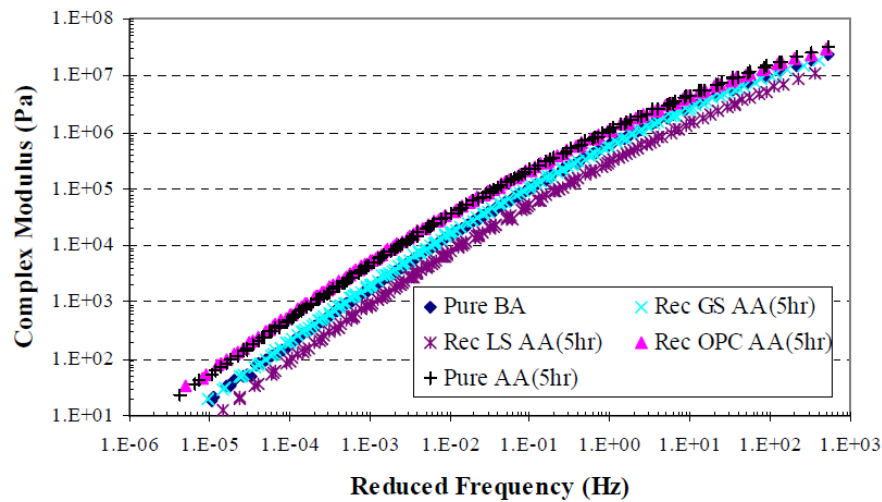


**Figure 2.33:** Complex shear modulus master-curves of Reference “fresh” and aged bitumen and recovered bitumen from 5-hours-aged mastics (Wu 2009).

The research was further extended by investigating the behavior of mastics containing the basic limestone and the acidic gritstone at different ageing times, namely 1, 3, 5, 10 and 20 hours. This extension was regarded as crucial for the deeper understanding of the influence of the mineral fillers on ageing of bitumen, since their adsorbing and/or catalytic ability changes as the ageing simulation goes on.  $G^*$  master-curves were constructed to evaluate the influence of the gritstone and limestone on ageing at different ageing times. Unlike the limestone mastic, the master-curves of the gritstone mastic, corresponding to the various ageing times, showed the expecting trend, that is, the complex shear modulus increased throughout the whole frequency range as the ageing time increased (Fig. 2.34). With respect to the former, however, an initial reduction of the complex shear modulus for ageing times of 1 and 3 hours was observed compared to the unaged mastic, or, in other words, the aged mastic (1 hour and 3 hours) appeared to be softer than the unaged mastic (Fig. 2.35). This phenomenon was attributed to the adsorption of polar functional groups from bitumen to the surface of the limestone particles.

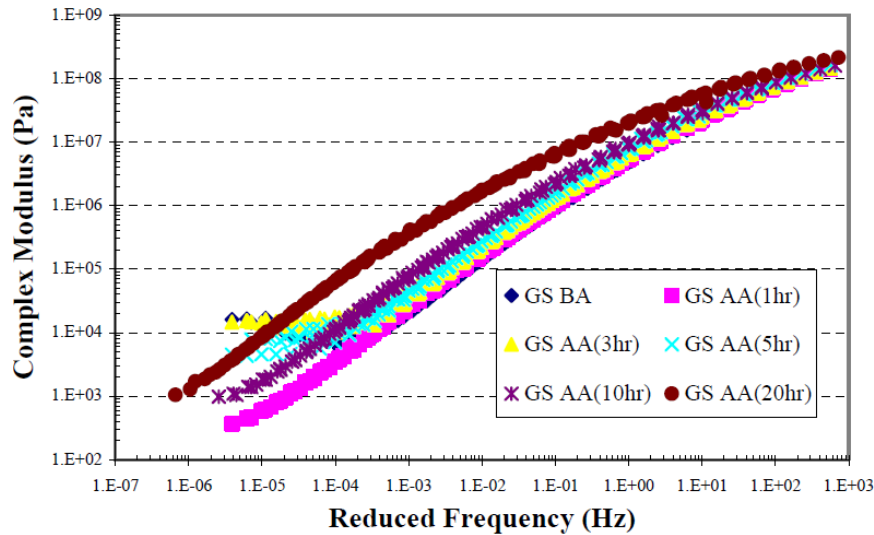


Figure 2.34: Complex shear modulus master-curves of gritstone mastics at various ageing times (Wu 2009).

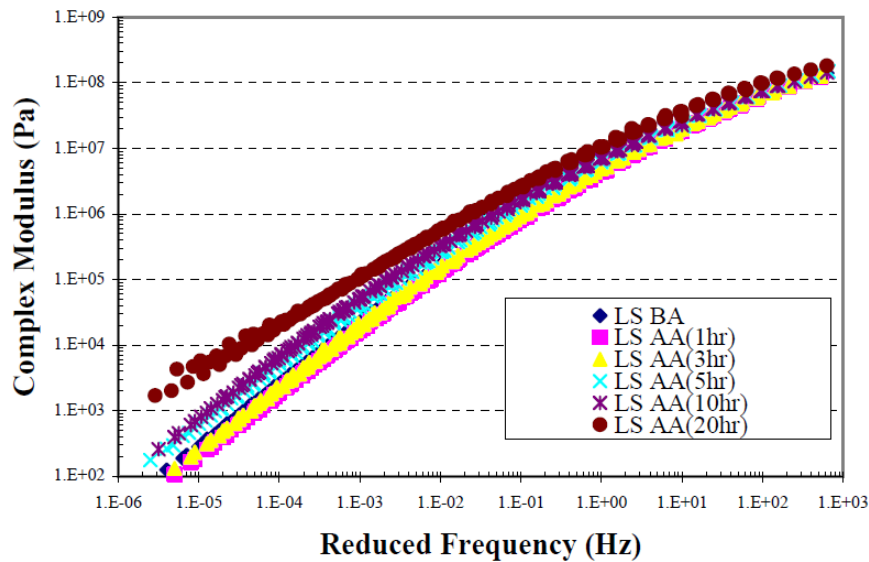
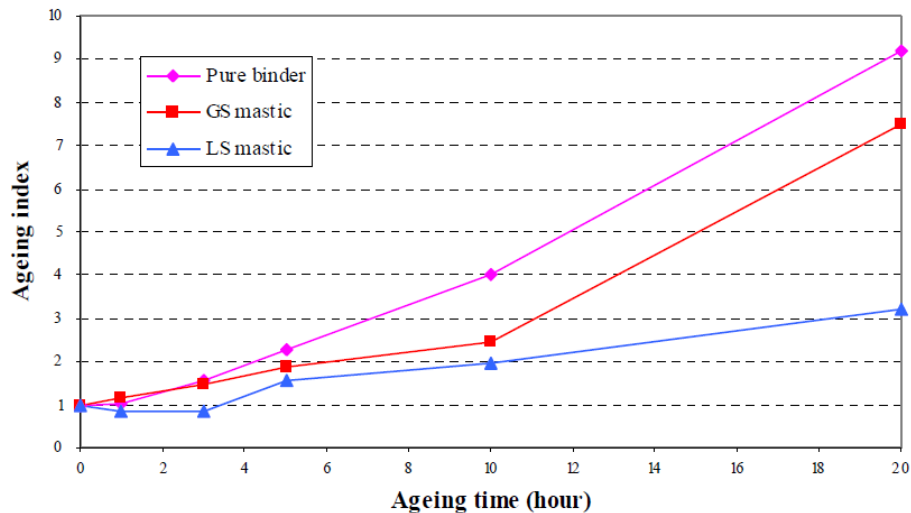


Figure 2.35: Complex shear modulus master-curves of limestone mastics at various ageing times (Wu 2009).

A comparative evaluation was also performed between the gritstone and limestone mastics and the neat bitumen by means of the ageing indices, for the various ageing times (Fig. 2.36). The limestone mastic showed lower ageing indices, than the other two tested materials, throughout the whole ageing simulation, which revealed the superior ability of the limestone mineral filler to adsorb polar functional groups from bitumen. The gritstone mastic demonstrated also lower ageing indices than the neat bitumen except for one case, that is, ageing time of 1 hour, at which the pure bitumen showed a slightly lower value. It was believed that this was due to the acidic nature of the gritstone particles which may have catalysed the bitumen oxidation at the initiation of the ageing simulation.



**Figure 2.36:** Ageing indices of neat bitumen, gritstone and limestone mastics at various ageing times (Wu 2009).

Furthermore, bitumen of the mastics with limestone and gritstone, at the different ageing levels, were recovered and evaluated by utilizing the DSR. Ageing indices were calculated based on the values of the complex shear modulus (*Fig. 2.37*). Interestingly, in most of the cases (ageing times) the ageing indices of the bitumen recovered from the limestone mastic were higher than the respective ones for the bitumen from gritstone mastic, which indicates that the bitumen in the limestone mastics had undergone more severe age-hardening. This finding is totally opposite to the one observed when the ageing indices of the mastics were evaluated FTIR analyses, indeed, confirmed that more oxygenated products were formed in the bitumen recovered from the limestone mastic during the ageing simulation (*Fig. 2.38*), which explains the higher stiffness, and by extension the higher ageing indices, with respect to the bitumen recovered from the gritstone mastic. In an effort to correlate the results observed at mastic and bitumen level, the researcher claimed that, even though there were evidently more oxygenated products in the bitumen recovered from the limestone mastic, a substantial portion of them did not contribute to the hardening of the mastic by virtue of the relatively greater ability of the limestone mineral filler to adsorb and hold these components on its surface.

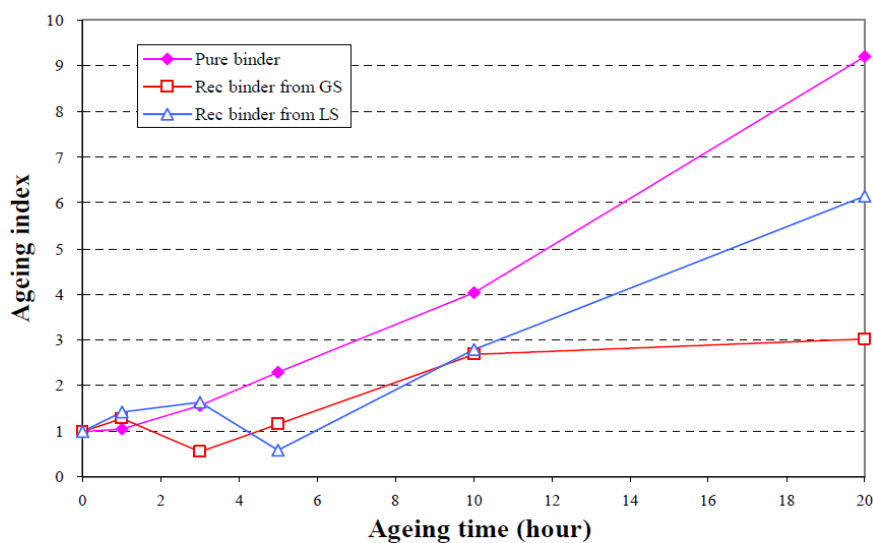


**Figure 2.37:** Ageing indices of neat bitumen and recovered bitumen from gritstone and limestone mastics at various ageing times (Wu 2009).

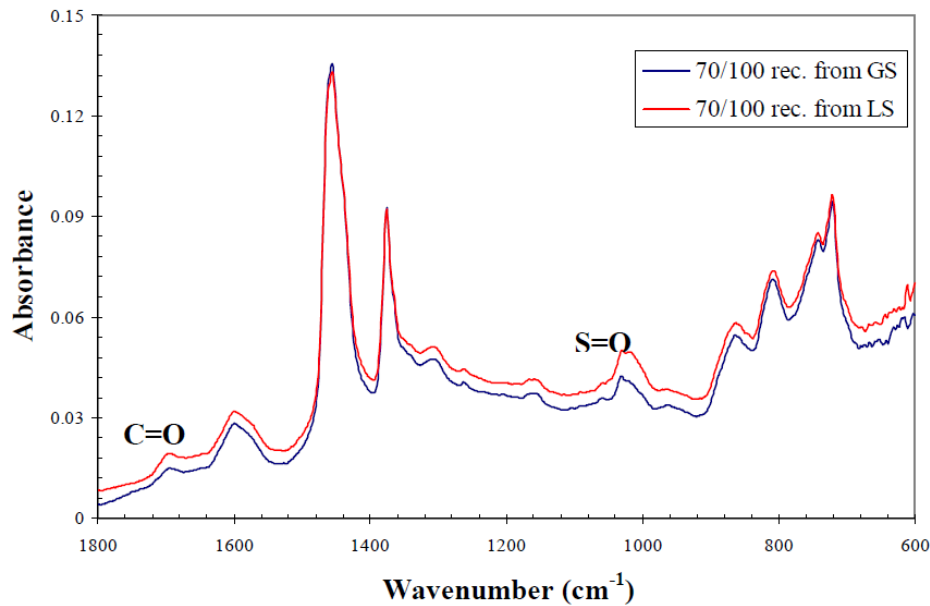


**Figure 2.38:** FTIR analyses on bitumen recovered from the 3-hour aged gritstone and limestone mastics (Wu 2009).

#### 2.4.2.1 Effect of hydrated lime on ageing of bitumen

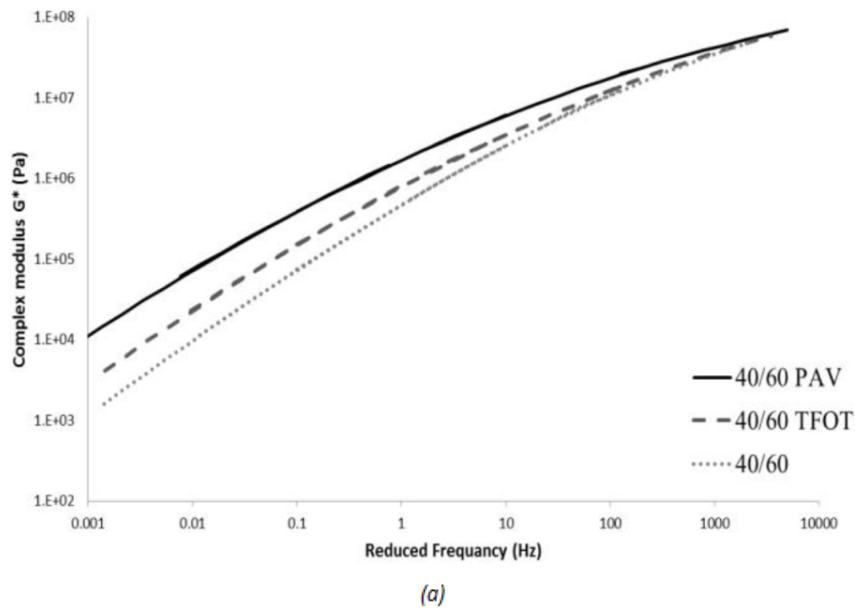
Numerous of laboratory studies and field evaluations have demonstrated the ability of hydrated lime to reduce the ageing susceptibility of bitumen, amongst other special features it provides to asphalt mixtures (Lesueur et al. 2012). An important aspect was underlined by Gundla et al. (2015) when ageing studies on mastic level utilizing hydrated lime, or any other additive, are performed. The researchers stated that even though the benefits of hydrated lime on bitumen ageing are evidently demonstrated, these findings do not necessarily reflect the real effect of the additive on asphalt mixture level. This is because, in several studies, high concentrations of hydrated lime are utilized, in the absence of a base mineral filler, whereas in an asphalt mixture hydrated lime is only a partial replacement of another mineral matter. Thus, it is of immense importance for the reliability and soundness of the experimental results and the direct correlation to practical applications, that the multiple scales (e.g. mastic scale) are represented as they will exist in the final asphalt mixture.

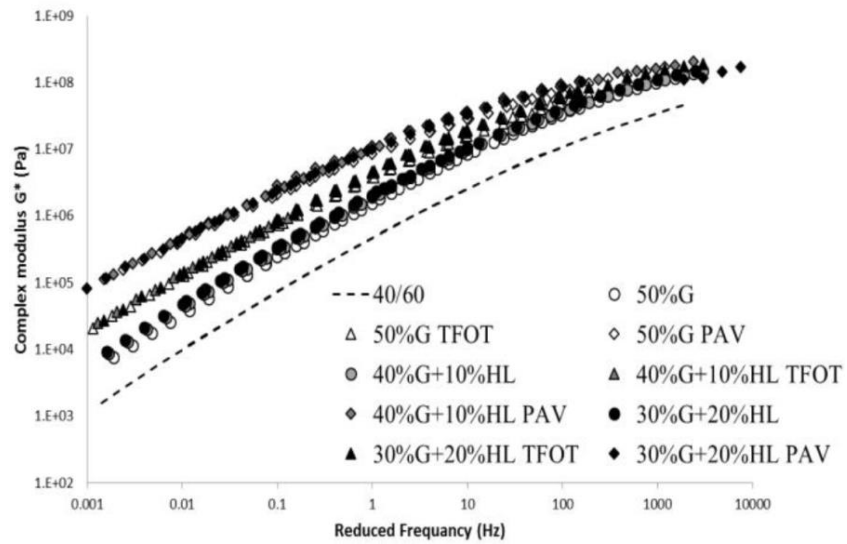
Plancher & Petersen (1976) attempted to explain the mechanism through which hydrated lime has an effect on oxidative ageing. According to the authors, highly polar functional groups of bitumen are adsorbed on the surface of the lime. This adsorption mechanism has at least two effects on the ageing process. For one, the removal of oxidation promoters leads to a decrease of the formation of oxidation products. For another, the adsorption and immobilization of highly polar functional groups on the lime surface prevents them from interacting with oxygenated products leading to a reduced viscosity build-up rate.

Alfaqawi et al. (2017) performed an ageing study on mastic level to examine the effect of different mineral fillers on the ageing process. A Penetration Grade 40/60 bitumen and three types of mineral fillers, namely granite, limestone and hydrated lime, were included in the study. The mastics were prepared with a filler concentration of 50% by mass. Hydrated lime was added as a partial replacement of the granite and limestone at concentrations of 10% and 20% by mass. Prior to testing, all materials were artificially aged by utilizing the TFOT and subsequently the PAV test.

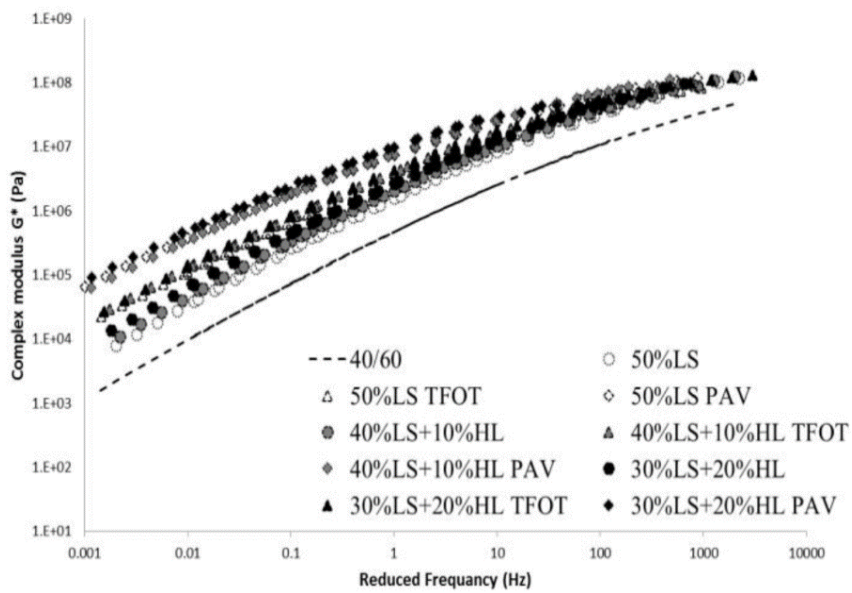


Rheological evaluation of the resulting materials and base bitumen, by means of DSR, led to the same conclusion drawn by Moraes & Bahia (2015a), that is,  $G^*$  master-curves of mastics only shifted towards higher complex shear modulus and frequency values (Fig. 2.39b and c), with respect to the master-curve of the unaged bitumen, without showing any decrease in the material's time dependency, as in the case of the neat aged bitumen (Fig. 2.39a). Moreover, master-curves of the phase angle ( $\delta$ ) were constructed and analysed (Fig. 2.40). As it was expected, the addition of mineral filler (any type at any concentration) led to the decrease of the phase angle, highlighting the more elastic response of mastics compared to neat bitumen. In addition, hydrated lime-treated mastics showed higher values of phase angle compared to mastics with pure granite or limestone after ageing. The latter is an indication of the relatively superior ability of the hydrated lime-treated mastics to dissipate shear stresses in the aged state, leading to an overall reduced susceptibility of the aged asphalt pavement in cracking-related failure modes. The influence of hydrated lime on the phase angle was more pronounced in the case of granite mastics rather in limestone mastics. The favourable effect of hydrated lime on the phase angle was also observed by Petersen et al. (1987). Hydrated lime-treated bitumen demonstrated higher values for the phase angle compared to untreated control bitumen after ageing, indicating an increased stress relaxation ability.





(b)



(c)

**Figure 2.39:** Complex shear modulus master-curves. (a) “Fresh” and aged bitumen. (b) “Fresh” and aged granite mastics. (c) “Fresh” and aged limestone mastics (Alfaqawi et al. 2017).

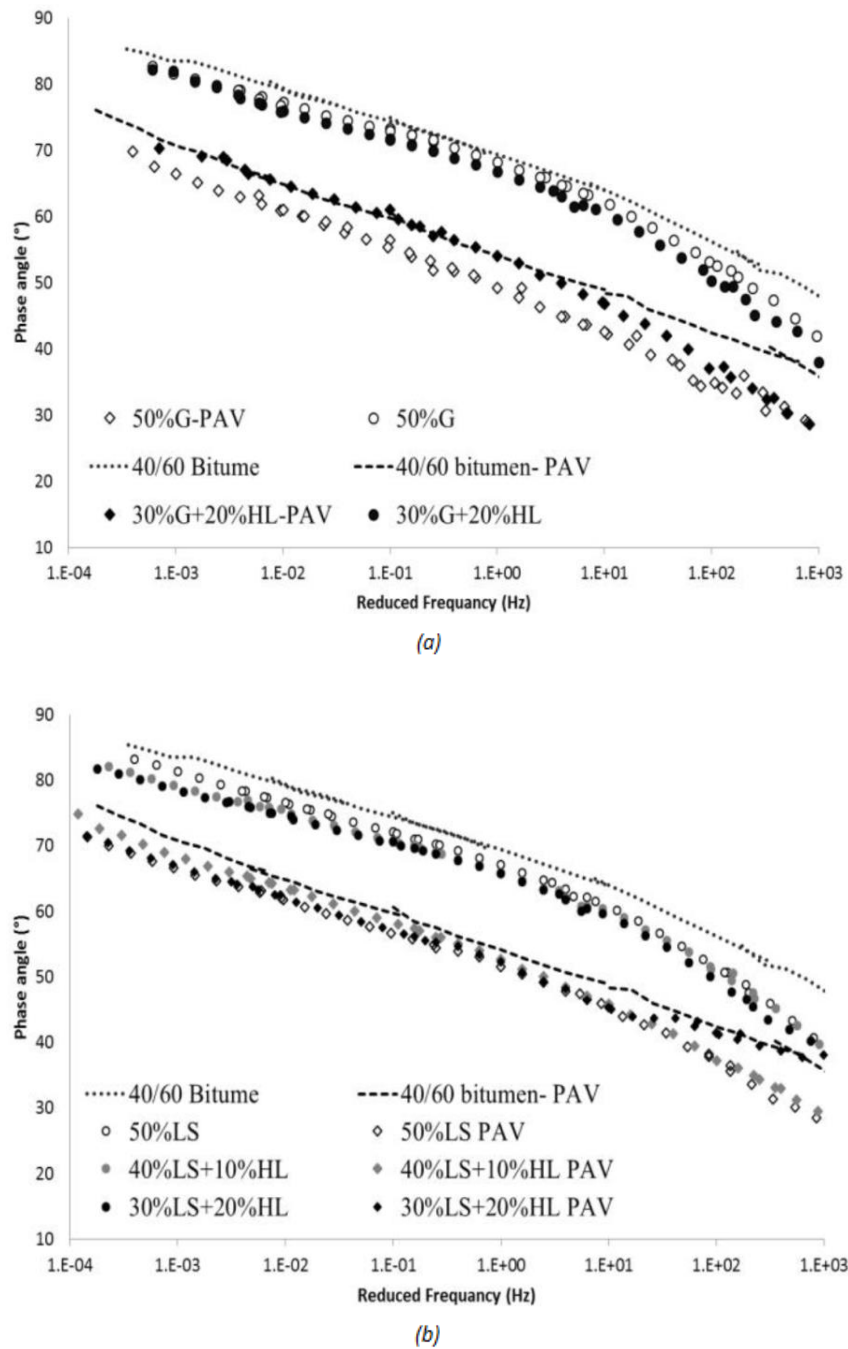


**Figure 2.40:** Phase angle master-curves. (a) “Fresh” and aged neat bitumen and granite mastics. (b) “Fresh” and aged neat bitumen and limestone mastics (Alfaqawi et al. 2017).

The prepared mastics were evaluated by means of ageing indices calculated through the complex shear modulus values at specific temperature and frequency before and after ageing (*Fig. 2.41*). The results demonstrated that mastics containing limestone were less aged than mastics with granite. When hydrated lime was added to either of the two base fillers, the ageing indices reduced even more which confirms the statement of Lesueur et al. (2012) regarding the effectiveness of hydrated lime in decelerating the ageing process. The combination of limestone and hydrated lime was the most beneficial in terms of reducing the rate of bitumen ageing.

The effectiveness of hydrated lime was also verified on bitumen level. Recovered bitumen from mastics with granite and granite with partial replacement of hydrated lime were chemically evaluated by utilizing the FTIR test. The results indicated that less oxygenated products were formed in the bitumen recovered from the hydrated lime-treated mastic (Fig. 2.42). These results were in good agreement with the rheological evaluation. Overall, the researchers concluded that, in the presence of hydrated lime, physico-chemical interactions take place between the mineral matter and the bitumen which are not present with pure limestone or granite fillers. These interactions lead to a less severe ageing process.

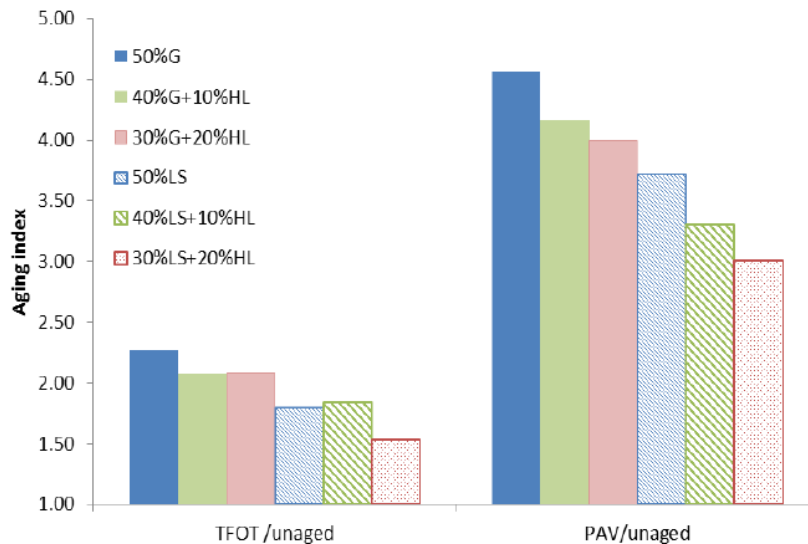


Figure 2.41: Ageing indices of granite and limestone mastics (Alfaqawi et al. 2017).

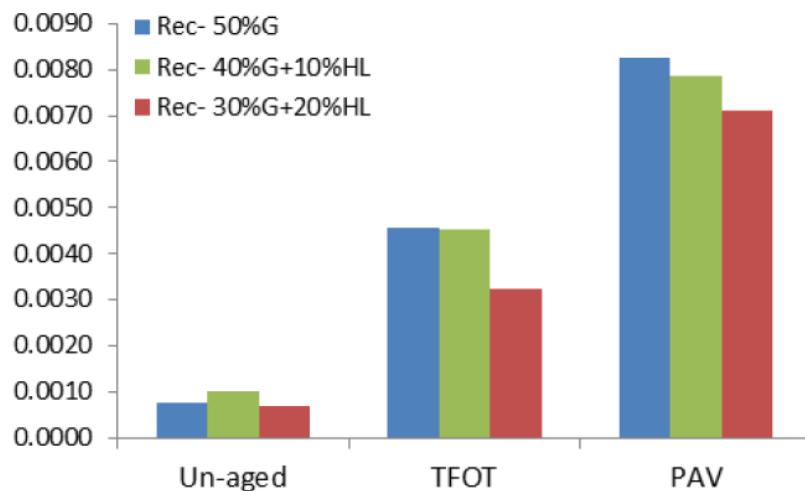


Figure 2.42: Carbonyl index of recovered bitumen from granite mastics (Alfaqawi et al., 2017).

The results presented by Alfaqawi et al. (2017) are in line, to an extent, with previous research on hydrated lime carried out by Little & Petersen (2005). In their study, hydrated lime was compared to a similar size limestone mineral filler. Through an extensive research on mastic and asphalt mixture level, the researchers concluded that the effect of hydrated lime is at least equal to other mineral fillers and in some cases considerably greater. The latter is a function of the physico-chemical interactions that occur between the bitumen and the hydrated lime which, in extension, are highly affected by the type of bitumen used.

Gundla et al. (2015) investigated the mitigating potential of hydrated lime and Portland cement on bitumen ageing. A multi-scale experimental approach was utilized according to which the materials were evaluated on mastic as well as on asphalt mixture level. The purpose of the latter was to determine whether the performance of the materials, as evaluated on mastic level, is also captured when the whole asphalt mixture is investigated.

A control mastic was prepared with ordinary mineral filler and it was subsequently modified with hydrated lime or Portland cement at equal mass contents. The resulting materials as well as neat bitumen were aged by utilizing the PAV test following the standard protocol. The rheological parameter  $G^*$  was then determined through DSR testing for all materials before and after ageing. The test was performed at a frequency of 10 rad/s and temperatures 10, 20, 30, 58, 64 and 70°C. The anti-ageing effect of the mineral matters was evaluated by means of ageing indices calculated through values of the complex shear modulus at fixed temperatures and frequency equal to 10 rad/s, before and after ageing (Fig. 2.43).

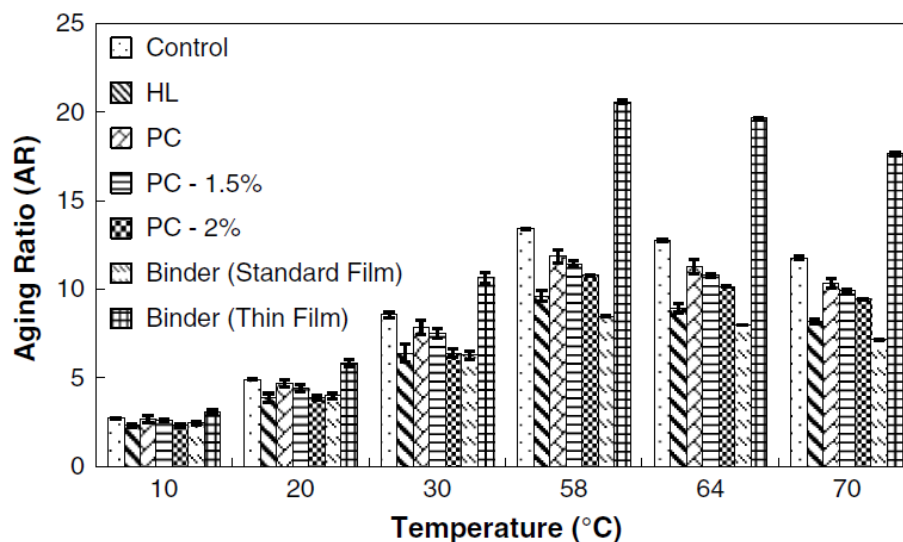
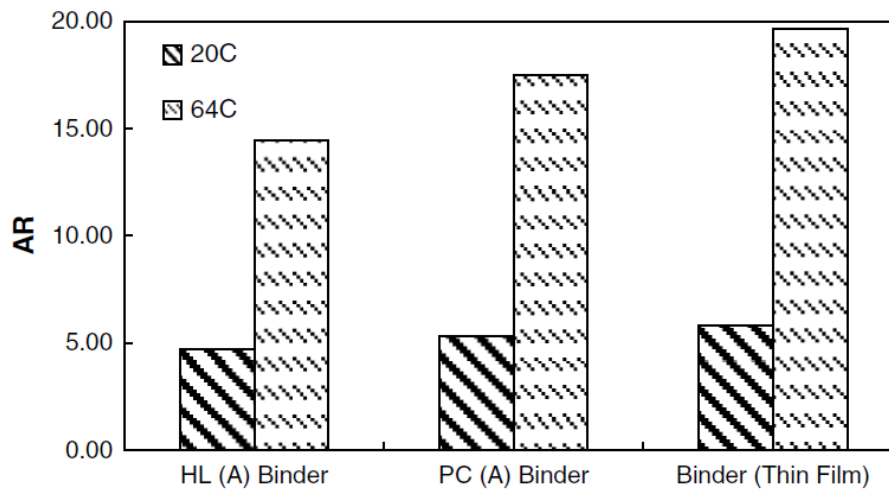


Figure 2.43: Ageing indices for neat bitumen and mastics at 10 rad/s (Gundla et al. 2015).

The results indicated the greater capability of hydrated lime over Portland cement to reduce ageing of bitumen. Nevertheless, both modified mastics demonstrated lower ageing indices compared to control mastic. In addition, the research revealed the importance of the binder film thickness during the ageing simulation when neat bitumen and mastics are to be compared. One interesting observation, that underlines the significance of the filler's specific surface area, is that when Portland cement was dosed at a double rate (2%) compared to hydrated lime the value of the surface area of the two materials was similar and the ageing mitigation potential of Portland cement was almost the same with the one of hydrated lime. However, this was the case only at lower testing temperatures, whereas at higher testing temperatures hydrated lime clearly prevailed. The researchers attributed this phenomenon to the gradual temperature sensitivity of active mineral fillers and/or the increased bitumen mobility which lead to a more pronounced effect at higher temperatures.

Bitumen was extracted and recovered by the modified mastics, with equal mineral filler concentration, and were subjected to DSR testing under the conditions described above. The ageing indices of the recovered bitumen as well as of the neat bitumen were

calculated based on complex shear modulus values at certain frequency (10 rad/s) and temperatures (20 and 64°C), before and after ageing (*Fig. 2.44*). Both bitumen recovered from the modified mastics appeared to be less aged than the neat bitumen, with the one coming from the hydrated lime-modified mastic demonstrating the lowest ageing index.



**Figure 2.44:** Ageing indices for neat bitumen and recovered bitumen from hydrated lime and Portland cement mastics (Gundla et al. 2015).

The research was further extended by producing and testing asphalt mixtures that contained ordinary mineral filler and ordinary mineral filler partially replaced with hydrated lime or Portland cement. The asphalt mixtures were aged in a forced draft oven at 85°C for 8 days, which constitutes a modified version of the standard long-term ageing protocol specified in AASHTO R30. The Dynamic Modulus and Uniaxial Fatigue tests were employed to evaluate the performance of the different asphalt mixtures. Ageing indices were calculated based on dynamic modulus ( $E^*$ ) values at a frequency of 10 Hz and temperatures of 4, 20 and 46°C (*Fig. 2.45*).

The results indicated the superior mitigating potential of hydrated lime on ageing compared to neat ordinary mineral filler and Portland cement, which is in good agreement with the results obtained on mastic level. The asphalt mixture containing Portland cement demonstrated the highest ageing index, however, due to the great variability observed with the Portland cement samples, the researchers could not derive a safe conclusion. The results from the fatigue evaluation (*Fig. 2.46*) highlighted the effectiveness of hydrated lime, ageing-wise, which showed longer fatigue life after ageing, implying lower stiffness, and by extension, lower susceptibility to oxidative hardening.

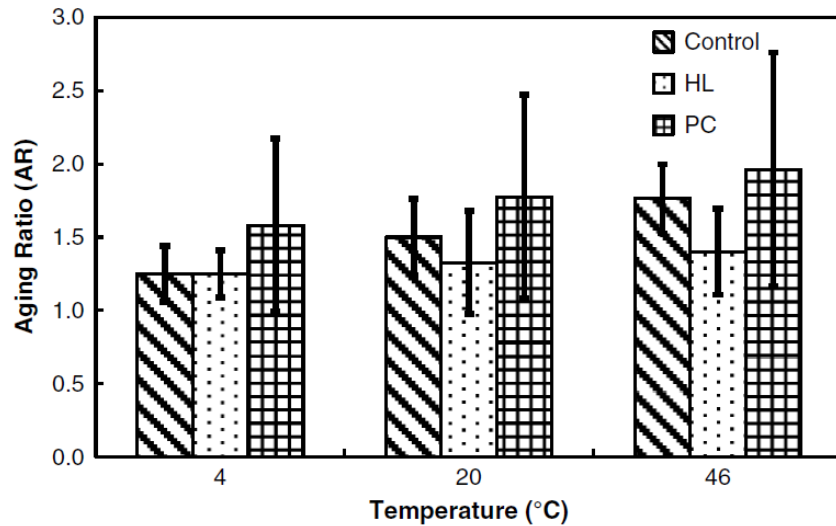


Figure 2.45: Ageing indices for control, hydrated lime and Portland cement mixtures (Gundla et al. 2015).

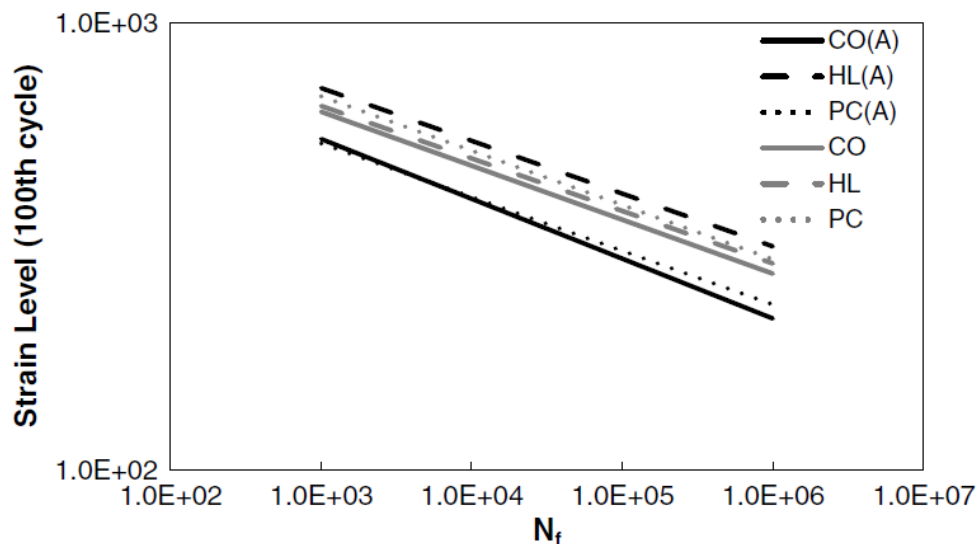


Figure 2.46: Predicted fatigue life for “fresh” and aged mixtures (Gundla et al. 2015).

## 2.5 Conclusions on literature review

- Oxidation is the major mechanism that leads to irreversible ageing of bitumen. Its effect on the material’s chemical composition, and by extension, on its physical properties is of paramount importance in bitumen/bituminous mixtures ageing studies.
- Different bitumen may present different response upon ageing, depending on their initial chemical composition and the resulting arrangement of their molecular structure. The degree of age-hardening of a certain bitumen is controlled by other factors as well (e.g. dispersing capacity of the non-polar fraction, polarity formed in bitumen etc.), rather than the amount of the developed oxygenated products alone. As a result, in a fundamental study, where the effect of a certain material and/or condition on ageing of bitumen is investigated, the utilization of various bitumen from different sources may lead to difficulties in interpreting correctly the obtained results.

- Amongst the reviewed accelerated laboratory ageing techniques, the PAV seems to be the most appropriate method when it comes to ageing of bituminous blends (e.g. mastics). Regarding other methods (i.e. TFOT and RTFOT) there seem to be several problems associated with ageing of mastics that could lead to biased results. The latter is especially crucial when the ageing study involves a comparative analysis between neat bitumen and mastics.
- The ageing level of a bituminous binder is possible to be assessed through the evaluation of its physical properties by means of DSR and/or the penetration and ring & ball tests, before and after ageing, and the derivation of ageing indices. On compositional level, the chemical changes of the material upon ageing can be investigated through techniques such as the FTIR and GPC.
- Bitumen-aggregates adhesion studies have provided a solid background on the interaction of the two materials that can be further utilized for the interpretation of the results when the effect of mineral aggregates on ageing of bitumen is considered.
- Several studies, investigating the effect of mineral fillers on the ageing of bitumen, are reported in literature. Among these studies, the vast minority claims a catalyzing effect of the mineral matter. Most of them are aligned by demonstrating a mitigating effect of the mineral matter on the ageing process of bitumen. Nevertheless, among the latter studies, contradicting results exist with respect to the effectiveness of different mineral fillers, that present different physico-chemical properties, in decelerating the bitumen ageing process. The latter highlights that deep understanding of the role of the mineral filler, and the effect of its various properties, in the ageing process is yet to be achieved, dictating the necessity for further fundamental research.
- It is commonly recognized that the compositional (i.e. mineralogical/elemental composition) and physical (e.g. specific surface area, gradation) properties of the mineral fillers as well as the design parameters of the mastics (filler to bitumen ratio) are the major factors affecting ageing of bitumen. The occurring physico-chemical interactions between the two materials have been in the center of focus of the reported studies, whereas the effect of the physical presence of mineral fillers in the diffusion medium and the effect it may have on the oxygen diffusion path has received limited attention, as it is regarded negligible compared to the former.
- A common line between relevant studies is that the utilization of hydrated lime, either as base filler or as partial replacement of another one, enhances the mitigating action of the mineral matter on the ageing of bitumen. In the case, however, that hydrated lime is mixed with another base filler, its effectiveness still varies and is a function of its concentration and the type of the base mineral filler.



### 2.6 Research objectives

The overall objective of the present thesis is to establish a solid theoretical background and provide the necessary fundamental experimental work that will assist in gaining (further) insight regarding the effect of mineral fillers on ageing of bituminous mixtures. By extension, the findings of the current research can be utilized as benchmark for more advanced and specialized future studies regarding this very topic and/or studies where coupled phenomena, such as ageing and moisture, are to be investigated on mineral filler-bitumen systems. The particular objectives of the present research are to:

- Determine whether the mineral fillers are active participants in the ageing process of bituminous mixtures and, if they do so, what is their effect (i.e. catalysing or mitigating).
- Examine whether the mineral matters' possible effect on ageing of bituminous mixtures is triggered by physico-chemical interactions and/or by their physical presence in the mastics.
- Identify the mineral fillers' properties that govern their potential effect on the ageing of bituminous mixtures.
- Establish the mechanisms through which the mineral fillers' effect on ageing of bituminous mixtures occurs.

## 2.7 Research methodology

The research objectives of the present thesis are attempted to be achieved through a comparative study between various materials. The experimental plan can be distinguished in three main parts: a) Mineral fillers' characterization, b) investigation on mastic level and c) investigation on bitumen level. The comparative analysis lies in the evaluation of the raw/resulting materials within the individual parts and the derivation of conclusions. The performed comparative analysis assists in the subsequent drawing of particular (within the phases) correlations and global correlations between the three main parts, leading to the derivation of the overall conclusions. Fig. 2.47 schematically illustrates the adopted research methodology.

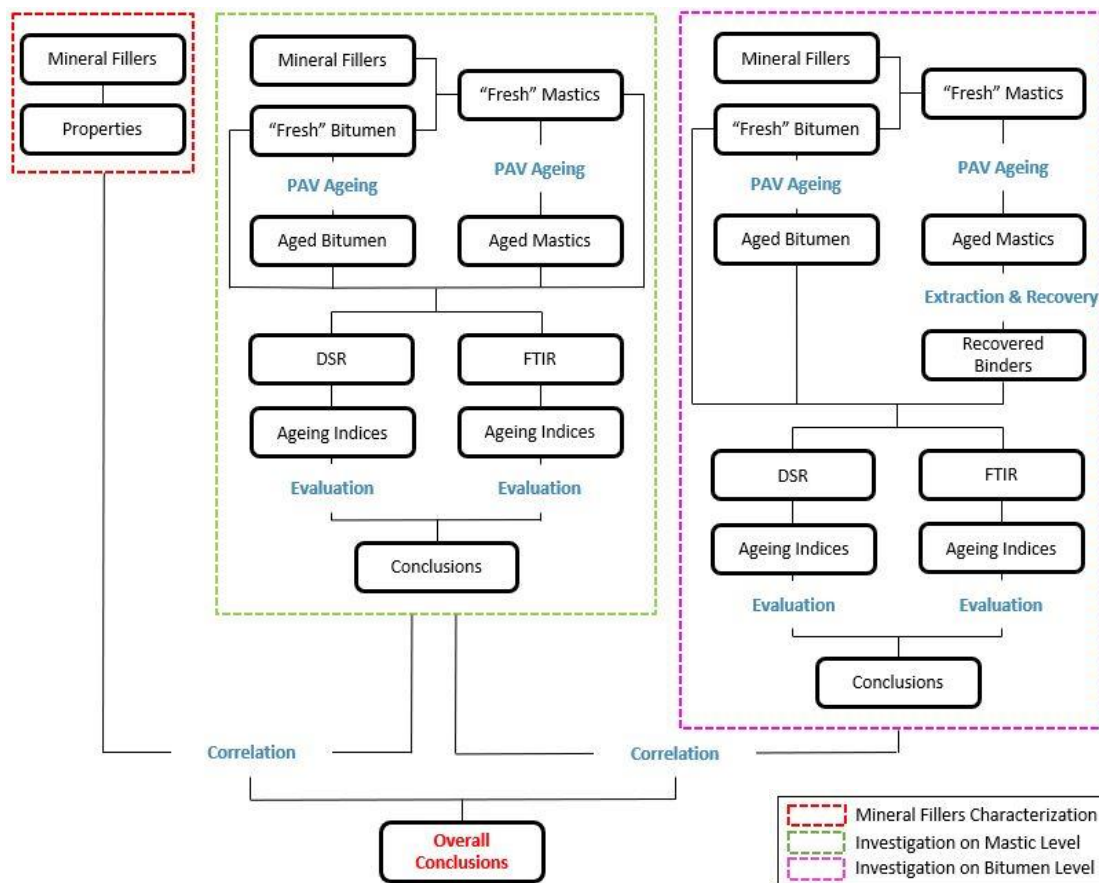


Figure 2.47: Research approach flow diagram.

# 3

## Materials and methods

### 3.1 Bitumen

An unmodified penetration grade bitumen, available in the laboratory of the Pavement Engineering of TU Delft, was used in the experimental study of the present thesis. The bitumen was initially characterized based on its conventional properties i.e. penetration grade and softening point. The density of the bitumen was assumed to be equal to 1.03 gr/cm<sup>3</sup>.

#### 3.1.1 Penetration grade

The needle penetration test was performed in accordance with NEN-EN 1426 to classify the utilized bitumen based on the Penetration Grade scale. The operating parameters of the test were: temperature 25°C, applied load 100 grams and loading duration 5 seconds.

More specifically, 100 grams of heated bitumen were poured in a metal can and the sample was left to cool down at ambient temperature for 2 hours. Then the sample was placed in a water bath at 25°C for another 2 hours to reach the necessary temperature for the performance of the test. During the test, the sample was immersed in a water bath to maintain the testing temperature at the specified value (25°C) throughout the whole duration of the measurements. Three measurements were performed, with separate needles, at different locations of the sample's surface. The difference between the lowest and highest measurement complied with the requirements dictated by the norm and all three measurements were accepted as they showed great repeatability. The results of the needle penetration test are presented in *Table 3.1*. Based on the results the utilized bitumen is classified as a 40/60 penetration grade bitumen.

**Table 3.1:** Needle penetration test results.

Measurement	Penetration @ 25°C (dmm)	Average Penetration (dmm)
1	50.0	
2	51.0	50.3
3	50.0	

#### 3.1.2 Softening point

The softening point of the utilized bitumen was determined by performing the Ring & Ball test in accordance with NEN-EN 1427.

Heated bitumen was poured in the rings (*Fig 3.1a*) and was left to cool down for approximately 30 minutes. Then the bitumen excess on the top of the ring was gently removed with a heated knife. The test was assembled and the bath was filled with distilled water (*Fig. 3.1b*) at an initial temperature approximately 5°C. The heater beneath the bath was controlled to provide temperature increments of 5°C/min. For each ring and ball, the indication in the thermometer is recorded as soon as the bitumen surrounding each ball touches the bottom plate (*Fig. 3.1c*), which is placed at a specified distance from the bottom level of the samples ( $25 \pm 0.4$  mm). Two sets of samples were tested in total, which yielded four different values for the softening point. All measurements showed great repeatability and complied with the allowable variation specified in the norm. The declared value for the softening point of the examined bitumen is the average of the four measurements. *Table 3.2* summarizes the results of the Ring & Ball test.

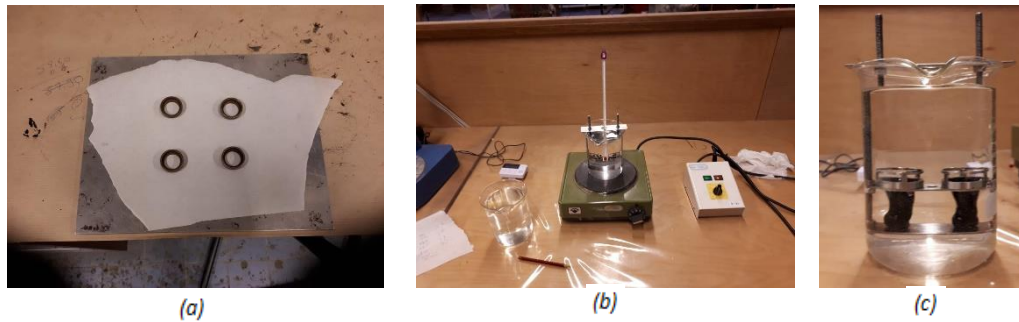


**Figure 3.1:** Ring & Ball test. (a) Rings. (b) Overall apparatus. (c) Bitumen after test completion.

**Table 3.2:** Ring & Ball test results.

Measurement	Softening point (°C)	Average softening point (°C)
1	48.0	48.4
2	48.2	
3	48.5	
4	48.8	

In *Table 3.3* the overall conventional properties of the utilized bitumen are summarized.

**Table 3.3:** 40/60 penetration grade bitumen conventional properties.

Penetration @ 25°C (dmm)	Softening point (°C)	Density (gr/cm <sup>3</sup> )
50.3	48.4	1.03

## 3.2 Mineral fillers

Six different mineral fillers were employed for the purpose of the present research including both commercial and non-commercial materials. A brief description of each material and its purpose of usage is provided in *Sub-Section 3.2.1*.

### 3.2.1 Types of mineral fillers considered in the study

#### *Wigro 60K*

Wigro 60K was provided by Sibelco-Winterswijk. This mineral filler is composed of limestone with the incorporation of 25wt% of hydrated lime (calcium hydroxide:  $\text{Ca}(\text{OH})_2$ ). Mineral fillers with hydrated lime are specified by the specifications and are typically used in the production of PA mixtures in the Netherlands. Wigro 60K was included in the study for two main reasons. For one, since it is the mineral filler used in practice in the Netherlands, the obtained results may assist in assessing the current practice with respect to ageing. For another, the effect of a basic aggregate in conjunction with hydrated lime on the ageing of bitumen can be evaluated.

#### *Wigro*

Wigro was provided by Sibelco-Winterswijk and is composed of limestone, or calcium carbonate ( $\text{CaCO}_3$ ). In essence, Wigro is the same material as Wigro 60K, in the absence of the hydrated lime. This mineral filler was included in the study to represent basic aggregates. In addition, the effect of hydrated lime on ageing of bituminous mixtures can be evaluated, when its performance is compared to that of Wigro 60K.

*Baghouse dust*

During the production of HMA, mineral aggregates enter the mixing drum, where they are dried, prior to mixing with bitumen. The drying process leads to the generation of fines which are removed and collected in a baghouse (Fig. 3.2), hence the name baghouse dust. The utilization of baghouse dust as mineral filler in the asphalt mixture production may lead to a (considerable) reduction of the production costs. In the guidelines for asphalt research (VBW Asphalt 1995) it is stated that in the production of asphalt mixtures it is allowed to dose 1.5% more baghouse dust in comparison with the type testing. This means that if no baghouse dust was used during type testing, a maximum of 1.5% baghouse dust may be added during the asphalt production, but if X% of baghouse dust was used in the type testing, it is allowed to dose X+1.5%. In addition, it is worth mentioning that since different types of mineral aggregates may be used in a single asphalt plant, it is quite possible that there is great variability in the minerals present in the collected dust.

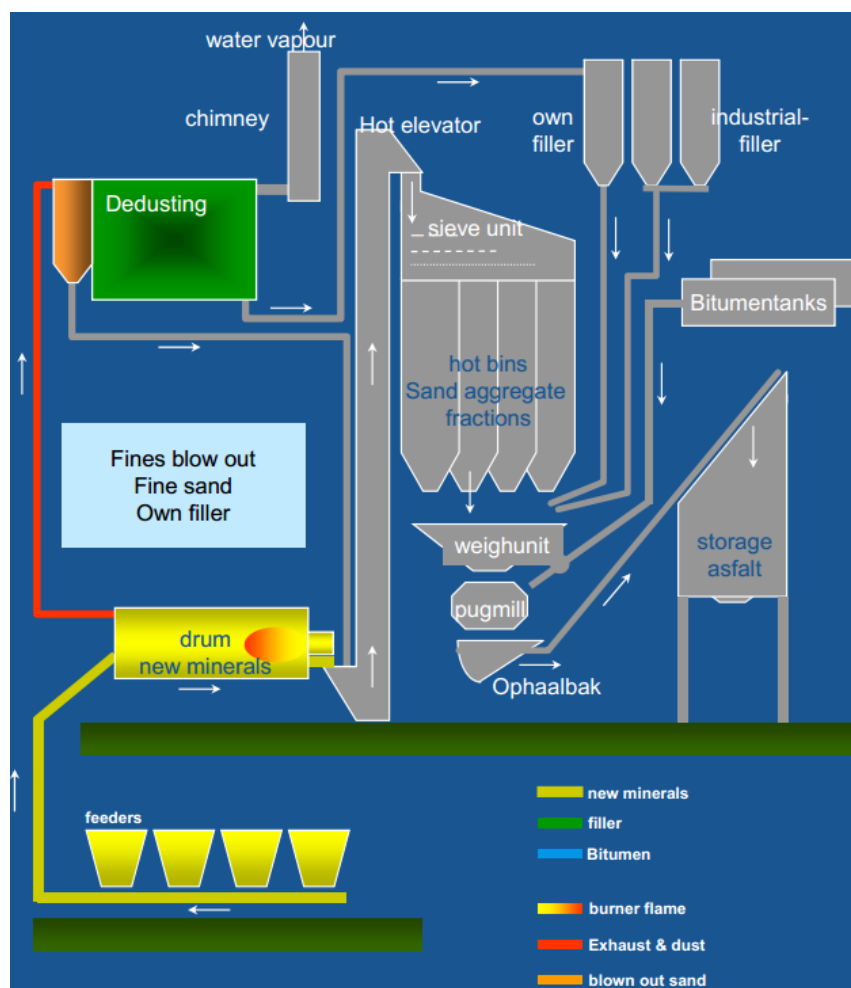


**Figure 3.2:** Schematic representation of batch type asphalt production unit including a dust collector.

Despite the fact that baghouse dust is derived from natural aggregates and its usage may be cost-effective, several concerns are raised for the quality and performance of the end product. For instance, Dukatz & Anderson (1980) reported that some baghouse fines led to a considerable stiffening of the asphalt mixtures resulting in low workability and embrittlement. Eick & Shook (1978) demonstrated that some baghouse fines increased the susceptibility of asphalt mixtures in moisture-induced damage. Currently

in the Netherlands, the susceptibility of PA pavements to moisture damage is addressed by incorporating in the standard PA mix design carbonate mineral fillers with the addition of hydrated lime (i.e. Wigro 60K) (Varveri 2017).

All above reasons establish baghouse dust as a very interesting candidate material for the present research, the inclusion of which provides the opportunity to evaluate the effect of the collected dust on the ageing of bituminous mixtures and how its performance, ageing-wise, ranks relatively to the specified mineral filler (Wigro 60K). The baghouse dust considered in this study was provided by an asphalt plant operating in the region of the Netherlands. According to the contractor the collected dust is most likely bestone (sandstone), since this is the main aggregate they use in their production site.

#### *Granite*

Granite was included in the study to represent acidic aggregates. The utilized material originates from a Scottish quarry. Coarse granite particles were received from the quarry which were milled in the laboratory of TU Delft to produce powder to be used as mineral filler.

#### *Silverbond M6 (Quartz)*

Silverbond M6 is a commercial filler provided by Sibelco-Dessel, which is exclusively comprised of quartz. Silverbond M6, hereafter designated simply as quartz, was included in the research due to its “inert” nature. It was hypothesized that, by virtue of its “inert” nature, no chemical interactions will occur between the mineral filler particles and bitumen during the ageing process. Having excluded the latter, quartz can be used to demonstrate any potential effect of the mineral fillers on the ageing of bituminous mixtures due to their physical presence in the mastics (effect on oxygen diffusion path).

#### *Norwegian sandstone (bestone)*

Bestone was acquired by a Norwegian quarry. This type of filler was incorporated in the research for comparison reasons with the baghouse dust.

In *Table 3.4* the abbreviations of the mineral fillers are presented.

**Table 3.4:** Mineral fillers abbreviations.

<b>Mineral filler</b>	<b>Abbreviation</b>
Wigro 60K	WG60K
Wigro	WG
Baghouse Dust	BD
Granite	GR
Quartz	QZ
Bestone	BE

### **3.2.2 Density of fine particles**

The density of the mineral fillers is an important property when it comes to ageing of mastics, as it is discussed in *Sub-Section 3.4.2*. The density of the fine materials is calculated through *Eq. 3.1* by utilizing the pycnometer method in accordance with NEN-EN 1097-7. The liquid substance used in the applied method was the white mineral oil LYTOL.

$$\rho_f = \frac{m_1 - m_0}{V - \frac{m_2 - m_1}{\rho_l}} \quad (3.1)$$

where,

$m_0$  = The mass of the empty pycnometer with stopper ([M])

$m_1$  = The mass of the pycnometer with the filler test portion ([M])

$m_2$  = The mass of the pycnometer with the filler test portion topped up with liquid ([M])

$V$  = The volume of the pycnometer ([V])

$\rho_l$  = The density of the utilized liquid at 25°C ([M]/[V])

$\rho_f$  = The density of the mineral filler at 25°C ([M]/[V])

Two measurements were performed for each material and their average value was used for the declared density of the mineral fillers. The individual measurements and the final density of all mineral fillers are presented in *Table 3.5*.

**Table 3.5:** Mineral fillers particles' densities.

Mineral filler	Density (gr/cm <sup>3</sup> )		
	Measurement 1	Measurement 2	Average
WG60K	2.547	2.542	2.545
WG	2.769	2.766	2.768
BD	2.679	2.677	2.678
GR	2.644	2.644	2.644
QZ	2.639	2.640	2.640
BE	2.696	2.700	2.698

### 3.3 Materials preparation

Six different mastics and pure bitumen were prepared for testing. The necessary amount of bitumen for the production of the materials was obtained by a bitumen storage can by making use of a knife heated up at 150°C. This approach was followed to avoid any ageing of the material that would result from repeated cycles of heating up and cooling down.

The applied heating temperature and time, in the production process, were chosen in accordance with NEN-EN 12594. The norm specifies that the heating temperature of bitumen should be 80 to 90°C above its softening point and the duration of heating should not exceed 2 hours. Based on the softening point of the utilized bitumen (48.4°C), a heating temperature of 130°C was selected. The heating duration was limited to 1 hour as it was regarded sufficient for the bitumen to develop the necessary workability and for the mineral fillers to expel any moisture residue.

#### 3.3.1 Mastics preparation

All mastics were prepared with a filler to bitumen mass ratio equal to 1 (f/b=1 by mass), following the standard Dutch mix design. As concluded in *Chapter 2* the concentration of the mineral filler has an impact on the ageing of bituminous mixtures. In this study, this parameter was kept constant and, thus, the effect of the mineral matter on bitumen ageing due to variations in its content was not investigated. The production of mastics was performed according to the following steps:



- i. Bitumen and mineral filler were heated-up in the stove for 1 hour at 130°C.
- ii. The appropriate amount of mineral filler, to achieve the intended filler to bitumen ratio ( $f/b=1$ ), was added to bitumen and the materials were manually stirred for 5 minutes. The applied stirring time ensured that a homogeneous blend was achieved while the workability of the mastic was kept at a tolerable level. The latter was enhanced by making use of a heating plate, set at 130°C, during blending of the materials.
- iii. The initial blending was followed by placing the mastic in the stove for 30 minutes at 130°C. This step was added to enhance the bonding of the materials through application of heat.
- iv. The mastic was manually re-stirred for 1 minute to regain any mineral filler particles that might have migrated towards the bottom of the can and could affect the homogeneity of the mixture.
- v. “Fresh” mastic samples were obtained for the imminent tests while portion of the mastic was stored for the ageing procedure.

The abbreviations of the various mastics are presented in *Table 3.6*.

**Table 3.6:** Mastics abbreviations.

<b>Mastic</b>	<b>Abbreviation</b>
40/60 Pen + Wigro 60K	40/60_WG60K
40/60 Pen + Wigro	40/60_WG
40/60 Pen + Baghouse Dust	40/60_BD
40/60 Pen + Granite	40/60_GR
40/60 Pen + Quartz	40/60_QZ
40/60 Pen + Bestone	40/60_BE

### 3.3.2 Bitumen preparation

In addition to the various mastics also neat bitumen samples were prepared for the purpose of the present research. It should be noted that it is of immense importance for this study that all materials (i.e. mastics and bitumen) undergo the same ageing. In order to avoid any undesired effects in the production phase that could lead to variant ageing level between the different materials, the preparation of bitumen was slightly modified to match the heating times of the mastics.

More specifically, in the mastics production process, after the initial blending of the materials the composite was placed in the stove for 30 minutes at 130°C (step iii, *Sub-Section 3.3.1*). As it is easily conceivable, this extra heating time may (slightly) contribute to the age-hardening of the mastics. For that reason, prior to sampling, bitumen was heated-up in the stove for a total of 1 hour and 30 minutes, instead of 1 hour, at 130°C, to compensate for the difference with the mastics. Analytically, the steps followed for the sampling of neat bitumen are listed below:

- i. Bitumen was heated-up in the stove for 1 hour at 130°C.
- ii. After the initial heating-up, bitumen was manually alligated for 5 minutes on a heating plate set at 130°C.
- iii. The material was placed in the stove for another 30 minutes at 130°C, to match the age-hardening of the mastics.
- iv. The bitumen was manually alligated for 1 minute.
- v. “Fresh” samples were obtained for further testing, while a portion of the bitumen was stored for the ageing process.

### 3.4 Ageing of bitumen and mastics

#### 3.4.1 Ageing protocol

Based on the available accelerated ageing methods in the laboratory of TU Delft and the findings from the literature review, the PAV was selected as the ageing method to be used in this study. The PAV test was performed in accordance with NEN-EN 14769, however, without prior STA of the materials. The STA was omitted due to some foreseen issues associated with the ageing of mastics with the STA equipment (i.e. TFOT and RTFOT). Specifically, these issues refer to the risk of the fillers’ settlement in the mastics in the case of TFOT, due to high utilized temperature (~163°C), and to the difficulty to control the materials’ film thickness during ageing in the RTFOT (see *Sub-Section 2.2.4*).

The norm, associated with the PAV ageing, specifies that for ageing temperatures of 90, 100 or 110°C, 20 hours were found to be an appropriate ageing duration. For the reasons discussed in *Sub-Section 2.2.4*, regarding the potential settlement of the mineral fillers in the mastics upon ageing, the lowest possible ageing temperature was selected for the execution of the test.

Overall, the test was conducted at a temperature of 90°C and 2.1 MPa (~300 psi) air pressure for a duration of 20 hours. It should be noted that the ageing time can be a parameter that could influence the effect of mineral fillers on the ageing of bitumen. In this study this parameter was kept constant (i.e. 20 hours) and no time intervals were considered in the ageing process.

The preparation of the mastics and neat bitumen, as described in *Section 3.3*, was followed by pouring an appropriate amount of the materials (see *Sub-Section 3.4.2*) in the PAV pans for the imminent ageing test. Due to the high viscosity of the mastics, it was not possible to achieve a uniform spread of the materials in the PAV pan by simply pouring the necessary amount. For that reason, the mastics in the PAV pans were placed in the stove for 15 minutes at 130°C to allow for a decrease in their viscosity, which led to a uniform distribution of the materials in the metal trays (*Fig. 3.3*). To preserve an equal ageing level between all materials, this added step was also applied for the neat bitumen, even though its viscosity was low enough, in the first place, to allow for its uniform spread in the PAV pan.

The completion of the accelerated ageing method was followed by placing the aged materials in the stove at 170°C for 30 minutes, as suggested in NEN-EN 14769. This step is performed so that the aged material becomes fluid enough to allow for the removal of

bubbles through manual stirring. The aged materials were manually stirred for 2 minutes, on a heating plate set at 170°C, and aged samples were obtained for further testing.

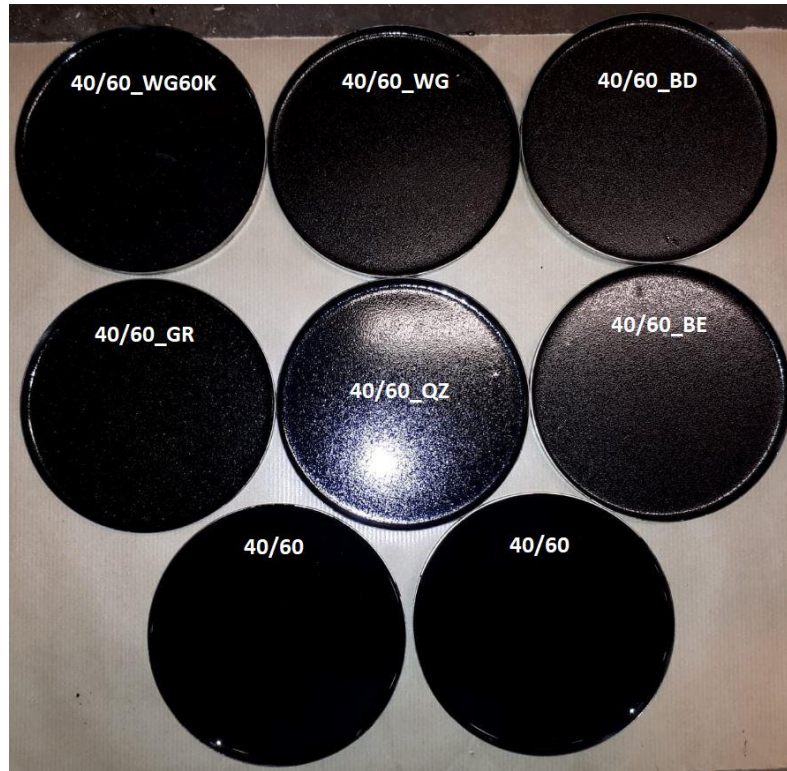


**Figure 3.3:** Materials in the PAV pans prior to ageing.

### 3.4.2 Materials' film thickness during ageing

During PAV ageing oxygen diffuses into the bituminous film. To allow for a comparison among the various materials, it is of immense importance that the geometry of the film, namely its thickness, is kept constant.

NEN-EN 14769 specifies that 50 grams of neat bitumen are placed in the PAV pan. Knowing the bitumen mass, the bitumen density (*Table 3.3*) and the PAV pan diameter (*Table 3.7*), one can obtain a film thickness in the metal tray approximately equal to 0.315 cm, through trivial calculations (*Eq. 3.2*).

**Table 3.7:** PAV pan dimensions.

Diameter (cm)	Thickness (cm)	Area (cm <sup>2</sup> )
14	0.95	153.94

$$t_i = \frac{4 \cdot m_i}{\rho_i \cdot \pi \cdot D_{\text{pan}}^2} \quad (3.2)$$

where,

$t_i$  = Thickness in the PAV pan of material (i) ([L])

$m_i$  = The mass of material (i) ([M])

$\rho_i$  = The density of material (i) ([M]/[V])

$D_{\text{pan}}$  = The diameter of the PAV pan ([L<sup>2</sup>])

All mastics were prepared with a  $f/b=1$  by mass. Knowing the mass and the density (*Tables 3.3 and 3.5*) of the individual mastic ingredients one can obtain their volume percentages in the final mastic blend. The density of the various mastics can be determined through *Eq. 3.3*. The results are presented in *Table 3.8*. With the densities of the mastics known, solving *Eq. 3.2* for the mass, with a predefined film thickness of 0.315 cm, the necessary amount of each mastic, that will lead to the desired material film thickness in the PAV pan (i.e. 0.315 cm), can be obtained (*Table 3.9*).

$$\rho_{M,i} = \rho_b \cdot V_{b,i} + \rho_{f,i} \cdot V_{f,i} \quad (3.3)$$

where,

$\rho_{M,i}$  = The density of mastic (i) ([M]/[V])

$\rho_b$  = The density of bitumen ([M]/[V])

$V_{b,i}$  = The volume percentage of bitumen in mastic (i)

$\rho_{f,i}$  = The density of mineral filler (i) ([M]/[V])

$V_{f,i}$  = The volume percentage of mineral filler (i) in mastic (i)

**Table 3.8:** Mastics densities.

Mastic	Density (gr/cm <sup>3</sup> )
40/60_WG60K	1.466
40/60_WG	1.501
40/60_BD	1.487
40/60_GR	1.482
40/60_QZ	1.481
40/60_BE	1.490

**Table 3.9:** Mass of mastics in the PAV pan that yields a film thickness of 0.315 cm.

Mastic	Mass in the PAV pan (gr)
40/60_WG60K	71.18
40/60_WG	72.88
40/60_BD	72.22
40/60_GR	71.97
40/60_QZ	71.93
40/60_BE	72.37

The above practice ensured that the ageing assessment of the different materials will not provide biased results due to variations in their film thicknesses during the ageing process, since a constant film thickness was achieved for all materials, regardless of their individual properties.

### 3.5 Mineral fillers characterization methods

#### 3.5.1 Laser diffraction

The laser diffraction is a volume-based technique for the determination of the particles' size. This method is based on the interaction between monochromatic light and matter. The tested matter particles pass through a laser light beam and scatter it. The angular distribution of the scattered light is captured by appropriate detectors and the collected data are used for the construction of the particles' size distribution curves (NCHRP 9-45 2010, Michel & Courard 2014). The operating principles of the laser diffraction method are schematically represented in *Fig. 3.4*.

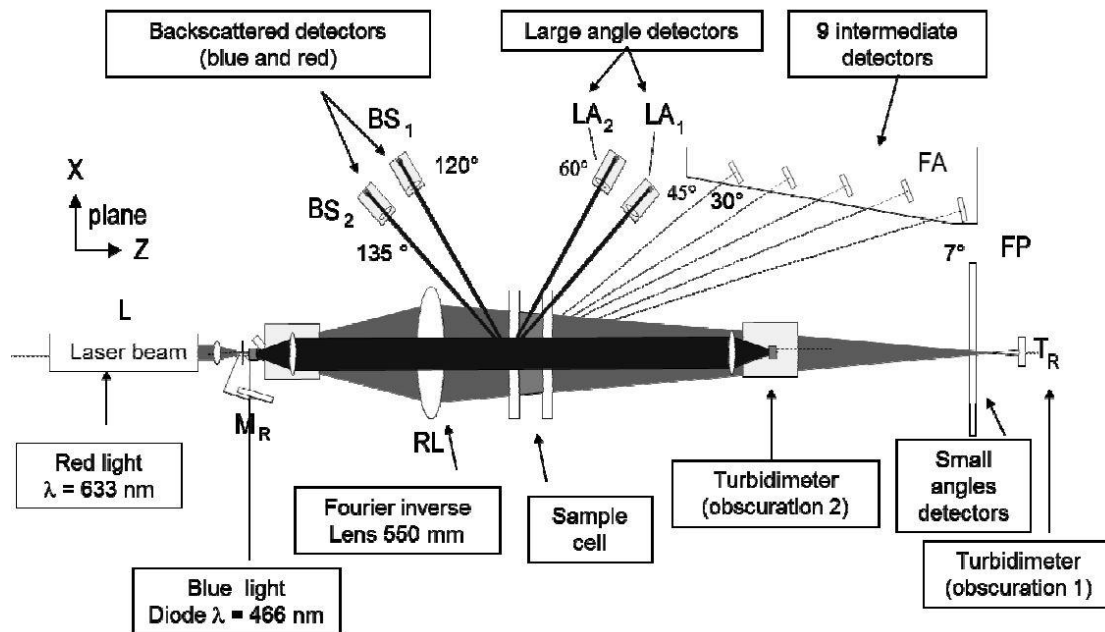


Figure 3.4: Laser diffraction operating principles (Michel & Courard 2014).

Two are the major theories that are used to convert the light scattering data into particles' size distribution information: a) the Mie theory and b) the Fraunhofer diffraction model. Both models assume that the material is isotropic and its particles can be approximated as perfect spheres. Hence, the size of a single particle, of arbitrary shape, is approximated as the size of a spherical particle with equivalent volume. The Fraunhofer diffraction model does not consider the optical properties of the tested material, since it assumes that the particles are opaque discs and only the diffracted light is used in the calculation of the projected area of a sample. On the contrary, the Mie theory prerequisites that the optical properties of the material under analysis are provided as inputs (Michel & Courard 2014).

Apart from the particles' size distribution, the laser diffraction test provides an estimation of the specific surface area (SSA) of the material under analysis. In general, the term "estimation" witnesses that one or more assumptions lie behind the determination of a particular property. As mentioned previously, in the laser diffraction analysis, the tested particles are treated as being perfect spheres. As a result, their surface texture and external porosity are completely disregarded (Fig. 3.5). The latter may have an (important) impact on the determination of the SSA, since both aforementioned features may (considerably) add to the total SSA of the material.

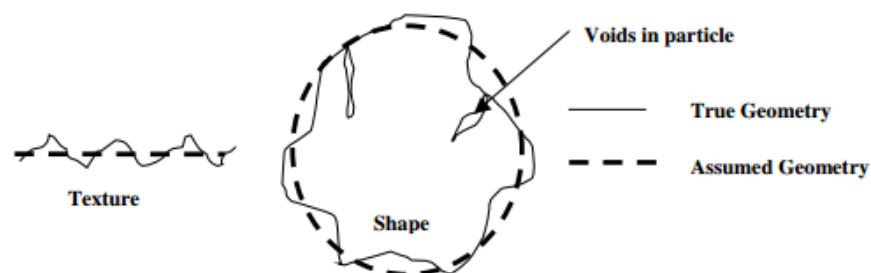
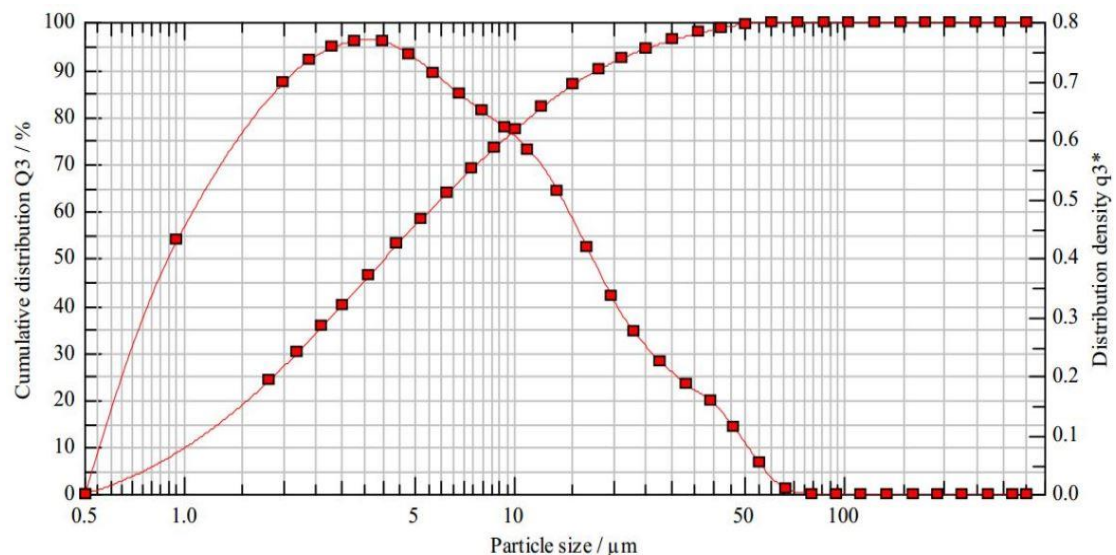


Figure 3.5: Laser diffraction test. Particles' geometry and texture assumptions (Taylor 2007).

In the present thesis, the particles' size distribution and the estimated specific surface area of the various mineral fillers were determined through dry dispersion measurements by utilizing a Sympatec HELOS instrument with a RODOS dry dispersion system combined with a VIBRI precise vibratory feeder (*Fig. 3.6*). The post-processing of the collected data, for the generation of gradation curves, was done based on the Fraunhofer diffraction model. In *Fig. 3.7*, an example of the exported data from the laser diffraction test is illustrated. The laser diffraction test results are presented and discussed in *Section 4.1*.



**Figure 3.6:** Laser diffraction equipment used in this study.



**Figure 3.7:** Laser diffraction analysis. Example of exported gradation curve.

### 3.5.2 Environmental scanning electron microscope (ESEM) imaging

The environmental scanning electron microscope (ESEM) imaging was utilized to investigate the morphology (i.e. shape, texture etc.) of the various mineral fillers' particles. Microscopy can be useful in observing the differences between the utilized mineral fillers, morphological-wise, and may provide information that can be correlated to other properties of the mineral matter.

For the purpose of the present research, a Philips XL30 ESEM-Tungsten filament electron microscope (*Fig. 3.8*) was employed for the observation of the mineral fillers. Four different magnification scales (i.e. 125x, 250x, 500x and 1000x) were applied for each material. The results of the ESEM imaging are presented and discussed in *Section 4.2*.



**Figure 3.8:** The ESEM utilized in this study.

### 3.5.3 Rigden voids

The fractional voids content refers to the entrapped voids of a compacted, at the maximum density, dry mineral filler. The measurement of this property was introduced by Rigden in 1947, hence, usually, the researchers refer to this test as the “Rigden voids” (RV) test. Four mineral filler geometrical characteristics have been found to have the most pronounced effect on the RV content: particles' size, size distribution, shape, angularity and texture (NCHRP 9-45 2010).

Rigden (1954) introduced the concepts of “fixed” and “free” binder in bitumen-mineral filler systems.” Fixed” binder is the portion of bitumen that is used to fill-in the Rigden voids, which is no longer available to contribute to the fluidity of the mastic. On the contrary, the bitumen in excess, responsible for the separation of the fine particles and the lubrication of the mastic, is referred to as “free” binder (*Fig. 3.9*) (Aburkaba & Muniandy 2016). Based on the aforementioned concepts, a good correlation is reported in literature between the RV content and the stiffening effect of the mineral fillers on bitumen. The latter stems from the fact that when the fractional voids content is high, more bitumen is occupied in filling-in the voids, leaving less “free” binder to separate the particles and provide the mastic with fluidity (NCHRP 9-45 2010).

The RV test constitutes a standardized test for the characterization of mineral fillers and it is performed in accordance with NEN-EN 1097-4. The percentage of fractional voids in a dry compacted mineral filler is calculated through *Eq. 3.4*. The RV test results are presented and discussed in *Section 4.3*.

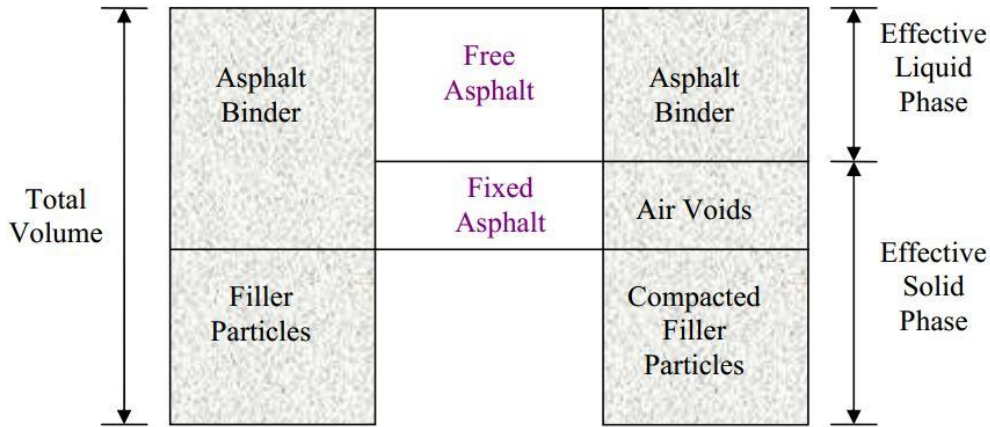


**Figure 3.9:** Concepts of “fixed” and “free” binder (Aburkaba & Muniandy 2016).

$$RV = \left[ 1 - \frac{4 \cdot m_f}{\pi \cdot D_c^2 \cdot (h - h_{\text{filter}})} \cdot \frac{1}{\rho_f} \right] \cdot 100\% \quad (3.4)$$

where,

RV = The Rigden voids percentage (%)

$m_f$  = The mass of the tested filler portion ([M])

$D_c$  = The diameter of the cylinder ([L])

$h$  = The height of the compacted mineral filler, plunger and filter paper ([L])

$h_{\text{filter}}$  = The thickness of the utilized filter paper ([L])

$\rho_f$  = The density of the mineral filler ([M]/[V])

### 3.5.4 Braunauer-Emmett-Teller (BET) method

In contrast to the laser diffraction test, as discussed in *Sub-Section 3.5.1*, gas sorption measurements constitute a more accurate mean for the determination of the SSA of the mineral fillers. The major advantage of the latter is that the surface texture, particles' shape as well as the surface of the external pores of the material are taken into account in the determination of its SSA (*Fig. 3.10*). Nevertheless, the determination of this property is biased by the molecular size of the adsorbate gas relatively to the size of the material's pores and crevices (Taylor 2007).

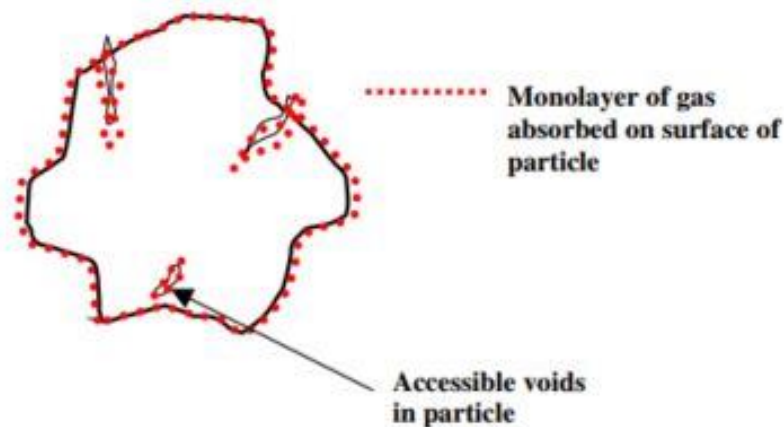


**Figure 3.10:** Solid particle in gas sorption measurement (Taylor 2007).



The most widely used method for the determination of the SSA, based on gas sorption measurements, is the Braunauer-Emmett-Teller (BET) method, named after its developers Braunauer et al. (1938). The method is based on the isothermal adsorption of gas molecules on the particles' surface, creating a monolayer. The SSA is derived based on the size and amount of the adsorbed gas molecules (Apostolidis 2015).

Braunauer et al. (1938) determined a relationship between the relative pressure of the gas and the volume adsorbed per unit mass of the sample (Eq. 3.5), by assuming that, during the formation of the first monolayer, the heat of adsorption is constant and that for the following monolayers the heat of adsorption is equal to the heat of condensation of the bulk liquid.

$$\frac{P}{V_{\text{ads}} \cdot (P_0 - P)} = \frac{1}{V_m \cdot c} + \frac{c - 1}{V_m \cdot c} \cdot \frac{P}{P_0} \quad (3.5)$$

where,

$P$  = The equilibrium pressure (Pa)

$P_0$  = The saturation pressure (Pa)

$V_{\text{ads}}$  = The volume of adsorbed gas at  $P/P_0$  ( $\text{mm}^3 \cdot \text{gr}^{-1}$ )

$V_m$  = The volume of adsorbate corresponding to one monolayer ( $\text{mol} \cdot \text{gr}^{-1}$ )

$c$  = The BET constant (-) (Eq. 3.6)

$$c = e^{\frac{E_1 - E_L}{R \cdot T}} \quad (3.6)$$

where,

$E_1$  = The heat of adsorption for the first monolayer ( $\text{KJ} \cdot \text{mol}^{-1}$ )

$E_L$  = The heat of adsorption for the higher monolayers ( $\text{KJ} \cdot \text{mol}^{-1}$ )

$R$  = The universal gas constant ( $8.314 \text{ J} \cdot \text{mol}^{-1} \cdot \text{K}^{-1}$ )

$T$  = The absolute temperature (K)

A plot of  $P/V_{\text{ads}}(P_0 - P)$  versus  $P/P_0$  yields a straight line of the type  $y = a + bx$  (Fig. 3.11), where the slope ( $b$ ) corresponds to the term  $1/V_m c$  and the intercept ( $a$ ) corresponds to the term  $c - 1/V_m c$  (see Eq. 3.5). The volume of the gas required to form a monolayer ( $V_m$ ) and the BET constant ( $c$ ) can be calculated through Eq. 3.7 and 3.8 respectively.

$$V_m = \frac{1}{a + b} \quad (3.7)$$

$$c = 1 + \frac{b}{a} \quad (3.8)$$

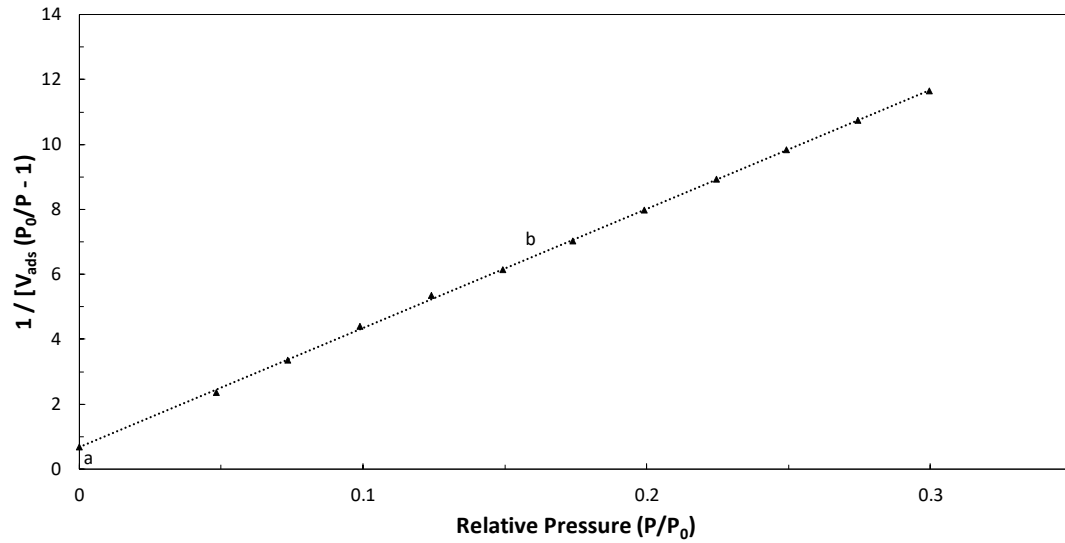


**Figure 3.11:** Example of a typical BET plot.

The total surface area and the SSA of the tested sample are calculated through Eq. 3.9 and 3.10 respectively.

$$S_{\text{total}} = V_m \cdot A_{\text{mol}} \cdot L \quad (3.9)$$

where,

$S_{\text{total}}$  = The total surface area of the sample ( $\text{m}^2$ )

$V_m$  = The volume of adsorbate corresponding to one monolayer ( $\text{mol} \cdot \text{gr}^{-1}$ )

$L$  = The Avogadro's constant ( $6.022 \cdot 10^{23} \text{mol}^{-1}$ )

$$\text{SSA}_{\text{BET}} = \frac{S_{\text{total}}}{m} \quad (3.10)$$

where,

$\text{SSA}_{\text{BET}}$  = The BET specific surface area ( $\text{m}^2/\text{gr}$ )

$m$  = The mass of the tested sample (gr)

For the purpose of the present research, the BET specific surface area measurements were performed with a Gemini VII 2390p analyzer. The utilized carrier gas and adsorbate were nitrogen ( $\text{N}_2$ ) and liquid nitrogen, respectively. The measuring equipment was calibrated by utilizing glass powder reference material with an SSA of  $5.1 \pm 0.3 \text{ m}^2/\text{gr}$ . The relative pressure was gradually increased up to 30% with ten intermediate steps. The mineral matters were dried in the oven at  $105^\circ\text{C}$  for 24 hours prior to testing.

The BET SSA results are presented and discussed in Section 4.4. The isothermal curves and BET plots of all measured materials are presented in Appendix A. It should be noted that the SSA of QZ was not measured by the author. Instead the declared value in the material's specification sheet, as measured by Sibelco-Dessel by utilizing the BET method, was considered.

### 3.5.5 Swelling test

The swelling test is a non-standard method developed by Sibelco-Winterswijk to evaluate the swelling tendency of the mineral fillers in the presence of water. The test is characterized by its executional simplicity and its straightforwardness. Even though the swelling tendency of the mineral fillers is not a parameter that would assist in achieving the research objectives of the present thesis, the results may be useful for future studies, where the same mineral fillers are used and moisture considerations are included. For the reason stated above, the outcome of the swelling test will just be reported without providing any further interpretation of the obtained results.

For the execution of the test, approximately the same mass of mineral filler is placed in two volumetric tubes and the weights of the mineral filler portions are recorded. Then, one tube is filled with methanol and the other one with water. The mineral fillers in the tubes are allowed to completely settle under the effect of gravity. Usually 48 hours are required for the complete material to settle at the bottom of the tube. After 48 hours, the indications on the volumetric tubes, as specified by the surface of the (swelled) material, are recorded. It should be noted that, due to non-uniform settlement of the material, the volume indication may vary along the circumference of the volumetric tube. In that case, an average value of the various indications is declared as the final volume. In *Fig. 3.12*, an example of completed swelling test is illustrated. The swelling percentage (SP) of the material under analysis is calculated through *Eq. 3.11*. The results of the swelling test are reported in *Section 4.5*.

$$SP = \left( \frac{m_{f,m} \cdot V_w}{m_{f,w} \cdot V_m} - 1 \right) \cdot 100\% \quad (3.11)$$

where,

SP = The swelling percentage (%)

$m_{f,m}$  = The mass of the mineral filler in methanol ([M])

$m_{f,w}$  = The mass of the mineral filler in water ([M])

$V_{f,w}$  = The volume indication on the water volumetric tube ([V])

$V_{f,m}$  = The volume indication on the methanol volumetric tube ([V])

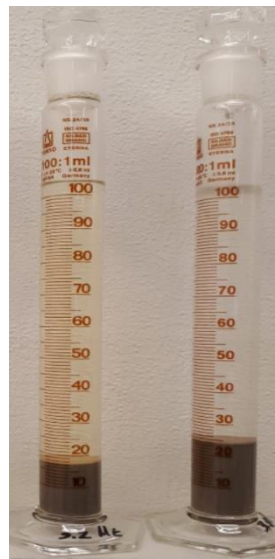


**Figure 3.12:** Completed swelling test. Volumetric tubes with methanol (left) and water (right).

### 3.5.6 Methylene blue

The methylene blue value (MBV) is a method applied for the determination of harmful fines in the mineral matter, such as clay and organic materials (NCHRP 9-45 2010). When liquid, the methylene blue is a cationic dye which is adsorbed on negatively charged clay surface areas (Santamarina et al. 2002). The test principal lies in the gradual addition of the methylene blue in the test sample until adsorption of the dye ceases (Kandhal et al. 1998).

In this study, the methylene blue test was performed in accordance with NEN-EN 933-9. The tests were conducted with the addition of kaolinite. In *Fig. 3.13*, the overall setup of the methylene blue test is illustrated. The MBV, expressed in grams of dye per kilogram of the tested sample, is calculated through *Eq. 3.12*. The results are presented and discussed in *Section 4.6*.

$$MBV = \frac{V_{d,total} - V_{d,k}}{m_f} \cdot 10 \quad (3.12)$$

where,

MBV = The methylen blue value (gr/kg)

$V_{d,total}$  = The total volume of added dye (ml)

$V_{d,k}$  = The volume of dye adsorbed by kaolinite (ml)

$m_f$  = The mass of the test sample (gr)



**Figure 3.13:** Methylene blue test setup.

### 3.5.7 X-ray fluorescence (XRF) spectroscopy

The X-ray fluorescence spectroscopy (XRF) spectroscopy constitutes a non-destructive method, which is employed for the identification of the types of elements and their respective concentrations in a powder sample. Its basic principle lies in the collection and post-processing of characteristic secondary radiation, that is emitted from the sample, when the latter is excited with X-rays (Gupta 2011).

More specifically, when an X-ray is directed to the sample, it can be either absorbed by an atom or scattered in the material. In the first case, and provided that the X-ray has adequate energy, electrons are ejected from the inner shells of the atom leading to the creation of vacancies at these very orbits. This constitutes an unstable state for the atom. In order for stability to be restored, electrons from the outer shells migrate towards the “deficient” inner shells. During this process, energy is released in the form of X-rays, known as fluorescent radiation, whose energy is the difference between the binding energies of the involved shells. The various elements in a sample can be identified by virtue of their unique characteristic emitted X-ray signature. In most of the cases, the K and L shells participate in the XRF detection measurements (Gupta 2011). *Fig. 3.14* schematically illustrates the principle of XRF spectroscopy. For a detailed review of X-rays treatment, the reader is directed to Jenkins (1999).

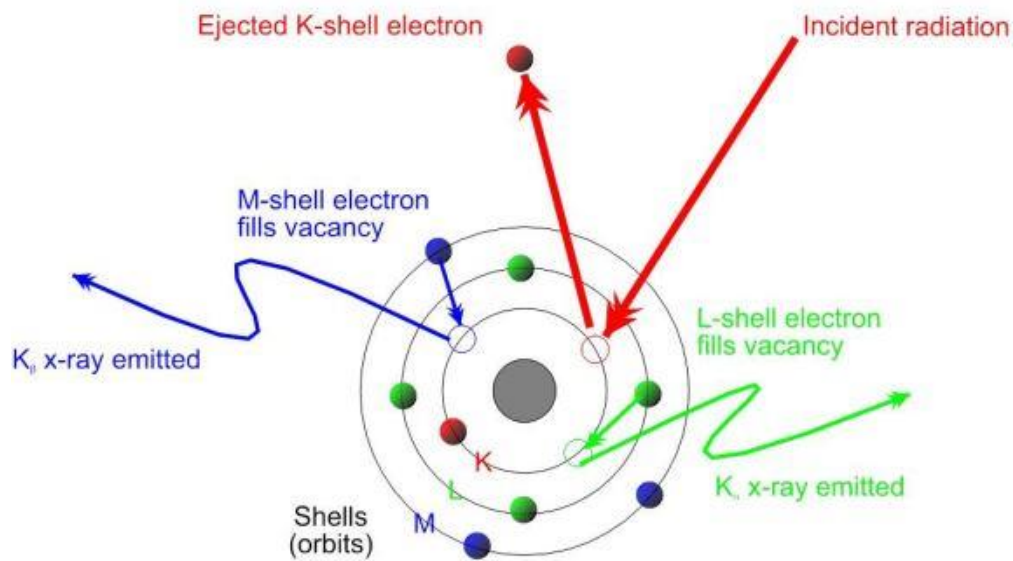


**Figure 3.14:** Principle of XRF (Nageswaran 2016).

The elemental analysis of the mineral fillers, considered in this study, is presented and discussed in *Section 4.7*. The elemental composition analysis of the materials is accompanied with the results of the loss-on-ignition (LOI) test. LOI is performed to allow for the escape of volatile components in the mineral fillers.

### 3.5.8 X-ray diffraction (XRD)

The X-ray diffraction (XRD) is a technique widely used for the identification of minerals in rocks and soils. During an XRD analysis the tested sample (usually in the form of powder) is scanned with X-rays over a range of different angles. Under certain circumstances the incoming X-ray is diffracted and its intensity is recorded by a diffractometer. The mineralogical composition of the specimen is obtained by matching

the recorded intensity at specific angles with standard reference patterns (Gupta 2011). In *Fig. 3.15*, an example of an XRD spectrum is depicted. The mineralogical composition of the mineral fillers, utilized in this study, is reported and discussed in *Section 4.7*.

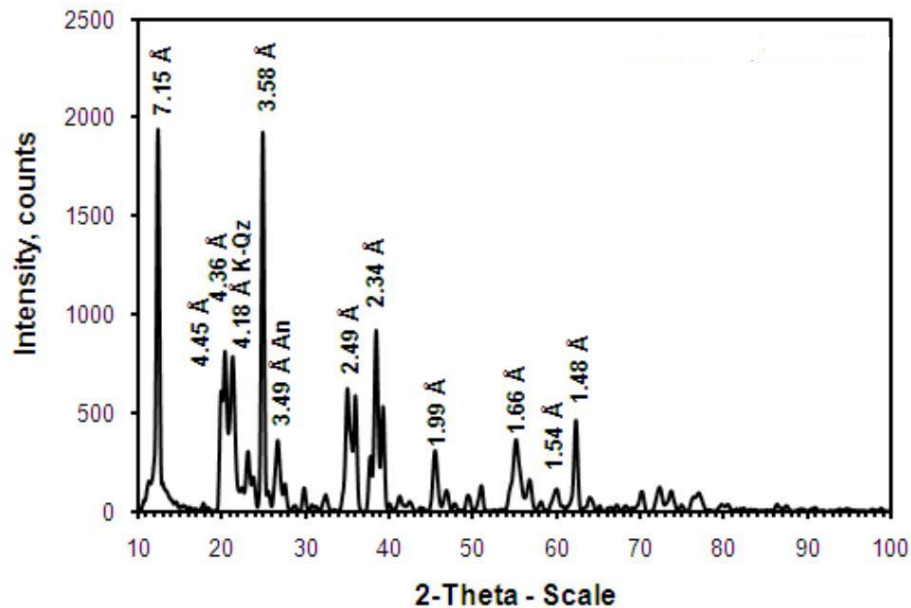


**Figure 3.15:** Example of an XRD spectrum (Gupta 2011).

### 3.6 Bitumen and mastics test methods

#### 3.6.1 Dynamic shear rheometer (DSR)

##### *Basic principles*

The dynamic shear rheometer (DSR) is used for the rheological evaluation of time (loading rate) dependent materials, such as bituminous binders. Measurements with the DSR yield the fundamental properties of bituminous binders, namely the Complex Shear Modulus ( $G^*$ ) and the Phase Angle ( $\delta$ ).

The standard testing procedure involves the application of sinusoidal stress or strain on a sample sandwiched between the Parallel Plates (PP), also referred to as test geometries, of the rheometer. The most frequently used test geometries, are, for low to intermediate test temperatures (i.e.  $\sim -10$  to  $20^\circ\text{C}$ ), an 8 mm-diameter plate (*Fig. 3.16a*) with a gap of 2 mm between the PP, while for higher temperatures, a 25 mm-diameter plate (*Fig. 3.16b*) with a gap of 1 mm (Woldekidan 2011).

During the dynamic measurements, the top plate of the DSR configuration oscillates while the lower plate remains fixed (*Fig. 3.17*). The test can be conducted in either the stress-controlled mode or the strain-controlled mode. In the first case, a sinusoidal stress is applied and the corresponding strain is determined by measuring the displacement in response to the applied stress. In the second case, the stress amplitude is determined by measuring the torque in response to the applied strain. The maximum shear stress ( $\tau_{\max}$ ) and the maximum shear strain ( $\gamma_{\max}$ ) occur at the edge of the specimen (*Fig. 3.18a and b*) and are calculated according to *Eq. 3.13* and *3.14*, respectively (Van den Bergh 2011).



Figure 3.16: (a) 8 mm-diameter oscillating plate. (b) 25 mm-diameter oscillating plate.

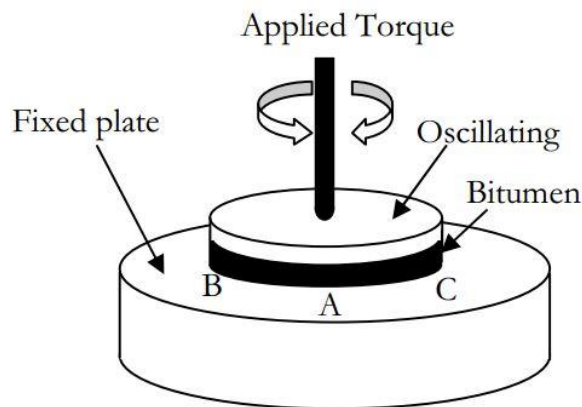


Figure 3.17: DSR operating principal (Woldekidan 2011).

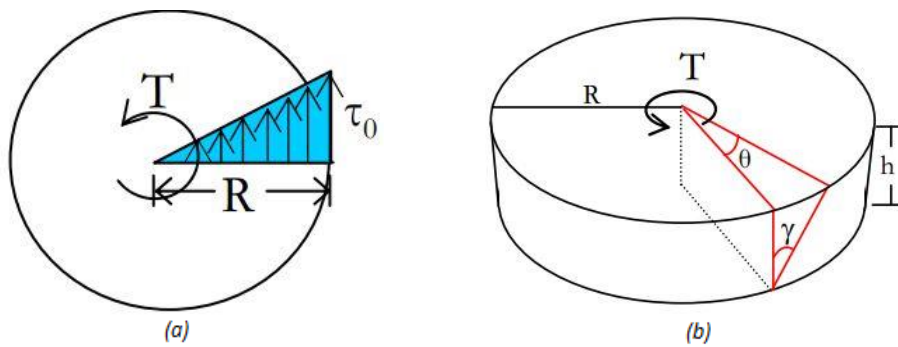


Figure 3.18: (a) Maximum shear stress location. (b) Maximum shear strain location (Woldekidan 2011).

$$\tau_{\max} = \frac{2 \cdot T}{\pi \cdot R^3} \tag{3.13}$$

$$\gamma_{\max} = \frac{\theta \cdot R}{h} \tag{3.14}$$

where,

$\tau_{\max}$  = The maximum shear stress ([F]/[A])

T = The applied torque ([F] · [L])

R = The radius of the plates (specimen) ([L])

$\gamma_{\max}$  = The maximum shear strain

$\theta$  = The deflection angle (rad)

h = The specimen height/gap between the PP ([L])

The complex shear modulus is a measure of the resistance of the material against deformation when repeatedly sheared (Apostolidis 2015), and is calculated as the ratio of the maximum stress amplitude and the maximum strain amplitude (Eq. 3.15) (Van den Bergh 2011).

$$G^* = \frac{\tau_{\max}}{\gamma_{\max}} \quad (3.15)$$

The phase angle describes the phase lag between the stress and strain signals (Fig. 3.19) (Van den Bergh 2011). Purely elastic materials present a phase angle equal to  $0^\circ$  whereas purely viscous materials show a phase angle equal to  $90^\circ$ . For visco-elastic materials,  $\delta$  lies in between the two extremes (Fig. 3.20) and its value depends on the testing temperature and frequency. The phase angle is calculated through Eq. 3.16 (Van den Bergh 2011).

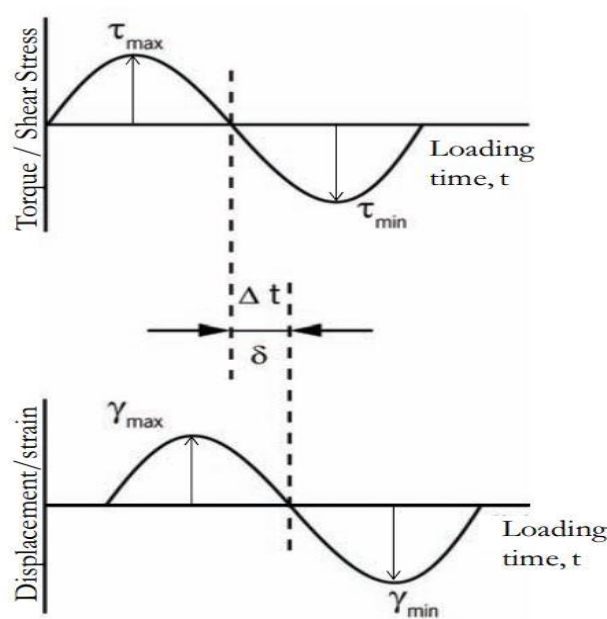


Figure 3.19: Phase lag between loading and response (Van den Bergh 2011).

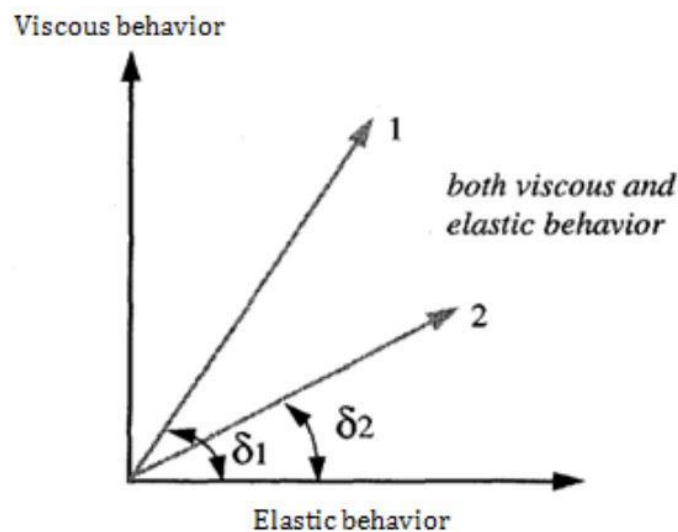


Figure 3.20: Phase angle as a function of material's behavior (Apostolidis 2015).



$$\delta = \omega \cdot \Delta t = 2 \cdot \pi \cdot f \cdot \Delta t \quad (3.16)$$

where,

$\delta$  = The phase angle (rad) or ( $^{\circ}$ )

$\omega$  = The angular frequency (rad)

$\Delta t$  = The time lag between the loading and response signals (sec).

$f$  = The frequency (Hz)

The complex shear modulus is composed by two components. An elastic component, the Storage Modulus ( $G'$ ) and a viscous component, the Loss Modulus ( $G''$ ). The relation between complex  $s$ ,  $G'$ ,  $G''$  and  $\delta$  is graphically represented in *Fig. 3.21* and is described through *Eq. 3.17, 3.18, 3.19* and *3.20* (Van den Bergh 2011).

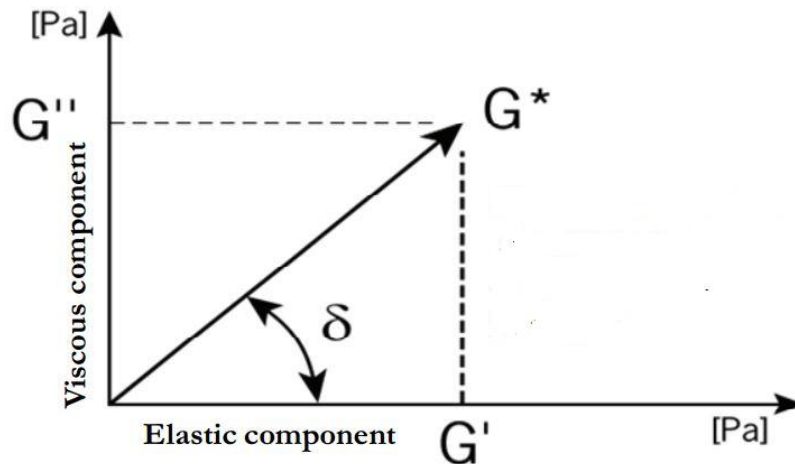


**Figure 3.21:** Relationship between complex shear modulus, storage modulus, loss modulus and phase angle (Van den Bergh 2011).

$$G'(f) = G^*(f) \cdot \cos \delta \quad (3.17)$$

$$G''(f) = G^*(f) \cdot \sin \delta \quad (3.18)$$

$$G^* = G' + i \cdot G'' = \sqrt{(G')^2 + (G'')^2} \quad (3.19)$$

$$\delta = \tan^{-1} \left( \frac{G''}{G'} \right) \quad (3.20)$$

The dynamic measurements were performed with a dynamic shear rheometer Anton Paar MCR 502 with temperature control chamber, available at the laboratory of the Pavement Engineering Section of TU Delft.

### 3.6.1.1 Preliminary study on DSR configuration

Woldekidan (2011) reported that testing of mortars (i.e. bitumen-filler-sand system) by using the Cone and Plate (CP) configuration (*Fig. 3.22*) did not provide consistent results due to the presence of the fine particles in the material. Instead, the testing of these materials was carried out by adopting a different testing geometry, the mortar column (*Fig. 3.23*), which was developed during the first phase of the PA design tool project (Huurman 2008).

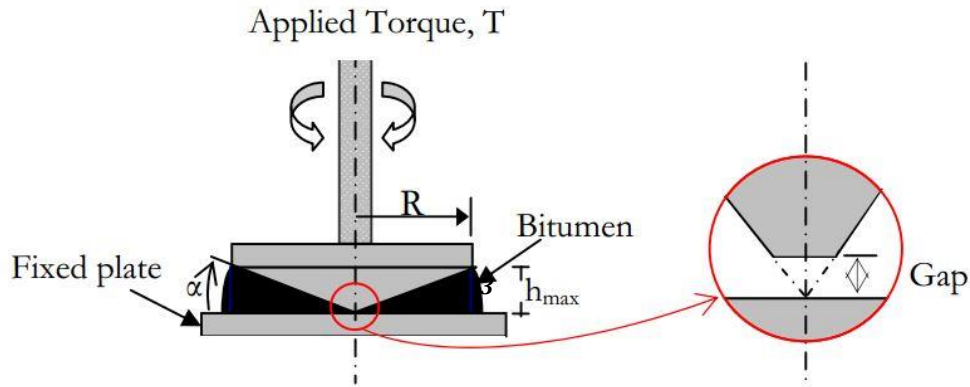


**Figure 3.22:** DSR CP configuration (Woldekidan 2011).

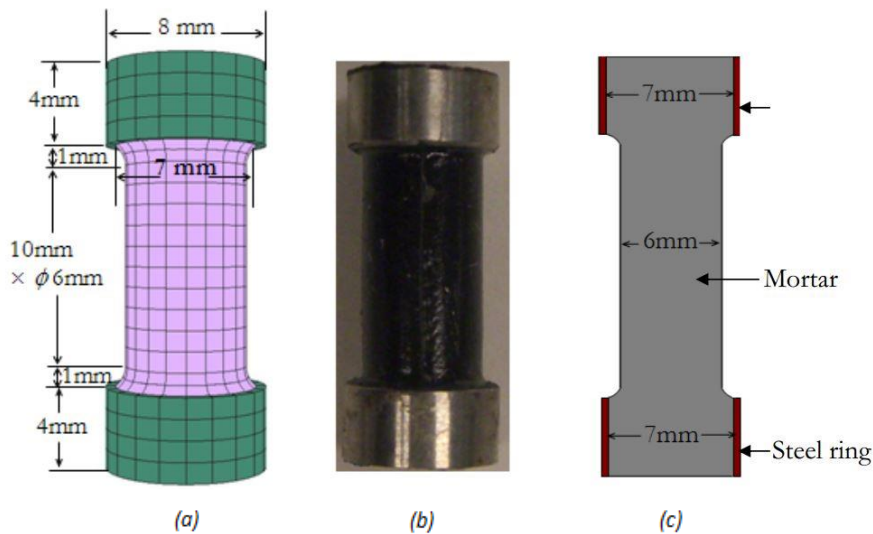


**Figure 3.23:** DSR mastic column configuration. (a) FEM model. (b) Real specimen. (c) Specimen cross-section (Woldekidan 2011).

The experimental plan of the present thesis includes the rheological evaluation of mastics by utilizing the DSR. Despite the fact that the CP configuration was not a potential candidate for the dynamic measurements and, despite the fact that the mastics, in contrast to mortars, contain only mineral filler particles (extremely fine particles), the experience of Woldekidan (2011) raised the concern whether the PP configuration is a suitable one for testing mastics, or Mastic Columns (MC) should be used instead.

To address this concern a preliminary study on the DSR configuration was conducted, prior to any further measurements for the main experimental part of this research. The frequency sweep test was performed on a mastic by utilizing the two different configurations of interest (i.e. PP and MC configurations) (*Fig. 3.24*) and the results were compared through the  $G^*$  master-curves.

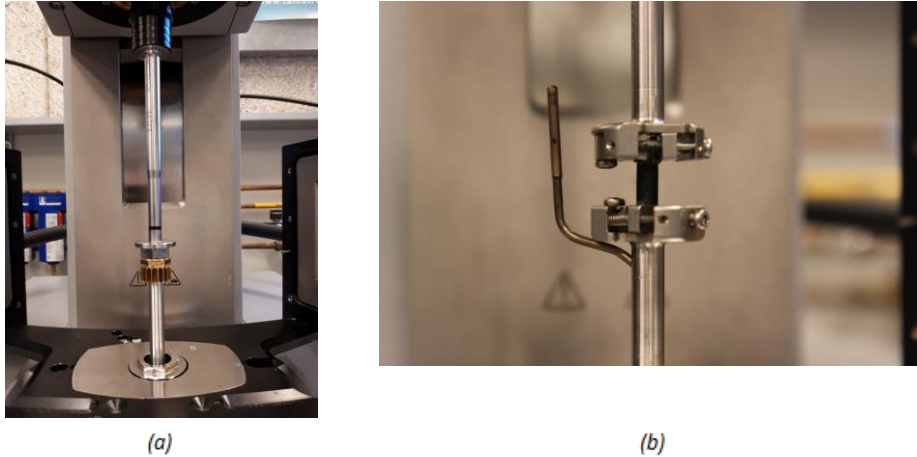


**Figure 3.24:** (a) PP configuration. (b) MC configuration.

#### *Mastic and DSR specimens' preparation*

One type of mastic was used for the purpose of the preliminary study, namely the 40/60\_WG. It should be noted that the mineral filler used in this phase is not the same with the one used in the main experimental part, since, for the latter, new materials were provided by Sibelco-Winterswijk. The production of the mastic was carried out as described in *Sub-Section 3.3.1* and specimens for the PP and MC configuration were prepared.

In the case of the MC specimens, after the mastic was poured in the silicon mold (*Fig. 3.25a*), the filled mold was placed in the oven at 130°C for 15 minutes. This step was added to remove the air bubbles in the mastic specimens. The mold was then left to cool down at room temperature for 1 hour and afterwards it was stored in the freezer for approximately 2 hours. When the mastic became stiff enough, the specimens were detached from the mold, placed on fine sand, to avoid self-weight bending (*Fig. 3.25b*), and stored in the refrigerator until the imminent test.



**Figure 3.25:** (a) Mastic column silicon mold. (b) Mastic column specimens.

#### *Frequency sweep test and complex shear modulus master-curves*

In both configuration cases the frequency sweep test was carried out in the stress-control mode. In this phase no amplitude sweeps were conducted prior to the frequency sweep tests, to identify the Linear Visco-Elastic (LVE) region of the tested material. The applied stress levels, at each testing temperature, were arbitrarily chosen, but kept sufficiently low to ensure that the material's response is evaluated within its LVE region. The frequency sweep tests were conducted at temperatures from -10°C to 30°C, with 10°C increments, and frequencies ranging from 0.02 to 20 Hz. In the PP configuration an 8 mm-

diameter plate was used for all testing temperatures. The construction of the master-curves was done according to the procedure described in *Sub-Section 3.6.1.4*.

In *Fig. 3.26* the  $G^*$  master-curves for the two different configurations are presented. The graph indicates that the two cases yield approximately the same results. More specifically, the PP configuration seem to provide a slightly lower complex shear modulus values compared to the MC configuration, with the difference being more pronounced at low and high frequencies. Based on the outcome of the preliminary study the PP configuration was selected to be used for the DSR measurements of the mastics.

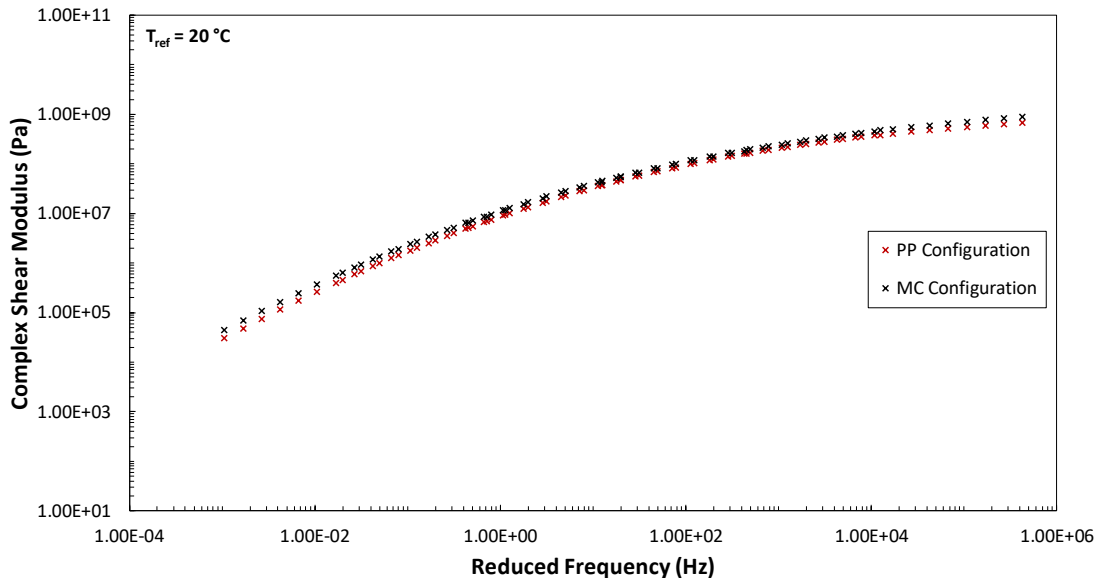


**Figure 3.26:** Complex shear modulus master-curves PP and MC configurations.

### 3.6.1.2 Amplitude sweep test - materials' linear visco-elastic (LVE) region

Bituminous binders present a non-linear relationship between stress and strain, which becomes negligible at very low stresses (or strains), where the material is assumed to display Linear Visco-Elastic (LVE) behavior. When the fundamental visco-elastic properties of the material (i.e.  $G^*$  and  $\delta$ ) are determined in its LVE region of response, the stress-strain relationship is only affected by the testing temperature and frequency and not by the magnitude of the stress or strain (Airey 2002). Moreover, the application of analysis methods, such as the generation of master-curves by making use of the Time-Temperature Superposition (TTS) principal, prerequisites that the rheological data are defined within the LVE region of the considered material (Bahia 1998).

Therefore, prior to the frequency sweep tests, stress (or strain) sweeps, also frequently referred to as amplitude sweeps, are performed, during which the stress (or strain) is gradually increased while the temperature and frequency remain constant. The LVE region of the tested material can be determined as the range of stress (or strain) at which the complex shear modulus is relatively independent of the stress (or strain) magnitude (plateau in *Fig. 3.27*). The complex shear modulus is plotted against stress (or strain) and an amplitude limit is defined beyond which the non-linear behavior of the material becomes significant. According to a study carried out within the framework of the SHRP, the LVE limit is defined as the point in the stress (or strain) amplitude axis at which the maximum measured complex shear modulus value is reduced by 5% (*Fig. 3.27*) (Petersen 1994).

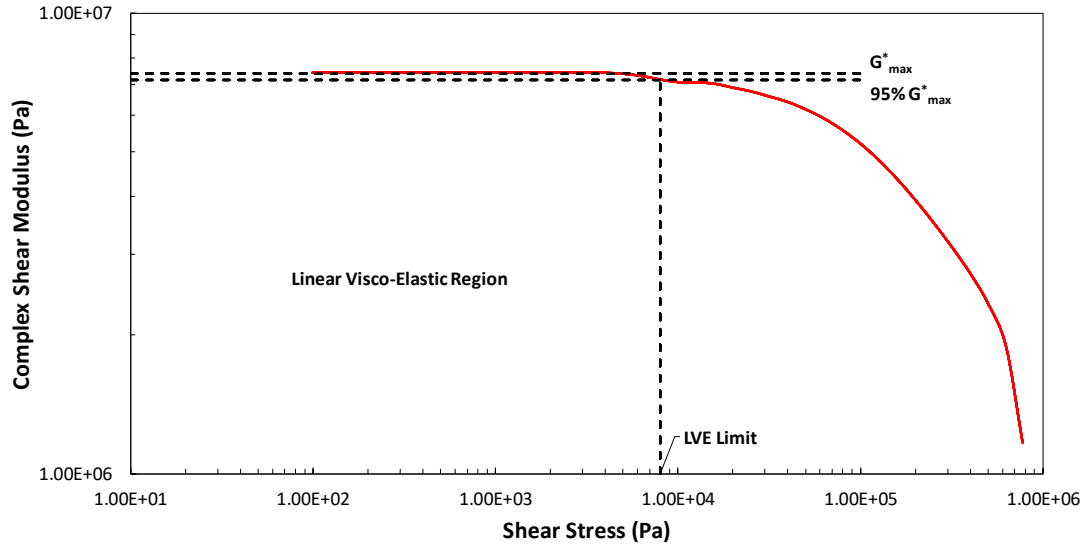


**Figure 3.27:** Example of the determination of the LVE limit. Stress amplitude sweep.

The amplitude sweep test was performed on all materials (i.e. mastics and bitumen) at both the “fresh” and the aged state. The test was carried out at six different temperatures (-10 to 40°C, with 10°C increments) and frequency of 1 Hz. The LVE limit is affected by the test temperature and, based on the TTSP, so does by the applied frequency (Fig. 3.28). The chosen test frequency (i.e. 1 Hz) represents, approximately, the mid-value of the frequencies applied in the imminent frequency sweep tests.

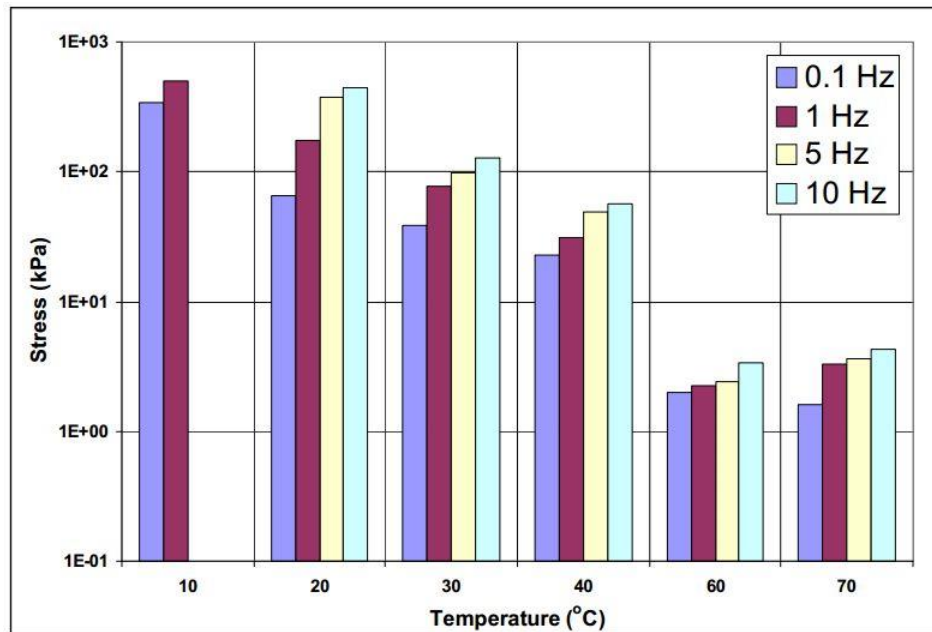


**Figure 3.28:** LVE region stress limit as a function of temperature and frequency for aged 40/60 Pen bitumen (Rahimzadeh 2002).

The above practice allowed to determine a governing LVE limit for each testing temperature and select a stress level (for each temperature), to be applied in the stress-controlled frequency sweep tests, which would ensure that all materials are evaluated within their LVE region of response. It should be noted that different sets of stress levels were determined for the mastics and the bitumen. *Table 3.10* summarizes the amplitude sweep test conditions.

The amplitude sweeps results for all materials, as well as the determination of their LVE limits and selection of appropriate stress levels, are reported in Appendix B. The chosen stress levels, applied in the frequency sweep tests, per type of material and temperature, are presented in *Table 3.11*.

**Table 3.10:** Amplitude sweep test conditions.

Feature	Material	
	Mastic	Bitumen
Loading Mode	Stress-Controlled	Stress-Controlled
Stress Range (KPa)	0.1-1000	0.01-1000
Testing Points	41	51
Test Temperatures (°C)	-10, 0, 10, 20, 30 and 40	-10, 0, 10, 20, 30 and 40
Test Frequency (Hz)	1	1
Test Geometry (-ies)	8 mm Plate 2 mm Gap	-10÷20°C: 8 mm Plate 2 mm Gap 30 and 40°C: 25 mm Plate 1 mm Gap
Specimen Temperature Equilibrium	600 sec ± 0.2°C Tolerance	600 sec ± 0.2°C Tolerance

**Table 3.11:** Chosen stress levels applied in the frequency sweep tests.

Temperature (°C)	Chosen stress level (Pa)	
	Mastics	Bitumen
-10	150000	12000
0	100000	10000
10	50000	8000
20	7000	5000
30	2500	3000
40	2000	2000

### 3.6.1.3 Frequency Sweep Test

The frequency sweep test was performed on all materials to obtain their fundamental rheological properties (i.e.  $G^*$  and  $\delta$ ) in different temperatures and in a range of frequencies. To increase the accuracy of the obtained data, 3 replicates were tested for each material and their average was used to obtain the  $G^*$  and  $\delta$  isothermal curves (*Fig 3.29a and b*) to be post-processed. All three measurements showed great repeatability, for all materials.

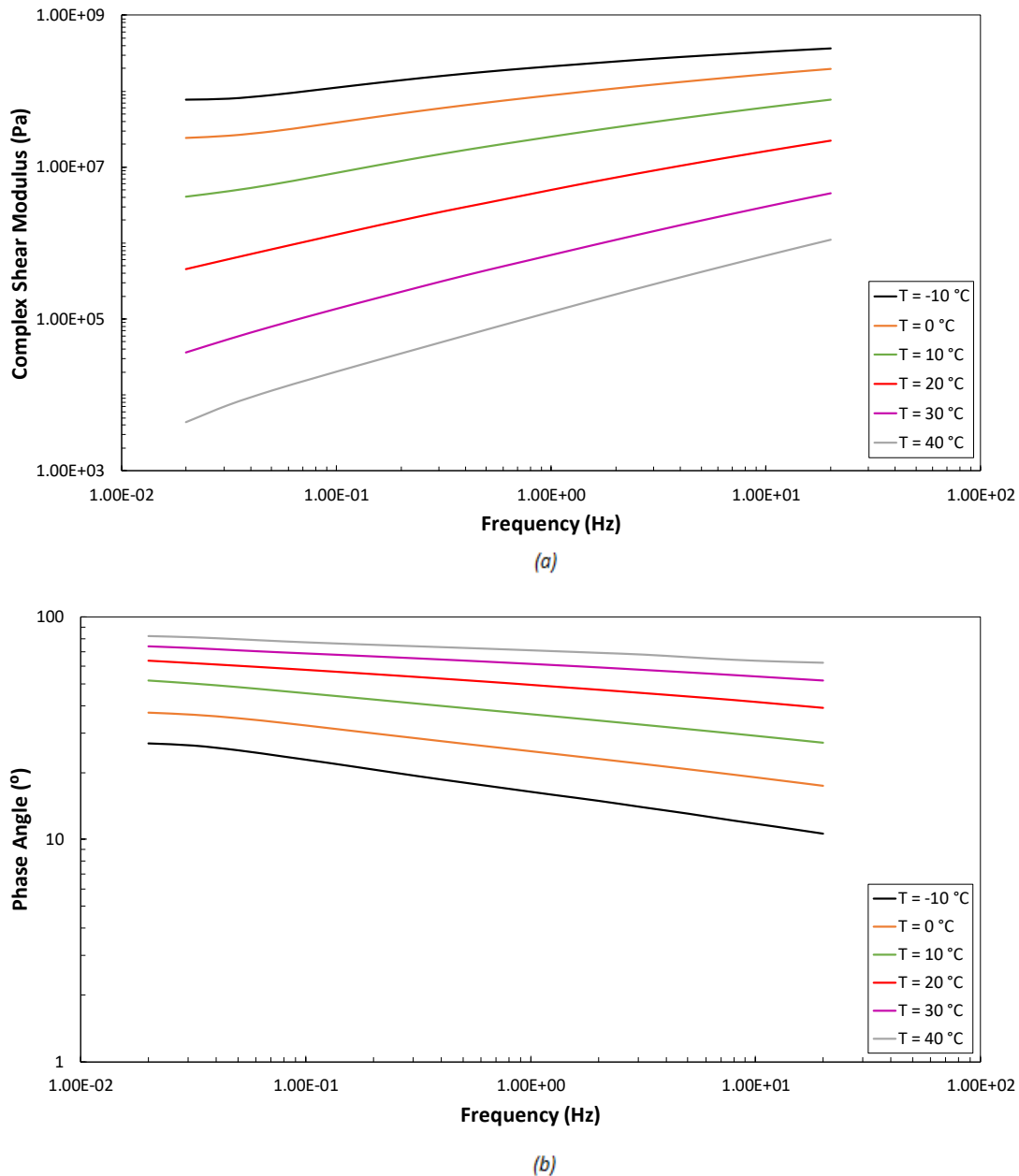


**Figure 3.29:** Example of average isothermal plots. (a) Complex shear modulus. (b) Phase angle.

The test was conducted in the stress-control mode, at temperatures from  $-10$  to  $40^{\circ}\text{C}$ , with  $10^{\circ}\text{C}$  increments, and frequencies ranging from  $0.02$  to  $20$  Hz. The applied sinusoidal stress level, per testing temperature and material, was selected in accordance with the results presented in *Sub-Section 3.6.1.3*. For neat bitumen measurements, the  $8$  mm plate was used for low to intermediate temperatures (i.e.  $-10$  to  $20^{\circ}\text{C}$ ), whereas the  $25$  mm plate was utilized for the remaining higher temperatures (i.e.  $30$  and  $40^{\circ}\text{C}$ ). In the case of mastics, keeping in mind that they are (quite) stiffer than pure bitumen, the  $8$  mm plate was found to provide consistent results at all testing temperatures and no change of the testing geometry was necessary. The material in the DSR chamber was allowed to reach thermal equilibrium for  $600$  sec with a tolerance of  $\pm 0.2^{\circ}\text{C}$ . *Table 3.12* summarizes the test conditions for the frequency sweep tests.

**Table 3.12:** Frequency sweep test conditions.

Feature	Material	
	Mastic	Bitumen
Loading Mode	Stress-Controlled	Stress-Controlled
Stress Levels	<i>Table 3.11</i>	<i>Table 3.11</i>
Testing Points	16	16
Test Frequencies (Hz)	0.02, 0.03, 0.05, 0.08, 0.13, 0.20, 0.32, 0.50, 0.80, 1.26, 2.00, 3.17, 5.02, 7.96, 12.60 and 20.00	0.02, 0.03, 0.05, 0.08, 0.13, 0.20, 0.32, 0.50, 0.80, 1.26, 2.00, 3.17, 5.02, 7.96, 12.60 and 20.00
Test Temperatures (°C)	-10, 0, 10, 20, 30 and 40	-10, 0, 10, 20, 30 and 40
Test Geometry (-ies)	8 mm Plate 2 mm Gap	-10÷20°C: 8 mm Plate 2 mm Gap  30 and 40°C: 25 mm Plate 1 mm Gap
Specimen Temperature Equilibrium	600 sec ± 0.2°C Tolerance	600 sec ± 0.2°C Tolerance

#### 3.6.1.4 Construction of complex shear modulus and phase angle master-curves

The generation of master-curves allows the visco-elastic analysis of the tested materials in a wide range of frequencies and/or temperatures, that cannot be obtained by normal measurements, due to certain limitations of the utilized equipment.

The construction of master-curves is based on the TTS principle. The TTS principle advocates that temperature and loading time impose the same changes on the rheological properties of the tested sample. The relation of time-temperature is only valid for thermo-rheological simple materials. The latter are materials whose structural character does not fundamentally change in the considered temperature range (Mezger 2002). This principle allows the horizontal shifting (*Fig. 3.30*) of the isothermal curves (*Fig. 3.29*), along the frequency axis, to a predefined reference temperature. The end result is a continuous, smooth curve, called the master-curve (*Fig. 3.30*). The extended frequency scale in a master-curve is referred to as reduced frequency scale, or simply reduced frequency (Hunter et al. 2015).

The amount of required shifting for each temperature is expressed through the shift factors ( $\alpha_T$ ). The shift factors are only dependent on temperature and, therefore, describe the temperature dependency of the visco-elastic behavior of the examined material. By plotting the  $\log(\alpha_T)$  against temperature (*Fig. 3.31*), a visual representation can be obtained with regards to the way the visco-elastic properties of the material change with temperature, since these values ( $\log(\alpha_T)$ ) can be interpreted as viscosity changes, always with respect to the viscosity at the reference temperature (Hunter et al. 2015).



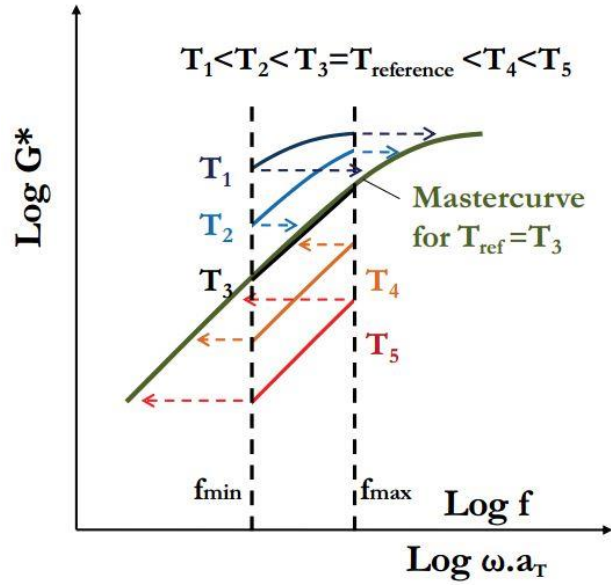


Figure 3.30: Example of the generation of master-curve (Van den Bergh 2011).

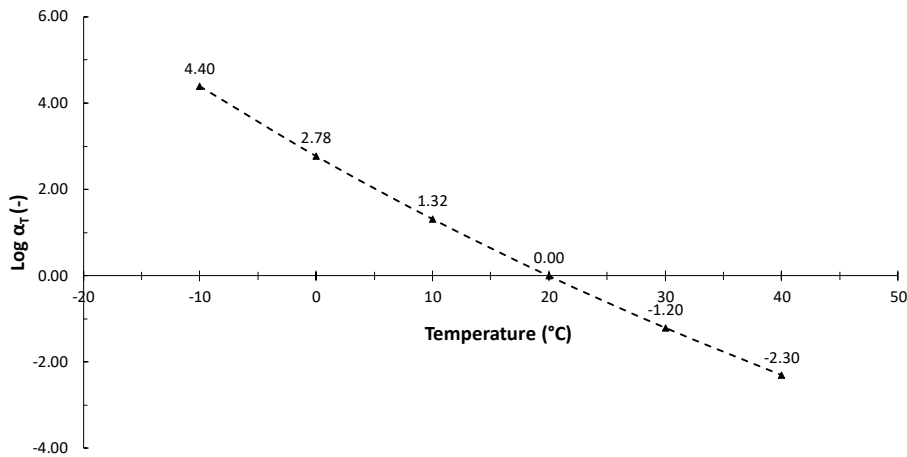


Figure 3.31: Example of plotting the  $\log(aT)$  against temperature with reference temperature of 20°C.

For the derivation of the shift factors several techniques can be employed, ranging from manual shifting and determination of the shift factors, to the utilization of mathematical equations that describe the relationship between the shift factors and temperature. With respect to the latter, the most widely used mathematical expressions are the Williams-Landel-Ferry (WLF) (Eq. 3.21) and Arrhenius (Eq. 3.22) functions.

$$\log(\alpha_T) = -\frac{C_1 \cdot (T - T_{ref})}{C_2 + T - T_{ref}} \quad (3.21)$$

where,

$\alpha_T$  = The shift factor

T = The analyzed temperature (°C)

$T_{ref}$  = The reference temperature (°C)

$C_1, C_2$  = Coefficients

$$\log(\alpha_T) = \frac{\Delta H_\alpha}{2.303 \cdot R} \cdot \left( \frac{1}{T} - \frac{1}{T_{\text{ref}}} \right) \quad (3.22)$$

where,

$\alpha_T$  = The shift factor

$\Delta H_\alpha$  = The activation energy (kJ/mol)

R = The universal gas constant (8.314 J/mol/K)

T = The analyzed temperature (K)

$T_{\text{ref}}$  = The reference temperature (K)

In this study, the WLF equation was used to obtain the shift factors and construct the various master-curves. The procedure included manual shifting of the isothermal plots to a reference temperature of 20°C and determination of the estimated shift factors. The derivation of the shift factors based on the WLF equation was done by minimizing the squared summed error of the estimated (manual) and predicted (WLF) shift factors by using as variables the coefficients  $C_1$  and  $C_2$ . The WLF generated master-curves, calculated shift factors and corresponding  $C_1$  and  $C_2$  coefficients, for all materials, are presented in Appendix C.

The modified Christensen, Anderson and Marasteanu (CAM) model was employed to describe the resulting master-curves of the complex shear modulus (Eq. 3.23) (Yusoff et al.). The same mathematical expression was used for fitting a smooth curve in the  $\delta$  master-curves (Eq. 3.24), as it was observed that the generated phase angle data correlated more than satisfactorily with the experimental ones.

$$G^*(f) = G_e^* + \frac{G_g^* - G_e^*}{\left[ 1 + \left( \frac{f_c}{f} \right)^k \right]^{\frac{m}{k}}} \quad (3.23)$$

$$\delta(f) = \delta_e + \frac{\delta_g - \delta_e}{\left[ 1 + \left( \frac{f_d}{f} \right)^k \right]^{\frac{m}{k}}} \quad (3.24)$$

where,

$G^*(f)$  = The complex shear modulus as a function of the reduced frequency ( $[F]/[A]$ )

f = The reduced frequency (Hz)

$G_e^*$  = The complex shear modulus at equilibrium state,  $f \rightarrow 0$  ( $[F]/[A]$ )

$G_g^*$  = The glassy complex shear modulus,  $f \rightarrow \infty$  ( $[F]/[A]$ )

$f_c$  = Location parameter (Hz)

k, m = Shape parameters

$\delta(f)$  = The phase angle as a function of the reduced frequency (°)

$\delta_e$  = The phase angle at equilibrium state,  $f \rightarrow 0$  (°)

$\delta_g$  = The phase angle when  $f \rightarrow \infty$  (°)

$f_d$  = Location parameter (Hz)

Fig. 3.32 and 3.33 illustrate an example of the fitting potential of the utilized equations in the case of aged mastic and “fresh” neat bitumen, respectively. The results indicate that the considered model can describe accurately enough the  $G^*$  master-curve, whereas, in the case of the  $\delta$  master-curve, a rather small deviation is observed between the experimental and predicted data at low frequencies (i.e.  $\sim 0.001\text{--}0.01$  Hz). The latter remarks hold true for all materials considered in this study. The modified CAM model fitting parameters, for all tested materials, are reported in Appendix D.

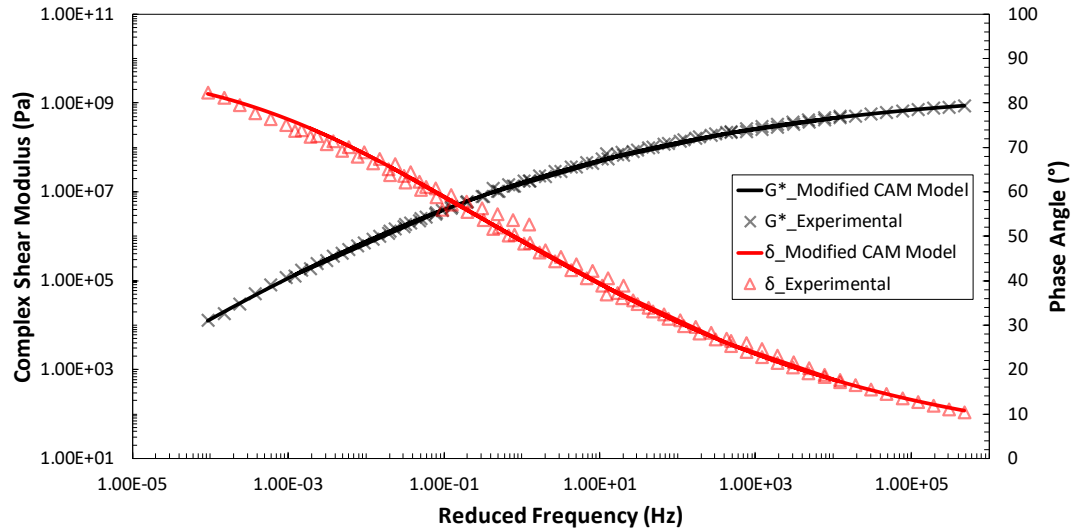


Figure 3.32: Fitting potential of the modified CAM model. Example of an aged mastic.

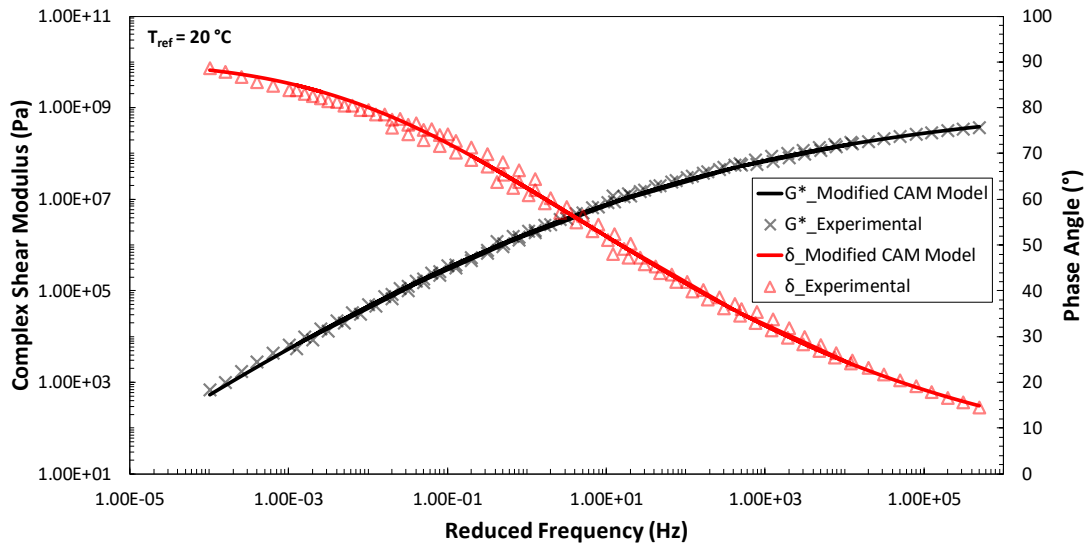


Figure 3.33: Fitting potential of the modified CAM model. Example of “fresh” bitumen.

### 3.6.2 Fourier transform infrared (FTIR) spectroscopy

#### Basic principles

The Fourier transform infrared spectroscopy (FTIR) is one of the most widely used methods to characterize the chemical composition of materials. The method is based on the interaction between infrared radiation and the existing bonds in a material, defining its chemical composition. From a technical point of view, an infrared light beam is charged into the sample leading to vibrations and rotations of the molecule bonds at distinct frequencies (Van den Bergh 2011). The FTIR spectroscopy utilizes the infrared spectrum, which constitutes part of the electromagnetic spectrum (*Fig. 3.34*) (Hagos 2008).

Radio wave	Microwave	Infrared	Visible and ultraviolet	X-Ray	γ-ray.
	10	10 <sup>3</sup>	10 <sup>5</sup>	10 <sup>7</sup>	10 <sup>9</sup>
Energy (J mol <sup>-1</sup> )					
10 <sup>3</sup>	10 <sup>-2</sup>	10 <sup>-5</sup>	0,5.10 <sup>-6</sup>	10 <sup>-10</sup>	10 <sup>-12</sup>
1	10 <sup>-3</sup>		10 <sup>-6</sup>	10 <sup>-8</sup>	10 <sup>-11</sup>
Wavelength λ (m)					

**Figure 3.34:** Various regions of the electromagnetic spectrum (Van den Bergh 2011).

Regarding the electromagnetic radiation, the velocity of propagation in a vacuum is constant, throughout the whole electromagnetic spectrum, and equal to the speed of light ( $c$ ). The propagation can be conceived as a wave with velocity defined as the product of the wavelength ( $\lambda$ ) and the frequency ( $\nu$ ). The former (wavelength) is defined as the distance between two successive peaks while the latter (frequency) as the number of cycles per second. The energy of an infrared photon is related to these two quantities through Bohr's equation (*Eq. 3.25*), by utilizing Planck's constant ( $h$ ). *Eq. 3.25* demonstrates that the photon energy is proportional to the frequency and the wave number (Van den Bergh 2011).

$$E = h \cdot \nu = \frac{h \cdot c}{\lambda} = h \cdot c \cdot \bar{\nu} \quad (3.25)$$

where,

$E$  = The energy of photon (J)

$h$  = Planck's constant ( $6.626 \cdot 10^{-34}$  J · s)

$\nu$  = The frequency (cycles/s)

$c$  = The speed of light ( $2.997925 \cdot 10^8$  m/s)

$\lambda$  = The wavelength (m)

$\bar{\nu}$  = The wave number ( $\text{cm}^{-1}$ )

The chemical composition of a material is described by the bond energy between its components. Molecules should present a specific bond or structure, such as a dipole moment which changes upon atomic vibrations, in order for infrared absorption to be used. When infrared radiation is charged in the material, different types of bonds will absorb different frequencies. This frequency is in essence energy of a specific photon that brings the particular bond to a specific excited state (vibrations). The interaction of infrared radiation should be conceived as changes in molecular dipoles resulting from rotations and vibrations of the atoms, the latter being very important for the identification

of the types of functional groups present in the examined material. Two general modes of atomic vibrations can be distinguished: a) stretching and b) bending (*Fig. 3.35*). The former refers to the modification of the distance of two atoms along their bond-axis while the latter to the change of the angle between two bonds (Van den Bergh 2011).

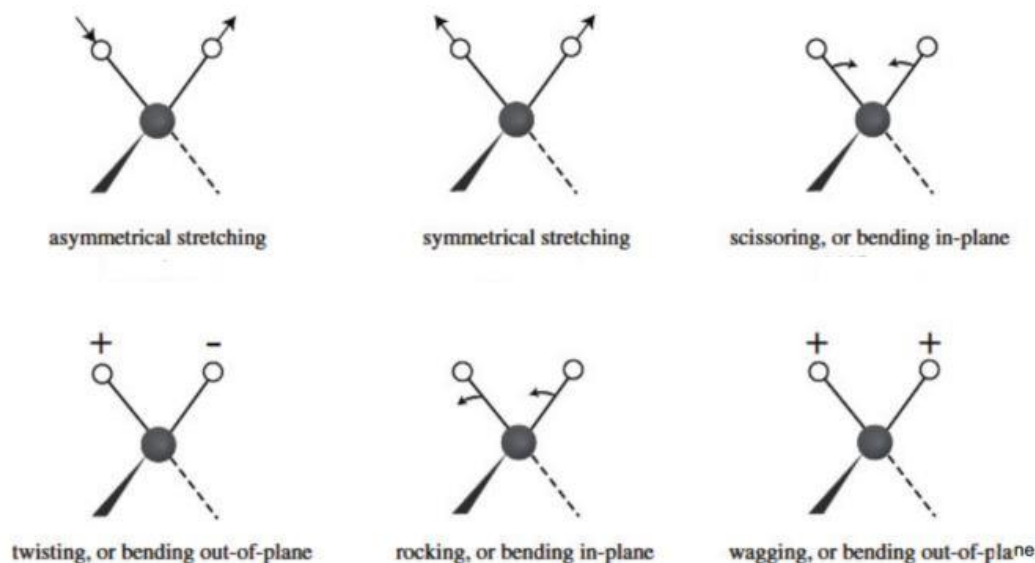


**Figure 3.35:** Different types of stretching and bending vibrations (Van Lent 2013).

### 3.6.2.1 Attenuated total reflectance (ATR) spectrometer

Depending on the way that the infrared beam is charged to the sample, two modes of conducting FTIR measurements can be distinguished: a) Transmittance of the beam through the sample and b) reflection of the beam within the sample (Van den Bergh 2011).

In the first method, radiation is sent through the sample and specific wavelengths are absorbed. In this way, transmission absorption spectra can be derived. Transmission spectroscopy constitutes the oldest infrared method and involves a relatively demanding sample preparation (Van den Bergh 2011). Moreover, for materials with high absorption coefficients, such as bitumen, there exists the drawback that transmission is extremely low, or even impossible, leading to an unacceptably low signal to noise ratio (Hofko et al. 2017). For all above reasons, transmission spectroscopy is nowadays replaced by the reflectance spectroscopy (second method).

Reflectance spectroscopy can be realized in three modes: a) Diffuse Reflectance Infrared Fourier Spectroscopy (DRIFTS), b) Ranging Angle Infrared Reflectance Spectroscopy (RAIRS) and c) Attenuated Total Reflectance (ATR). In the first mode, the sample must be in powder form and the measurements rely on the particles' scattering and refraction. RAIRS involves specialized sample preparation and requires an absolutely plane film. Hence, ATR is the method widely used for the analysis of bitumen (Hofko et al. 2017).

The ATR method is based on the principal of total internal reflection. An evanescent light wave is attenuated, by virtue of the vibrations of molecules at the interface between the tested sample and a crystal, which possesses a high refraction index (Hofko et al. 2017). For measurements in the mid-infrared region, crystals of diamond, Zinc Selenide (ZnSe) or Germanium (Ge) are considered suitable (Van den Bergh 2011). The ATR can be further distinguished in multiple-ATR (*Fig. 3.36a*) and single-point-ATR

(Fig. 3.36b). In the first case, the light beam is reflected more than once in the crystal (multiple), thus, “hitting” the tested sample in multiple positions, whereas in the second case the beam is reflected only once by the sample and only in a single position.

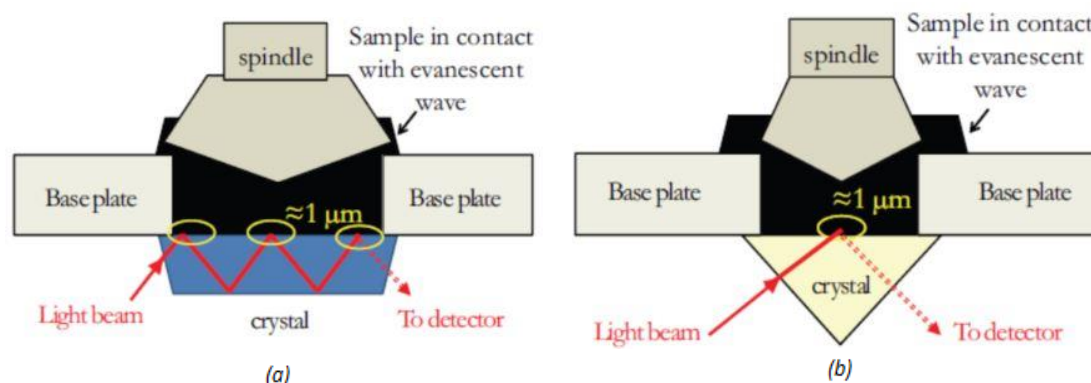


**Figure 3.36:** FTIR/ATR spectrometer. (a) Multiple FTIR/ATR. (b) Single point FTIR/ATR (Van den Bergh 2011).

The outgoing attenuated evanescent light is collected and analyzed by a detector and an interferogram is derived. The latter is expressed as a plot of the absorbance or transmittance on the vertical axis against wave number on the horizontal axis (Fig. 2.14, Sub-Section 2.2.3.2). The absorbance and transmittance are related through Eq. 3.26. The absorbance is equal to the difference of the logarithms of the intensity of the entering light beam and the intensity of the transmitted one (Eq. 3.27) (Van den Bergh 2011).

$$A = \log \frac{1}{T} \quad (3.26)$$

$$A = \log I_0 - \log I = \log \frac{I_0}{I} = -\log T \quad (3.27)$$

where,

$A$  = The absorbance

$T$  = The transmittance

$I_0$  = The intensity of light beam entering the sample

$I$  = The intensity of light beam transmitted by the sample

### 3.6.2.2 FTIR/ATR spectrometer test method

For the purpose of the present research, the chemical evaluation of the various materials was performed by utilizing the Spectrum 100 FTIR spectrometer of Perkin Elmer with a single-point-ATR add-in (Fig. 3.37). The considered wave number region, during measurements, was set in between 600 and 4000  $\text{cm}^{-1}$ . Background checks and samples' scans were carried out with individual 20 scans and a resolution of 4  $\text{cm}^{-1}$ . The ultimate derived interferogram for each sample constitutes the mean record of the 20 individual scans.

For reproducibility reasons, three replicates were tested for each analysed material. The demonstrated infrared spectrum of each material (Chapters 5 and 6) was determined as the mean value of its replicates' spectra, while the indices of interest were calculated for each replicate individually and reported as the mean value with its standard deviation.



**Figure 3.37:** Spectrum 100 FTIR spectrometer Perkin Elmer with a single-point-ATR fixture.

### 3.6.2.3 Analysis method of infrared spectra

Amongst the various methods for infrared spectra analyses, the recommendations provided by Hofko et al. (2017) (see *Sub-Section 2.2.3.2*) were considered in this study, for the post-processing of the FTIR/ATR raw data and the derivation of ageing indices. The absorbance of the asymmetric stretching vibration of the aliphatic group, at wave number  $2923\text{ cm}^{-1}$ , was utilized for the spectrum normalization, which is performed according to *Eq. 3.28* (Hofko et al. 2017).

$$y_{\text{normalized}}(x) = \frac{y(x)}{y(2923\text{ cm}^{-1})} \quad (3.28)$$

where,

$y_{\text{normalized}}(x)$  = Normalized absorbance value at wave number (x)

$y(x)$  = Original absorbance value at wave number (x)

$y(2923\text{ cm}^{-1})$  = Original absorbance value at wave number  $2923\text{ cm}^{-1}$

The boundary-wave numbers for the carbonyls and sulfoxides groups are presented in *Table 3.13* (Hofko et al. 2017). It should be noted that, in the research of Hofko et al. (2017), these boundaries were applied for the conventional bitumen, while, in the case of polymer modified bitumen they were slightly altered. The present thesis does not deal with polymer modified bitumen and, thus, only information of interest are cited. The integration of areas was performed by approximating the area below the infrared spectrum as a sequence of trapezoids. *Eq. 3.29* and *3.30* were employed for the calculation of the CI and SI, respectively.

**Table 3.13:** Area integration boundary-wave numbers (Hofko et al. 2017).

Functional group	Lower boundary (cm <sup>-1</sup> )	Upper boundary (cm <sup>-1</sup> )
Carbonyls	1666	1746
Sulfoxides	924	1066

$$CI = \int_{1666}^{1746} y_{\text{normalized}}(x) dx \quad (3.29)$$

$$SI = \int_{924}^{1066} y_{\text{normalized}}(x) dx \quad (3.30)$$

where,

$y_{\text{normalized}}(x)$  = Normalized absorbance value at wave number  $x$

The utilization of *Eq. 3.29* for the derivation of the CI yields also a non-zero value for the unaged materials, regardless if there is a peak or not at the region around the wave number  $1700 \text{ cm}^{-1}$ . As Hofko et al. (2017) mention in their study, this is, of course, an artificial effect and the CI of the unaged materials should be reported as zero, if visual inspection of the infrared spectrum verifies that there is no peak at the carbonyls' group region.



# 4

## Mineral fillers tests results and discussion

#### 4.1 Particles' size distribution and specific surface area

In this section, the results of the laser diffraction test are presented and discussed. Two samples were tested for each material. The reported gradation curves and estimated SSAs are the average of the two measurements.

##### *Particle's size distribution*

In Fig. 4.1, the gradation curves for the six considered mineral fillers are presented, while Table 4.1 shows the particles' size distribution in terms of figures.

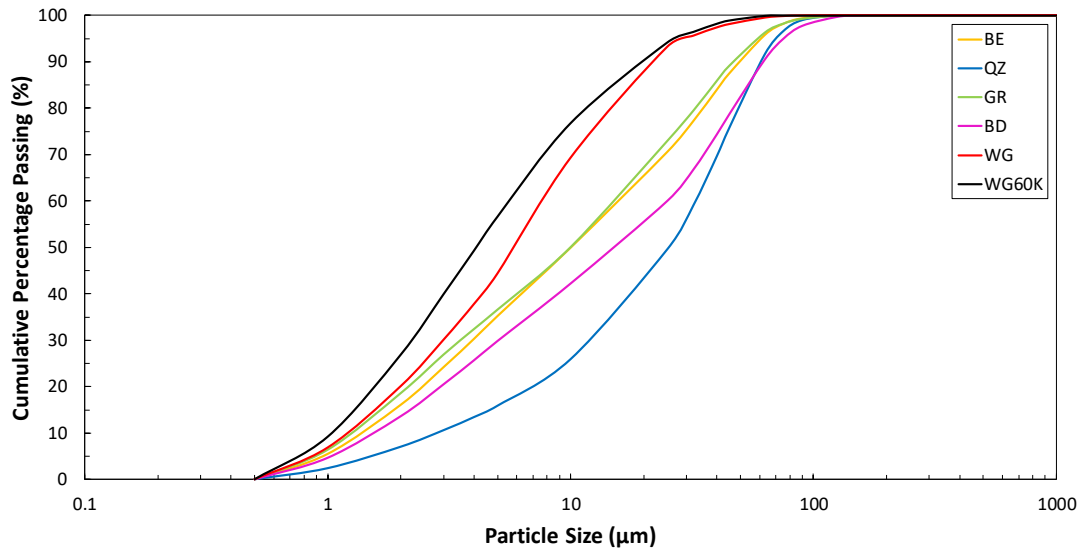


Figure 4.1: Mineral fillers gradation curves.

Table 4.1: Mineral fillers cumulative percentage passing.

Particle size (µm)	Cumulative percentage passing (%)					
	WG60K	WG	BD	GR	QZ	BE
0.5	0.00	0.00	0.00	0.00	0.00	0.00
1.0	9.18	6.85	4.63	6.38	2.40	5.47
2.0	26.90	20.10	13.60	18.59	7.03	16.08
3.0	39.94	30.09	20.47	26.89	10.59	24.19
4.0	49.31	37.77	25.63	32.37	13.40	30.27
5.0	56.64	44.36	29.79	36.56	15.85	35.20
10.0	76.81	69.30	42.18	50.04	25.89	49.94
25.0	94.21	93.20	59.97	72.92	49.56	70.60
32.0	96.49	95.58	66.71	79.44	59.00	77.25
40.0	98.25	97.36	74.32	85.89	69.63	84.02
45.0	98.95	98.09	78.65	89.13	75.72	87.53
63.0	99.95	99.48	90.43	96.27	91.58	95.81
75.0	100.00	99.81	94.88	98.20	96.55	98.21
90.0	100.00	99.95	97.71	99.25	98.95	99.41
125.0	100.00	100.00	99.63	99.92	100.00	100.00
150.0	100.00	100.00	99.92	100.00	100.00	100.00
180.0	100.00	100.00	100.00	100.00	100.00	100.00

The mineral fillers' particles size can be described with a single figure through the Fineness Modulus (FM). FM determines the relative fineness of an aggregate and is derived by dividing the sum of the percentages larger than 75, 50, 30, 20, 10, 5, 3 and 1  $\mu\text{m}$ , or in other words the sum of the retained cumulative percentages of these "sieves", by 100 (Eq. 4.1). The finer the mineral filler the lower its corresponding FM (NCHRP 9-45 2010). Fig. 4.2 illustrates the calculated FM of the six mineral fillers.

$$FM = \frac{\sum P_{i,Ret}}{100}, i = 75, 50, 30, 20, 10, 5, 3 \text{ and } 1 \mu\text{m} \quad (4.1)$$

where,

FM = The fineness modulus

$P_{i,Ret}$  = The percentage retained on "sieve" (i) (-)

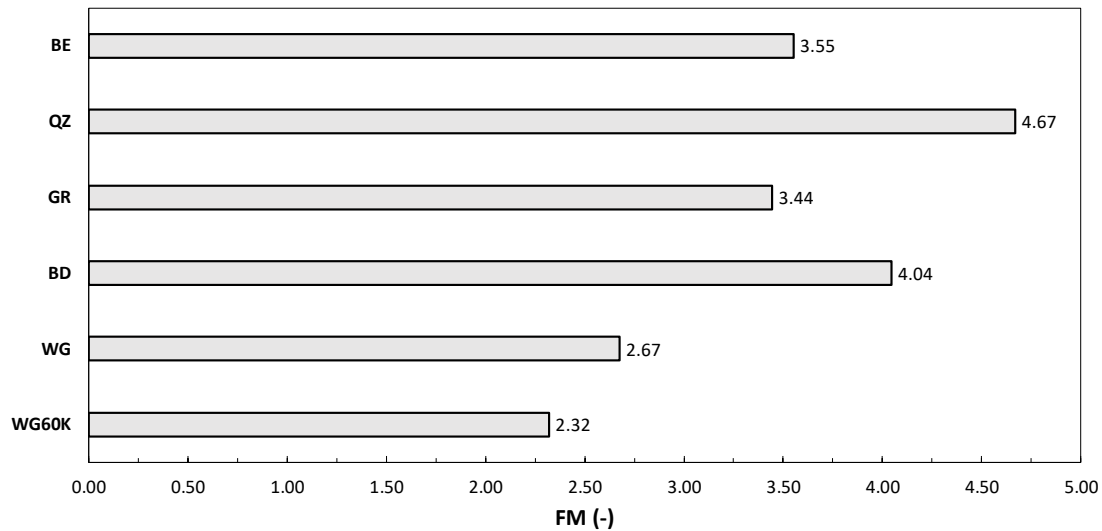


Figure 4.2: Mineral fillers fineness modulus.

The analysis of the mineral fillers' particles size distribution indicates that the considered materials cover a wide range of different gradations. More specifically, WG60K and WG constitute the finest mineral fillers, followed by GR and BE, which show a rather similar gradation. BD and QZ are the coarser mineral fillers, amongst the considered materials, with the latter presenting the highest percentage of large particles.

As mentioned in *Sub-Section 3.2.1*, QZ was included in the study to demonstrate any potential effect of the mineral matter on the oxygen diffusion path, during ageing of the mastics. The coarse nature of this particular mineral filler is considered to be advantageous for capturing the aforementioned effect, since, provided that such mechanism exists, the larger the mineral filler particles the higher their influence is expected to be.

### Specific surface area

In *Fig. 4.3* the SSA of the mineral fillers, as determined by the laser diffraction test, is presented. It can be observed that the finer the mineral matters the larger the estimated SSA. Having mentioned the latter, a nice correlation was found between the FM and the estimated SSA (*Fig. 4.4*).

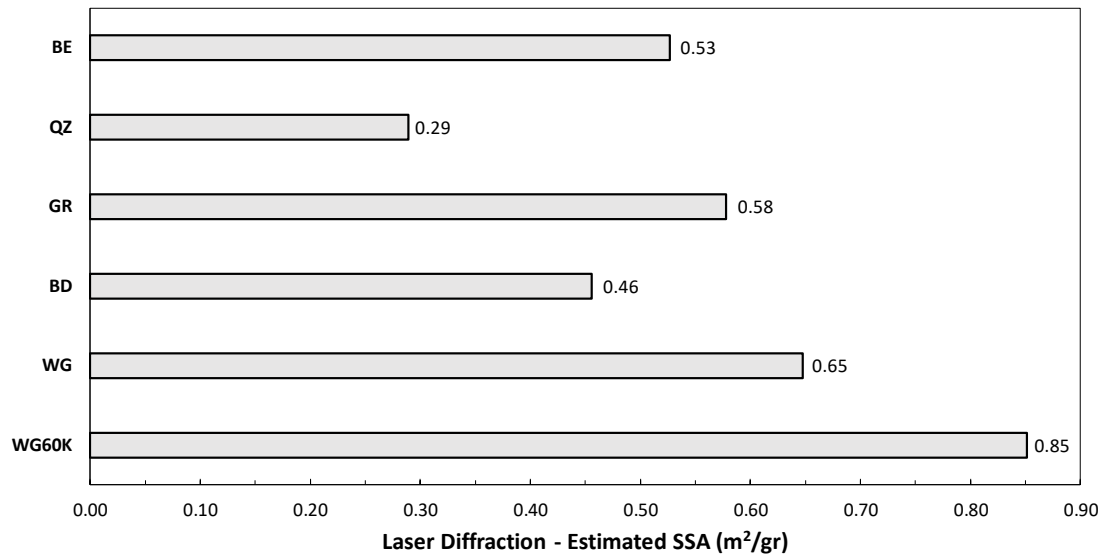


**Figure 4.3:** Mineral fillers estimated specific surface area.

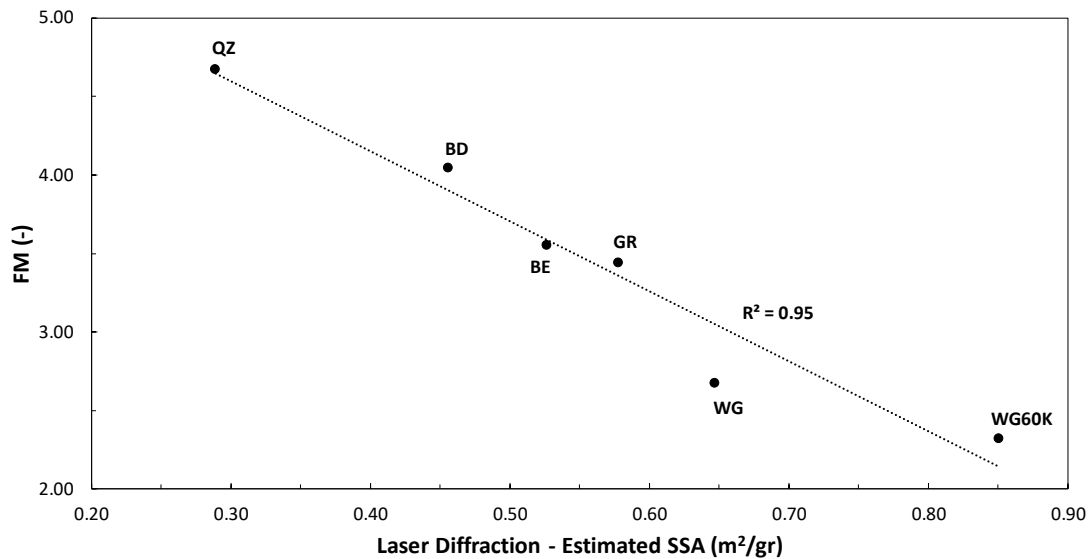


**Figure 4.4:** Mineral fillers fineness modulus and estimated specific surface area correlation.

### 4.2 Microscopic imaging

In this section the morphology of the mineral fillers is presented and discussed. In *Fig. 4.5*, *4.6*, *4.7*, *4.8*, *4.9* and *4.10* the microscopic images of WG60K, WG, BD, GR, QZ and BE, at four magnification scales, are presented, respectively.

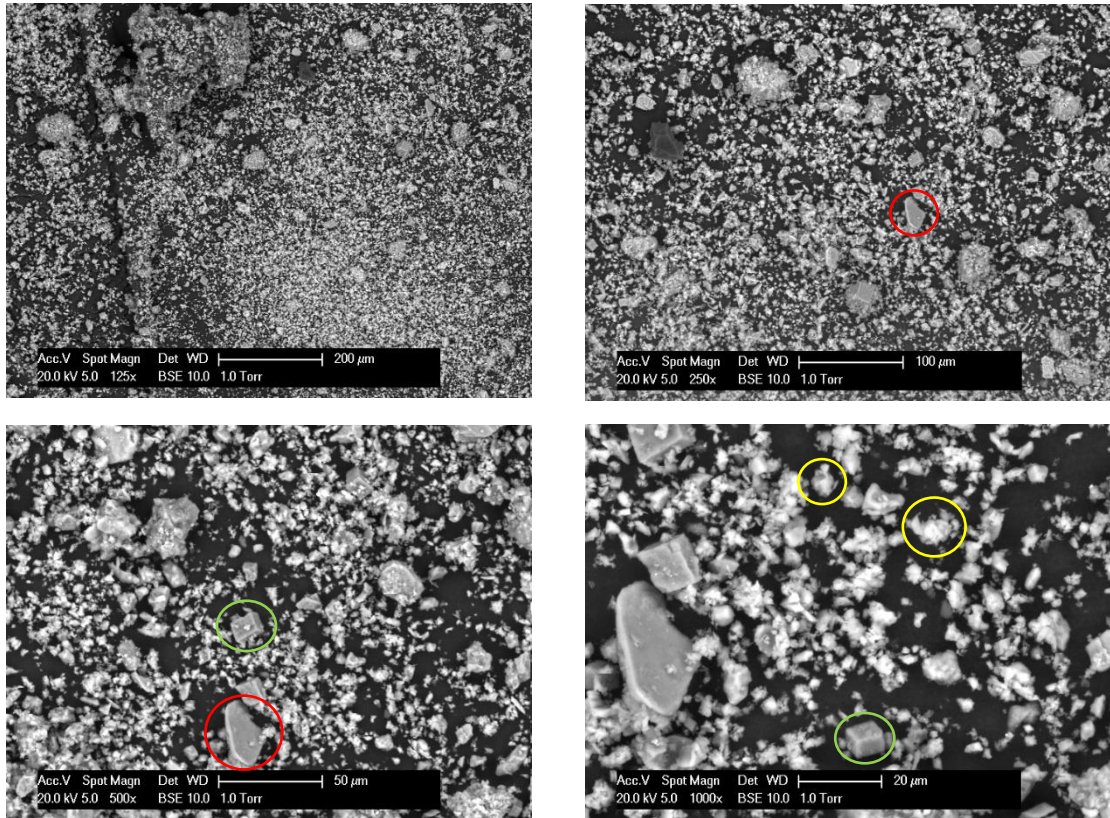


Figure 4.5: Microscopic imaging of WG60K.

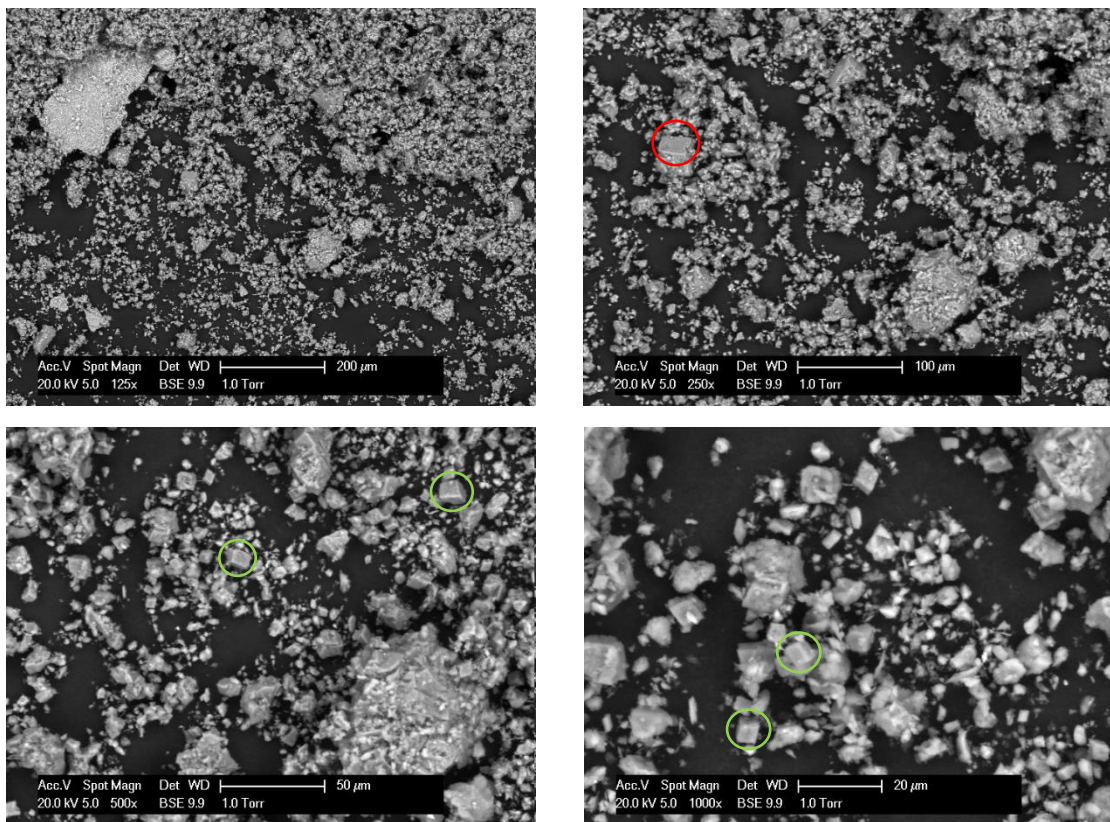


Figure 4.6: Microscopic imaging of WG.

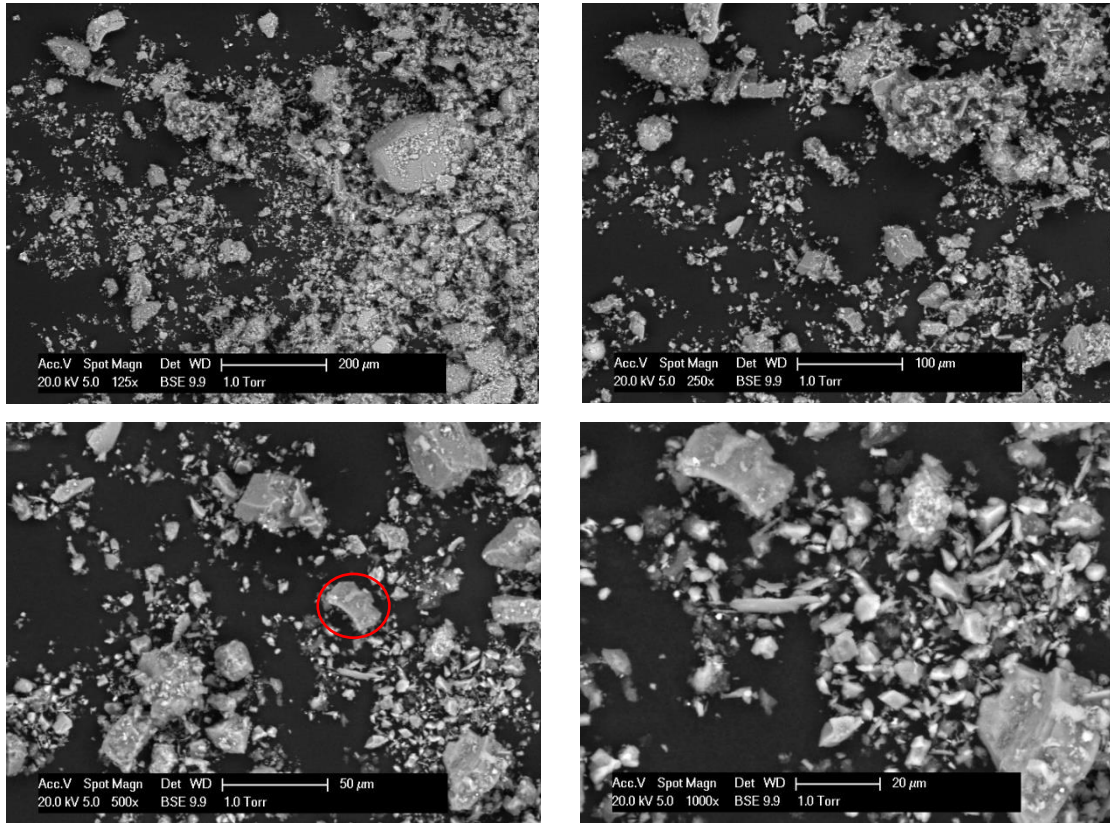


Figure 4.7: Microscopic imaging of BD.

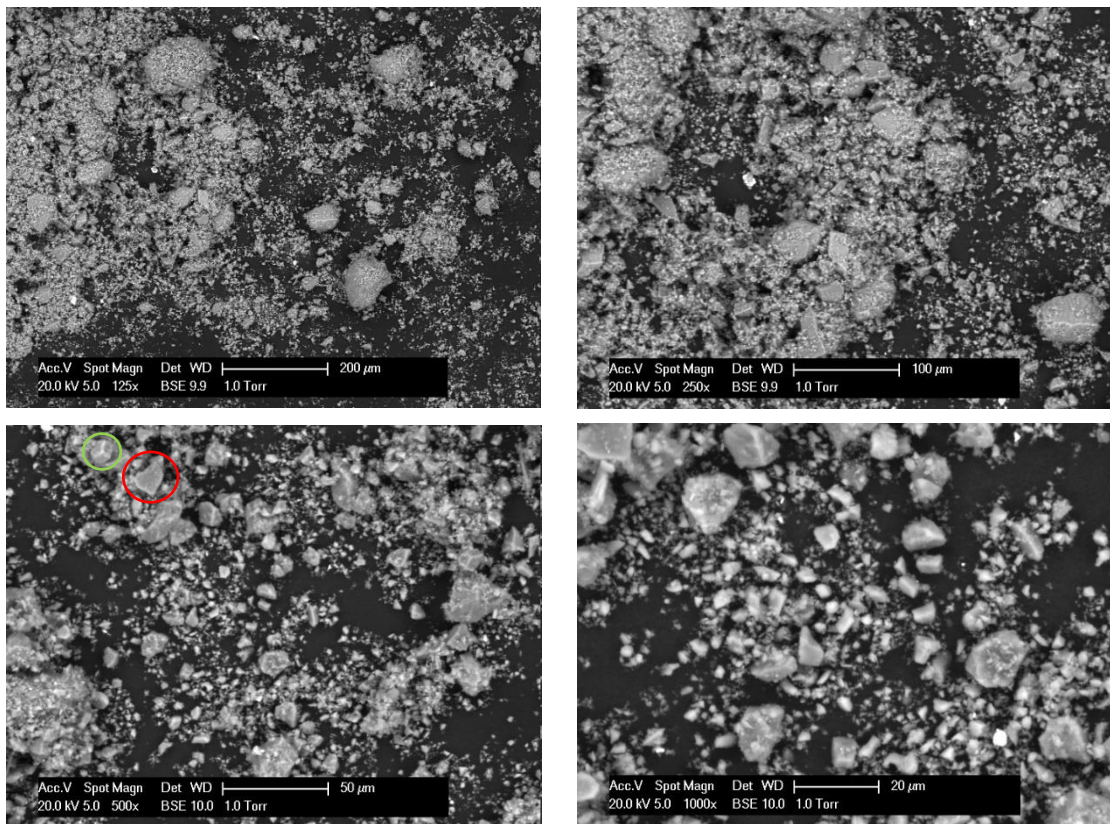


Figure 4.8: Microscopic imaging of GR.

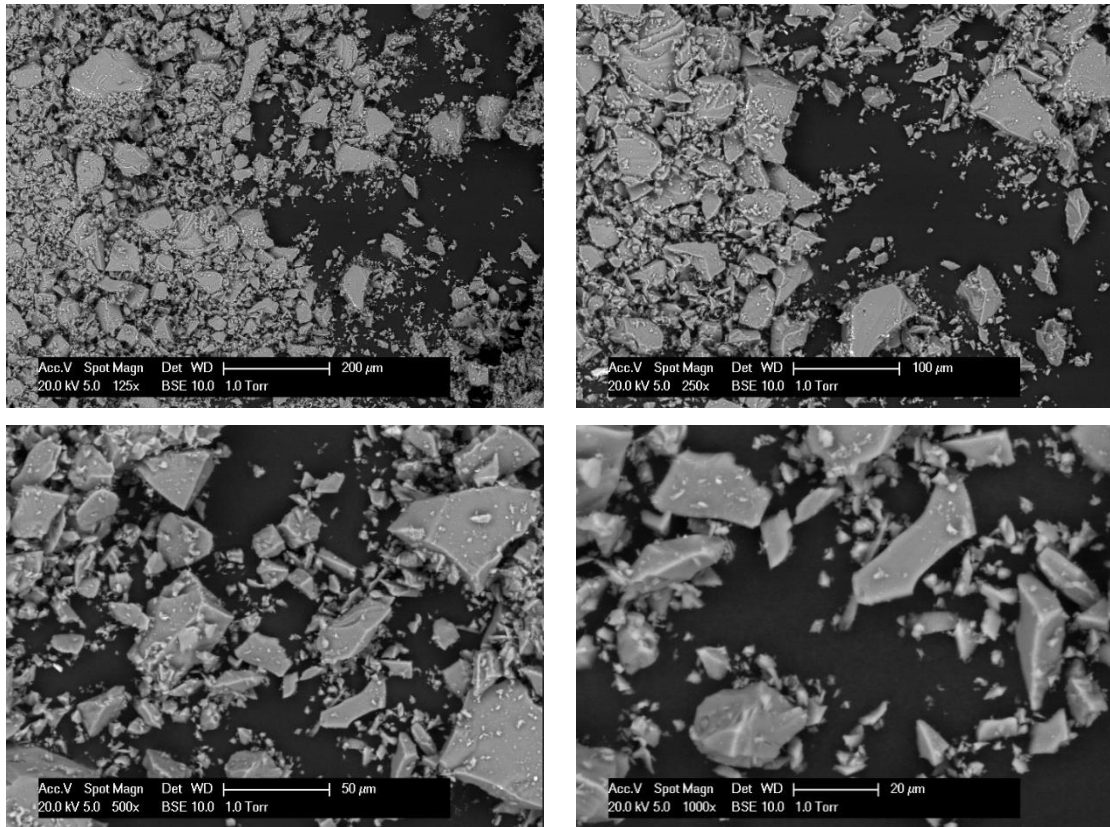


Figure 4.9: Microscopic imaging of QZ.

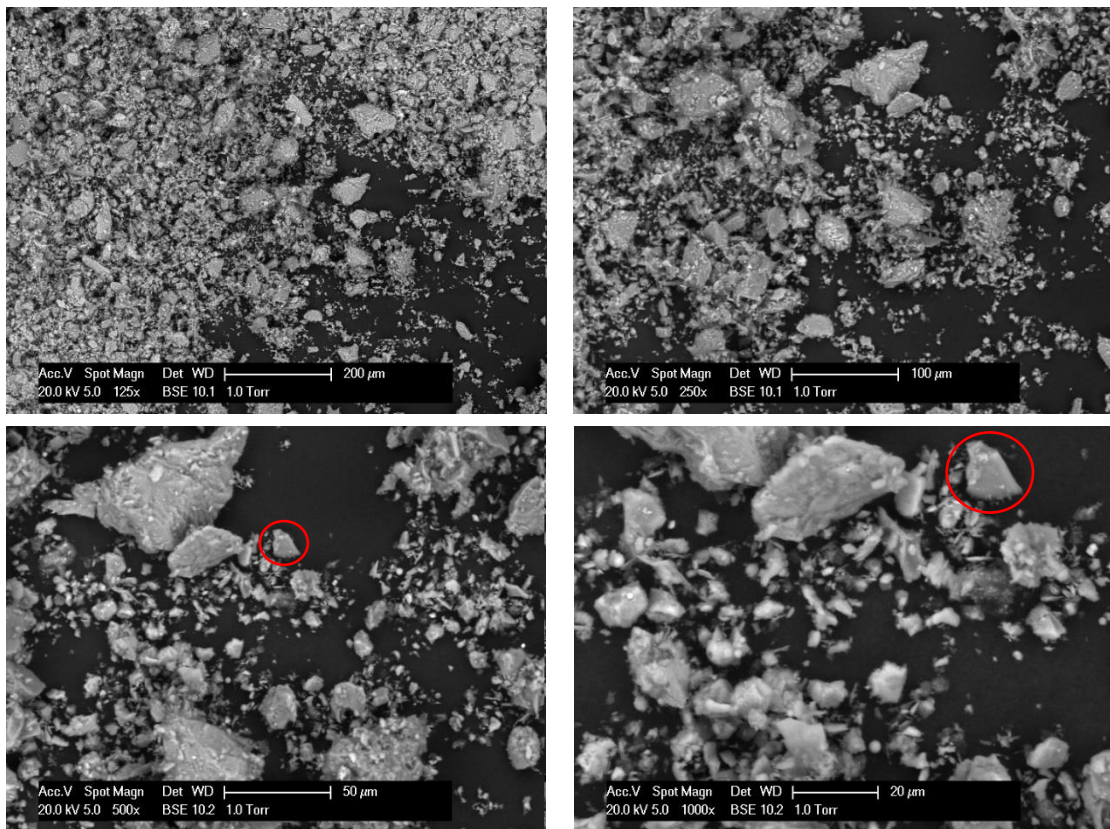



Figure 4.10: Microscopic imaging of BE.

By investigating the microscope images of the mineral fillers several information can be derived for their composition as well as their particles' size and surface characteristics.


With respect to the composition of the mineral fillers, by comparing WG60K (*Fig. 4.5*) and WG (*Fig. 4.6*), one can observe the particles of hydrated lime in the former (yellow marks), which are absent in the pure limestone (i.e. WG). Based on their mineralogical analysis (*Section 4.7*) both mineral fillers are rich in calcite, which is also found in their microscopic analysis (green marks), and, finally, a rather limited amount of quartz particles, which are characterized by their extremely smooth surface texture, can also be observed (red marks). Quartz particles are found in all mineral fillers, with QZ consisting exclusively of such particles (*Fig. 4.9*).

With respect to particles' characteristics, the microscope images seem to correlate very well with the particles' size distribution analysis presented in *Section 4.1*. Talking in extremes, the (very) fine nature of WG60K and WG as well as the coarseness of QZ are nicely captured in *Fig. 4.5, 4.6* and *4.9*, respectively. In addition, the intermediate state of the rest of the mineral fillers is also a fact. Regarding, particles' morphology a relative ranking was established for the various mineral fillers with respect to their particles' type (i.e. granular or angular) and surface texture (i.e. rough or smooth). The results are presented in *Tables 4.2* and *4.3*, respectively.

**Table 4.2:** Mineral fillers particles type ranking.

Mineral filler	Particles type
WG60K	Granular
WG	
BE	
BD	
GR	
QZ	
	Angular

**Table 4.3:** Mineral fillers particles surface texture ranking.

Mineral filler	Particles surface texture
WG60K	Rough
BE	
WG	
GR	
BD	
QZ	
	Smooth

### 4.3 Fractional voids

In this section the results of the RV test for the mineral fillers are reported and discussed. Three samples were tested for each material and their individual measurements are summarized in *Table 4.4*. The final results are presented in *Fig. 4.11* by means of the average of the three measurements including the standard deviation.



Table 4.4: Mineral fillers Rigden voids measurements.

Mineral filler	RV (%)			
	Measurement 1	Measurement 2	Measurement 3	Average
WG60K	47.30	46.90	47.40	47.20
WG	39.60	39.70	39.40	39.57
BD	33.50	33.7	33.50	33.57
GR	32.10	31.70	32.00	31.93
QZ	32.90	33.40	32.90	33.07
BE	35.80	35.90	36.20	35.97

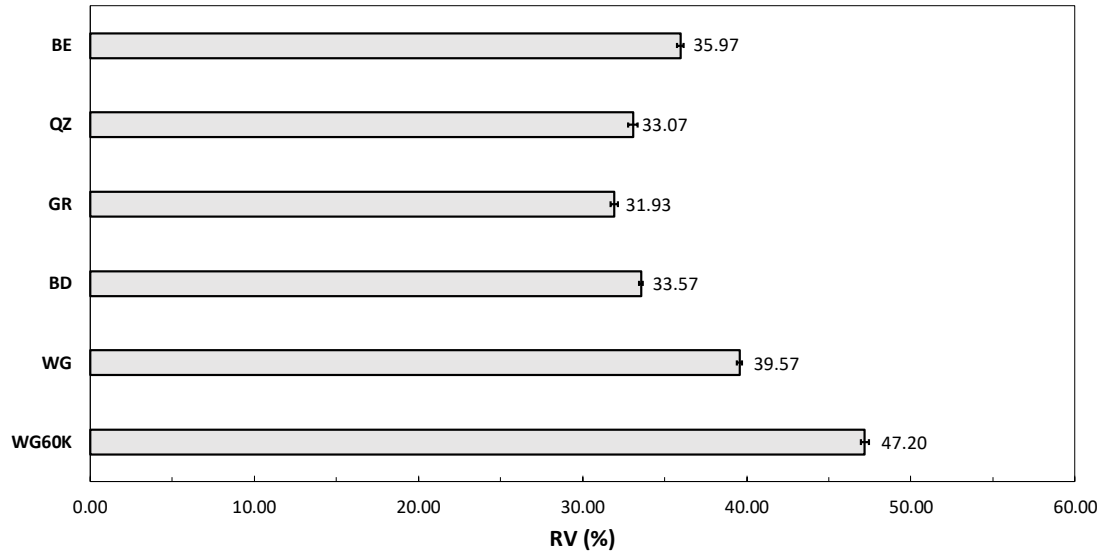


Figure 4.11: Mineral fillers Rigden voids.

Fig. 4.11 demonstrates that WG60K possesses the highest RV value of all mineral fillers, which is very well expected due to the presence of the granular with rough surface hydrated lime particles. This result is consistent with findings from literature, where it is reported that when mixed fillers are considered (i.e. blend of a base mineral filler with hydrated lime), the WG60K in this case (see *Sub-Section 3.2.1*), the RV content increases with increasing amount of hydrated lime. Typical values in the range of 45-50% are found for 25wt% of hydrated lime in a mineral filler mixture (Schellenberg & Eulitz 1999, Grabowski 2009). Finally, GR presents the lowest RV content followed by QZ.

The RV results can be correlated to the ESEM images of the mineral fillers presented in *Section 4.2*. As mentioned in *Sub-Section 3.5.2* the RV content is regulated by the particles' size, distribution, shape and surface texture. WG60K consists mostly of granular particles with very rough texture, compared to the other materials, which justifies its higher RV value. To cancel out the effect of the particles' size and size distribution it would be interesting to compare GR and BE, since their gradation is fairly similar (*Fig. 4.1*). The morphological analysis of these fillers reveals that GR consists mostly of angular particles with intermediate surface roughness, whereas in BE mostly granular particles with rough surface are found. The latter observed differences, shape and texture-wise, are considered to entail a higher RV value for BE compared to GR. Overall, the RV results seem to correlate quite satisfactorily with the results presented in *Tables 4.2 and 4.3 (Section 4.2)*. Nevertheless, QZ presents a slightly higher RV value than GR, despite the fact that it evidently consists of exclusively angular type particles with the smoothest surface texture observed amongst the considered materials. This could be the

result of the coarseness of QZ compared to GR in the context that the smaller particles of GR fill the voids between its larger particles, thus reducing the RV content.

#### 4.4 Specific surface area – BET method

In this section the results of the mineral fillers' SSA are presented, as determined through gas sorption measurements and by utilizing the BET method. Moreover, a comparison and evaluation of the two methods for the determination of the SSA (i.e. laser diffraction and BET method) is provided.

A high SSA value implies a large interface between the mineral matter and the bitumen. As a result, it is expected that the larger the value of the SSA the more intensive the physico-chemical interactions between the two materials. In *Fig. 4.12* the SSAs of the mineral fillers are shown. The utilized equipment provides the value of the measured parameter along with the standard deviation.

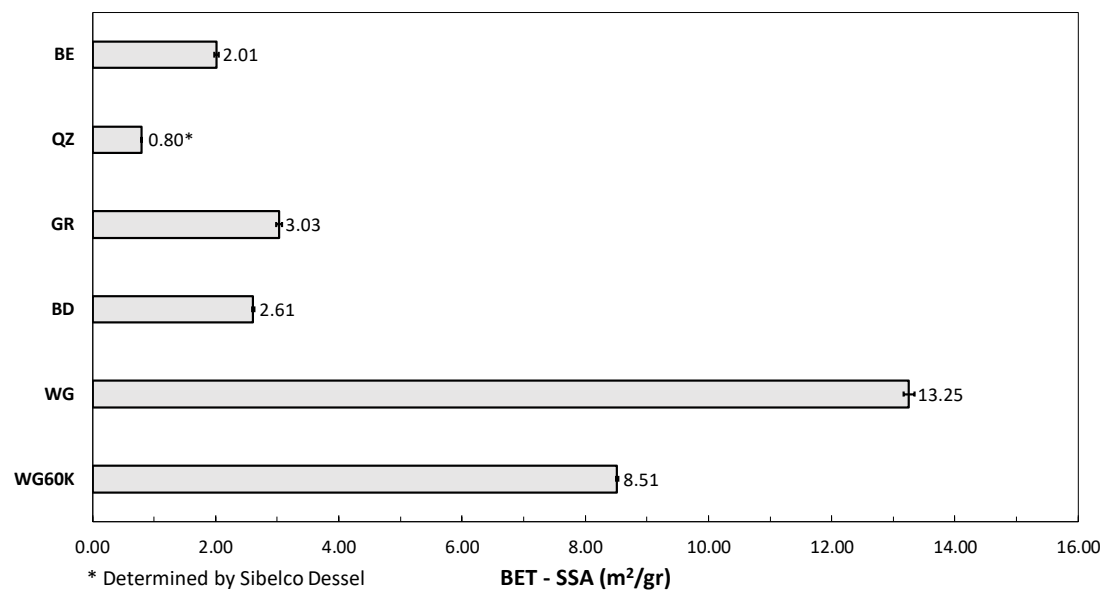


**Figure 4.12:** Mineral fillers BET specific surface area.

The results indicate that WG presents the highest SSA followed by WG60K. These two mineral fillers differentiate themselves from the rest of the materials by demonstrating noticeably higher values. GR possesses a value of 3.03 m<sup>2</sup>/gr followed by BD and BE. QZ presents the lowest SSA. The latter is advantageous for the purpose of this research. In *Sub-Section 3.2.1*, QZ was introduced as the “inert” mineral filler that was hypothesized not to chemically interact with bitumen when the two materials are brought in contact. This hypothesis was solely based on its mineralogical composition. However, even if this hypothesis will be proved wrong and chemical interaction will occur between the two materials, QZ's extremely low SSA, compared to the other mineral fillers, may establish these interactions as negligible. The latter stems from the fact that less interface between the filler particles and bitumen will be available for interactions.

In *Sub-Section 3.5.4* it was stated that gas sorption measurements, for the determination of a material's SSA, are able to take into account the particles' shape and surface texture. Hence, the results of the BET analysis can be correlated, to some extent, with the results from the ESEM imaging presented in *Tables 4.2* and *4.3*. For instance, WG and WG60K show the highest values of SSA, which is in good agreement with their granular type particles and rough particles' surface texture. On the same grounds, QZ

possesses a very low SSA, which is very well justified by its angular type particles and extremely smooth particles' surface texture. Nevertheless, an absolute correlation is not possible due to the fact that there are also other factors affecting the SSA value, such as the external porosity of the filler particles, which is not possible to be evaluated through visual inspection of the microscope images.

*Evaluation of various methods for the determination of the specific surface area*

Tables 4.5 and 4.6 show the relative ranking of the mineral fillers based on their SSA, as determined by the laser diffraction and BET method, respectively. In Fig. 4.13 the correlation of the two methods is illustrated.

**Table 4.5:** Mineral fillers laser diffraction estimated specific surface area ranking.

Mineral filler	Laser diffraction -SSA
WG60K	Large ↑ ↓ Small
WG	
GR	
BE	
BD	
QZ	

**Table 4.6:** Mineral fillers BET specific surface area ranking.

Mineral filler	BET - SSA
WG	Large ↑ ↓ Small
WG60K	
GR	
BD	
BE	
QZ	

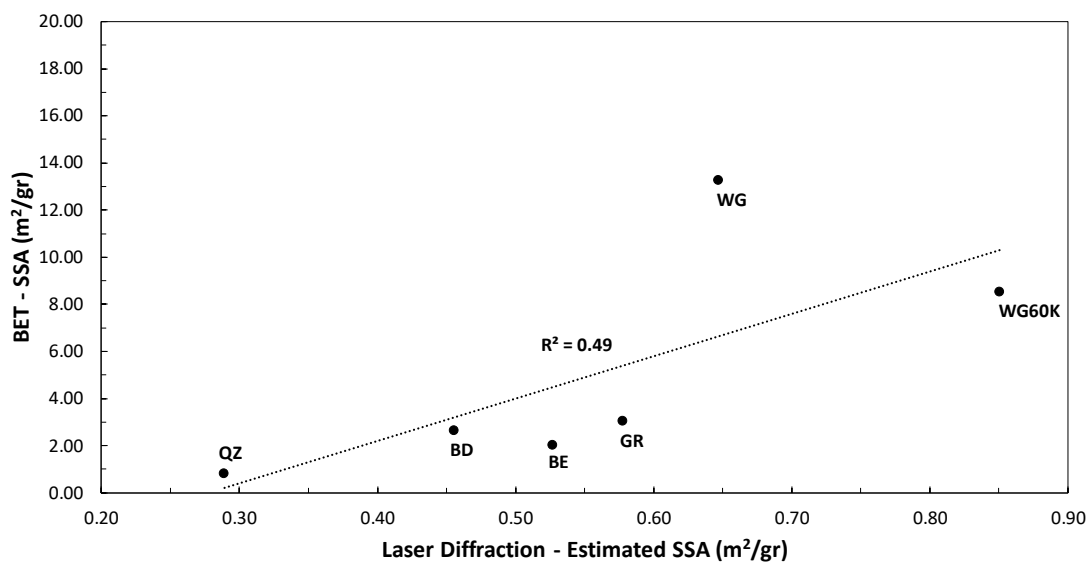


**Figure 4.13:** Mineral fillers laser diffraction estimated specific surface area and BET specific surface area correlation.

The results highlight the severity of the assumptions made when the laser diffraction is utilized for the determination of the materials' SSA. These assumptions not only lead to a considerable underestimation of the magnitude of this property but also to

a slight alternation of the relative ranking of the materials. This could be of high importance in a comparative study. Keeping in mind that gas sorption measurements provide a more accurate description of the actual case, the results of the BET method are used in this thesis for further considerations.

#### 4.5 Swelling percentage

In this section the results of the swelling test are reported and discussed. Two samples were tested for each material and the final SP is declared as the average value of the two measurements along with the standard deviation. *Table 4.7* summarizes the individual measurements of all mineral fillers while *Fig. 4.14* shows the swelling test results.

**Table 4.7:** Mineral fillers swelling test measurements.

Mineral filler	SP (%)		
	Measurement 1	Measurement 2	Average
WG60K	5.90	4.50	5.20
WG	25.00	24.70	24.85
BD	32.80	33.10	32.95
GR	16.30	16.00	16.15
QZ	-8.30	-3.30	-5.80
BE	39.10	41.10	40.10

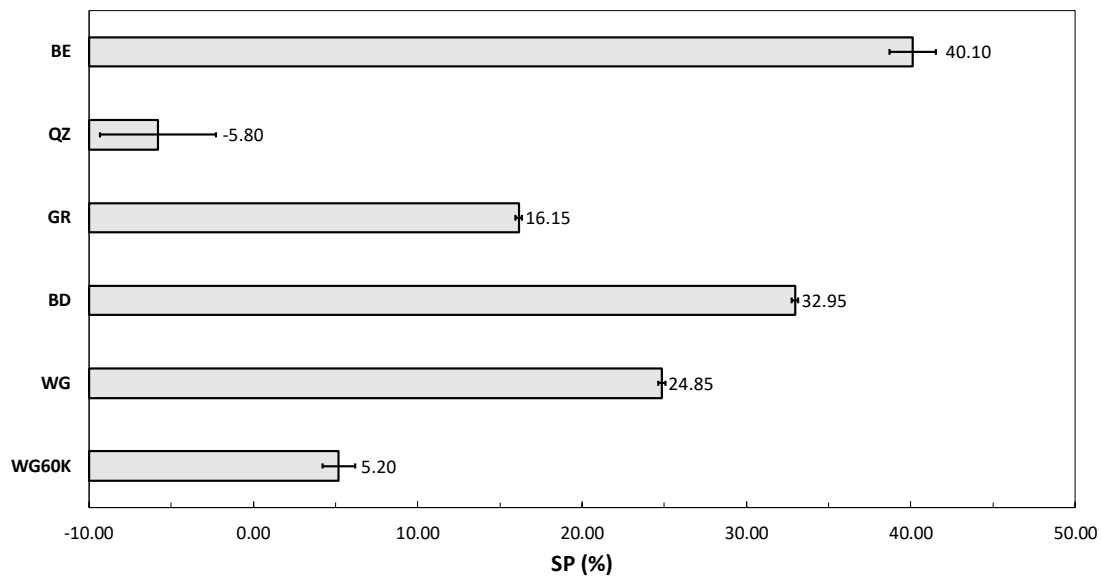


**Figure 4.14:** Mineral fillers swelling percentage.

The highest swelling tendency is observed in BE, followed by the BD. WG shows a noticeable SP which is almost 10% higher than GR. WG60K demonstrated a rather small swelling tendency. Interestingly, QZ presented a negative SP. Following *Eq. 3.11*, a negative value is produced due to a higher volume in the methanol containing volumetric tube than in the one containing water. A possible explanation for this outcome is that QZ reacted with methanol. Another explanation could be that the mineral filler had not completely settled, under the effect of gravity, in the water containing volumetric tube. To verify whether the latter was indeed the case a new measurement was taken after another 48 hours (total settlement time of 96 hours), however, still a negative value was obtained.

#### 4.6 Harmful fines – methylene blue value

This section provides the results of the methylene blue test. Two samples were tested for each material. In *Table 4.8* the individual measurements for each material are presented. *Fig. 4.15* shows the average MBV, for the tested mineral fillers, with its standard deviation.

**Table 4.8:** Mineral fillers methylene blue measurements.

Mineral filler	MBV (gr/Kg)		
	Measurement 1	Measurement 2	Average
WG60K	4.40	4.40	4.40
WG	16.80	17.20	17.00
BD	2.80	3.20	3.00
GR	2.40	2.40	2.40
QZ	0.00	0.00	0.00
BE	3.40	3.40	3.40

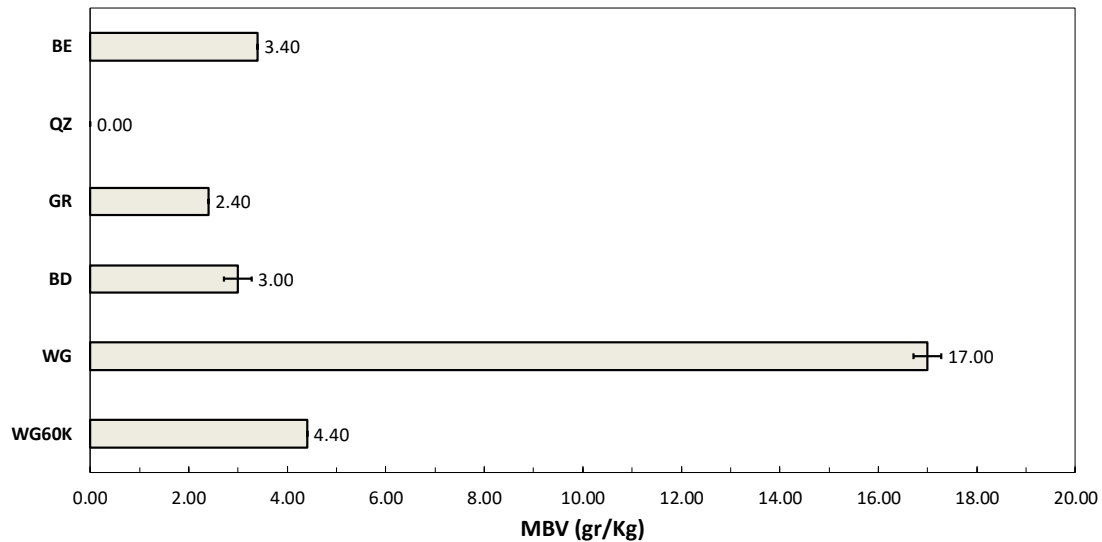


**Figure 4.15:** Mineral fillers methylene blue value.

According to the results, WG differentiates itself from the rest of the mineral fillers by showing the highest MBV value. WG is followed by WG60K, while BD and BE show quite similar MBVs. Finally, GR possesses the lowest MBV amongst the materials that seem to contain impurities, whereas QZ appears to be free of harmful fines by demonstrating no adsorption of the blue dye.

The purpose of the methylene blue test is to identify, amongst others, the existence of active clays in the mineral fillers. Active clays have the tendency to retain water and swell (Ødegård 2015). Having mentioned the above, it would be reasonable to expect a correlation between the swelling test (*Section 4.5*) and methylene blue test results. However, no good correlation was found between the two approaches. For instance, BE and BD showed a rather low MBVs while they were the mineral fillers with the highest SPs.

#### 4.7 Elemental and mineralogical analysis

In this section the XRF, LOI and XRD analyses results of the mineral fillers are reported and discussed. *Table 4.9* summarizes the XRF results. *Table 4.10* shows the materials' LOI while *Table 4.11* their mineralogical analysis (XRD).

Table 4.9: Mineral fillers elemental composition.

Oxide	Chemical formula	Concentration (%)					
		WG60K	WG	BD	GR	QZ	BE
Iron	Fe <sub>2</sub> O <sub>3</sub>	1.193	2.377	3.015	1.958	0.034	3.711
Aluminium	Al <sub>2</sub> O <sub>3</sub>	2.933	5.526	9.242	14.485	0.150	11.533
Titanium	TiO <sub>2</sub>	0.133	0.257	0.495	0.310	0.046	0.563
Potassium	K <sub>2</sub> O	1.118	2.136	2.330	3.633	0.040	2.917
Calcium	CaO	49.510	30.240	16.457	2.015	0.026	8.657
Magnesium	MgO	3.950	9.430	1.953	0.720	0.008	2.266
Sodium	Na <sub>2</sub> O	0.134	0.194	1.318	4.297	0.011	1.916
Silicon	SiO <sub>2</sub>	9.960	16.570	51.880	70.719	99.571	60.716
Chromium	Cr <sub>2</sub> O <sub>3</sub>	-	-	0.014	0.012	0.001	0.016
Barium	BaO	0.009	0.021	0.076	0.127	0.004	0.087
Zirconium	ZrO <sub>2</sub>	0.003	0.007	0.041	0.021	0.007	0.035
Strontium	SrO	0.044	0.147	0.042	0.046	-	0.049

Table 4.10: Mineral fillers loss on ignition.

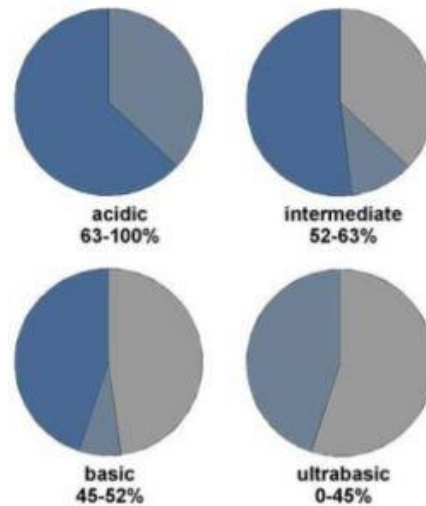
Mineral filler	LOI (%)	Testing temperature (°C)
WG60K	31.67	1100
WG	33.21	1100
BD	12.96	950
GR	1.34	1100
QZ	0.10	1100
BE	7.24	950

Table 4.11: Mineral fillers mineralogical composition.

Mineral	Concentration (%)					
	WG60K	WG	BD	GR	QZ	BE
Quartz	2.50	3.50	36.60	30.70	100.00	40.00
Plagioclase	-	-	12.10	40.20	-	17.80
K-Feldspar	2.50	6.30	6.70	21.00	-	7.20
Mica+Illite	7.00	12.80	12.10	2.10	-	15.80
Calcite	41.70	31.70	25.70	1.20	-	12.40
Chlorite	-	4.10	4.10	2.70	-	6.80
Pyroxene	-	-	-	2.10	-	-
Dolomite	17.30	41.30	2.10	-	-	-
Hematite	0.50	0.30	0.60	-	-	-
Portlandite	28.50	-	-	-	-	-

The elemental analysis (Table 4.9) shows that the highest calcium compounds content appears in the limestone-based mineral fillers (WG60K and WG). Moreover, WG60K incorporates approximately 20% more calcium than WG, which is very well expected due to the added hydrated lime. QZ demonstrates a negligible calcium concentration, whereas SiO<sub>2</sub> is the governing element found in it. The presence of Al<sub>2</sub>O<sub>3</sub> may witness the existence of clay particles in the mineral matters. GR shows the highest concentration in Al<sub>2</sub>O<sub>3</sub> followed by BE. Overall, CaO or SiO<sub>2</sub> are the two elements in abundance in all mineral fillers. It is noticeable that the higher the CaO concentration the lower the respective one of SiO<sub>2</sub>, and vice versa.

The mineral matter may be classified as acidic or basic based on its SiO<sub>2</sub> content (Nageswaran 2016) (*Fig. 4.16*). *Table 4.12* illustrates the classification of the considered mineral fillers as (super-)acidic or (ultra-)basic based on their SiO<sub>2</sub> content. It should be noted that this classification shows QZ to be super-acidic, which from an elemental (mineralogical) point of view is absolutely valid. The term “inert” used to describe this particular mineral filler, from the very beginning of this thesis, refers to its behavior when it is brought in contact with bitumen and it is based on the repelling principal between two similarly (i.e. positively or negatively) charged components.



**Figure 4.16:** Classification of mineral matter based on its silicon content (Nageswaran 2016).

**Table 4.12:** Mineral fillers classification as acidic or basic.

<b>Mineral filler</b>	<b>Classification</b>
WG60K	(Ultra-)Basic
WG	
BD	
BE	
GR	
QZ	(Super-)Acidic

The highest values of LOI are observed in WG60K and WG which are the results of the presence of hydrated lime and the mineral dolomite (*Table 4.11*), respectively. GR and QZ demonstrate the lowest contents of organic substances.

Regarding the mineralogical analysis of the mineral fillers, the governing minerals in WG60K and WG are calcite and dolomite, which justifies their high calcium compounds content, as shown in *Table 4.9*. In addition, a high percentage of portlandite is found in WG60K, which is associated with the incorporation of hydrated lime. The latter is the reason why this mineral is only found in WG60K. Quartz is the only mineral found in QZ, which is in full agreement with the elemental analysis (*Table 4.9*). The presence of the mineral chlorite witnesses the contamination of the mineral matter. Interestingly, the commercial mineral filler WG (pure limestone) demonstrates a relatively high percentage of chlorite concentration, which was not expected. However, according to the supplier, this result is possible. Last but not least, BD presents the largest diversity of minerals, which seems as an expected result, considering that BD is a by-product collected in the asphalt plant, where different types of aggregates with distinct mineralogy may be used.





# 5

## Bitumen and mastics tests results and discussion

## 5.1 Rheological evaluation

In this section, the rheological data of the considered mastics and neat bitumen, prior and after ageing, are reported and discussed. The analysis of the master-curves and the ageing assessment of the various materials are performed both in a qualitative and quantitative way. *Fig. 5.1* and *5.2* demonstrate the  $G^*$  and  $\delta$  master-curves, respectively, for all materials at both the “fresh” and aged state.

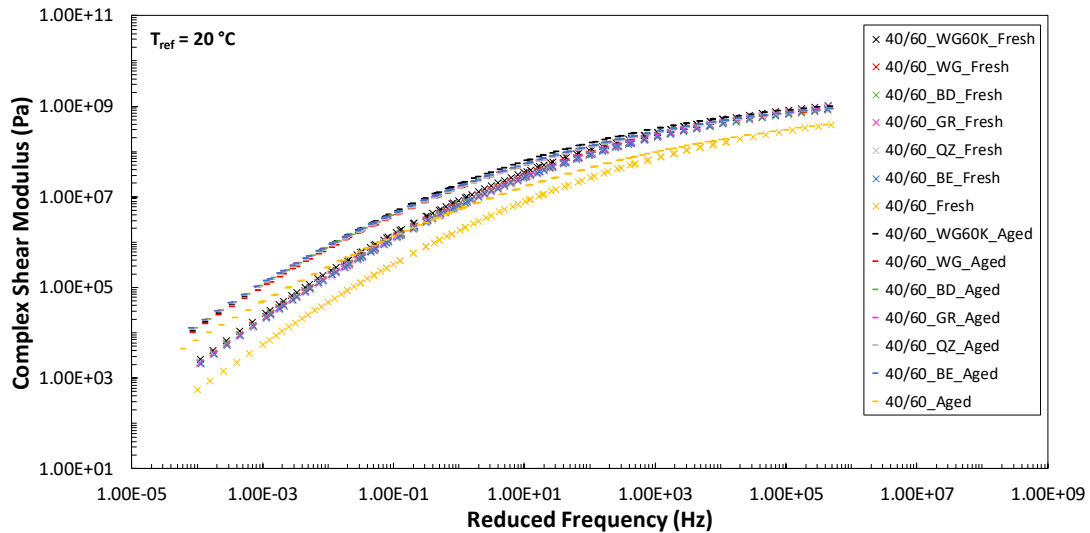


Figure 5.1: Bitumen and mastics complex shear modulus master-curves at “fresh” and aged state.

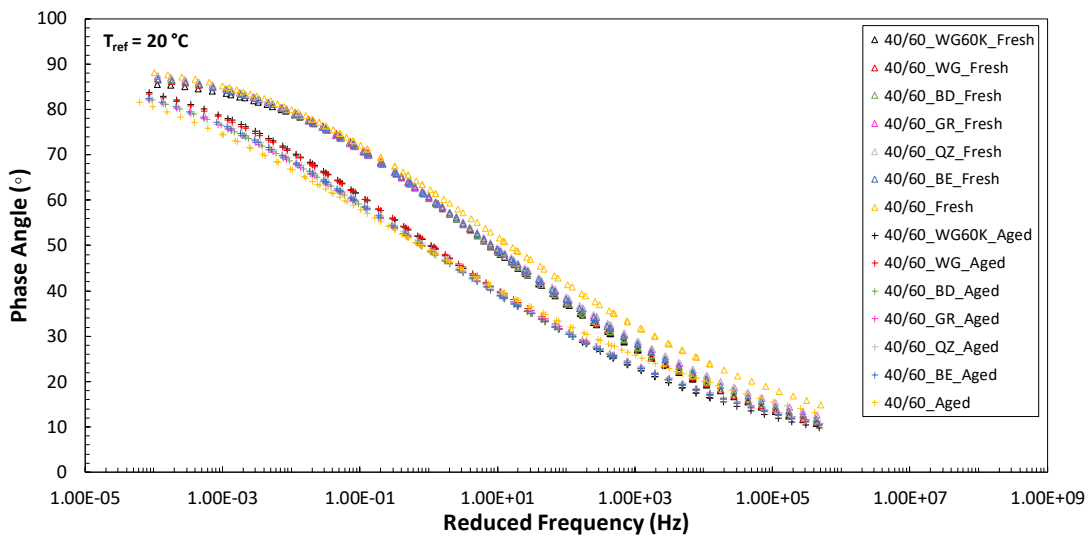


Figure 5.2: Bitumen and mastics phase angle master-curves at “fresh” and aged state.

### 5.1.1 Complex shear modulus and phase angle master-curves analysis

#### “Fresh” materials’ master-curves

It is well-known that the addition of mineral filler in bitumen entails a stiff behavior and a relatively more elastic response of the resulting mastic. This effect is captured in both the  $G^*$  and  $\delta$  master-curves.

More specifically, with regards to the  $G^*$  plots (Fig. 5.1), the master-curves corresponding to the mastics are offset towards higher values of complex shear modulus and slightly higher frequencies, with respect to the neat bitumen master-curve, implying a more elastic response. Moreover, it is noticeable that the stiffer behavior of the mastics over neat bitumen is relatively more pronounced at intermediate frequencies, while a tendency is observed of the mastics' and neat binder's  $G^*$  master-curves to converge at extreme frequencies. The latter implies that at very low frequencies (or high temperatures) the materials' temperature susceptibility increases and that the properties of the mastics are predominantly governed by the bitumen, hence the observed tendency of the master-curves for convergence. This is in line with previous reported rheological evaluation of "fresh" neat bitumen and mastics (Hagos 2008).

The effect of the mineral fillers on bitumen properties is also quite clear in the  $\delta$  master-curves (Fig. 5.2). The less viscous response of the mastics, compared to neat bitumen, is demonstrated by their lower phase angle values, throughout the whole considered frequency range, as well as by the movement of their master-curves to slightly higher frequencies. The greatest difference between the phase angle values of mastics and neat bitumen is observed at intermediate to high frequencies, where the mineral fillers' stiffening effect is corroborated by the simultaneous effect of low testing temperatures, whereas at lower frequencies the effect of the mineral fillers is hindered by the viscous behavior of the binder.

The mineral filler WG60K appears to have the most pronounced stiffening effect on bitumen, compared to the other mineral matters, as captured by the higher complex shear modulus values of the mastic's 40/60\_WG60K\_Fresh master-curve, throughout the whole frequency range (Fig. 5.1). This is verified in Fig. 5.3, which shows the complex shear modulus values of the mastics at selected frequencies and temperature of 20°C. Moreover, the stiffer nature of 40/60\_WG60K\_Fresh is also demonstrated in the  $\delta$  master-curves at low and intermediate to high frequencies (Fig. 5.2), where the relatively more elastic response of this particular material is a fact.

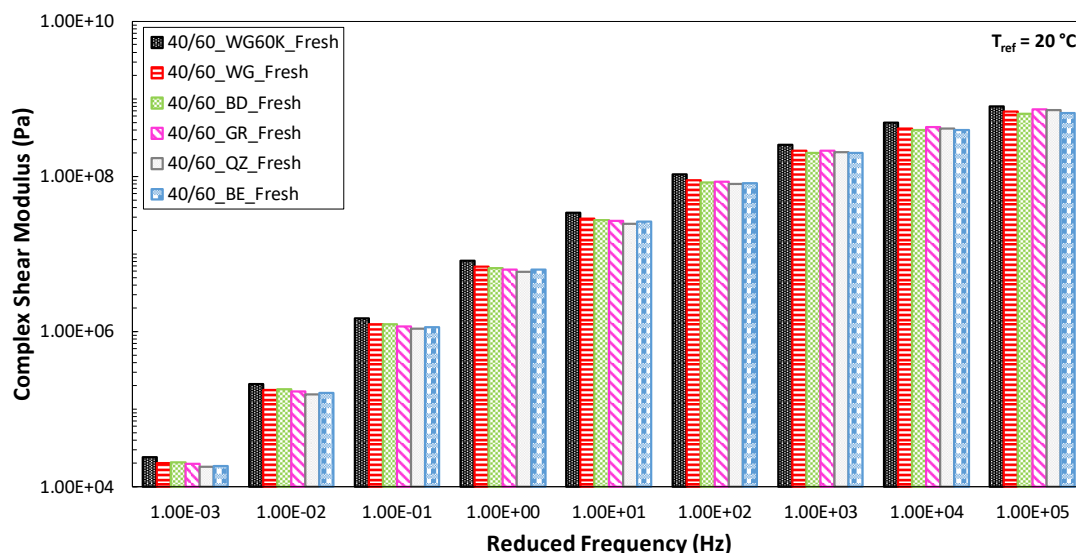


Figure 5.3: "Fresh" mastics complex shear modulus at various frequencies and temperature of 20°C.

Finally, a comparison between the 40/60\_WG60K\_Fresh and 40/60\_WG\_Fresh complex shear modulus values (*Fig. 5.3*) shows the enhanced stiffening effect of the mixed mineral filler, when 25wt% of hydrated lime is added in the limestone-based mineral matter. This is in line with observations reported elsewhere (Alfaqawi et al. 2017).

#### *Aged materials' master-curves*

*Fig. 5.1* shows the effect of (oxidative) ageing on the shape of the  $G^*$  master-curves. It can be observed that ageing leads to the reduced time-dependency of the materials' response in the considered frequency range, which is expressed through the rotation (reduced slope) of the aged materials' master-curves, always with respect to the ones corresponding to the "fresh" state. The point of rotation is located at the region of high frequencies, where all pairs of master-curves (i.e. fresh and corresponding aged) converge to approximately the same value (i.e. glassy modulus). This effect of the ageing on the materials' mechanical properties is expected and is in full agreement with previous research (Anderson & Bonaquist 2012).

In addition, the shape of the master-curves reveals another feature regarding the influence of ageing on the materials' properties. As mentioned above, the point of the observed rotation of the master-curves is located at the high frequency range, whereas the difference of the "fresh" and aged complex shear moduli gradually increases when lower frequencies, or equivalently higher temperatures, are considered. Bituminous binders possess a viscous and an elastic component. At high temperatures the viscous component dominates over the elastic one. This implies that ageing has a greater influence on the viscous component rather on the elastic one of a bituminous binder (*Fig. 5.1*).

The materials' ageing level can be assessed through the amount of rotation of the aged  $G^*$  master-curves. More severe ageing results in a greater difference between the complex shear modulus values corresponding to the "fresh" and aged state of a material at the region of intermediate to low frequencies. The  $G^*$  master-curves show that bitumen had undergone more severe age-hardening than all considered mastics. The effect of ageing on the complex shear modulus of the materials is investigated and discussed, in more detail, in *Sub-Section 5.1.2* through the derivation and evaluation of the complex shear modulus  $A_1$ .

According to Moraes & Bahia (2015a) and Alfaqawi et al. (2017) observed the  $G^*$  master-curves of aged mastics appeared to only shift towards higher complex shear modulus values, with respect to the "fresh" bitumen master-curve, without showing the distortion (large rotation) that characterizes the aged bitumen master-curve. This behavior of the materials is also verified by the rheological data of the present thesis, as it can be seen in *Fig. 5.4*. According to Moraes & Bahia (2015a) this result indicates that the changes in the mechanical properties of bitumen attributed to ageing may be of lower significance to the overall asphalt mixture performance, when the effect of mineral fillers in the mastic phase is considered. In other words, the effect of ageing on bitumen properties differs when the latter is aged alone and in the presence of the mineral matter.

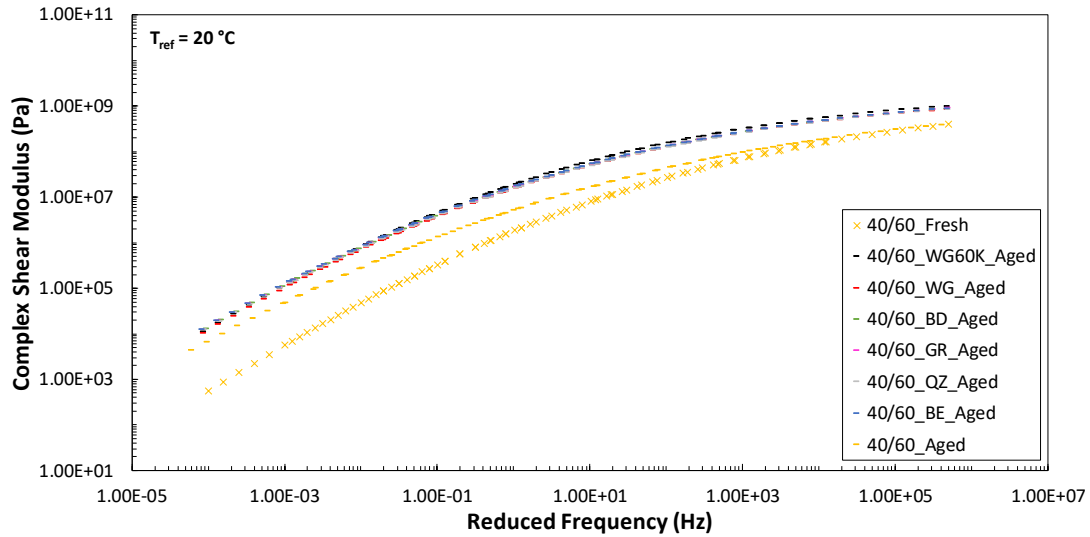


**Figure 5.4:** “Fresh” bitumen, aged bitumen and aged mastics complex shear modulus master-curves.

With respect to the  $\delta$  master-curves (*Fig. 5.2*), ageing leads to the reduction of the phase angle through the whole range of frequencies and for all materials, thus, denoting their more elastic response after ageing. It is noticeable that, bitumen demonstrates lower phase angle values after ageing than all mastics, at the intermediate to low frequencies range. For one thing, this is an indication that bitumen had undergone more severe ageing than the mastics. For another, it highlights that mastics possess a greater ability to dissipate shear stress through a more viscous response, at high loading durations, after ageing. On the contrary, at intermediate to high frequencies, the mastics demonstrate lower values of the phase angle than bitumen, implying a more elastic behavior. It is believed that this is due to the intrinsic stiff nature of mastics and simultaneous effect of low temperatures.

Nevertheless, what is of more interest to examine is the change of the phase angle at these high frequencies, from the “fresh” to the aged state, and not the relative ranking of bitumen and mastics at the aged state alone. *Eq. 5.1* was used to evaluate the change of the phase angle, from the “fresh” to the aged state, at selected frequencies and temperature of 20°C. The outcome is illustrated in *Fig. 5.5*. The results indicate that, indeed, the neat bitumen experienced the greatest change in the phase angle, upon ageing, throughout the whole range of the considered frequencies, despite the fact that it shows a more viscous response than the mastics at the high frequencies’ region.

$$\Delta\delta_i = |\delta_{i,Aged} - \delta_{i,Unaged}| \quad (5.1)$$

where,

$i = 0.001, 0.01, 0.1, 1, 10, 100, 1000, 10000, 100000$  Hz

$\Delta\delta_i$  = The difference of the phase angles at reduced frequency ( $i$ ) (°)

$\delta_{i,Aged}$  = The phase angle of the aged material  
at reduced frequency ( $i$ ) (°)

$\delta_{i,Unaged}$  = The phase angle of the “fresh” material  
at reduced frequency ( $i$ ) (°)

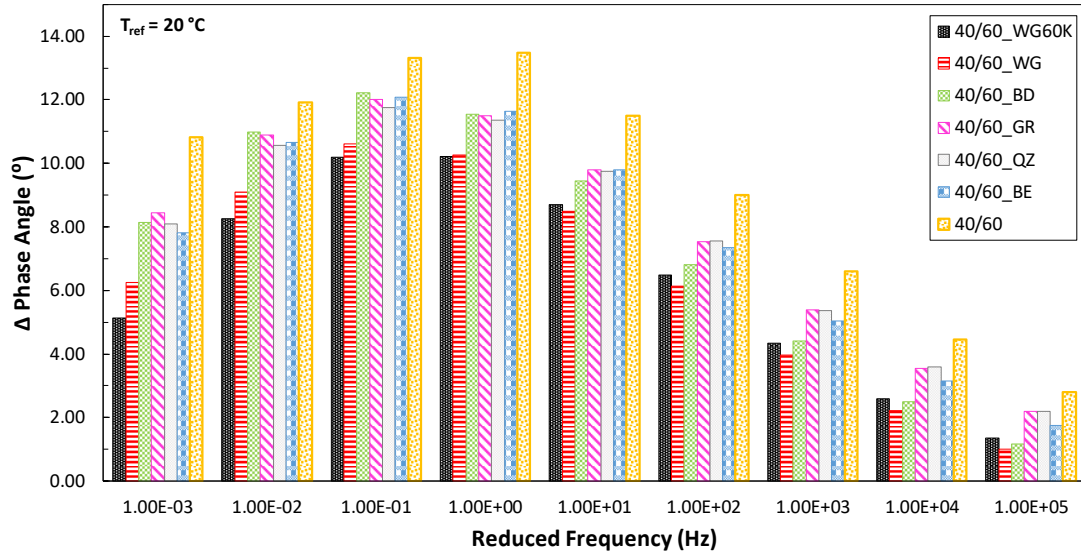


**Figure 5.5:** Change of the phase angle upon ageing at various frequencies and temperature of 20°C.

Amongst the various aged mastics, 40/60\_WG60K\_Aged and 40/60\_WG\_Aged show the highest values of phase angle in the intermediate to low frequencies' region (*Fig. 5.2*), with the former demonstrating the most viscous response at low frequencies while an equal response of the two materials is observed at the intermediate ones. From *Fig. 5.5* it can be deduced that these two mastics had undergone the least age-hardening based on the change of the phase angle upon ageing.

### 5.1.2 Complex shear modulus ageing indices

The quantitative evaluation of the ageing level of the materials was performed through the derivation of ageing indices based on the  $G^*$  master-curves (*Fig. 5.1*). For that purpose, the generic form of the ageing index was employed (*Eq. 2.1*) and the complex shear modulus, at selected frequencies and temperature of 20°C, was utilized as the assessed physical property for the calculation of the Ageing Indices (AI) (*Eq. 5.2*).

In *Fig. 5.6* the calculated AI, as a function of a wide range of loading frequencies or, equivalently, testing temperatures, is presented. As it was discussed previously, the effect of ageing is more pronounced at the low frequencies range. This is also demonstrated in *Fig. 5.6*, where the differences of the ageing level of the materials become apparent at higher temperatures (lower frequencies), while the AI curves converge to unit as the frequency increases. The latter is the result of the "fresh" and aged  $G^*$  master-curves' convergence to the glassy modulus, at very high frequencies (*Fig. 5.1*).

$$AI_i = \frac{G_{i,Aged}^*}{G_{i,Unaged}^*} \quad (5.2)$$

where,

$i = 0.001, 0.01, 0.1, 1, 10, 100, 1000, 10000$  Hz

$AI_i$  = The ageing index at reduced frequency (i) (–)

$G_{i,Aged}^*$  = The complex shear modulus of the aged material  
at reduced frequency (i) ([F]/[A])

$G_{i,Unaged}^*$  = The complex shear modulus of the "fresh" material  
at reduced frequency (i) ([F]/[A])

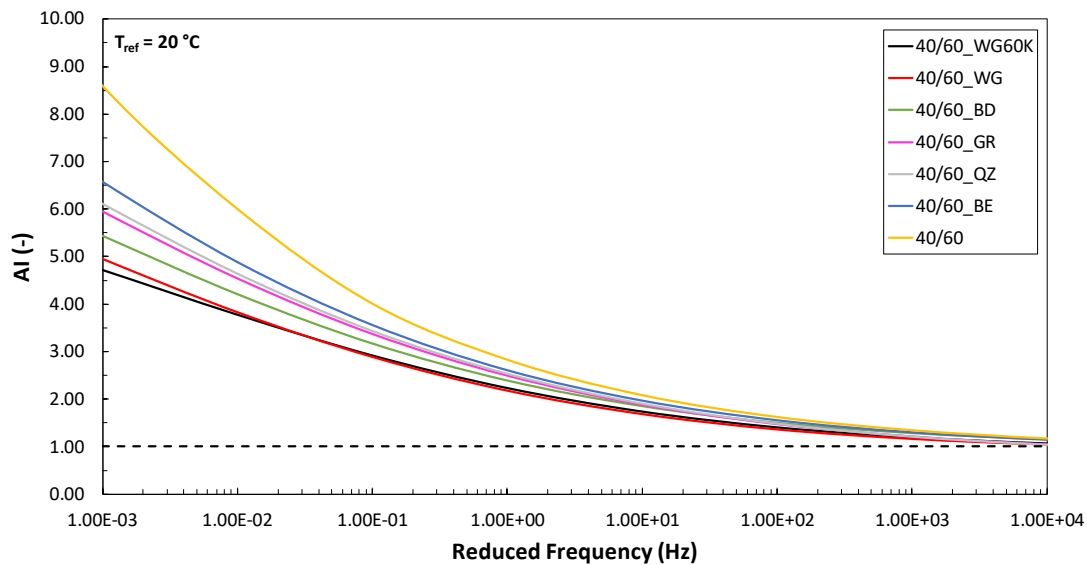


**Figure 5.6:** Complex shear modulus ageing indices as a function of the reduced frequency at 20°C.

The results presented in *Fig. 5.6* suggest, first and foremost, that all mineral fillers, regardless of their individual properties, have a positive effect on ageing of bituminous mixtures, as it can be deduced by the mastics' lower complex shear modulus AI, compared to the neat bitumen, throughout the whole range of the considered frequencies. The observed favourable effect of the mineral matters is in full agreement with the results and conclusions reported elsewhere (Curtis et al. 1993, Wu 2009, Moraes & Bahia 2015a, Moraes & Bahia 2015b, Gundla et al. 2015, Alfaqawi et al. 2017).

Mastics 40/60\_WG60K and 40/60\_WG show the least ageing amongst all materials. Evidently, their performance is quite comparable, as can be deduced by the close packing of their corresponding AI curves (*Fig. 5.6*). More specifically, 40/60\_WG60K appears to be less aged than 40/60\_WG, when the AI is evaluated at very low frequencies, while the opposite holds at higher frequencies. A crossing point between the two AI curves is observed at a frequency approximately equal to 0.049 Hz (*Fig. 5.7*). These results suggest that the addition of 25wt% of hydrated lime in the limestone-based mineral filler not only did not result in a pronounced reduction of mastic ageing, as suggested elsewhere (Gundla et al. 2015, Little & Petersen 2015, Alfaqawi et al. 2017) but also led to a slightly poorer performance of the mixed mineral filler (i.e. WG60K), when the AI is evaluated at intermediate to high frequencies. The potential reasons behind such relative behavior of these mastics are attempted to be established in *Sub-Section 5.1.4*, where the correlation of the mastics ageing level and mineral fillers' properties is investigated.

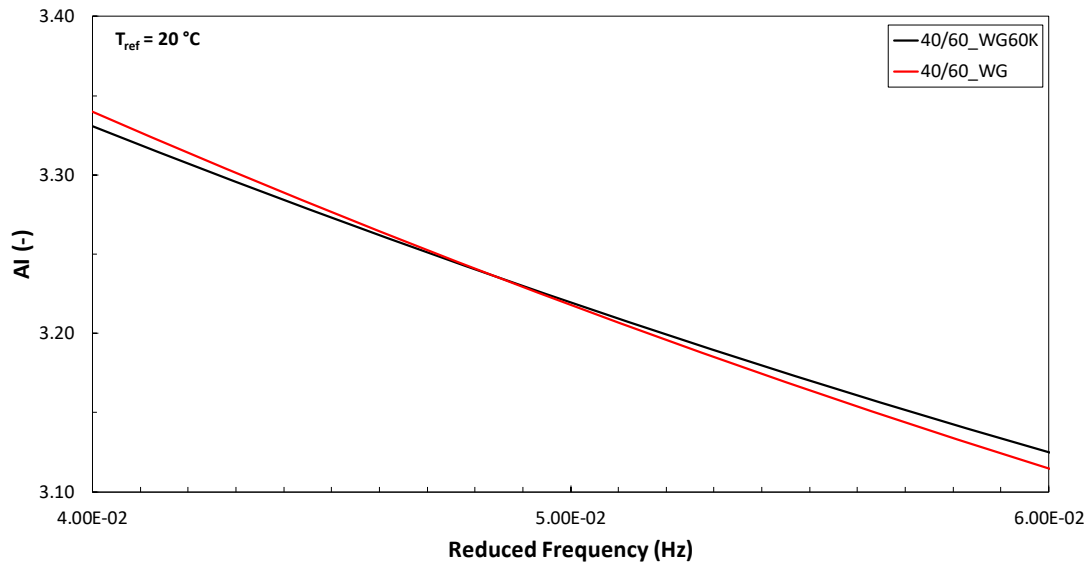


**Figure 5.7:** Crossing point of 40/60\_WG60K and 40/60\_WG AI curves at  $\sim 0.049$  Hz and 20°C.

The mastic produced with the BD (i.e. 40/60\_BD) shows more severe ageing than the two limestone-based mastics, 40/60\_WG60K and 40/60\_WG, but less ageing than the rest of the materials. This result shows that the utilization of the BD, collected in the asphalt plant, as a mineral filler in the asphalt mixtures production may lead to the deceleration of bitumen ageing but its performance, ageing-wise, is still poorer than the one of the standardized mineral filler currently used in the production of PA mixtures in the Netherlands (i.e. WG60K). In terms of higher ageing level, 40/60\_BD is followed by 40/60\_GR and 40/60\_QZ, which show a fairly similar behavior. Nevertheless, it is believed that their resulting ageing level is controlled by two different mechanisms, as it is discussed in *Sub-Section 5.1.4*.

Finally, 40/60\_BE appears to be the most aged mastic. This result was unexpected for two major reasons. For one, the mineral filler BE was included in the study for comparison reasons with the BD, since it was suggested that the supplied BD is most likely bestone, as mentioned in *Sub-Section 3.2.1*. Thus, it was expected that the resulting mastics would have had a comparable performance upon ageing, which is not the case. For another, BE is a mineral filler that it is expected to develop chemical interactions with bitumen, in contrast to QZ. Hence, and solely based, at the moment, on the statement of Moraes & Bahia (2015a) that the major contribution to the mitigation of bitumen ageing stems from the physico-chemical interactions between the bitumen and the mineral matter and not from the physical presence of the mineral fillers in the mastics, it was expected that 40/60\_BE would demonstrate at least lower age-hardening from 40/60\_QZ.



### 5.1.3 Relation between mastics' rheological ageing indices and properties of mineral fillers

The complex shear modulus AI at 0.001 Hz and 20°C was chosen for the ageing comparison of the various materials in terms of figures. The results are presented in *Fig. 5.8*. The relative ranking of bitumen and mastics is shown in *Table 5.1*.

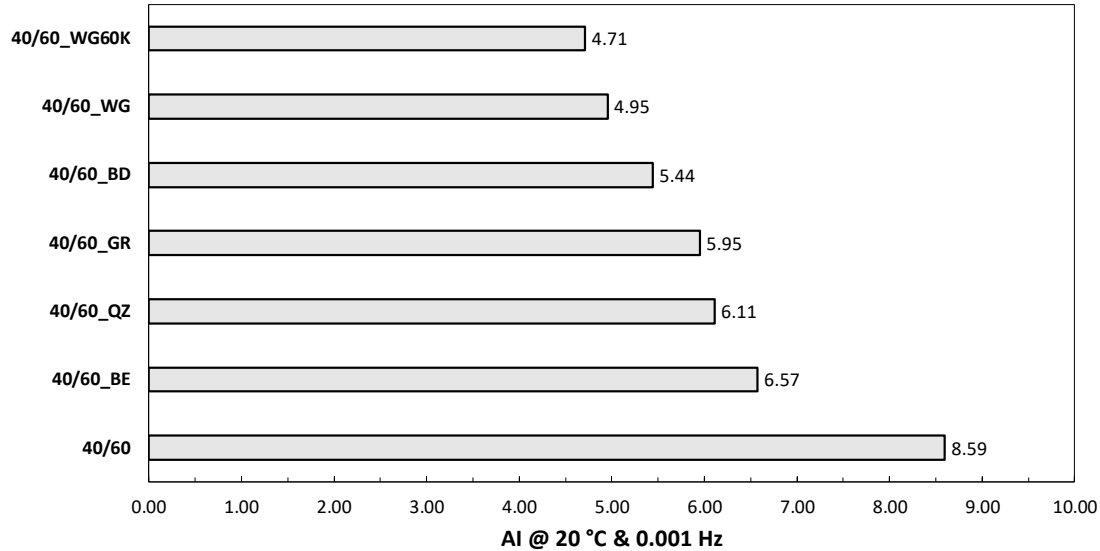


**Figure 5.8:** Complex shear modulus ageing indices at 20°C and 0.001 Hz.

**Table 5.1:** Bitumen and mastics ranking based on the complex shear modulus ageing indices at 20°C and 0.001 Hz.

Material	Ageing level
40/60	High
40/60_BE	↑ ↓
40/60_QZ	
40/60_GR	
40/60_BD	
40/60_WG	
40/60_WG60K	Low

#### *Particles' size distribution*

The mastic prepared with the mineral filler QZ (i.e. 40/60\_QZ) shows a lower complex shear modulus AI than the neat bitumen (*Fig. 5.8*). This implies that the presence of the mineral fillers' particles in the mastics (diffusion mediums) affect the oxygen diffusion path during ageing. The fact that 40/60\_QZ presents a relatively substantial difference in its complex shear modulus AI compared to neat bitumen, could be attributed to the coarseness of QZ (*Fig. 4.1* and *4.2, Section 4.1*). The reasoning behind that is that the coarser the mineral filler's particles the greater the resistance that the oxygen molecules encounter in diffusing into the medium, entailing a reduced rate of oxidative ageing of bitumen. This finding further supports the statement of Han (2011), in the context that the mineral matter compels the oxygen molecules to follow a more tortuous path through the diffusion medium, thus, lengthening the diffusion path.

Nevertheless, the fact that considerably finer mineral fillers, such as WG60K and WG (*Fig. 4.1* and *4.2, Section 4.1*), resulted in less aged mastics than 40/60\_QZ, reveals the

existence of another mechanism, stemming from the physico-chemical interactions between the mineral matter and bitumen, that led to the resulting mastics' behavior upon ageing. In addition, this outcome suggests that the effect of the mineral fillers' particles on the oxygen diffusion path is a mechanism of secondary importance, whereas the developed physico-chemical interactions seem to contribute the most in the mitigation of bitumen ageing. This observation is in line with the statement of Moraes & Bahia (2015a) that the major contribution to the mitigation of bitumen ageing stems from the physico-chemical interactions between the bitumen and the mineral matter and not from the physical presence of the mineral fillers in the mastics.

#### *Elemental/mineralogical composition*

The complex shear modulus AI results, presented in *Fig. 5.8*, show a good relationship with the mineral fillers ranking as basic or acidic (*Table 4.12, Section 4.7*). The mineral filler BE deviates from this relationship, whose case is discussed separately later.

More analytically, the basic limestone-based mineral fillers, WG60K and WG, led to the mastics with the least ageing. On the other hand, more acidic aggregates, such as GR, promoted the mitigation of bitumen ageing to a lesser extent. BD lies in between the ultra-basic and acidic mineral fillers (*Table 4.12, Section 4.7*), which is in good agreement with its corresponding mastic's ageing level. Finally, QZ shows the highest complex shear modulus AI, by virtue of its lack of chemical reactivity. Having mentioned the above, a nice relationship was found between the CaO content of the mineral fillers, which is a relative measure of the mineral matters' basicity (or acidity), and the mastics' complex shear modulus AI at 0.001 Hz and 20°C. The latter relationship is described by a power law (*Fig. 5.9*).

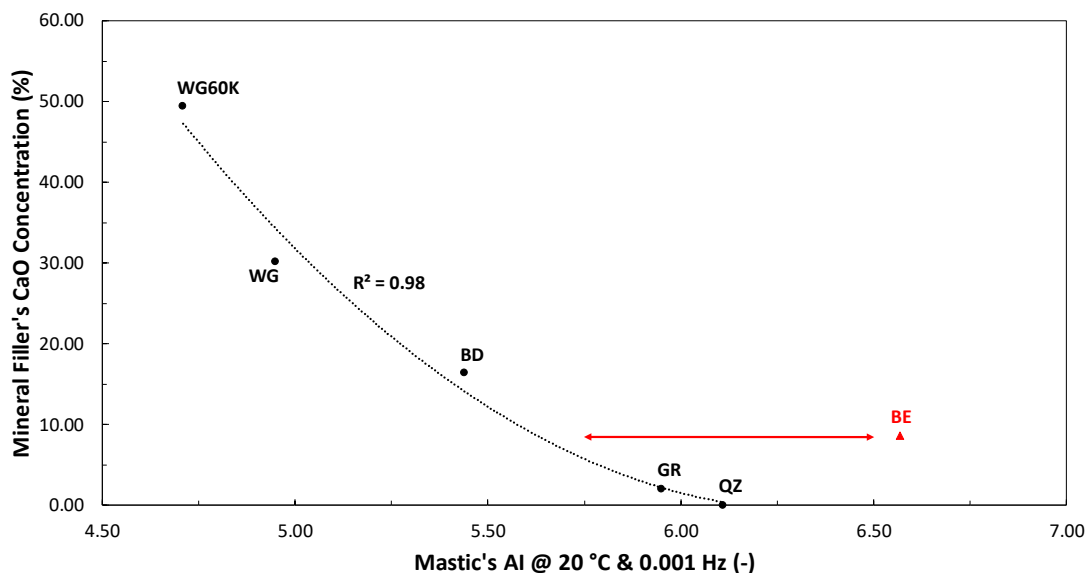


**Figure 5.9:** Relationship between mineral fillers' CaO content and mastics' AI at 20°C and 0.001 Hz.

The relationship depicted in *Fig. 5.9* indicates that, basic mineral fillers (e.g. WG60K and WG) possess a greater ability in intensifying the interactions between the bitumen and the mineral filler's particles, compared to more acidic mineral fillers (i.e. BD and GR), thus leading to less aged-hardened mastics. This finding is in absolute agreement with the observations of Wu (2009), but opposite to the results reported by Moraes & Bahia (2015a) and Moraes & Bahia (2015b).

*Specific surface area (SSA)*

Another property, that is believed to affect the mastics' ageing level, is the SSA of the mineral fillers. As stated in *Section 4.4*, a high value of the SSA implies a large interface between the mineral filler's particles and the bitumen to interact. Thus, it is reasonable to expect that, when the mineral fillers present a large SSA, the physico-chemical interactions between the two materials are intensified.

WG60K and WG, possess the largest SSAs, amongst the various mineral fillers (*Fig. 4.12, Section 4.4*), which is in line with the ageing level of their corresponding mastics, compared to the rest of the materials. A further analysis reveals that, when the complex shear modulus AI is evaluated at 0.001 Hz and 20°C (*Fig. 5.8*), 40/60\_WG60K appears to be slightly less aged than 40/60\_WG, despite the fact that WG has a larger SSA than WG60K. This result indicates that the mineralogy of the mineral fillers prevails over their SSA.

Nevertheless, in *Sub-Section 5.1.2*, it was stated that the complex shear modulus AI curves of 40/60\_WG60K and 40/60\_WG are closely packed and that at higher frequencies 40/60\_WG appears to be slightly less aged than 40/60\_WG60K (*Fig. 5.6*). It is believed that the close packing of the curves and the reverse situation as the frequency increases is the result of the larger SSA of WG, compared to WG60K, compensating for their differences in mineralogy (i.e. CaO content). Moreover, the coarser nature of WG compared to WG60K may also slightly contribute to the close packing of the complex shear modulus AI curves. This analysis may lead to the conclusion that both the mineral fillers' elemental/mineralogical composition and SSA have an effect on the physico-chemical interactions between the bitumen and the mineral matter, and, by extension, a primary role to the ageing of bituminous mixtures.

A comparison between BD and GR entails that even though GR has a slightly higher value of SSA than BD (3.03 and 2.61 m<sup>2</sup>/gr, respectively) the mastic 40/60\_BD is less aged than the one produced with GR. This result, further corroborates the above statement, that the effect of the elemental/mineralogical composition of the mineral fillers prevails over the effect of their SSA. In addition, the less age-hardening of 40/60\_BD, compared to 40/60\_GR, could also partially result from the coarser nature of BD compared to GR (*Fig. 4.1 and 4.2, Section 4.1*).

It is believed that the effect of the materials' SSAs on mastics' ageing cannot be clearly demonstrated by the data presented in this section. This is because the mastics' ageing results correlate very well with the mineralogical properties of the mineral fillers, thus, its effect is concealed. Only indirect indications of the influence of the SSA can be derived, as was done through evaluating the ageing level of 40/60\_WG60K and 40/60\_WG and their relative relationship. Despite that, there are some strong evidence from the literature review in *Chapter 2* that there is an (important) effect of the SSA on the interactions of bitumen and the mineral matter. The more pronounced example was reported by Moraes & Bahia (2015a), who showed that an acidic mineral filler performed better, ageing-wise, than a basic one, by virtue of its higher SSA.

*Analysis of bestone*

The reasons behind the behavior of mastic 40/60\_BE, upon ageing, are attempted to be established through a comparison of this particular material with the mastics 40/60\_BD, 40/60\_GR and 40/60\_QZ, based on their respective mineral fillers' properties.

BD and BE possess a similar elemental composition (*Table 4.9, Section 4.7*) except for the CaO concentration. Hence, BD is classified as a more basic mineral filler than BE. Moreover, BD presents a (slightly) larger SSA than BE (difference of 0.6 m<sup>2</sup>/gr), thus, BD provides a larger interface between the mineral filler particles and bitumen for interactions. Both above features, would result in more pronounced physico-chemical interactions in the case of BD, which is in very good agreement with the relative ageing ranking of mastics 40/60\_BD and 40/60\_BE (*Table 5.1*). Moreover, the coarser nature of BD, compared to BE (*Fig. 4.1 and Fig. 4.2, Section 4.1*), may also partially contribute to the less age-hardening of mastic 40/60\_BD. The comparison of these two materials demonstrates the simultaneous favourable effect of the mineral fillers' particles' size distribution, basicity and SSA on ageing of mastics.

By comparing GR and BE, the effect of their particles' size distribution can be considered equivalent, since the differences in their gradation can be regarded as negligible (*Fig. 4.1 and 4.2, Section 4.1*). GR is ranked as a more acidic material than BE, which, based on the trend illustrated in *Fig. 5.9*, cannot justify the higher complex shear modulus AI of the mastic 40/60\_BE. Nevertheless, GR possesses a higher SSA than BE, which could be a potential reason for more intensified interactions, resulting in a less aged mastic. This analysis, highlights the prevalence of the effect of SSA over mineralogy.

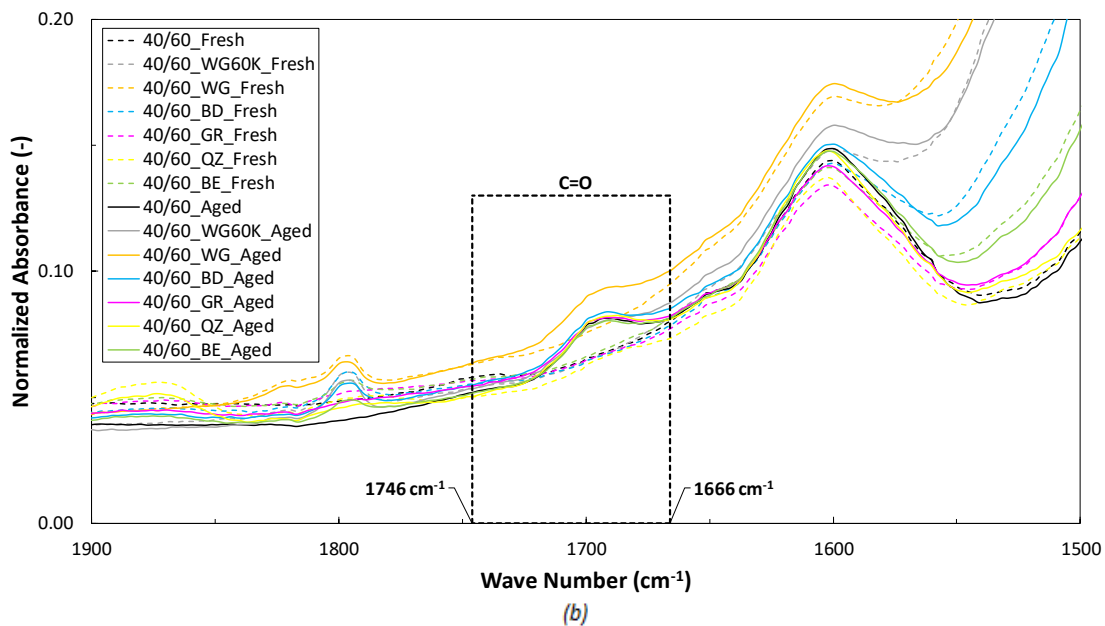
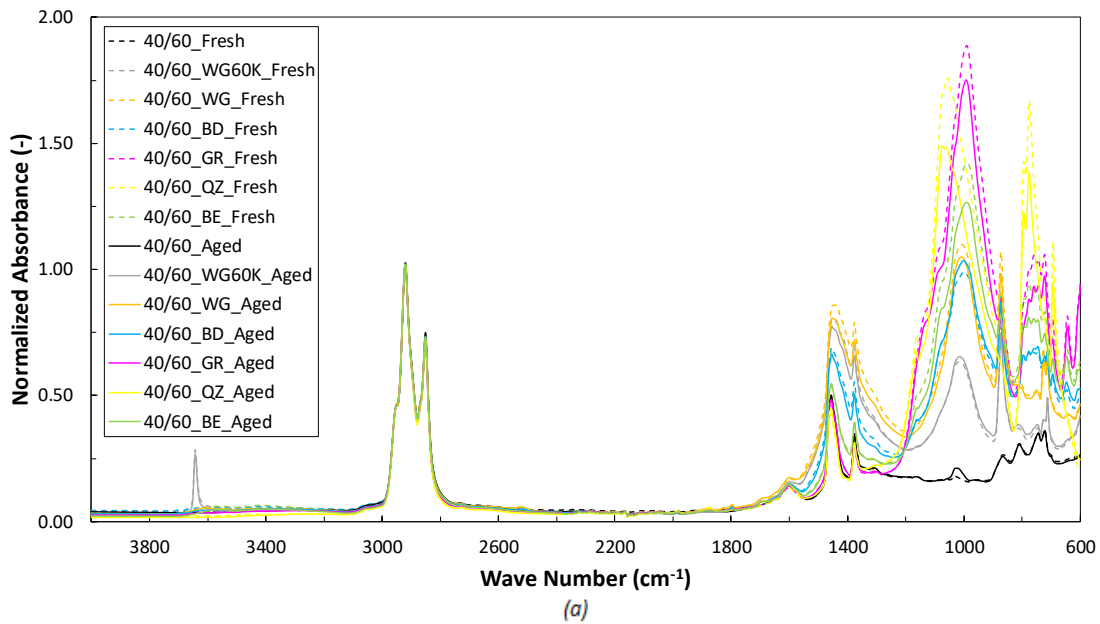
Finally, despite the fact that both above analyses are possible ways to justify the ageing ranking of 40/60\_BE, with respect to the mastics that physico-chemical interactions were expected to occur between the bitumen and the mineral fillers, the question why this particular material appears to be more aged than the mastic 40/60\_QZ, prepared with the "inert" mineral filler QZ, still remains. This question triggers the derivation of another possible explanation regarding the behavior of 40/60\_BE. It is well known, from bitumen-aggregate adhesion studies, that, in the presence of moisture, acidic aggregates (hydrophilic aggregates) show a greater affinity towards water molecules than bitumen components (Van Lent 2013). This means that, if there was moisture residue in BE upon mastic preparation and ageing, the interaction of bitumen components and the mineral filler's particles would be hindered by the presence of water molecules. Having excluded the interactions between the particles and bitumen, BE would behave as an "inert" mineral filler, similar to QZ, meaning that the only remaining mechanism that would contribute to the mitigation of the mastic's ageing is the effect of its particles on the oxygen diffusion path. The analysis for the potential chemical inertness of BE seems to justify its relative ranking with the chemically active mineral fillers. Moreover, considering its remaining "anti-ageing" mechanism, the finer nature of BE compared to QZ, could be the reason why 40/60\_BE appears to be more aged than 40/60\_QZ.

## 5.2 Chemical evaluation

This section deals with the chemical evaluation of the considered materials. The infrared spectra of all mastics and bitumen, both prior and after ageing, as well as ageing-related indices are presented and discussed. The post-processing of the FTIR data and spectra analysis are carried out according to the guidelines provided by Hofko et al. (2017)

### 5.2.1 Infrared spectra

In Fig. 5.10a the normalized infrared spectra of all materials are illustrated, while Fig. 5.10b and 5.10c show the close-ups of the carbonyls' (C=O) and sulfoxides' (S=O) regions, respectively.



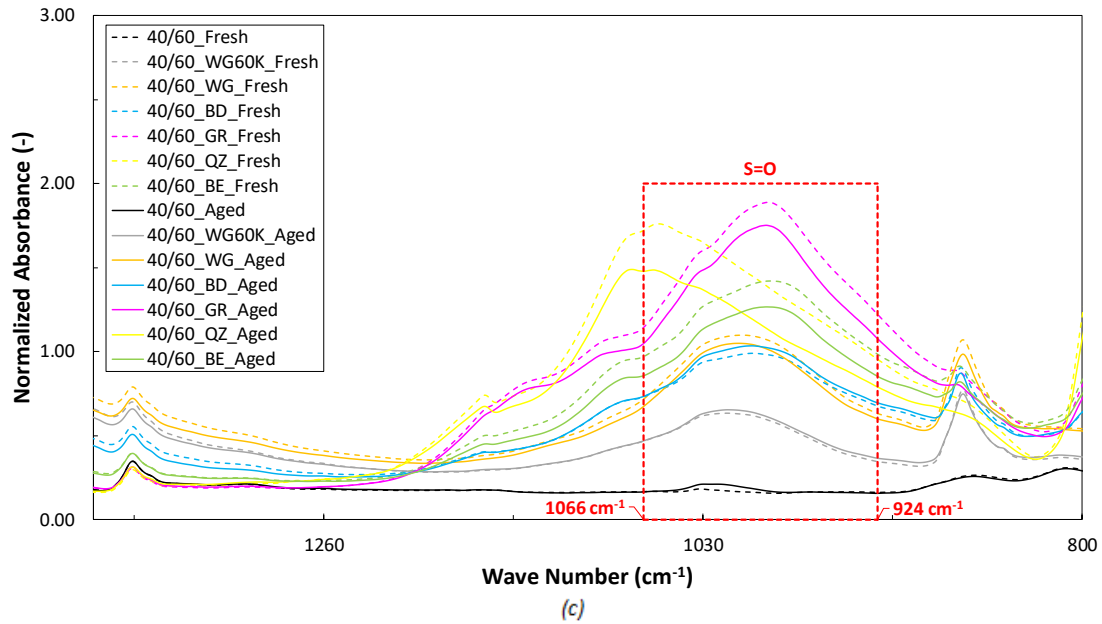


**Figure 5.10:** “Fresh” and aged bitumen and mastics infrared spectra. (a) Total spectra. (b) Carbonyls close-up. (c) Sulfoxides close-up.

From *Fig. 5.10a* it can be deduced that the interferogram of a mastic is a “mix” of the individual interferograms of its constituent materials and consists of peaks that are attributed both to the bitumen and the mineral filler. The latter is verified in *Fig. 5.11*, which shows an example of the infrared spectra of the two mastic’s phases as well as of the resulting composite material.

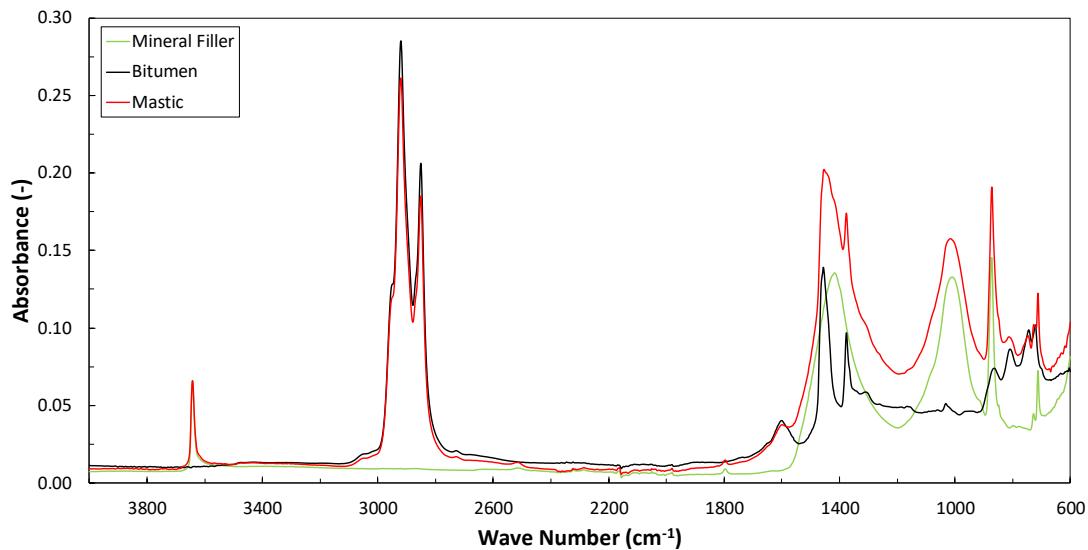


**Figure 5.11:** Example of infrared spectra of mineral filler, bitumen and resulting mastic.

The “fresh” mastics’ sulfoxides area (i.e.  $\sim 1030 \text{ cm}^{-1}$ ) is very much affected by the presence of the mineral fillers. On the contrary, their carbonyls area presents the same shape as in the case of “fresh” neat bitumen, which implies no effect of the mineral matter at these wave numbers.

Upon ageing, the increase of carbonyls is traced through visible peaks around the wave number  $1700 \text{ cm}^{-1}$  (*Fig. 5.10b*), which is solely attributed to the formation of C=O bonds in the bitumen phase. However, this is not the case when it comes to the sulfoxides

area. As it can be seen in *Fig. 5.10c*, for four out of seven materials the infrared spectra corresponding to their “fresh” state show a higher peak than the respective ones of the aged state. This is in contradiction with what is normally expected and observed, that is, the formation of S=O bonds in the bitumen microstructure upon ageing is translated through an increase in the sulfoxides peak. The reason behind such results is the presence of the mineral fillers in the mastics, and more specifically, the interference of the infrared beam, charged into the sample, with the solid particles. The effect of ageing on bitumen’s microstructure, in terms of sulfoxides formation, is in there, but it is hindered by the simultaneous contribution of the mineral matter to the aged mastic spectrum. The recorded absorbance value, during measurements, is very much depended on whether the infrared beam “hits” a mineral filler particle, pure bitumen or a combination of the two. The latter is also corroborated by the variability in the absorbance observed between the three tested replicates for each mastic. The variability was more apparent at the sulfoxides’ areas but extremely negligible at the carbonyls’ areas, or in other words, apparent at wave numbers where the peaks of the two phases interfere and negligible at regions where only one phase prevails.

The above qualitative analysis of the infrared spectra entails that the SI is not a reliable index for the ageing assessment of the materials, from a chemical point of view, as it would yield irrational results. On the other hand, the calculation of the CI seems a reliable and sound way to track down the effect of ageing on the various mastics and neat bitumen, through the formation of C=O bonds in the binders’ matrices.

### 5.2.2 Carbonyls index


The CI was calculated according to *Eq. 3.29*. The results are presented in *Fig. 5.12*.

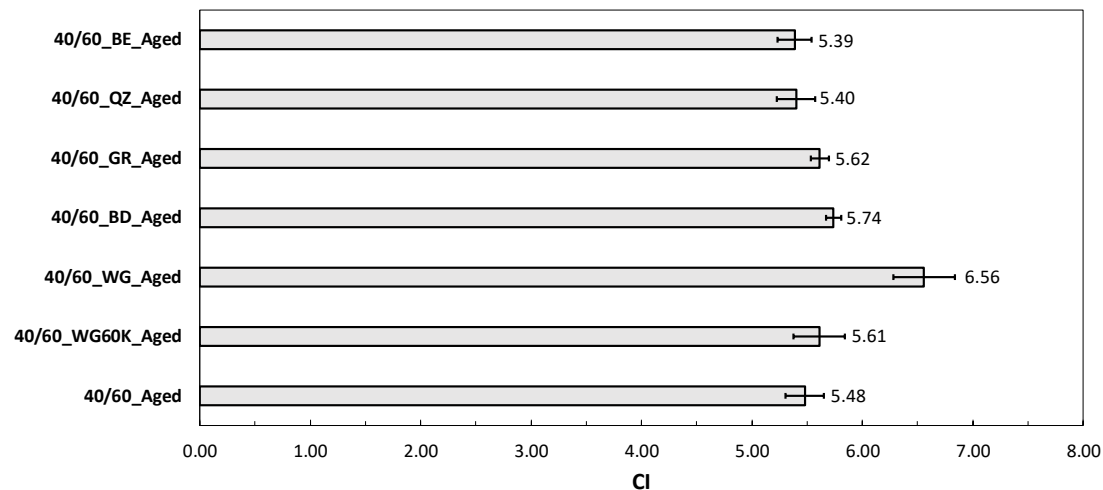


**Figure 5.12:** Aged bitumen and mastics carbonyls’ index.

The results in *Fig. 5.12* show that there is no significant difference in the CI between the materials, from a statistical point of view, except for 40/60\_WG\_Aged, as it can be concluded by the overlapping of the error-bars. Hence, the formation of carbonyls in the various materials can be considered, approximately, equivalent, excluding 40/60\_WG\_Aged, which differentiates itself by demonstrating a higher value of CI. *Table 5.2* presents the ranking of the aged materials, as a function of their ageing level, as defined based on the average calculated CI.

**Table 5.2:** Aged bitumen and mastics ranking based on the carbonyls' indices.

Material	Ageing level
40/60_WG_Aged	High
40/60_BD_Aged	
40/60_GR_Aged	
40/60_WG60K_Aged	
40/60_Aged	
40/60_QZ_Aged	Low
40/60_BE_Aged	

A comparison between *Tables 5.1 (Sub-Section 5.1.3)* and *5.2* yields that there is no correlation between the materials' ageing ranking based on the rheological and chemical evaluations. Analytically, mastics 40/60\_WG\_Aged, 40/60\_BD\_Aged, 40/60\_GR\_Aged and 40/60\_WG60K\_Aged appear to have undergone more severe ageing than pure bitumen, as shown by their higher CI, whereas the complex shear modulus AI (*Fig. 5.8, Sub-Section 5.1.3*) established these mastics as less aged than the neat bitumen. Only the mastics prepared with QZ and BE are shown to be less aged than pure bitumen, by both evaluations. Despite the fact that the results presented in this sub-section may seem irrational at a first glance, they may, in fact, provide insight regarding the interactions between the mineral fillers and the bitumen and, ultimately, correlate with the rheological results reported in *Sub-Section 5.1.3*. The latter is attempted in the analysis carried out in the next few paragraphs. It should be noted that BE and its corresponding aged mastic will be, again, excluded from the bulk analysis and will be discussed separately at a later stage.

First and foremost, it can be observed in *Fig. 5.12* that the aged mastics corresponding to the mineral fillers that are expected to develop physico-chemical interactions with bitumen (i.e. WG60K, WG, BD and GR) show a higher CI compared to neat aged bitumen, which indicates the catalysis of bitumen oxidation in the mastics. Curtis et al. (1993) claimed that the ageing of bitumen in the presence of mineral matter entails a delay in its viscosity build-up, when compared to ageing of neat bitumen, aged under identical conditions. The researchers believed that the difference in the viscosities' development was the result of the adsorption of polar functional groups from bitumen on the mineral matters' particles, which prevented the formation of viscosity build-up. This mechanism was also supported by the results reported by Wu (2009), Moraes & Bahia (2015a) and Moraes & Bahia (2015b), in their respective studies. This mechanism seems to be corroborated by the results presented in this chapter as well.

The CI results, in combination with the rheological behavior of the materials, verify the existence of the "anti-ageing" mechanism, related to the physico-chemical interactions between the bitumen and the mineral fillers in the mastics, introduced in *Sub-Section 5.1.3*. This mechanism refers to the adsorption, by the mineral fillers' particles, of polar functional groups, formed upon oxidation, from bitumen. More specifically, the mineral fillers WG60K, WG, BD and GR catalyzed the oxidation of bitumen, leading to a higher concentration of carbonyls in the mastics compared to pure aged bitumen (*Fig. 5.12*). The complex shear modulus AI results, presented in *Fig. 5.8*, is the outcome of the different abilities of these mineral fillers to adsorb and hold the polar functional groups of bitumen (e.g. carbonyls) on their particles' surface, thus, removing the viscosity-build-up-promoters from the bitumen matrix, leading to apparent less aged mastics.



Regarding mastic 40/60\_WG\_Aged, its noticeably high concentration of carbonyls may be the result of WG's high SSA (i.e. 13.25 m<sup>2</sup>/gr). The latter, however, is not supported by the data of the rest of the mineral fillers and a clear trend could not be established to support such a conclusion. The fact that 40/60\_WG\_Aged shows the highest CI and still ranks as one of the least aged mastics, based on the complex shear modulus AI (*Fig. 5.8, Sub-Section 5.1.3*), underlines the great ability of limestone-based mineral fillers in adsorbing polar components from bitumen. In addition, with the FTIR/ATR results at hand, the statement, cited in *Sub-Section 5.1.3*, that the close packing of the 40/60\_WG60K and 40/60\_WG AI curves (*Fig. 5.6, Sub-Section 5.1.2*) and the relative ageing ranking of these two materials as the frequency increases is the result of the larger SSA of WG compensating for their differences in mineralogy, seems to be verified. The latter is maybe the first clear indication of the favourable effect of the mineral fillers' SSA on ageing of bituminous mixtures, expressed through an intensified adsorption mechanism.

The mastic 40/60\_QZ\_Aged shows a slightly lower CI than pure aged bitumen, implying that the mineral filler QZ did not lead to any catalysis of the bitumen oxidation in the mastic. This can be attributed to its chemical inertness, in contrast to the mineral fillers discussed previously. The lower CI of 40/60\_QZ\_Aged compared to pure aged bitumen correlates well with the rheological evaluation performed in *Sub-Section 5.1.3*. The formation of less carbonyls is believed to be the result of the lengthening of the oxygen diffusion path caused by the physical presence of the mineral filler's particles in the mastic.

Nevertheless, it would be interesting to investigate the FTIR/ATR results of the mastic 40/60\_QZ\_Aged and neat aged bitumen by taking into account their CIs' variation. From a statistical point of view the CI of both materials can be considered equivalent. This cannot directly explain the ageing ranking of the materials based on the complex shear modulus AI (*Fig. 5.8, Sub-Section 5.1.3*). Petersen (2009) observed that bitumen which showed a fairly similar amount of formed oxygenated products, exhibited quite different age-hardening, based on viscosity measurements. The researcher attributed this behavior to their components' compatibility and, more specifically, to the variant capacity of the non-polar components of bitumen to effectively disperse the polar functional groups formed upon ageing. Having mentioned the above, it is believed that, despite the fact that the two materials show a similar amount of carbonyls, this is not translated into the rheological measurements by virtue of the different capacities of these materials to disperse the polar functional groups. A high dispersion capacity entails that the polar components can flow past each other with greater easiness under the application of shear stress resulting in an apparent softer material.

The above explanation is based on the following reasoning: Ageing in the PAV includes an oxygen diffusion-reaction mechanism. The test set-up leads to more severe ageing of the tested materials at the upper part of the diffusion medium, whereas the material at the bottom of the PAV pan can be expected to be less aged, if any at all. When the oxygen diffuses into the mastic 40/60\_QZ the mineral filler particles act as obstacles to oxygen molecules. As a result, the latter are compelled to follow a more spiral path and limit their action, with respect to the formation of C=O bonds, at the very upper part of the diffusion medium. For equal ageing times, the saturated by oxygen thickness would be larger for the neat bitumen compared to the mastic. At the end of the ageing process, the upper severe aged parts of the materials were diluted with the lower less aged, or even unaged, parts and samples were obtained for further testing. The mixing of the two parts (i.e. upper and lower) and the difference in the materials' thicknesses, which were

saturated by oxygen molecules, led to the variant dispersity of the polar components, entailing the observed rheological differences.

With respect to BE and its corresponding aged mastic (i.e. 40/60\_BE\_Aged) it can be observed that its CI is, almost, identical to the CI of the mastic 40/60\_QZ\_Aged and, statistically speaking, equivalent to the CI of neat aged bitumen (*Fig. 5.12*). In *Sub-Section 5.1.3* the ageing ranking of the mastic 40/60\_BE, based on the complex shear modulus AI, was attempted to be explained through its comparison with three other mastics. Amongst the latter, only the explanation claiming that a potential chemical inertness of the mineral filler (i.e. BE) might have led to the resulting mastic's ageing behavior, seemed to completely justify, from all aspects, its relative ranking with the rest of the materials. The CIs' equivalency of 40/60\_BE\_Aged and 40/60\_QZ\_Aged suggests that the explanation provided above may hold true. The mineral filler BE do not show any catalysis of bitumen oxidation, as was noticed for the rest of the chemically active mineral fillers, and its rheological results do not support, with confidence, the development of the adsorption mechanism. These two features might indeed manifest the inertness of BE.

The correlation of the mastic's 40/60\_BE(\_Aged) rheological and chemical evaluations may be performed as in the case of QZ, through the concept of the dispersion of the polar functional groups by the maltenes phase of the binder. The finer nature of BE compared to QZ would lead to the faster penetration of oxygen into the diffusion medium, but still the diffusion path in the mastic 40/60\_BE would be longer than in the case of neat bitumen. Hence, it seems that the mastic 40/60\_BE\_Aged experiences an intermediate dispersion capacity of polar functional groups in comparison to mastic 40/60\_QZ\_Aged and pure aged bitumen which can justify its relative ranking based on the complex shear modulus AI (*Fig. 5.8, Sub-Section 5.1.3*).

# 6

## Bitumen extraction and recovery from aged mastics

## 6.1 Preliminary information

### 6.1.1 “Fresh” bitumen

The preparation of mastics for the ageing and extraction and recovery procedures was carried out by utilizing the same type of bitumen, as described in *Section 3.1*, but from a different storage can. The “fresh” bitumen used in this phase is designated, hereafter, as 40/60\_ExPh (ExPh = Extraction Phase). *Fig. 6.1* shows the  $G^*$  and  $\delta$  master-curves of the “fresh” bitumen utilized at this stage of the research and the one used at the mastics’ evaluation stage. The results indicate that the newly used “fresh” binder is slightly softer than the former one. Bitumen 40/60\_ExPh is used for further considerations in this part of the research to avoid any effect on the results interpretation that might originate from the difference of the “fresh” binders coming from two different storage cans.

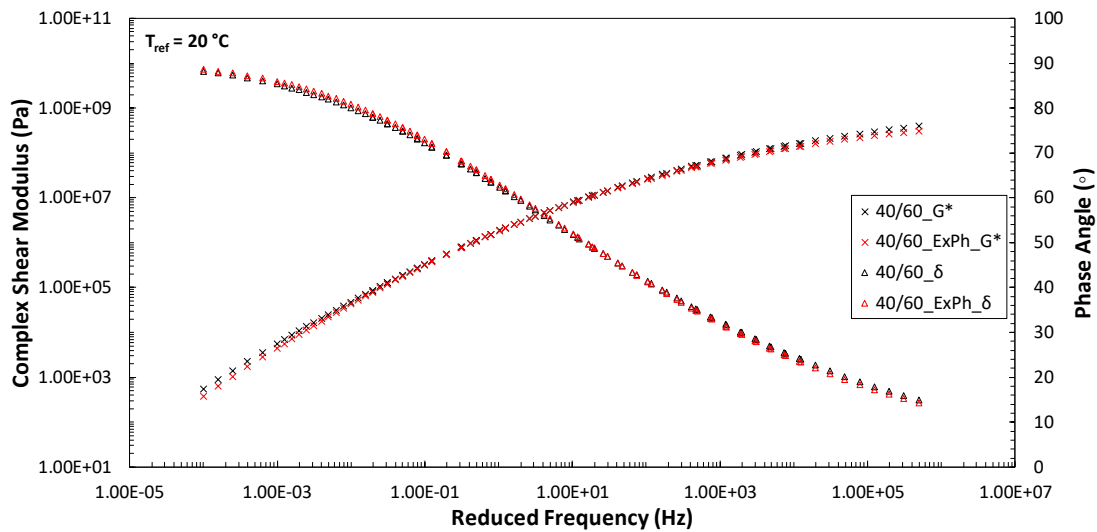


**Figure 6.1:** Complex shear modulus and phase angle master-curves of “fresh” bitumen utilized at mastics evaluation phase and bitumen extraction phase.

### 6.1.2 Materials preparation and ageing protocol

The preparation of neat bitumen and mastics and the ageing of the materials were done according to the procedures described in *Section 3.3* and *Section 3.4*, respectively. Bitumen 40/60\_ExPh was aged along with the mastics in the PAV to preserve the concept of identical ageing conditions between the materials that are about to be compared. The ageing of mastics was followed by the extraction and recovery of their bitumen for further testing.

## 6.2 Bitumen extraction and recovery process

The extraction and recovery of bitumen from the aged mastics was performed at the TNO MEC-laboratory. The description of the processes is summarized in the next steps:

- i. 130 ml of dichloromethane were added to each aged mastic (*Fig. 6.2*) 24 hours prior to the extraction of the mastic-dichloromethane solution in the asphaltanalysator.



**Figure 6.2:** Aged mastic-dichloromethane solution.

- ii. After 24 hours, the mastic-dichloromethane solution was transferred into the centrifuge of the asphaltanalysator. A sieve was used to remove the insoluble parts larger than 63  $\mu\text{m}$  (*Fig. 6.3*). The sieve and centrifuge were washed with 800-820 ml of dichloromethane.



**Figure 6.3:** Removal of mineral filler particles larger than 63  $\mu\text{m}$ .

- iii. The separation of the liquid phase from the mineral filler particles in the centrifuge of the asphaltanalysator (type 20-1100 from InraTest GmbH) (*Fig. 6.4*) was finalized in 30 minutes. Solid particles between 10-63  $\mu\text{m}$  were collected in the centrifuge beaker of the asphaltanalysator. This procedure was carried out according TNO MEC lab procedure WVS-MEC-16.



**Figure 6.4:** Centrifuge of the asphaltanalysator.

- iv. The reclaimed bitumen-dichloromethane solution was filtered through a glass filter (*Fig. 6.5*) of pores' size equal to  $10\ \mu\text{m}$ , to remove any residual mineral filler particles. The filtration was followed by the wash of the glass filter with 50-80 ml of dichloromethane.

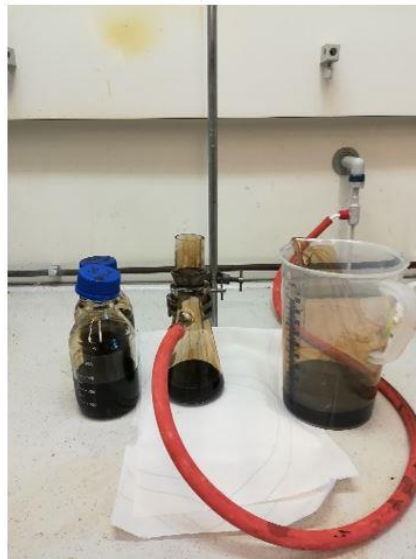


**Figure 6.5:** Glass filter of pores' size equal to  $10\ \mu\text{m}$ .

- v. The removal of the dichloromethane from the bitumen-dichloromethane solution was done by utilizing the rotary evaporator (*Fig. 6.6*). The procedure was carried out in two stages. *Table 6.1* summarizes the applied conditions during these stages. Approximately 99% of the dichloromethane was removed in the first stage. The recovery process was conducted according to the protocol WVS-MEC-16 (NEN-EN 12697-3) of TNO MEC-laboratory.



Figure 6.6: Rotary evaporator set-up.

Table 6.1: Bitumen recovery process conditions.

Stage	Conditions		
	Duration (hrs)	Temperature (°C)	Pressure (mbar)
1	1	85	850
2	1	150	20

- vi. The recovered bitumen from the bitumen-dichloromethane solution was stored at the refrigerator until the imminent dynamic and chemical tests.

In *Table 6.2* the abbreviations of the recovered bitumen are presented. During bitumen extraction the mineral fillers from the aged mastics were also reclaimed to be used in the efficiency assessment of the extraction and recovery process. *Table 6.3* shows the abbreviations of the reclaimed mineral fillers.

Table 6.2: Recovered bitumen abbreviations.

Treated mastic	Recovered bitumen abbreviation
40/60_WG60K_Aged	RB_40/60_WG60K_Aged
40/60_WG_Aged	RB_40/60_WG_Aged
40/60_BD_Aged	RB_40/60_BD_Aged
40/60_GR_Aged	RB_40/60_GR_Aged
40/60_QZ_Aged	RB_40/60_QZ_Aged
40/60_BE_Aged	RB_40/60_BE_Aged

Table 6.3: Reclaimed mineral fillers abbreviations.

Treated mastic	Recovered mineral filler abbreviation
40/60_WG60K_Aged	WG60K_Recovered
40/60_WG_Aged	WG_Recovered
40/60_BD_Aged	BD_Recovered
40/60_GR_Aged	GR_Recovered
40/60_QZ_Aged	QZ_Recovered
40/60_BE_Aged	BE_Recovered

### 6.3 Neat aged bitumen conditioning

Hot extraction and recovery methods may lead to (slight) ageing of the recovered bitumen (Wu 2009). *Table 6.1* shows the duration and applied temperatures during solvent evaporation from the bitumen-dichloromethane solution. It is expected that these conditions may have led to some change of the ageing level of the recovered bitumen. As repeatedly stated in this thesis, it is of immense importance that all materials undergo, as much as possible, similar ageing, due to the research's comparative character. For that reason, the heating conditions presented in *Table 6.1* were also applied for the neat aged bitumen (i.e. 40/60\_Aged\_ExPh). It should be noted that the conditioning of neat aged bitumen differs from the actual case of bitumen recovery by virtue of the absence of the solvent. Nevertheless, its conditioning was regarded as essential for a fairer comparison of the various materials with respect to their ageing level.

*Fig. 6.7* illustrates the  $G^*$  and  $\delta$  master-curves of the neat aged bitumen prior (40/60\_Aged\_ExPh\_Uncond) and after (40/60\_Aged\_ExPh\_Cond) conditioning. The results indicate that the applied heating temperatures and durations, shown in *Table 6.1*, led to a negligible age-hardening of the material. The latter is derived by the almost perfect overlapping of the  $G^*$  and  $\delta$  master-curves corresponding to the two states.

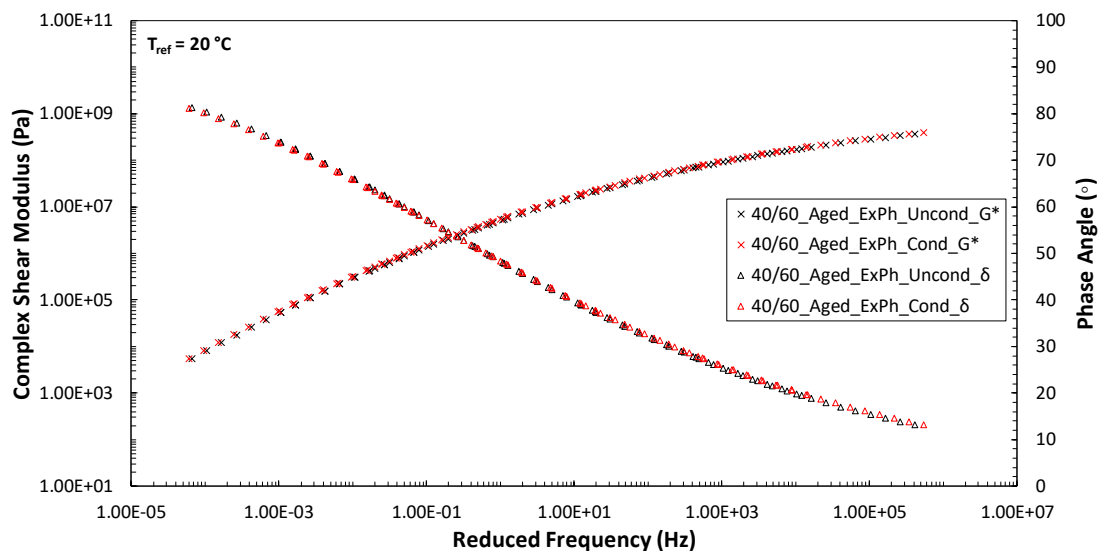


**Figure 6.7:** Complex shear modulus and phase angle master-curves of unconditioned and conditioned neat aged bitumen.

*Fig. 6.8* shows the infrared spectra of 40/60\_Fresh\_ExPh, 40/60\_Aged\_ExPh\_Cond and 40/60\_Aged\_ExPh\_Uncond. The CI and SI of the aforementioned materials were calculated based on *Eq. 3.29* and *3.30*, respectively. The results are presented in *Fig. 6.9* and *6.10*, respectively.

The outcome indicates that the neat aged bitumen treatment leads to the (slight) increase of the carbonyls and sulfoxides concentration, when compared to the unconditioned state. This implies that the bitumen recovery procedure may also have had a (minor) effect in the formation of C=O and S=O bonds in the recovered binders. Nevertheless, from a statistical point of view, the CIs and SIs of the neat aged binders, corresponding to the two conditioning states, can be considered equivalent. The conditioned neat aged bitumen (i.e. 40/60\_Aged\_ExPh\_Cond) is used for further considerations in this chapter.



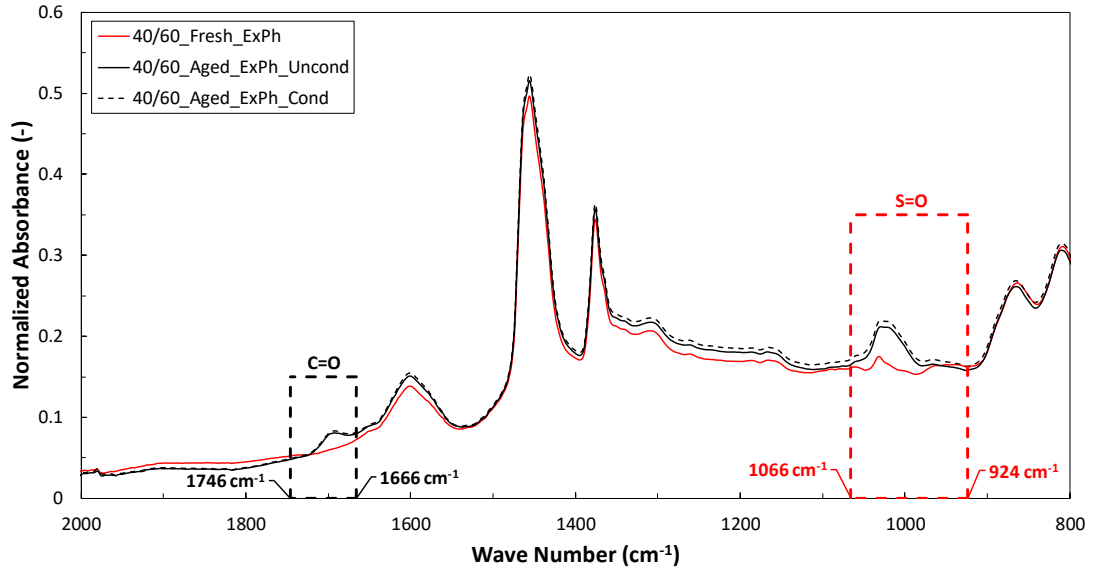


Figure 6.8: Infrared spectra of “fresh”, unconditioned and conditioned neat aged bitumen.

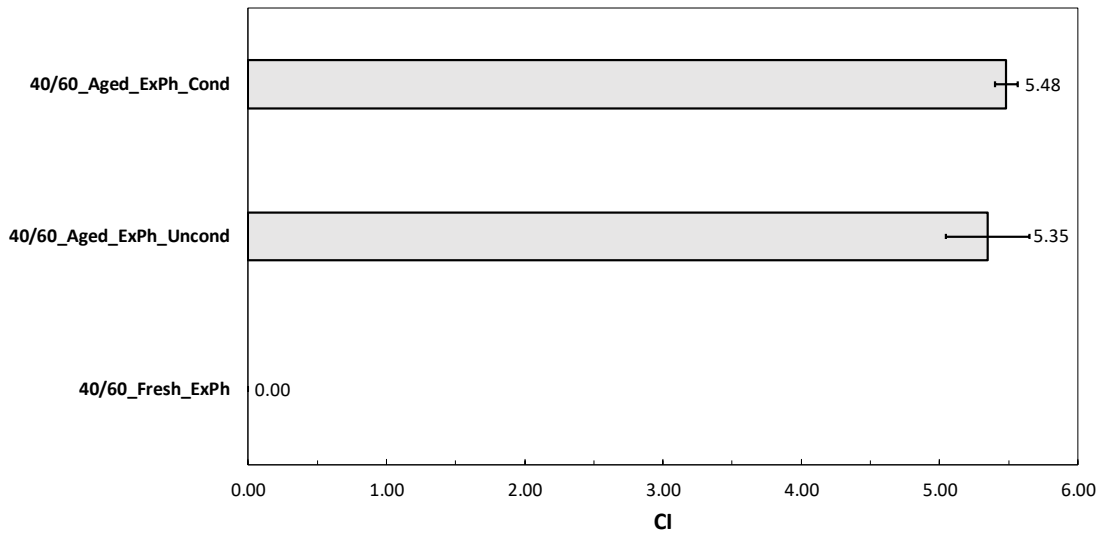


Figure 6.9: Carbonyls' index of “fresh”, unconditioned and conditioned neat aged bitumen.

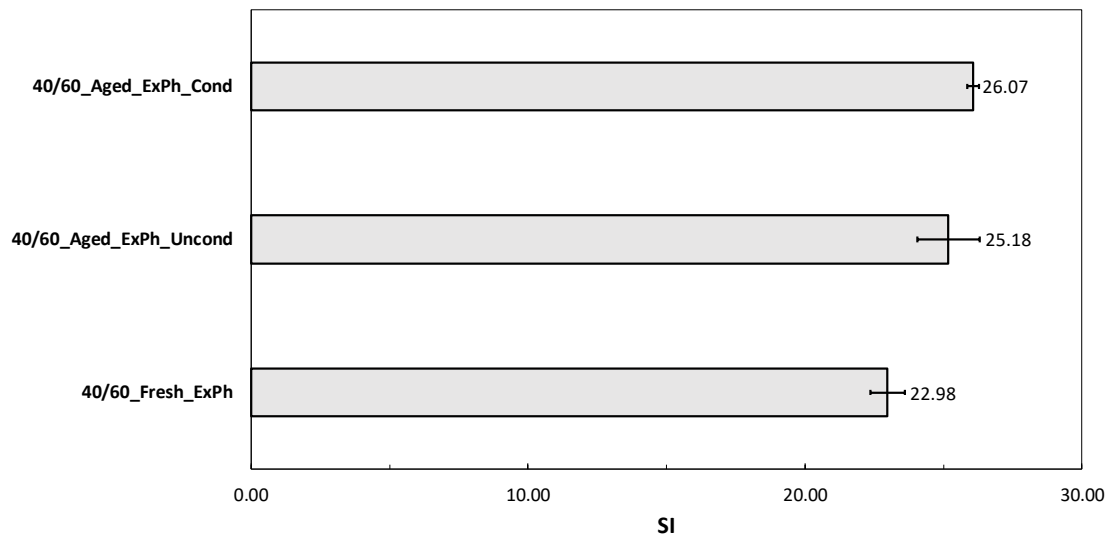


Figure 6.10: Sulfoxides' index of “fresh”, unconditioned and conditioned neat aged bitumen.

## 6.4 Assessment of extraction and recovery process

### 6.4.1 Mineral filler contamination and solvent residual

The utilization of the extraction and recovery procedure, described in *Section 6.2*, includes the removal of mineral filler particles larger or equal to 10  $\mu\text{m}$ . This implies, and by considering the mineral fillers' gradation (*Table 4.1, Section 4.1*), that part of the mineral matter remained in the recovered bitumen. Mineral filler residue in the recovered bitumen can lead to changes in the binder's rheological properties and disturbance of its infrared spectrum. The contamination of the recovered material by mineral matter can be traced through FTIR testing, when the infrared spectrum of the mineral filler is known (Van den Bergh 2011). Moreover, solvent residue in the recovered bitumen may lead to the softening of the binder (Wu 2009).

The FTIR test was employed to investigate any potential effect of the mineral matters' residue on the properties of the recovered bitumen. The latter was carried out by comparing the infrared spectra of the recovered bitumen and their corresponding mineral fillers. Moreover, the infrared spectrum of the neat aged bitumen (i.e. 40/60\_Aged\_ExPh\_Cond) was included in the comparison to identify possible relevant peaks in the recovered bitumen spectra that could manifest solvent residuals. The results, for all recovered materials, are presented in *Fig. 6.11 to 6.16*.

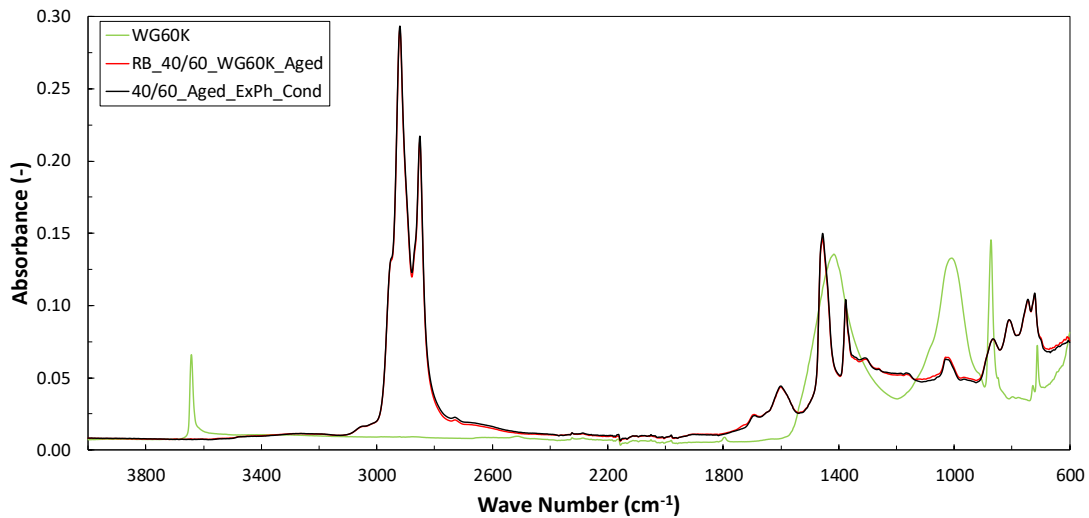


**Figure 6.11:** Mineral filler WG60K, recovered bitumen RB\_40/60\_WG60K\_Aged and neat aged bitumen 40/60\_Aged\_ExPh\_Cond infrared spectra.

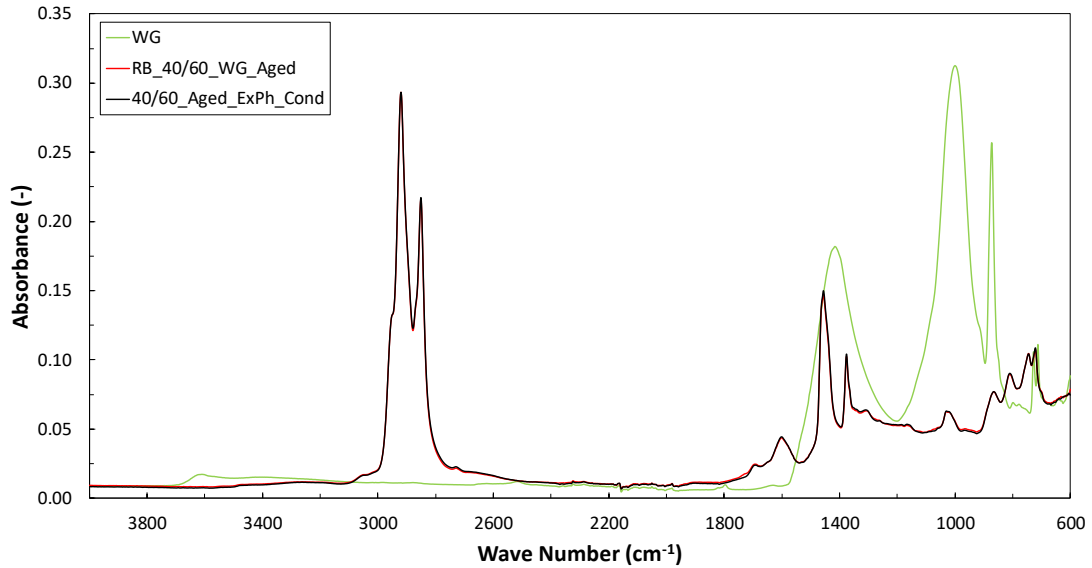


**Figure 6.12:** Mineral filler WG, recovered bitumen RB\_40/60\_WG\_Aged and neat aged bitumen 40/60\_Aged\_ExPh\_Cond infrared spectra.

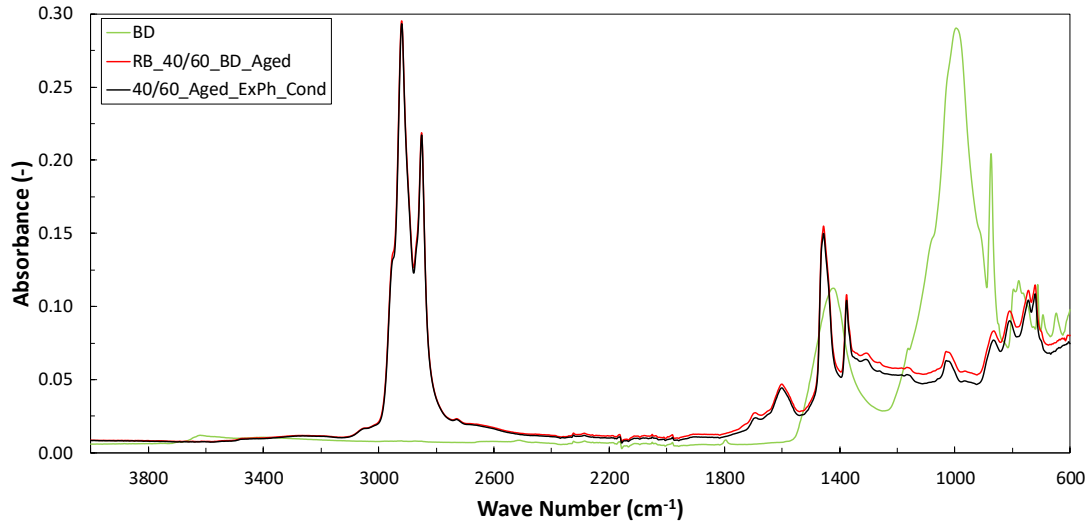


**Figure 6.13:** Mineral filler BD, recovered bitumen RB\_40/60\_BD\_Aged and neat aged bitumen 40/60\_Aged\_ExPh\_Cond infrared spectra.

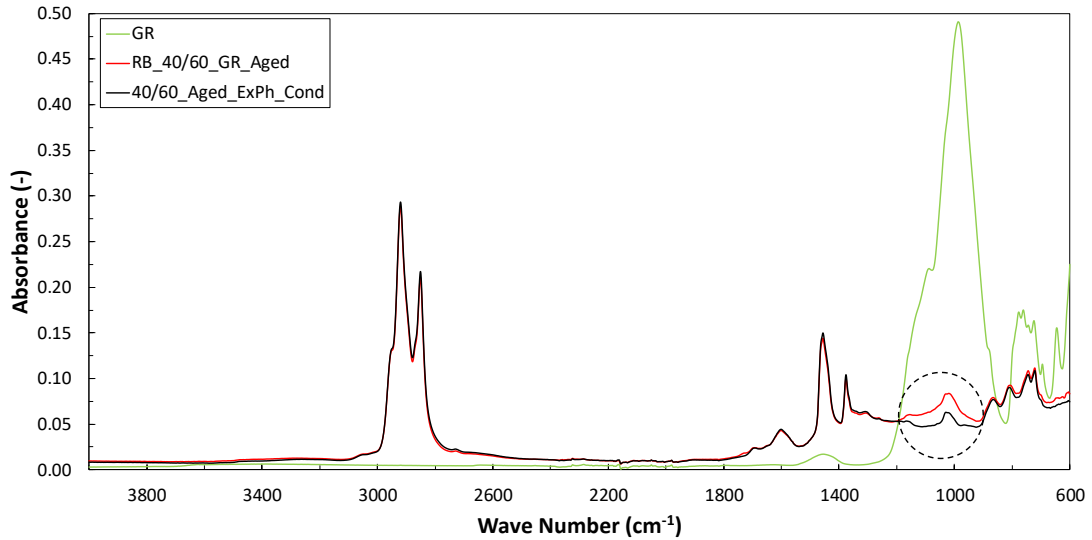


**Figure 6.14:** Mineral filler GR, recovered bitumen RB\_40/60\_GR\_Aged and neat aged bitumen 40/60\_Aged\_ExPh\_Cond infrared spectra.

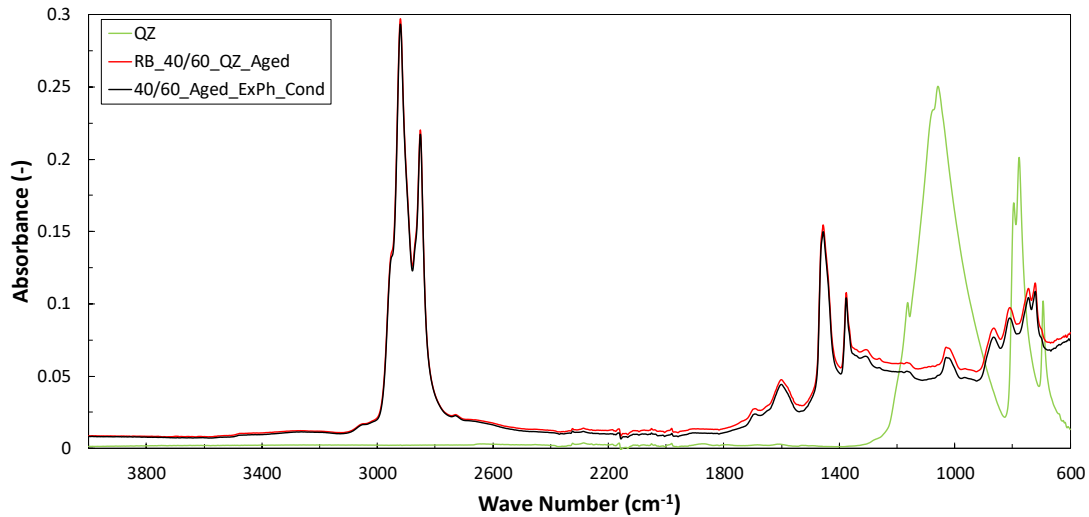


**Figure 6.15:** Mineral filler QZ, recovered bitumen RB\_40/60\_QZ\_Aged and neat aged bitumen 40/60\_Aged\_ExPh\_Cond infrared spectra.

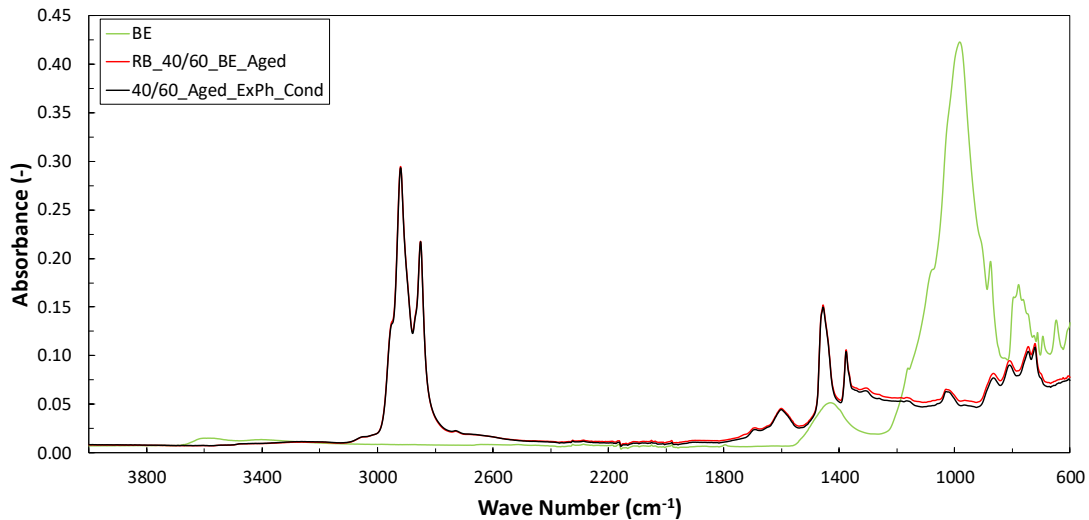


**Figure 6.16:** Mineral filler BE, recovered bitumen RB\_40/60\_BE\_Aged and neat aged bitumen 40/60\_Aged\_ExPh\_Cond infrared spectra.

The results indicate that there is no disturbance of the recovered bitumen infrared spectra, resulting from peaks that could be attributed to the mineral fillers' effect. This is not the case, however, for the bitumen recovered from the GR aged mastic (*Fig. 6.14*). The shape of the recovered bitumen infrared spectrum around the wave number  $1030\text{ cm}^{-1}$  (circled area in *Fig. 6.14*) shows that the binder is possibly affected by some residual mineral filler particles. The disturbance of this area can be ascribed to the peak of the infrared spectrum of mineral filler GR around the wave number  $1030\text{ cm}^{-1}$ . The latter will have an influence on the calculation of the SI of this particular recovered bitumen and should be taken into account in the declared SI value.

A comparison of the recovered bitumen and neat aged bitumen infrared spectra yields that all recovered binders are solvent-free, since no peaks are identified in the recovered materials' infrared spectra that would denote dichloromethane residue.

### 6.4.2 Recovery of bitumen components

In this sub-section the degree of reclamation of bitumen components upon binders' extraction is evaluated. The latter is done through a comparison of the infrared spectra of the mineral fillers prior and after the extraction procedure. The infrared spectra of the reclaimed mineral fillers are examined for the presence of new peaks, compared to the spectra of the original materials, that would manifest any possible irreversible absorption and/or adsorption of bitumen components into/onto the mineral matters' particles. The results are shown in *Fig. 6.17* to *6.22*.

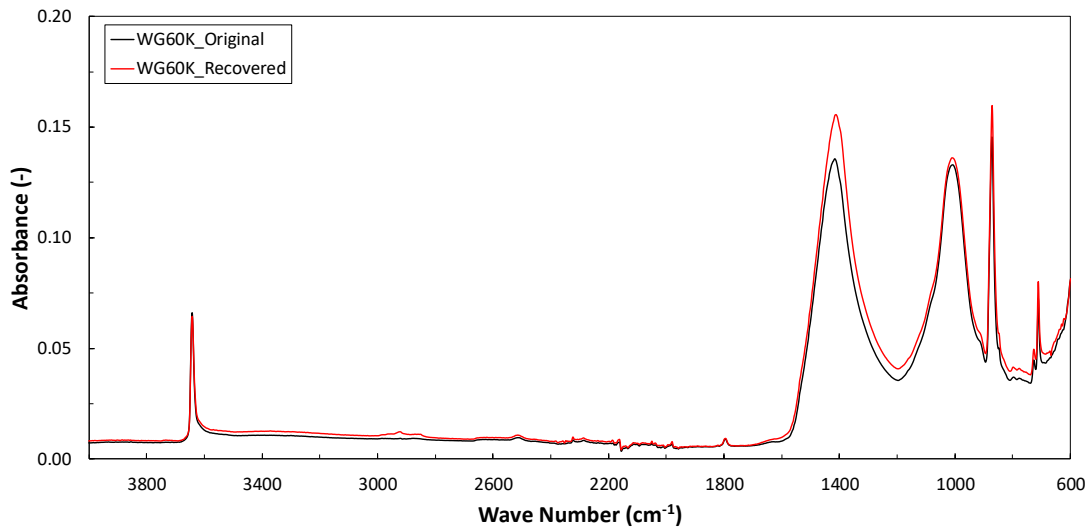


Figure 6.17: Original and recovered mineral filler WG60K infrared spectra.

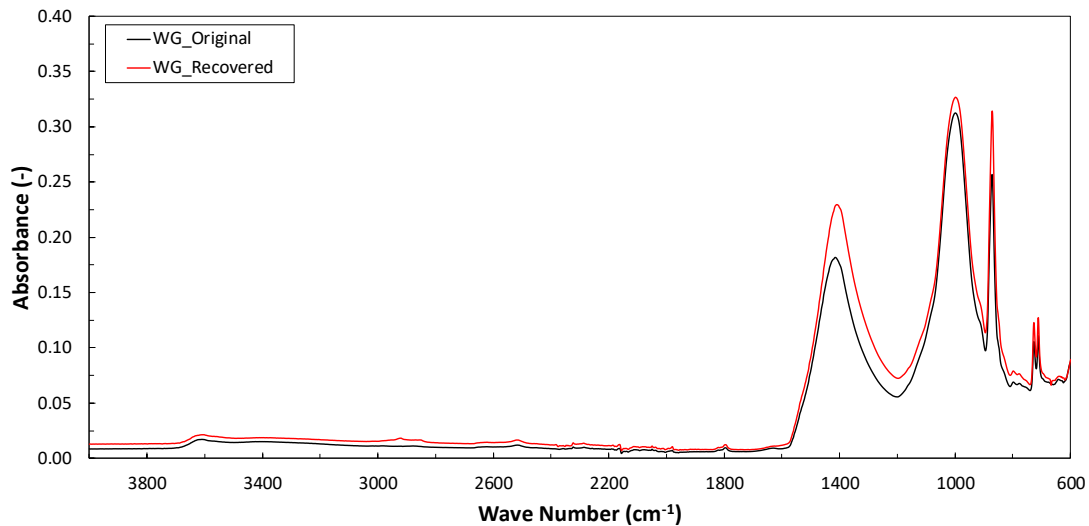


Figure 6.18: Original and recovered mineral filler WG infrared spectra.

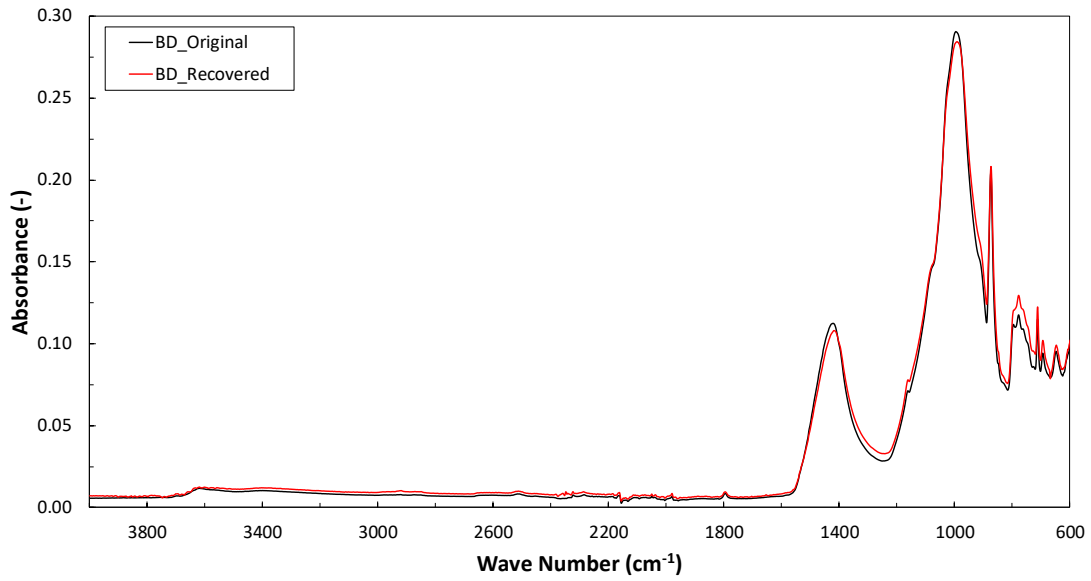


Figure 6.19: Original and recovered mineral filler BD infrared spectra.

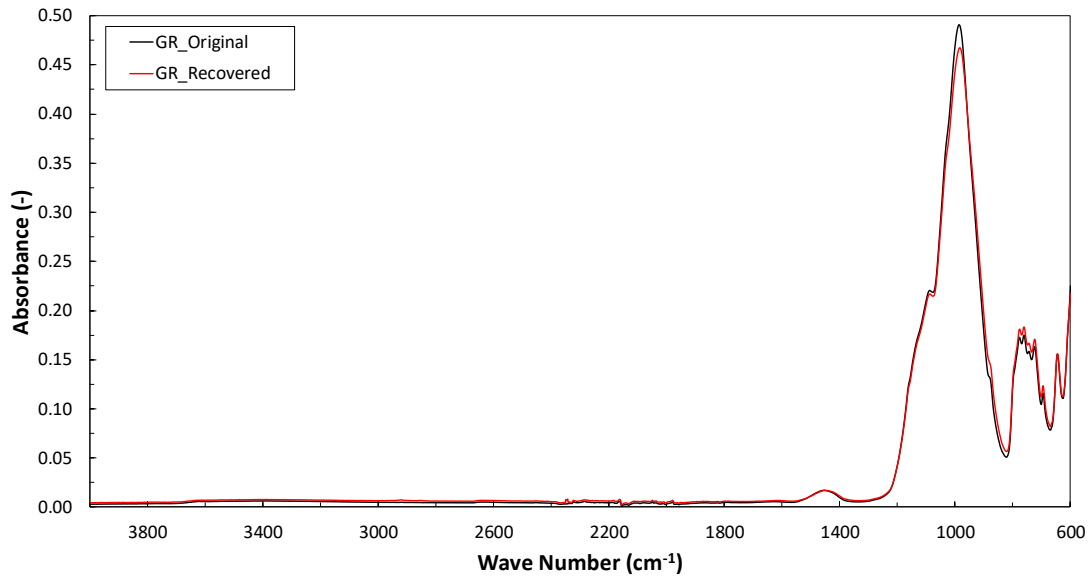


Figure 6.20: Original and recovered mineral filler GR infrared spectra.

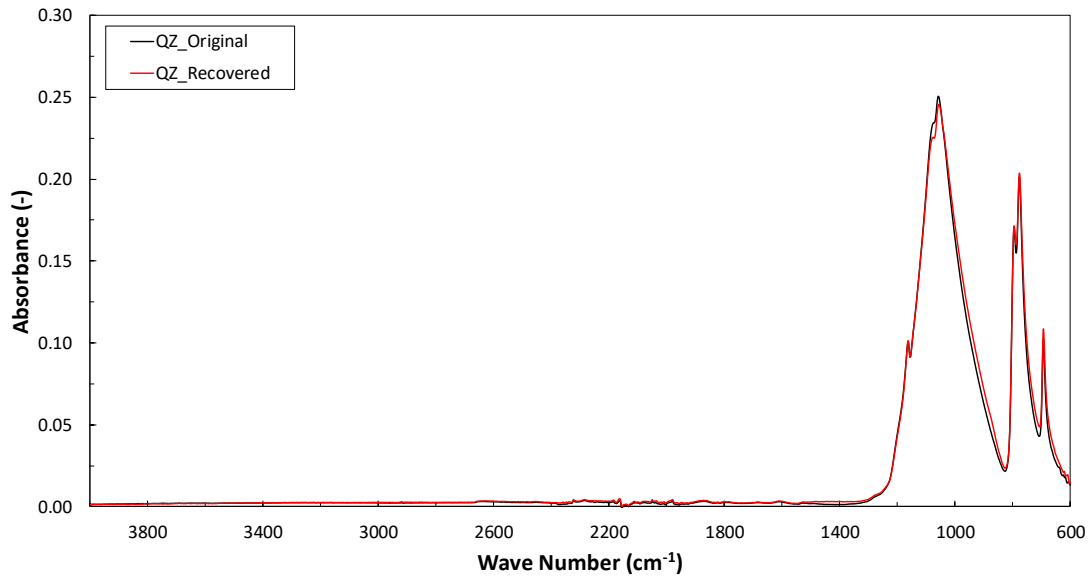


Figure 6.21: Original and recovered mineral filler QZ infrared spectra.

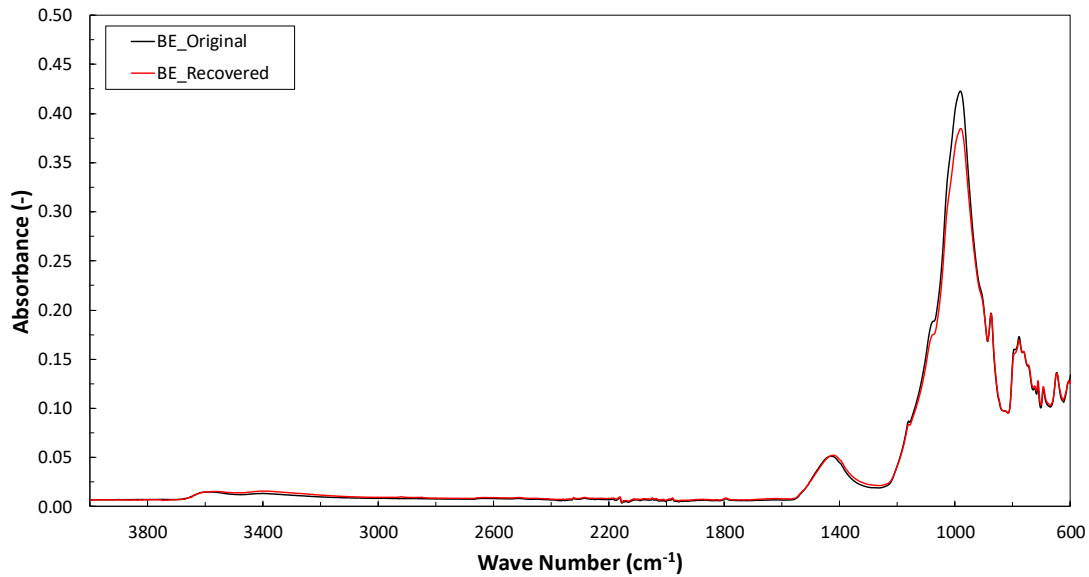


Figure 6.22: Original and recovered mineral filler BE infrared spectra.

Visual inspection of the infrared spectra yields that no new peaks appear in the reclaimed mineral fillers' infrared spectra that could be attributed to irreversible interactions between the bitumen components and the mineral matters' particles. This leads to the conclusion that upon bitumen extraction all bitumen components that might had been absorbed and/or adsorbed into/onto the mineral fillers' particles are reclaimed into the recovered bitumen matrices.

### 6.5 Rheological evaluation of recovered and neat bitumen – results and discussion

The  $G^*$  and  $\delta$  master-curves of the neat “fresh” bitumen (i.e. 40/60\_Fresh\_ExPh), neat aged bitumen (i.e. 40/60\_Aged\_ExPh\_Cond) and recovered binders are presented in Fig. 6.23 and 6.24, respectively.

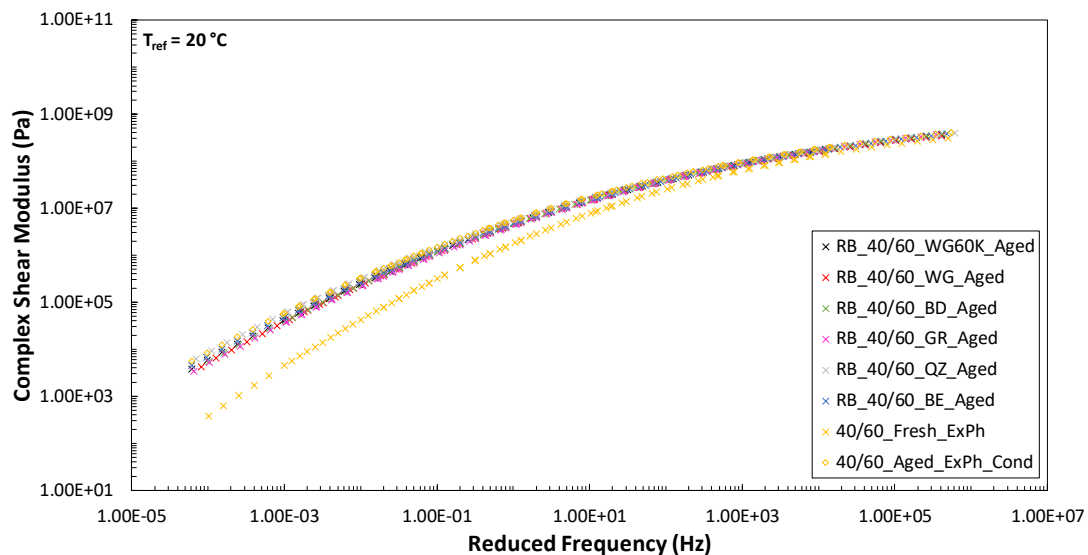


Figure 6.23: “Fresh”, neat aged and recovered bitumen complex shear modulus master-curves.

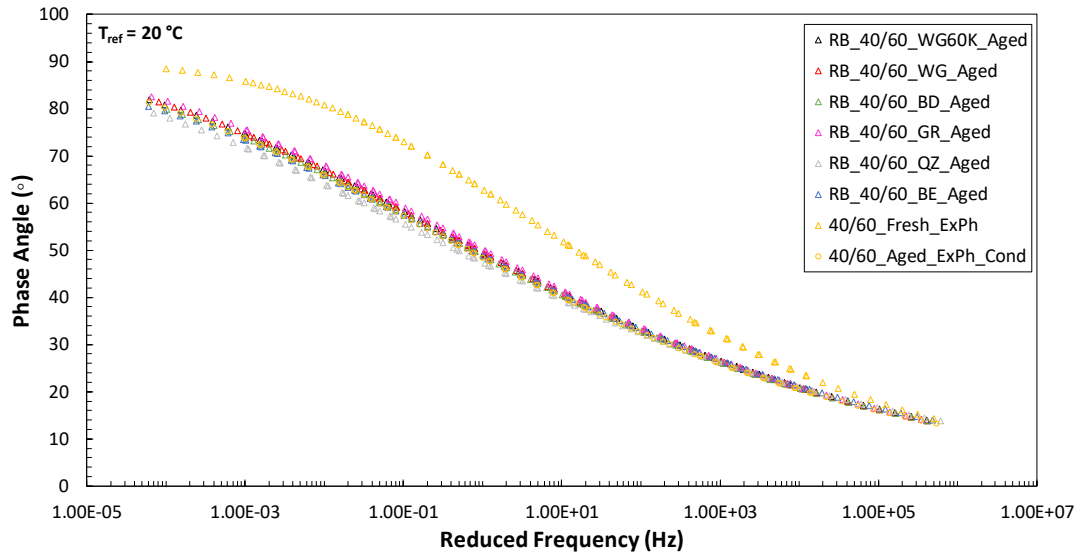


Figure 6.24: “Fresh”, neat aged and recovered bitumen phase angle master-curves.

### 6.5.1 Complex shear modulus and phase angle master-curves analysis

#### *Complex shear modulus master-curves*

It is obvious from *Fig. 6.23* that all recovered binders appear to be (slightly) softer than the neat aged one, except for the bitumen coming from the aged QZ mastic, whose  $G^*$  master-curve almost perfectly overlaps with the respective one of the neat aged binder. Amongst the various recovered bitumen, RB\_40/60\_GR\_Aged and RB\_40/60\_WG\_Aged demonstrate the lowest  $G^*$  values followed by the bitumen originating from the aged BD, WG60K and BE mastics. Nevertheless, by virtue of the close packing of the materials'  $G^*$  master-curves, their differences are not completely visible. The latter will become clearer through the calculation of the complex shear modulus AI performed in *Sub-Section 6.5.2*.

Another observation is that the rheological properties of all recovered binders are not affected by mineral fillers' residuals. This is based on the fact that all master-curves converge at very high frequencies and no increase in the  $G^*$  value of the recovered bitumen is observed, that could originate from the mineral fillers' stiffening effect (see *Fig. 5.1, Section 5.1*). This observation verifies the outcome of the infrared spectra investigation, performed in *Sub-Section 6.4.1*, regarding the identification of the possible effect of mineral fillers' residuals on the recovered bitumen properties. Even in the case of RB\_40/60\_GR\_Aged, which was found to be slightly affected by mineral filler residue (*Fig. 6.14, Sub-Section 6.4.1*), this effect seems to be negligible in the rheological evaluation. Hence, the position of the  $G^*$  master-curves can be solely attributed to the properties of the binders themselves.

#### *Phase angle master-curves*

The  $\delta$  master-curves (*Fig. 6.24*) show, excluding the case of the neat “fresh” bitumen, that RB\_40/60\_QZ\_Aged possesses the most elastic response from all tested materials, whereas a rather similar response can be observed between the recovered bitumen originating from the aged BD and BE mastics and the neat aged bitumen. The  $\delta$  master-curves of RB\_40/60\_WG60K\_Aged and RB\_40/60\_WG\_Aged almost perfectly overlap and their response is slightly more viscous than the respective one of



40/60\_Aged\_ExPh\_Cond. Finally, the recovered bitumen from the mastic 40/60\_GR\_Aged shows the most viscous response amongst the considered materials.

**6.5.2 Complex shear modulus ageing indices**

The comparative analysis of the ageing level of the various recovered bitumen with each other, as well as with the neat aged binder, was carried out through the calculation of complex shear modulus AI by utilizing Eq. 5.2. The  $G^*$  values used in the denominator of Eq. 5.2 correspond to the “fresh” bitumen (i.e. 40/60\_Fresh\_ExPh), while the  $G^*$  values of the nominator to the each-time evaluated material (i.e. recovered or neat aged bitumen).

Fig. 6.25 shows the AI of all materials as a function of the reduced frequency. The materials’ AI at 0.001 Hz and 20°C are presented in Fig. 6.26, while Table 6.4 shows the relative ageing ranking of the recovered and neat aged bitumen based on the latter indices.

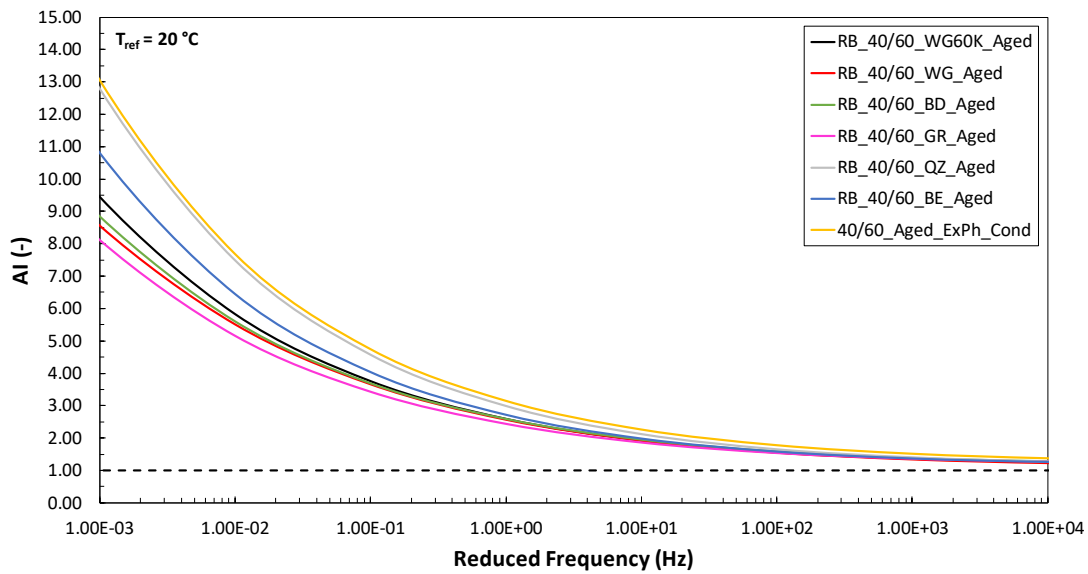



**Figure 6.25:** Recovered and neat aged bitumen complex shear modulus ageing indices as a function of the reduced frequency at 20°C.

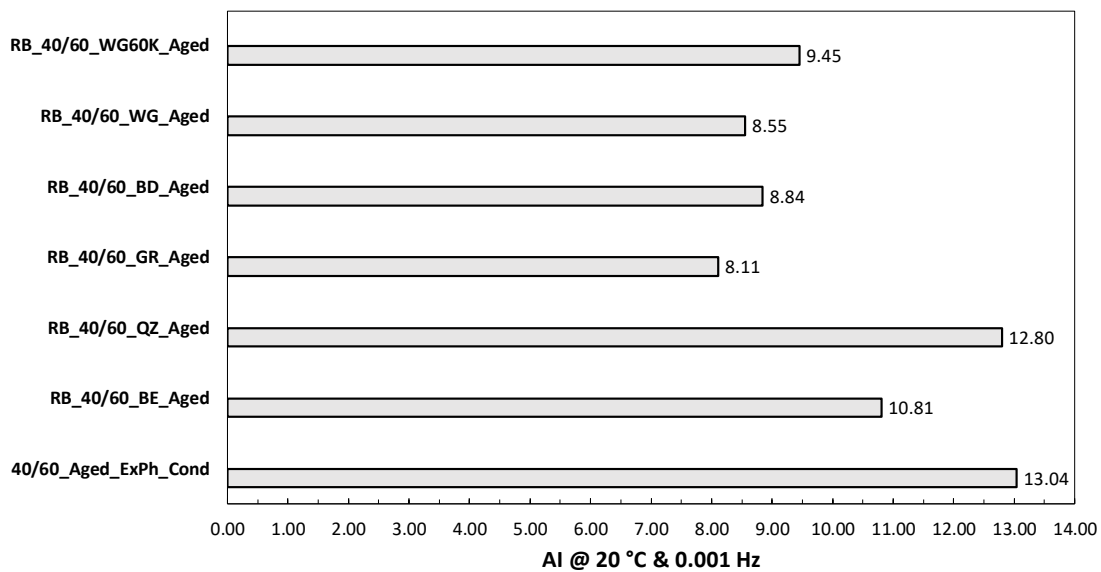


**Figure 6.26:** Recovered and neat aged bitumen complex modulus ageing indices at 20°C and 0.001 Hz.

**Table 6.4:** Recovered and neat aged bitumen ranking based on the complex shear modulus ageing indices at 20°C and 0.001 Hz.

Bitumen	Ageing Level
40/60_Aged_ExPh_Cond	High
RB_40/60_QZ_Aged	
RB_40/60_BE_Aged	
RB_40/60_WG60K_Aged	
RB_40/60_BD_Aged	
RB_40/60_WG_Aged	
RB_40/60_GR_Aged	

Based on the rheological data, a comparison between the materials' ageing ranking on mastic level (*Table 5.1, Sub-Section 5.1.3*) and on bitumen level (*Table 6.4*) yields a nice correlation, in the context that all mastics and their corresponding recovered bitumen appear to be less aged than the neat (aged) bitumen. Even though this seems to be a valid interpretation, a few observations suggest otherwise. For one, the materials' relative ranking differs significantly on mastic and on bitumen level. For instance, RB\_40/60\_GR\_Aged appears to be the least aged bitumen (*Fig. 6.25 and 6.26*) whereas the mastic prepared with the mineral filler GR was ranked as the fourth most aged one (*Fig. 5.8, Sub-Section 5.1.3*). For another, the rheological behavior of the recovered bitumen does not totally agree with the mastics' chemical evaluation, and more specifically their CI (*Fig. 5.12, Sub-Section 5.2.2*).

The CI results showed that in the aged mastics prepared with the mineral fillers WG60K, WG, BD and GR the concentration of carbonyls was greater than in the case of neat aged bitumen, whereas the rheological evaluation suggests that their recovered bitumen are softer (or less aged) than the neat aged binder. The recovered bitumen from the BE aged mastic appears to be less aged than the neat aged binder, which totally agrees with the mastics' CI evaluation. Nevertheless, the mastics' 40/60\_BE\_Aged and 40/60\_QZ\_Aged almost identical CI cannot justify the relative ranking of their respective recovered bitumen (*Fig. 6.25 and 6.26*). Only the ageing level of RB\_40/60\_QZ\_Aged, compared to neat aged bitumen (*Fig. 6.25 and 6.26*), seems to be in good agreement with the CI outcome.

Irreversible adsorption could be a potential reason behind the differences observed between the mastics' chemical evaluation and the recovered bitumen rheological behavior, in the context that if adsorbed bitumen components (i.e. polar functional groups) would remain on the recovered mineral matter, this would lead to a softer behavior of the recovered bitumen, when compared to the neat aged one. However, visual investigation of the infrared spectra of the original and recovered mineral fillers yielded that no irreversible adsorption of bitumen components on mineral fillers' particles occurred, suggesting that all the binders' components that might had reacted with the mineral matter were reclaimed back in the bitumen matrix, upon extraction and recovery. Having mentioned the above, it was expected that the recovered bitumen, apart from RB\_40/60\_BE\_Aged and RB\_40/60\_QZ\_Aged, would present higher  $G^*$  values, and, thus, higher ageing level than the neat aged binder, which is not the case. Two possible reasons can be identified that might had led to the lower AI (i.e. softening) of the recovered bitumen. The two below-discussed mechanisms may operate simultaneously as well as individually.

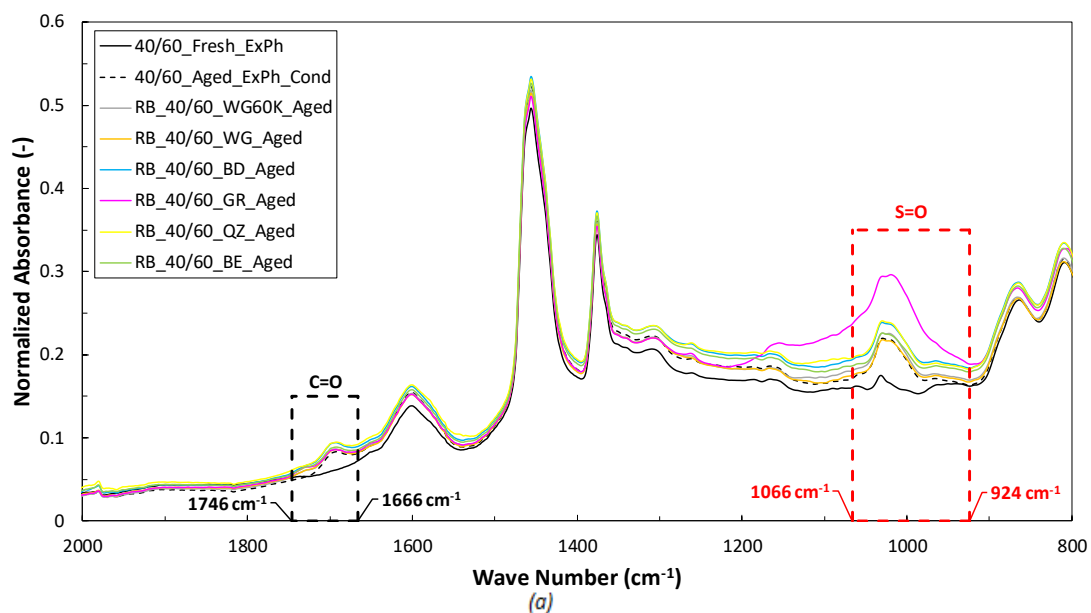
The first one is related to the absorption of bitumen components into the mineral fillers' particles' (micro-)pores, upon the preparation of mastics. In *Sub-Section 2.3.2.2* it was stated that, according to Van Lent (2013), previous research has demonstrated the preferential absorption of less viscous bitumen components into the aggregates. Moreover, in the very same sub-section, the experience and results' interpretation of Wu (2009) were cited regarding the encounter of characteristically softer recovered bitumen from aged mastics, compared to pure aged binder. By taking into account the information provided in the literature review, it is plausible that oily and/or less polar bitumen components were absorbed into the mineral matters' particles' (micro-)pores, during the mastics' production. These components were protected (or much less affected) from volatilization and oxidation during ageing of the materials. Upon bitumen extraction these components were reclaimed back in the bitumen's matrices, imparting softening in the recovered binders. The resulting complex shear modulus AI of the recovered binders (*Fig. 6.26*) and their relative ranking (*Table 6.4*) may be the outcome of the different abilities of the mineral fillers (mineral fillers' (micro-)porosity) to absorb bitumen components and, by extension, the subsequent various capacities of the reclaimed less or non-polar bitumen species to effectively disperse the polar functional groups within the bitumen matrix, leading to an apparent less aged material.

The second reason is related to the dichloromethane treatment of the aged mastics. Ageing at high temperatures and pressures (i.e. PAV) leads, apart from oxidation, also to physical hardening. As a result, the bitumen molecules form a dense network. Dissolving in dichloromethane entails the almost complete destruction of this dense network. Hence, the neat aged bitumen, which was not treated with solvent, still possesses this dense molecular structure making it slightly stiffer than the recovered bitumen (*Fig. 6.23* and *6.25*). The relative ranking of the recovered binders may be the result of the different dissolving efforts during the extraction process.

## 6.6 Chemical evaluation of recovered and neat bitumen – results and discussion

### 6.6.1 Infrared spectra

In *Fig. 6.27a* the normalized infrared spectra of the “fresh”, neat aged and recovered bitumen are illustrated, while *Fig. 6.27b* and *Fig. 6.27c* show the close-ups of the carbonyls' (C=O) and sulfoxides' (S=O) regions, respectively.



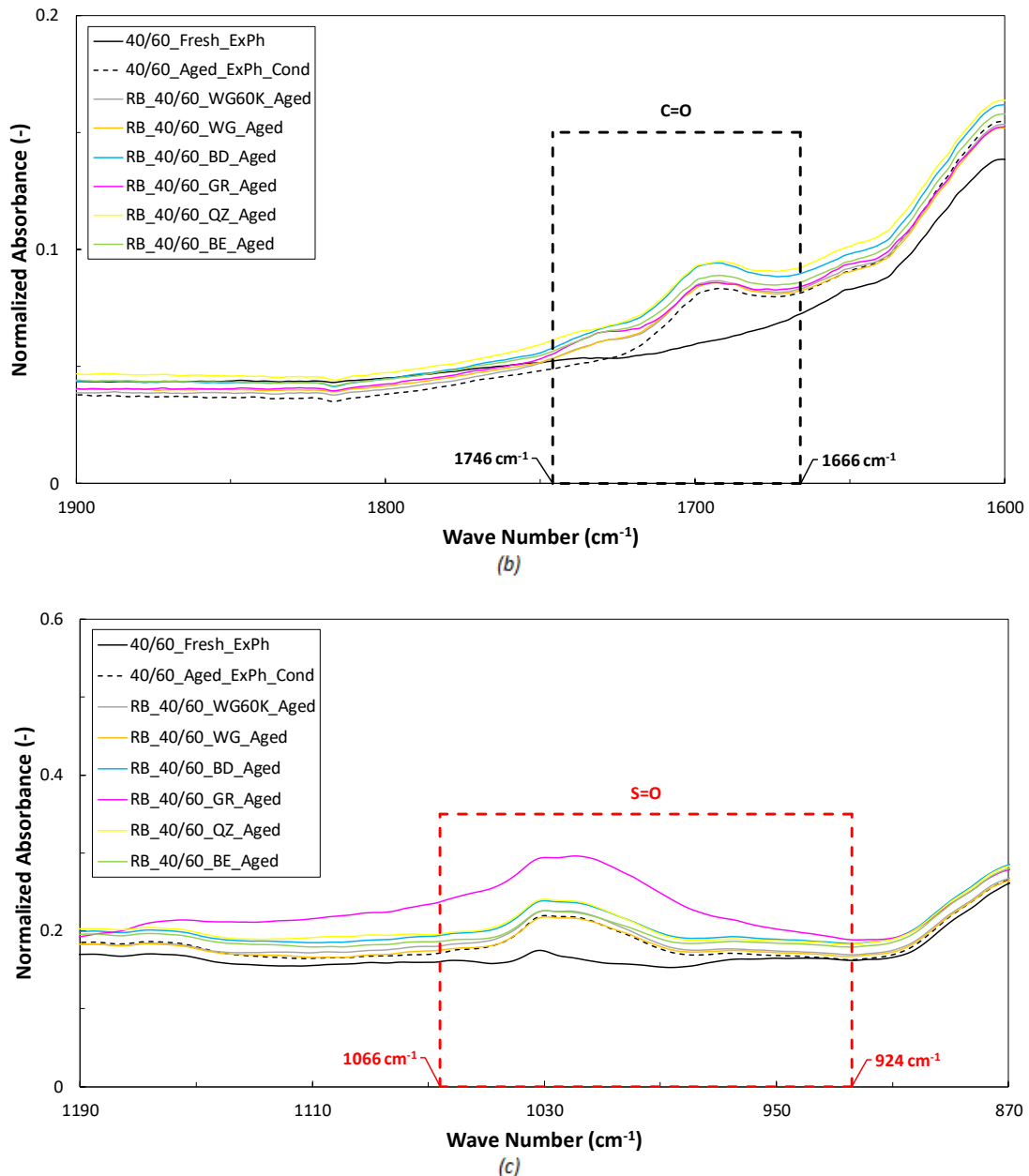


**Figure 6.27:** “Fresh”, neat aged and recovered bitumen infrared spectra. (a) Total spectra. (b) Carbonyls close-up. (c) Sulfoxides close-up.

A comparison of the infrared spectra of all bitumen yields that a disturbance is observed in the infrared spectrum of the recovered bitumen RB\_40/60\_GR\_Aged in the S=O region (*Fig. 6.27a* and *6.27c*), that most likely originates from the effect of mineral filler residue, as also stated in *Sub-Section 6.4.1*. Nevertheless, all of the rest of the examined materials appear to be free from the effect of other phases.

### 6.6.2 Carbonyls and sulfoxides indices

The CI and SI of all bitumen were calculated according to *Eq. 3.29* and *Eq. 3.30*, respectively. In *Fig. 6.28* the CI results are presented, while *Fig. 6.29* shows the SI of the materials. The combined carbonyls' + sulfoxides' index ((C+S)I) is presented in *Fig. 6.30*.

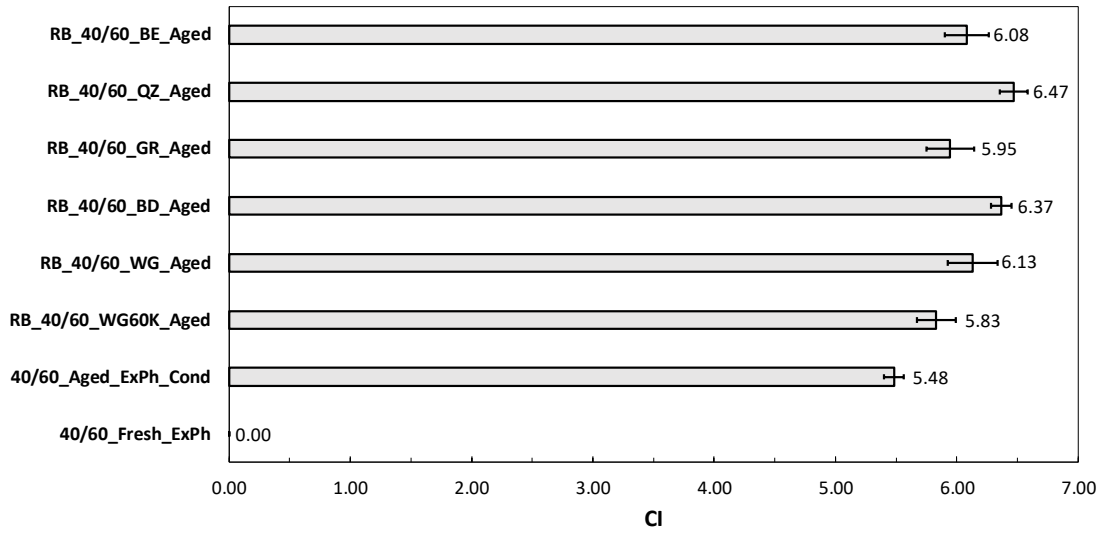


Figure 6.28: “Fresh”, neat aged and recovered bitumen carbonyls’ index.

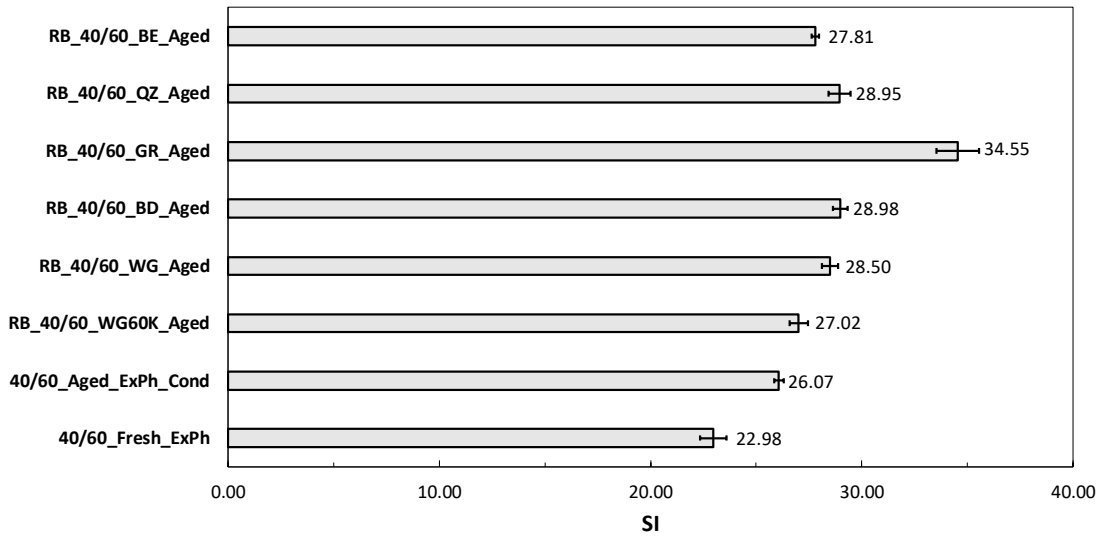


Figure 6.29: “Fresh”, neat aged and recovered bitumen sulfoxides’ index.

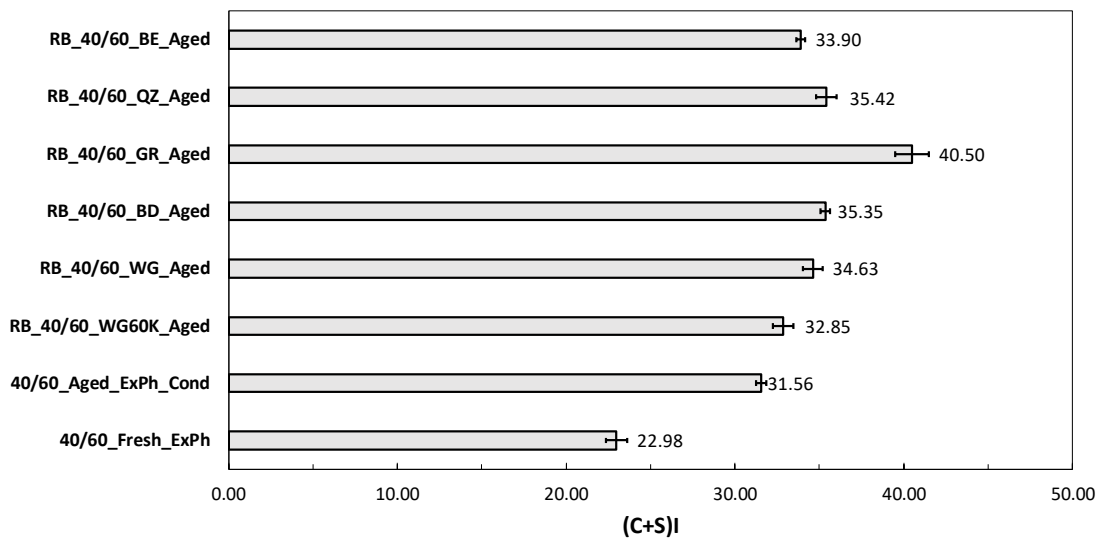


Figure 6.30: “Fresh”, neat aged and recovered bitumen carbonyls’ + sulfoxides’ index.

In *Fig. 6.29* it can be observed that RB\_40/60\_GR\_Aged demonstrates the highest SI from all considered materials. However, it is believed that this high SI value do not reflect the actual formation of S=O bonds in this particular recovered binder, but rather is the product of the combined effect of bitumen and mineral filler residue, as discussed previously.

The results in *Fig. 6.28* to *6.30* indicate that more carbonyls and sulfoxides were formed in the recovered bitumen, compared to the neat aged binder. This is in contrast to the complex shear modulus AI evaluation of the very same materials, presented in *Fig. 6.25* and *6.26* (*Sub-Section 6.5.2*), which showed that all recovered bitumen appeared to be less aged than the neat aged binder. This outcome suggests that the potential reasons cited in *Sub-Section 6.5.2* regarding the softening of the recovered binders (i.e. bitumen components absorption and reclamation and/or solvent treatment effect) may hold true.

The recovered binders from the aged mastics prepared with the mineral fillers WG60K, WG, BD and GR show higher CI and SI than the neat aged bitumen, implying a more severe ageing of the former compared to the latter. This result is in line with the chemical evaluation of mastics, by means of the CI (*Fig. 5.12*, *Sub-Section 5.2.2*). This finding may further corroborate the statement that, these mineral fillers catalyzed the bitumen oxidation, but this effect is not captured in the rheological evaluation of the mastics, due to the various abilities of the mineral matters to adsorb the oxygenated functional groups of bitumen, leading to apparent less aged mastics than the neat bitumen.

The recovered bitumen RB\_40/60\_BE\_Aged and RB\_40/60\_QZ\_Aged show a higher concentration of carbonyls and sulfoxides than the neat aged binder. This suggests that the binders in the mastics 40/60\_QZ and 40/60\_BE had undergone more pronounced ageing than the pure bitumen. The latter is in contrast to the mastic's rheological and chemical evaluation (i.e. CI). The increased CI on bitumen level may be the result of the hot extraction and recovery process.

### 6.7 Reflection on extraction and recovery of bitumen from aged mastics

The extraction and recovery of bitumen from aged mastics was carried out in an effort to gain further insight on the effect of mineral fillers on ageing of bituminous mixtures by investigating the involved materials on their individual level. Nevertheless, the obtained results seem to give rise to more questions, instead of providing answers to the already existing ones.

More specifically, the rheological data of the recovered binders could not be correlated to the respective ones on mastic level as well as to the chemical evaluation of the mastics. Two possible reasons were cited regarding this unexpected behavior of the materials on bitumen level. These explanations are not accompanied by experimental support, but rather are exclusively based on current observations and findings from literature. As a result, further investigation is necessary for their validation. A first indication of the potential validity of the aforementioned reasons was provided through the chemical investigation of the recovered binders, which was found to be in complete contrast to the rheological outcome.

The chemical evaluation of the recovered binders seems to correlate better than the rheological one to the outcome and results interpretation provided in the mastic level investigation phase. However, this correlation refers to a generic trend and particular conclusions, derived from the relative ranking of the various materials, could not be

established. It is believed that the sensitivity of the binders regarding the carbonyls' and sulfoxides' formation, upon application of heat and/or pressure (extraction and recovery process), could be the reason behind that. The latter also entails that the comparison of the neat aged bitumen with the recovered binders, by means of FTIR/ATR ageing indices, cannot be considered absolutely fair, due to the fact that the conditioning of the former is not equivalent to the effect of the extraction and recovery procedure on the recovered binders' properties.





## Conclusions and recommendations

## 7.1 Conclusions

- All considered mineral fillers, regardless of their individual properties, led to less aged mastics than the neat aged bitumen, aged under identical conditions. This indicates that:

Mineral fillers are active participants and play a role in the ageing process of bitumen and they have a positive effect on the ageing of mastics.

- The dust collected in the asphalt plant (i.e. Baghouse Dust) led to a mastic that demonstrated more severe ageing than the one prepared with the commercial material Wigro 60K. This result underlines that:

The substitution of the specified mineral filler Wigro 60K, currently used in the production of Porous Asphalt mixtures, by the cost-effective solution of the Baghouse Dust, could possibly lead to the production of Porous Asphalt mixtures that would be more prone to ageing and, by extension, to related failure modes.

- Mineral fillers Wigro 60K (Limestone + 25wt% Hydrated Lime) and Wigro (Limestone) led to mastics that demonstrated a rather equivalent performance, ageing-wise. This outcome entails that:

The addition of 25wt% of Hydrated Lime to the Limestone mineral filler (i.e. Wigro) does not result in an enhanced effectiveness of the mixed mineral matter (i.e. Wigro 60K) to mitigate the ageing of the mastic.

- The mastic prepared with the “inert” mineral filler Quartz appeared to have undergone less ageing than the neat aged bitumen. This outcome allowed the identification of the first mechanism through which the effect of the mineral fillers on ageing of bitumen occurs:

The physical presence of the mineral filler particles' in the mastic leads to the lengthening of the oxygen diffusion path, entailing the reduced rate of oxidative ageing of bitumen. The governing property of the mineral fillers, that controls the effect of this mechanism, is their particles' size distribution, implying that the coarser the mineral filler the more intense the effect of its particles on the oxygen diffusion path.

- The mineral fillers' particles' size distribution ranking is not in line with the ageing ranking of the examined mastics, based on the complex shear modulus ageing indices. This observation suggests that:

There exists a mechanism, originating from the physico-chemical interactions between the bitumen and the mineral filler, that leads the mastics prepared with finer mineral fillers than Quartz to develop less age-hardening. The latter indicates that the mechanism attributed to the physical presence of solid particles in the mastics is of secondary importance compared to the one referring to the materials' physico-chemical interactions.

- The prevailing mechanism, through which mineral fillers affect the ageing of bitumen-mineral filler systems, is related to the developed interactions between the mineral fillers' particles' and the bitumen. The FTIR/ATR results showed that the mineral fillers that were expected to interact with bitumen (i.e. Wigro 60K, Wigro, Baghouse Dust and Granite) catalyzed its oxidation, leading to the formation of more carbonyls in the aged mastics than in the neat aged bitumen. On the other hand, the DSR results displayed the mastics, corresponding to these mineral fillers, to be less aged than the pure bitumen. This leads to the conclusion that:

The (highly) polar functional groups of bitumen (e.g. carbonyls) in the mastics are adsorbed on the solid particles' surface and do not contribute to the mastics' viscosity build-up. The relative ranking of the mastics, based on the complex shear modulus ageing indices, is the result of the different abilities of the various mineral fillers to adsorb the polar functional groups from bitumen, thus, leading to mastics that appear to be less aged than the neat aged bitumen, aged under identical conditions.

- The established relationship (*Sub-Section 5.1.3*) between the mineral fillers' CaO content and the mastics' complex shear modulus ageing indices at 0.001 Hz and 20°C showed that the mineral fillers' adsorption ability is controlled by their elemental/mineralogical composition. Moreover, indications were cited that demonstrated the effect of the mineral fillers' specific surface area on the adsorption mechanism. The aforementioned findings lead to the conclusion that:

Basic mineral fillers (i.e. high CaO content) possess a greater ability in removing the oxygenated products from the bitumen matrix, compared to more acidic materials (i.e. rich in SiO<sub>2</sub>). In addition, a mineral filler with large specific surface area (e.g. Wigro) could lead to the intensification of the adsorption mechanism and, by extension, to less age-hardened mastics.

- The experimental results did not show any relationship between the mineral fillers' Rigden voids and methylene blue value with the derived ageing indices, both on mastic and bitumen level. This leads to the conclusion that:

The mineral fillers' particles' size distribution, specific surface area and elemental/mineralogical composition are the properties, in increasing significance, that govern the effect of the mineral matters on the ageing of bituminous mixtures, always amongst the measured in this research mineral fillers' properties.

- The mineral filler Bestone appeared to be a special case in this research. The mastics' rheological and chemical evaluations and their correlation led to the conclusion that:

It is highly possible that Bestone behaved as an "inert" material and no interactions with bitumen occurred. Nevertheless, this conclusion is not drawn with confidence and, undoubtedly, further research on this particular mineral filler is necessary.

- The extraction and recovery of bitumen from the aged mastics did not result in any further insight regarding the effect of mineral fillers on ageing of bituminous mixtures. Instead, the rheological evaluation on bitumen level revealed that the

recovered binders do not reflect the actual state of the effective bitumen in the bitumen-mineral filler systems. The latter was attributed to two possible reasons that might imparted softening in the recovered binders, resulting in establishing these binders as less aged than the neat aged bitumen, based on the complex shear modulus ageing indices. The FTIR/ATR results showed that the recovered binders, indeed, are not less aged than the pure aged bitumen, which confirms, to an extent, that the cited reasons for the observed rheological behavior of the recovered materials may hold true. Last but not least, the chemical evaluation of the recovered binders showed a similar trend to the results obtained on mastic level, but it is believed that the FTIR/ATR ageing indices include the effect of the hot extraction and recovery process on the recovered binders' properties and, thus, their reliability is questionable. The above remarks lead to the conclusion that:

The extraction and recovery of bitumen from the aged mastics could be useful in deriving information regarding the effect of mineral fillers on ageing of bituminous mixtures, provided that the reasons behind the observed behavior (mainly rheological) of the recovered materials are well-identified and experimentally validated. The latter could possibly allow the correlation of the results on bitumen level to the ones on mastic level. Moreover, a fairer comparison between the recovered and neat aged bitumen could be achieved by implementing the extraction and recovery process to the neat aged bitumen as well.

## 7.2 Recommendations

- In this research, the Pressure Ageing Vessel (PAV), with test conditions of 90°C and ~2.1 MPa, was used for the ageing of the materials. The utilization of a relatively low temperature (i.e. 90°C) prevented the settlement of the mineral fillers in the mastics during the ageing process, and, by extension, the hindrance of the mineral fillers' effect on the ageing of mastics. In addition, it is believed that the pressurized air, that is supplied during the PAV test, allowed for the effect of the mineral matters on the oxidation of bitumen to be more readily captured. Therefore, it is recommended that, in future ageing studies of mastics, the PAV, along with the aforementioned conditions, is used for the ageing of the materials.
- The effect of mineral fillers on ageing of bituminous mixtures was investigated by considering only one variable, that is, the type of the mineral filler and its intrinsic properties. Other parameters that could possibly influence their effect were kept constant. Hence, the following are recommended:

The mastics were prepared with a mineral filler-to-bitumen ratio, by mass, equal to one. It is suggested that different mineral filler-to-bitumen ratios are examined in future studies so that the effect of the variation of this design parameter can be evaluated. Based on the conclusions derived from the experimental research, regarding the mineral fillers' governing properties and the occurring mechanisms, it is highly plausible that the increase of the mineral filler content will entail a positive effect on the ageing behavior of the mastics, whereas a decrease of its content will lead to the opposite outcome. The latter should be experimentally investigated and validated.

The ageing duration, applied in this research, was constant and equal to 20 hours. The experimental results showed that the mineral fillers, that were expected to react with bitumen, led to the catalysis of its oxidation and that, at the same time, the ageing of the mastics was dependent on the ability of the various mineral fillers to remove (adsorb) the oxygenated functional groups from the bitumen matrix. However, it is unclear whether the catalysis of the bitumen oxidation and the bitumen components' adsorption are constant processes, taking place throughout the whole ageing simulation, or just occur at specific stages of the ageing procedure, and, in the case that they are constant, what is their intensities' profile during the ageing of the materials. With respect to the aforementioned features, insight may be gained through the fragmentation of the ageing process. Therefore, it is recommended that, in future related studies, time intervals in the ageing process are considered.

Last but not least, it is suggested that a study is performed on the effect of mineral fillers on ageing of bituminous mixtures that is focused on the influence of different types of bitumen, including polymer modified binders as well, with distinct physical properties and chemical structures. This will allow for the identification of the influence of the type of bitumen on the ageing of mastics, and will lead to a more comprehensive understanding of the overall topic.

- The addition of 25wt% of Hydrated lime in the Limestone-based mineral filler did not result in a pronounced effect of the mixed mineral matter on the ageing of mastics. It is recommended that higher contents of Hydrated Lime should also be investigated, to identify a potential threshold value of the Hydrated Lime percentage that could lead to a noticeable effect of the mixed mineral matter on the ageing of bituminous mixtures. Moreover, the modification with Hydrated Lime can also be done on other mineral fillers, beyond Limestone, (e.g. Granite), so that the effect of Hydrated Lime-modified mineral matters with various base-mineral fillers on the ageing of mastics can be evaluated.
- Three mineral fillers' properties were found to have an influence on the ageing of mastics, namely their particles' size distribution, specific surface area and elemental/mineralogical composition. Their identification allows for their isolation and more specialized investigation in future related studies. Having mentioned the above, the following are recommended:

The effect of the mineral fillers' particles' size distribution can be further investigated by utilizing various gradations of the "inert" mineral filler Quartz. By doing so, deeper understanding, with respect to the effect of the solid particles on the oxygen diffusion path, as a function of their size, as well as the importance of this mechanism, may be obtained. Within this framework, apart from rheological and chemical evaluations, also measurements regarding the diffusion of oxygen in the mastics (i.e. derivation of oxygen diffusion coefficients) are suggested to be carried out.

On the same grounds, the effect of the mineral fillers' specific surface area on the ageing of mastics can be further examined by incorporating, in future studies, mineral fillers with the same elemental/mineralogical composition but with various values of the specific surface area. In *Sub-Section 5.5.2* it was stated that the increased

carbonyls concentration in the aged mastic prepared with the mineral filler Wigro, could possibly originate from the large specific surface area of this particular mineral filler, which may have led to the more pronounced oxidation of bitumen. However, a concrete conclusion regarding the latter could not be derived, due to lack of support of such trend by the rest of the materials. The aforementioned recommended research methodology may provide insight whether or not a large specific surface area entails more severe oxidation of the bitumen in the mastics.

- The FTIR/ATR testing of mastics was proved very useful in deriving information regarding their ageing. The sulfoxides' index was regarded as unreliable but, on the contrary, the carbonyls' index appeared to be free from the effect of the mineral fillers in the mastics, hence, providing information solely related to the aged bitumen in them. Therefore, it is recommended that the carbonyls' index is used in future ageing studies of mastics to gain insight with respect to the formation of C=O bonds in the mixtures' binders.
- The relative rheological behavior of the recovered binders from the aged mastic, discussed in *Section 6.5*, was attributed to two possible reasons that might have imparted softening to the recovered bitumen.

The first reason is related to the reclamation of absorbed oily and/or less polar components of bitumen from the mineral filler particles. It is recommended that the validity of this explanation is experimentally examined by measuring the mineral fillers' porosity with the Mercury Intrusion Porosimeter and by investigating the molecular composition of the recovered binders by making use of the Gel Permeation Chromatography test.

The second reason is related to the dichloromethane treatment of the aged mastics, destroying the dense molecular network in the recovered binders. It is recommended that, in future ageing studies, where reclaimed bitumen from aged mastics are to be compared with pure aged bitumen, the neat aged binder is also subjected to the extraction and recovery process, so that the effect of this procedure on the binders' properties and chemical structure is cancelled out in the comparison of the materials.

**References**

- Abukarba E. & Muniandy R. *An Overview of the Use of Mineral Fillers in Asphalt Pavements*. Australian Journal of Basic and Applied Sciences, 10(9), pp 279-292, 2016.
- Airey G.D. *State of the Art Report on Ageing Test Methods for Bituminous Pavement Materials*. International Journal of Pavement Engineering, Vol. 4 (3), pp 165-176, 2003.
- Airey G.D., Rahimzadeh B. & Collop A.C. *Linear Viscoelastic Limits of Bituminous Binders*. Asphalt Paving Technology: Association of Asphalt Paving Technologists-Proceedings of the Technical Sessions, Vol. 71, pp 89-115, 2002.
- Alfaqawi R.M., Airey G.D., Lo Presti D. & Grenfell J. *Effects of Mineral Fillers on Bitumen Mastic Chemistry and Rheology*. University of Nottingham, 2017.
- Anderson D.A., Bahia H.U. & R. Dongre. *Rheological Properties of Mineral Filler-Asphalt Mastics and Their Relationship to Pavement Performance*. Effects of Aggregates and Mineral Fillers on Asphalt Mixture Performance: ASTM STP 1147. (Richard C. Meininger, ed.), American Society for Testing Materials, Philadelphia, Pa., 1992.
- Anderson D.A. & Bonaquist R. *NCHRP Report 709: Investigation of Short-Term Laboratory Ageing of Neat and Modified Asphalt Binders*. NCHRP Report 709, National Cooperative Highway Research Program, Transportation Research Board of the National Academies, Washington D.C., 2012.
- Apostolidis P. *Experimental and Numerical Investigation of Induction Heating in Asphalt Mixes*. Delft University of Technology, M.Sc. Thesis, 2015.
- Bagampadde U., Isacsson U. & Kiggundu B.M. *Influence of Aggregate Chemical and Mineralogical Composition on Stripping in Bituminous Mixtures*. The International Journal of Pavement Engineering, Vol. 6, No. 4, 2005.
- Bahia H.U., Hislop W.P., Zhai H. & Rangel A. *Classification of Asphalt Binders into Simple and Complex Binders*. Journal of the Association of Asphalt Paving Technologists, Vol. 67, pp 1-41, 1998.
- Bahia H.U., Moraes R., & Tabatabaee H.A. *Long Term Aging of Asphalt Binders in the Presence of Mineral Aggregates*. Federal Highway Administration (FHWA), Madison, Wis., 2014.
- Braunauer S., Emmett P.H. & Teller E. *Adsorption of Gases in Multimolecular Layers*. Journal of the American Chemical Society, Vol. 60, No. 2, pp 309-319, 1938.
- Cardone F., Frigio F., Ferrotti G. & Canestrani F. *Influence of Mineral Fillers on the Rheological Response of Polymer-Modified Bitumen and Mastics*. Journal of Traffic and Transportation Engineering, English Edition, 2 (6), pp 373-381, 2015.
- Charles J.G., Epps Martin A., Chowdhury A., Han R., Prapaitrakul N., Jin X., & Lawrence J. *Evaluation of Binder Aging and Its Influence in Aging of Hot Mix Asphalt Concrete: Literature Review and Experimental Design*. Federal Highway Administration (FHWA): Report No. FHWA/ TX-08/0-6009-1, Report 0-6009-1, Austin, Texas, 2009.

Choquet F.S. & Verhasselt A.F. *Aging of Bitumen: From the Road to the Laboratory and Vice Versa*. Strategic Highway program (SHRP) and Traffic Safety on Two Continents. Swedish Road and transport Research Institute, pp 194-213, 1994.

Christensen D.W. & Anderson D.A. *Interpretation of Dynamic Mechanical Test Data for paving Grade Asphalt Cements*. Proceedings of the Association of Asphalt Paving Technologists, Vol. 61, pp 67-116, 1992.

Corbett L.C. *Composition of Asphalt Based on Generic Fractionation Using Solvent Deasphalteneing, Elution-Adsorption Chromatography and Densitometric Characterization*. Analytical Chemistry, Vol. 41, pp 576-579, 1969.

Curtis C.W., Ensley K., & Epps J. *Fundamental Properties of Asphalt-Aggregate Interactions Including Adhesion and Absorption*. Strategic Highway Research Program: Report No. SHRP-A-341, National Research Council, Washington, D.C., 1993.

Domke C., Davison R. & Glover C. *Effect of Oxidation Pressure on Asphalt Hardening Susceptibility*. Transportation Research Record: Journal of the Transportation Research Board, No. 1661, pp 114-121, 1999.

Dorrence S.M., Barbour F.A. & Petersen J.C. *Direct Evidence of Ketones in Oxidized Asphalts*. Analytical Chemistry, Vol. 46, pp 2242-2244, 1974.

Dukatz E.L. & Anderson D.A. *The Effects of Various Fillers on the Mechanical Behavior of Asphalt and Asphaltic Concrete*. Proceedings of the Association of Asphalt Paving Technologists, Vol. 49, pp 530-549, 1980.

Eick J.H. & Shook J.F. *The Effect of Baghouse Fines on Asphalt Mixtures*. The Asphalt Institute Research Report 78-3, 1978.

Erkens S., Porot L., Glaser R. & Glover C.J. *Aging of Bitumen and Asphalt Concrete Comparing State of the Practice and Ongoing Developments in the United States and Europe*. TRB 95th Annual Meeting Compendium of Papers, 2016.

Fonsceca O.A & Witczak M.W. *A Prediction Methodology for the Dynamic Modulus of In-Place Aged Asphalt Mixtures*. Association of Asphalt Paving Technologies (AAPT), Vol. 65, 1996.

Francken L. *Long Term ageing of pure and modified Bitumen: Influence on the Rheological Properties and Relation with the Mechanical Performance of Asphalt Mixtures*. Proceedings of 8<sup>th</sup> International Conference on Asphalt Pavements, August 10-14, Seattle, USA, 1997.

Glover C.J., Davison R.R., Bullin J.A., Button J.W. & Donaldson G.R. *Chemical Characterization of Asphalt Cement and Performance Related Properties*. Transportation Research Record: Journal of the Transportation Research Board, No. 1171, Transportation Research Board of the National Academies, Washington, D.C., pp 71-81, 1988.

Goubert L., Hooghwerff J., The P. & Hofman R. *Two-Layer Porous Asphalt: An International Survey in the Frame of the Noise Innovation Programme (IPG)*. The 2005 Congress and Exposition on Noise Control Engineering, Rio de Janeiro, Brazil, 07-10, August 2005.



Grabowski W., Wilanowicz J. & Sobol T. *Structural and Functional Properties of Mineral Fillers Modified with Hydrated Lime*. Proceedings 6<sup>th</sup> International Conference on Maintenance and Rehabilitation of Pavements and Technological Control (MAIREPAV6), Torino (Italy), Paper 78, 2009.

Gubler R., Liu Y., Anderson D.A. & Partl M.N.. *Investigation of the System Filler and Asphalt Binders by Rheological Means*. Association of Asphalt Paving Technologists (AAPT), Vol. 68, pp 284-304, 1999.

Gundla A., Medina J., Gudipudi P. & Stevens R. *Investigation of Aging in Hydrated Lime and Portland Cement Modified Asphalt Concrete at Multiple Length Scales*. Journal of Materials in Civil Engineering, 2015.

Gupta V. Surface Charge Features of Kaolinite Particles and Their Interactions. University of Utah, Ph.D. Thesis, 2011.

Hagos E.T. Effect of Aging on Binder Properties of Porous Asphalt Concrete. Delft University of Technology, Ph.D. Thesis, 2008.

Han R. Improvement to a Transport Model of Asphalt Binder Oxidation in Pavements: Pavement Temperature Modeling, Oxygen Diffusivity in Asphalt Binders and Mastics, and Pavement Air Void Characterization. Texas A&M University, College Station, TX, Ph.D. Thesis, 2011.

Hofko B., Alavi M.Z., Grothe H., Jones D. & Harvey J. *Repeatability and Sensitivity of FTIR ATR Spectral Analysis Methods for Bituminous Binders*. Materials and Structures, 50:187, 2017.

Hunter R.N., Self A. & Read J. *The Shell Bitumen Handbook, 6<sup>th</sup> Edition*. 2015.

Huurman M. *Lifetime Optimization Tool, LOT, Main Report*. Report No. 07-170-1, Delft University of Technology, 2008.

Hveem F.N., Zube E. & Skog J. *Proposed New tests and Specifications for Paving Grade Asphalts*. Proceedings of the Association of Asphalt Paving Technologists, Vol. 32, pp 247-327, 1963.

Ishai I. *The Effect of Asphalt Composition on its Physical and Durability Characteristics*. Transportation Research Board, 75<sup>th</sup> Annual Meeting, Washington D.C., 1996.

Jenkins R. *X-Ray Fluorescence Spectrometry*. Chemical Analysis (N.Y.), 2<sup>nd</sup> Edition, Vol. 152, Wiley-Interscience Publication, 1999.

Kandhal P.S. & Chakraborty S. *Effect of Asphalt Film Thickness on Short and Long-Term Aging of Asphalt Paving Mixtures*. Transportation Research Record, No. 1535, 1996.

Kandhal P.S., Lynn C.Y. & Parker F. Jr. *Characterization Tests for Mineral Fillers Related to Performance of Asphalt Paving Mixtures*. Transportation Research Record 1638, Paper No. 98-0224, pp 101-110, 1998.

Kennedy T.W., Cominsky R.J., Harrigan E.T. & Leahy R.B. *Performance-Related Testing and Measuring of Asphalt-Aggregate Interactions and Mixtures*. Strategic Highway Research Program: Report No. SHRP-A-311, Contract A-003A, National Research Council, Washington, D.C., 1990.

King G., Anderson M., Hanson D. & Blankenship P. *Using Black Space Diagrams to Predict Age-Induced Cracking*. Proceedings of 7<sup>th</sup> RILEM International Conference on Cracking in Pavements, pp 453-463, 2012.

Lamontagne J., Dumas P., Mouillet V. & Kister J. *Comparison by Fourier Transform Infrared (FTIR) Spectroscopy of Different Ageing Techniques: Application to Road Bitumens*. Fuel, Vol. 80, No. 4, pp 483-488, 2001.

Leech D. & Nunn M.E. *Deterioration Mechanisms in Flexible Roads*. Proceedings of 2<sup>nd</sup> European Symposium on Performance and Durability of Bituminous Materials, Leeds, April 1997.

Lesueur D. *The Colloidal Structure of Bitumen: Consequences on the Rheology and on the Mechanisms of Bitumen Modification*. Advances in Colloid Interface Science, 145(1-2), pp 42-82, 2009.

Lesueur D., Petit J. & Ritter H.J. *The Mechanisms of Hydrated Lime Modification of Asphalt Mixtures: A State-of-the-Art Review*. Road Materials and Pavement Design 14: pp 1-16, 2012.

Lesueur D., Teixeira A., Lazaro M.M., Andaluz D. & Ruiz A. *A Simple Test Method in order to Assess the Effect of Mineral Fillers on Bitumen Ageing*. Construction and Building Materials, Vol. 117, pp 182-189, 2016.

Little D.N. & Petersen J.C. *Unique Effects of Hydrated Lime Filler on the Performance-Related Properties of Asphalt Cements: Physical and chemical interactions revisited*. Journal of Materials in Civil Engineering, 17(2), pp 207-218, 2005.

Martens E.W. & Wright J.R. *Cationic Emulsions, How They Differ from Conventional Emulsions in Theory and Practice*. Highway Research Board Proceedings, Vol. 38, pp 386-397, 1959.

Mezger T.G. *The Rheology Handbook*. Vincentz, Hannover, 2002.

Michel F. & Courard L. *Particle Size Distribution of Limestone Fillers: Granulometry and Specific Surface Area Investigations*. Particulate Science and Technology, 32 (4), 2014.

Mo L.T., Huurman R.M., Wu S.P. & Molenaar A.A.A. *Investigation into Stress States in Porous Asphalt Concrete on the Basis of FE Modelling*. Finite Element in Analysis and Design, 43(4), pp 333-343, 2007.

Moraes R. & Bahia H.U. *Effect of Mineral Fillers on the Oxidative Aging of Asphalt Binders: Laboratory Study with Mastics*. Transportation Research Record: Journal of the Transportation Research Board (2506): pp 19-31, 2015a.

Moraes R. & Bahia H.U. *Effect of Mineral Filler on Changes in Molecular Size Distribution of Asphalts During Oxidative Ageing*. Road Materials and Pavement Design 16(sup2): pp 55-72, 2015b.

Mortazavi M. & Moulthrop J.S. *SHRP Material Reference Library*, SHRP Report A-646, Washington D.C., National Research Council, 1993.

Nageswaran P.D.C. Adhesion of Aggregate-Binder Systems. Delft University of Technology, M.Sc. Thesis, 2016.

National Cooperative Highway Research Program (NCHRP). *Test Methods and Specification Criteria for Mineral Filler Used in HMA*. Project 9-45, University of Wisconsin-Madison, 2010.

Ødegård I. Effects of Mastic Ingredients and Composition on Asphalt Mixture Properties. Norwegian University of Science and Technology, M.Sc. Thesis, 2015.

Osman S.A. The Role of Bitumen and Bitumen/Filler Mortar in Bituminous Mixture Fatigue. University of Nottingham, Ph.D. Thesis, 2004.

Petersen J.C. *A Review of the Fundamentals of Asphalt Oxidation: Chemical, Physicochemical, Physical Property and Durability Relationships*. Transportation Research Circular, Number E-C140, 2009.

Petersen J.C. *Chemical Composition of Asphalt as Related to Asphalt Durability: State of Art*. Transportation Research record 999, Transportation Research Board, Washington D.C., pp 13-30, 1984.

Petersen J.C., Barbour F.A. & Dorrence S.M. *Catalysis of Asphalt Oxidation by Mineral Aggregate Surface and Asphalt Components*. Proc. Association of Asphalt Paving Technologists, Vol. 43, pp 162-177, 1974.

Petersen J.C., Plancher H., & Harnsberger P.M. *Lime Treatment of Asphalt to Reduce Age Hardening and Improve Flow Properties*. Proceedings of the Association Asphalt Paving Technologists, Lino Lakes, MN: Association Asphalt Paving Technologists (AAPT), Vol. 56, pp 632-653, 1987.

Petersen J.C., Robertson R.E., Branthaver J.F., Harnsberger P.M., Duvall J.J., Kim S.S., Anderson D.A., Christiansen D.W. & Bahia H.U., Dongre R., Sharma M.G., Antle C.E., Button J.W. & Glover C.J. *Binder Characterization and Evaluation*. Vol. 4, Strategic Highway Research Program: Report No. SHRP-A-370, Washington, D.C., 1994.

Petersen J.C., Robertson R.E., Branthaver J.F., Harnsberger P.M., Duvall J.J., Kim S.S., Anderson D.A., Christiansen D.W. & Bahia H.U. *Binder Characterization and Evaluation*. Vol. 1, Strategic Highway Research Program: Report No. SHRP-A-367, Contract A-002A, National Research Council, Washington, D.C., 1993.

Plancher H., Dorrence S.M. & Petersen J.C. *Identification of Chemical Types in Asphalt Strongly Adsorbed at the Asphalt-Aggregate Interface and Their Relative Displacement by Water*. Association of Asphalt Paving Technologists (AAPT), Vol. 46, pp 151-175, 1977.

Plancher H. & Petersen J.C. *Reduction of Oxidative Hardening of Asphalts by Treatment with Hydrated Lime-A Mechanistic Study*. Proceedings of the Association of Asphalt Paving Technologists, Vol. 45, pp 1-24, 1976.

Puzinauskas V.P. *Filler in Asphalt Mixtures*. The Asphalt Institute Research Report 69-2, 1969.

Rahimzadeh B. Linear and Non-linear Viscoelastic Behavior of Binders and Asphalts. University of Nottingham, Ph.D. Thesis, 2002.

Rigden D. J., Road Research Technical Paper No. 28, Road Research Laboratory, Hammondsworth, Middlesex, H. M., S.O., London, 1954.

Roberts F.L., Kandhal P.S., Ray Brown E., Lee D.Y. & Kennedy T.W. *Hot Mix Asphalt Materials, Mixture Design and Construction*. NAPA, Research and Education Foundation, Lanham, Maryland, 1996.

Rostler F.S. & White R.M. *Influence of Chemical Composition of Asphalts on Performance, Particularly Durability*. American Society for Testing Materials, No. 277, pp 64-88, 1959.

Santamarina J.C., Klein K.A., Wang Y.H. & Prencke E. *Specific Surface: Determination and Relevance*. Canadian Geotechnical Journal, Vol. 39, pp 233-241, 2002.

Schellenberg K. & Eulitz H.J. *Verbesserung von Asphalteigenschaften durch Einsatz von Kalkhydrat*. Bitumen1, pp 2-8, 1999.

Scott J.A.N. *Adhesion and Disbonding Mechanisms of Asphalt Used in Highway Construction and Maintenance*. Journal of the Association of Asphalt Paving Technologists, Vol. 47, pp 19-48, 1978.

Su Z. *Mineral Aggregates: Their Classification and Properties*. Report No. RT010-96-02, Esha, Groningen, The Netherlands, 1996.

Taylor R. *Surface Interactions Between Bitumen and Mineral Fillers and Their Effects on the Rheology of Bitumen-Filler Mastics*. University of Nottingham, B.Sc. Thesis, 2007.

Traxler R.N. *Durability of Asphalt Cements*. Association of Asphalt Paving Technologists, Vol. 32, pp 44-63, 1963.

Tunncliffe D.G. *A Review of Mineral Filler*. Proceedings of the Association of Asphalt Paving Technologists, Vol. 31, pp 118-150, 1962.

Van den Bergh W. *The Effect of Ageing on the Fatigue and Healing Properties of Bituminous Mortars*. Delft University of Technology, Ph.D. Thesis, 2011.

Van der Zwan J.Th., Goeman Th., Gruis H.J.A.J., Swart J.H. & Oldenburger R.H. *Porous Asphalt Wearing Courses in the Netherlands: State of the Art Review*. Porous Asphalt Pavements: An International Perspective. Transportation Research Record No. 1265, Washington, D.C., pp 95-110, 1990.

Van Lent D.Q. *Interfacial Interactions and Mass Transfer at the Interfacial Region of Bituminous Hydrocarbon Mixtures*. Delft University of Technology, Ph.D. Thesis, 2013.

Varveri A. *Moisture Damage Susceptibility of Asphalt Mixtures, Experimental Characterization and Modelling*. Delft University of Technology, Ph.D. Thesis, 2017.

Vassilyev N., Glover C.J. & Davison R.R. *Improved HMAC Plant Binder Aging Simulation Report of Preliminary Findings and Intended Project Direction*. Report FHWA/TX-01/1742-1, College Station (TX): Texas A & M University, 2001.

VBW Asphalt. *Richtlijn vooronderzoek van asfalt*. Bibliotheek RWS dienst weg- en waterbouwkunde, 1995.

Verra N., Bol M.v.d. & Gaarkeuken B. *De Levensduur van ZOAB*. Rep. No. DWW-2033-066, Road and Hydraulic Engineering Institute (DWW), 2003.

Voskuilen J.L.M., Tolman F. & Rutten E. *Do Modified Porous Asphalt Mixtures Have a Longer Service Life?* Euroasphalt and Eurobitumen Congress, Vienna, 2004.

Woldekidan M.F. Response Modelling of Bitumen, Bituminous Mastic and Mortar. Delft University of Technology, Ph.D. Thesis, 2011.

Woo W.J., Chowdhury A. & Glover C.J. *Field Ageing of Unmodified Asphalt Binder in Three Texas Long-Term Performance Pavements*. Journal of Transportation Research Board, No. 2051, Washington, D.C. pp 15-22, 2008.

Wu J. The Influence of Mineral Aggregates and Binder Volumetrics on Bitumen Ageing. University of Nottingham, Ph.D. Thesis, 2009.

Wypych G. *Handbook of Fillers*. Ontario: Chemtec Publishing, 1999.

Yusoff N.I.Md., Shaw M.T. & Airey G.D. *Modelling the Linear Viscoelastic Rheological Properties of Bituminous Binders*. Construction and Building Materials, Vol. 25, pp 2171-2189, 2011.



# **Appendix A**

Mineral fillers isothermal curves and  
BET plots

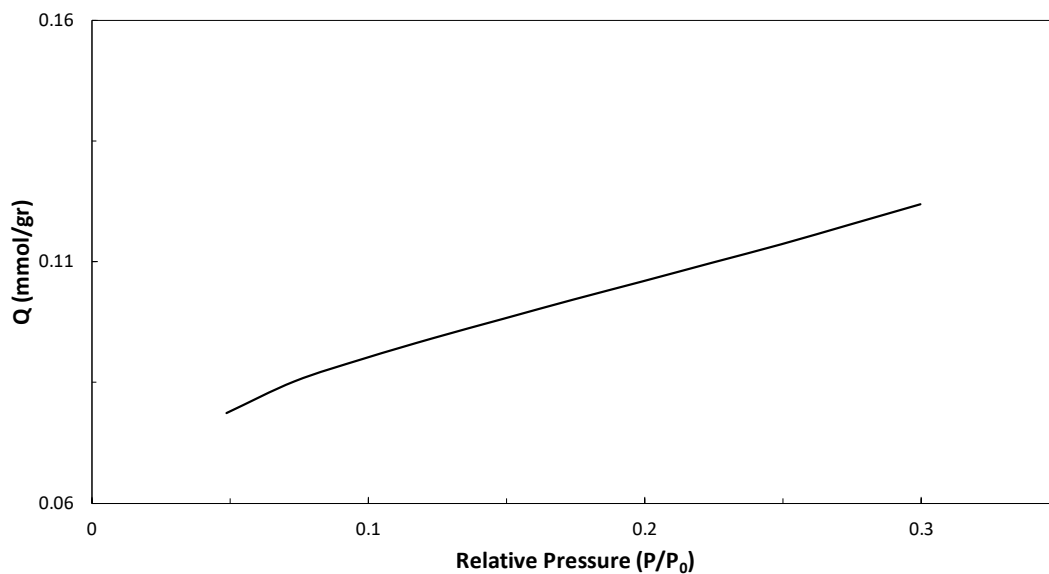


Figure A.1: WG60K isothermal curve.

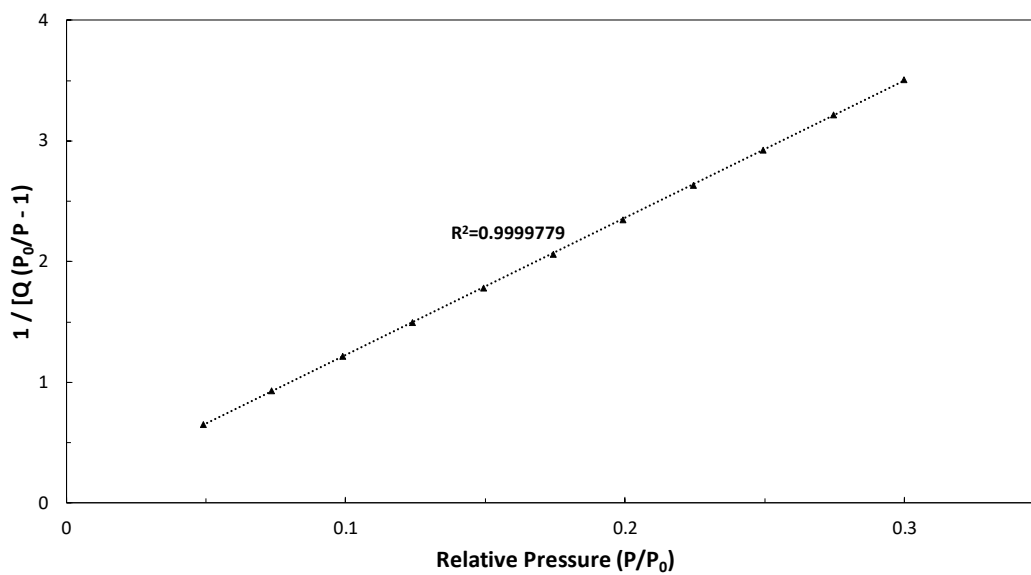


Figure A.2: WG60K BET plot.



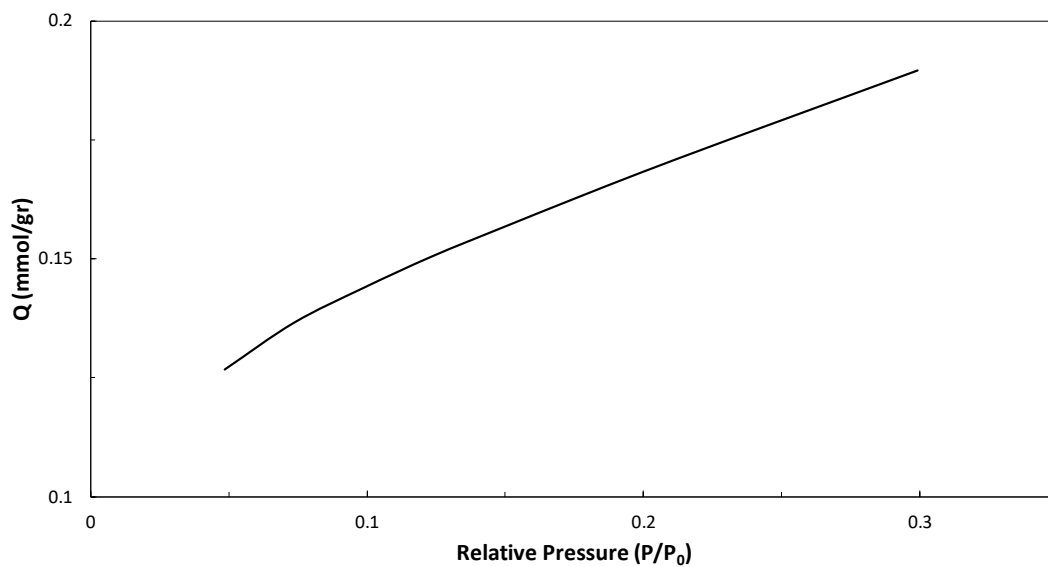


Figure A.3: WG isothermal curve.

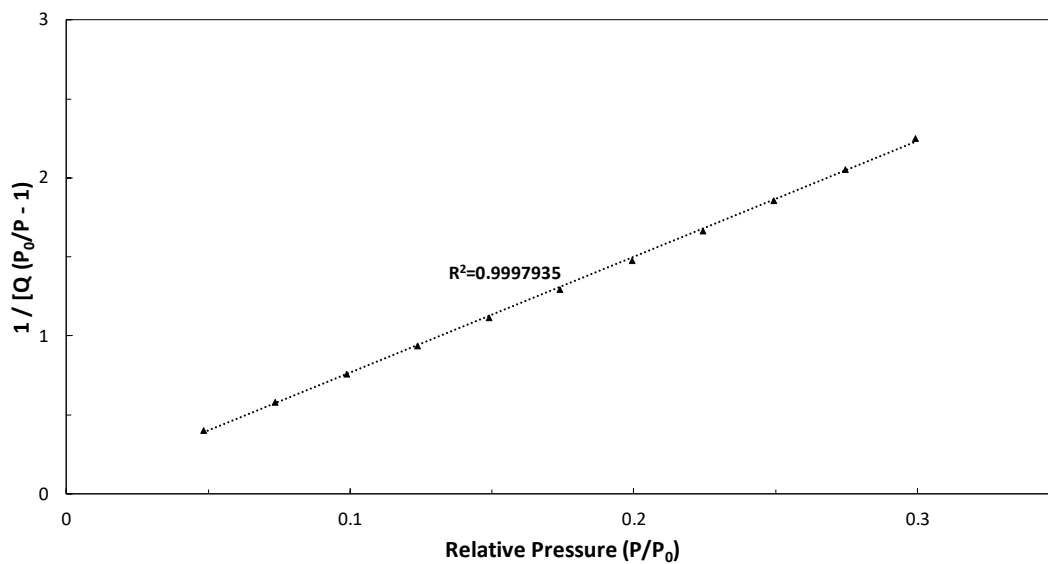


Figure A.4: WG BET plot.

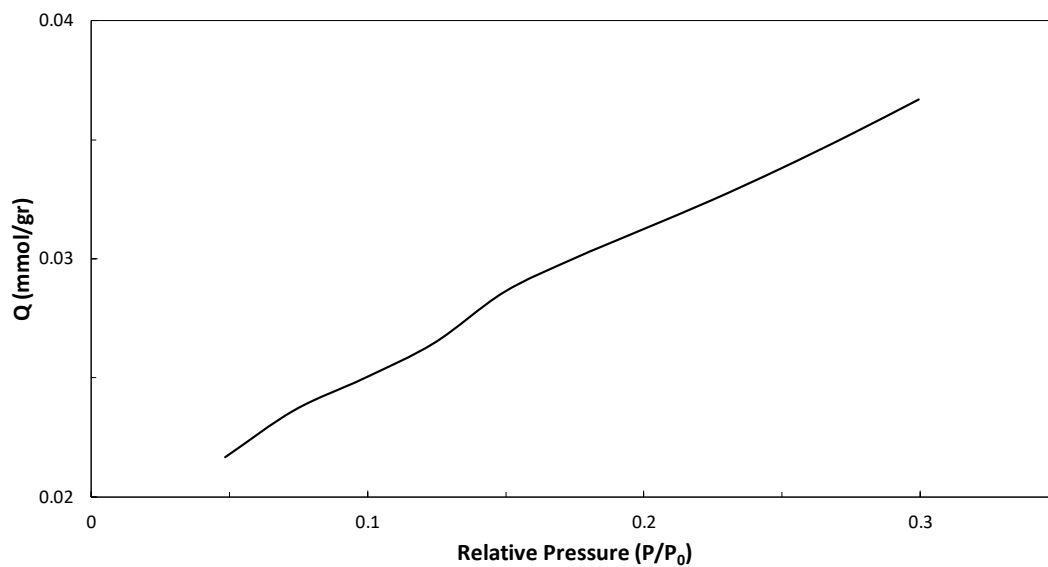


Figure A.5: BD isothermal curve.

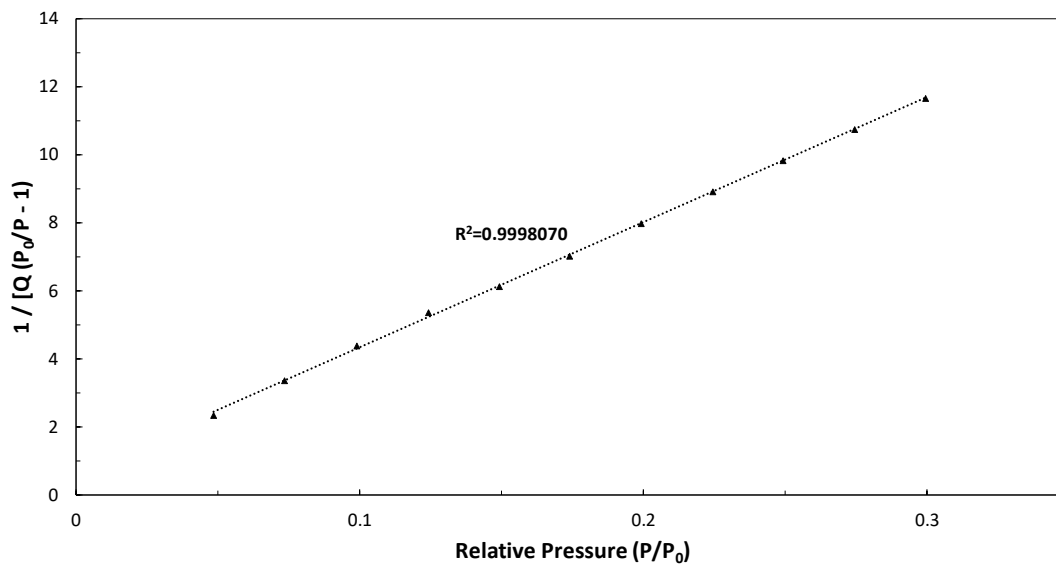


Figure A.6: BD BET plot.

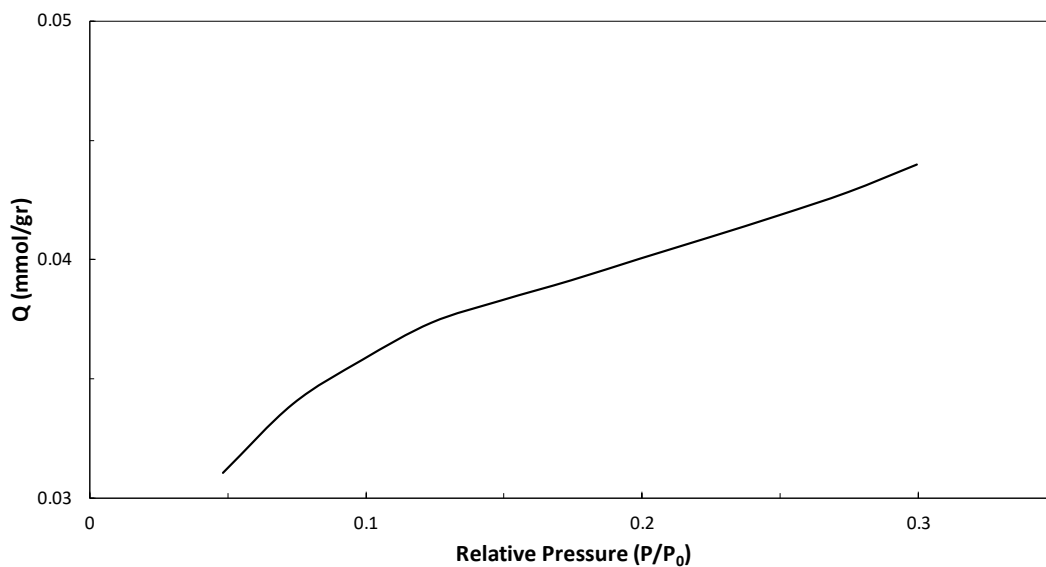


Figure A.7: GR isothermal curve.

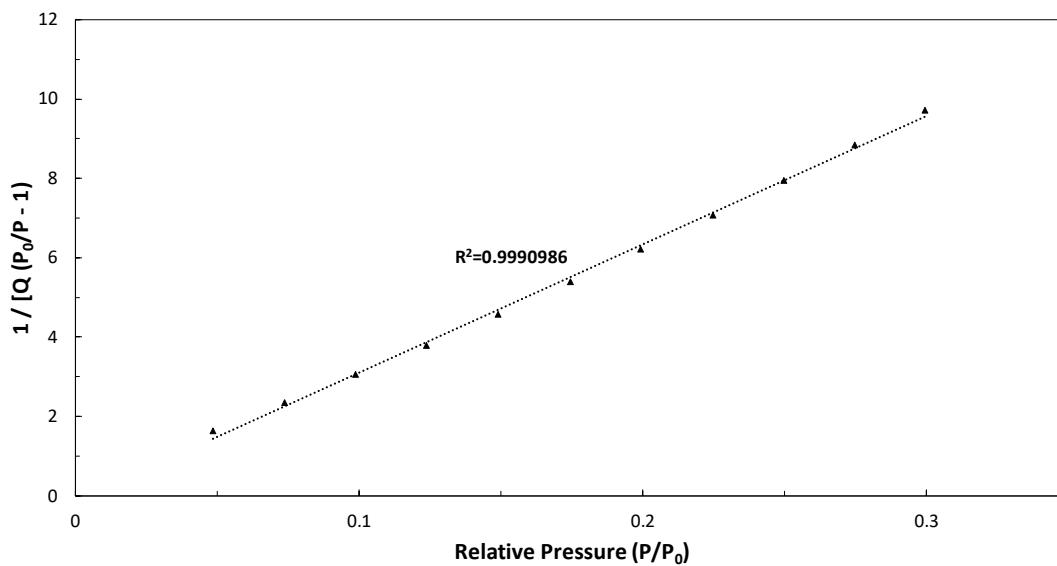


Figure A.8: GR BET plot.

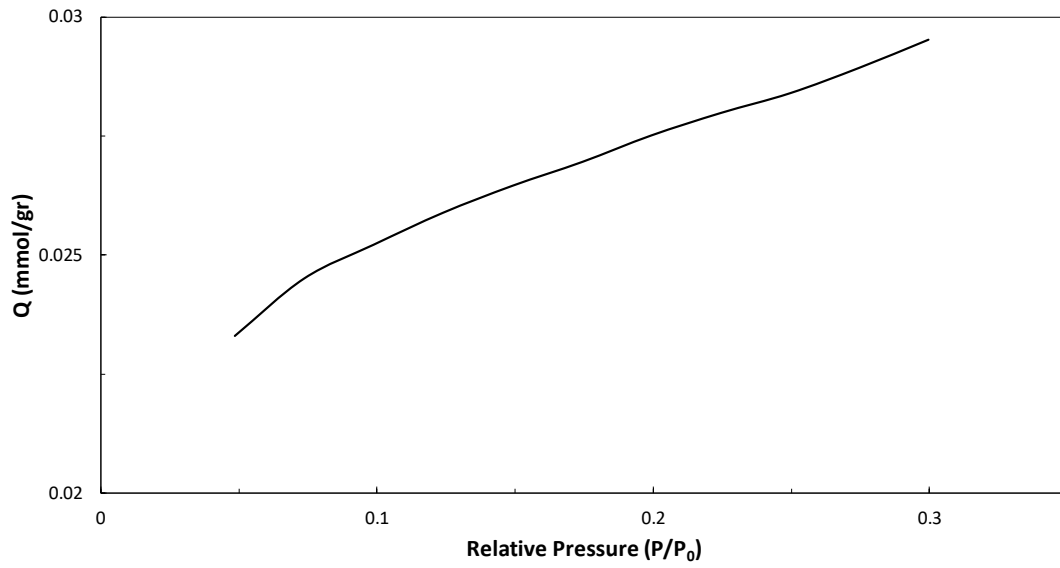


Figure A.9: BE isothermal curve.

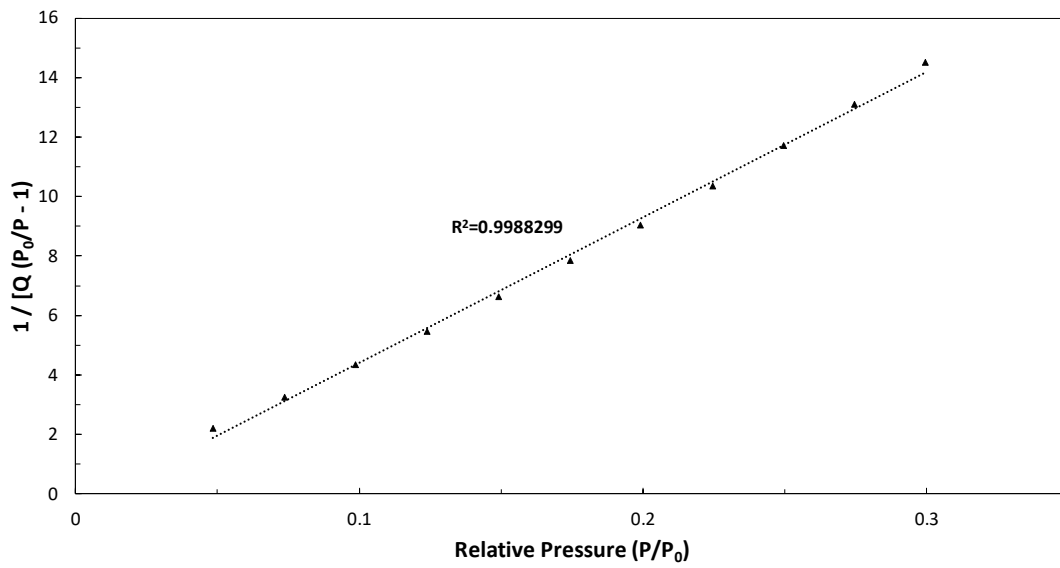


Figure A.10: BE BET plot.

# **Appendix B**

Amplitude sweep test results

Mastics LVE limit

In Fig. B.1 to B.6 the stress sweep test results for all mastics at each testing temperature are presented. On the graphs, the governing LVE limit as well as the chosen stress level for each case are also highlighted. In Tables B.1 to B.6 the determination of the materials' LVE limits, the governing LVE limit and the chosen stress level for the corresponding test temperature are summarized.

It should be noted that if the  $0.95G^*_{max}$  does not correspond to a recorded value (falls in between two measured complex shear modulus values) the one that corresponds to the lowest of the two stress levels is taken as the reduced complex shear modulus that determines the LVE region. This practice is on the “safe side”, since it ensures that the declared LVE region will always be (slightly) smaller than the actual one.

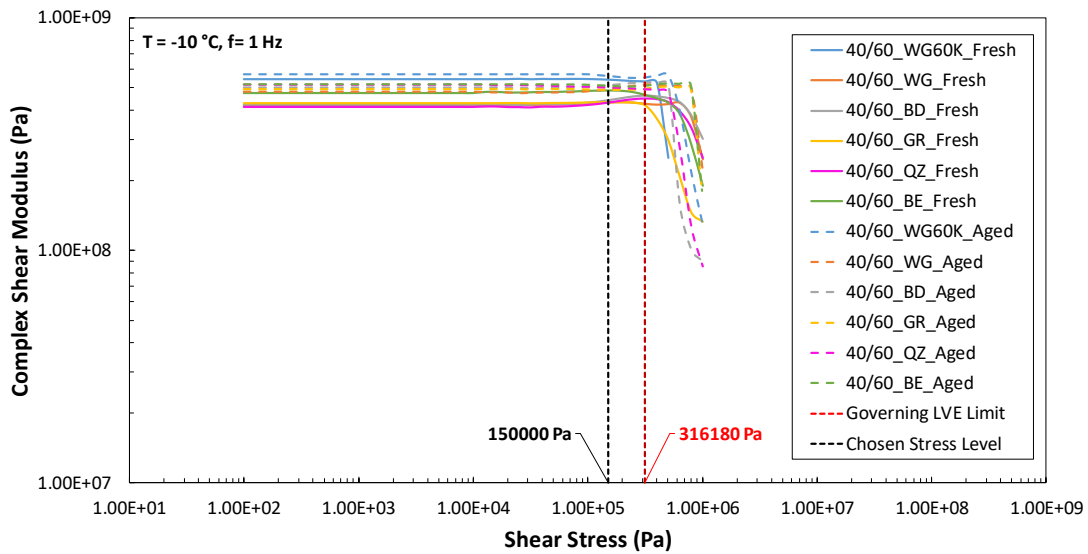


Figure B.1: Mastics amplitude sweep test results. T=-10°C, f=1 Hz.

Table B.1: Mastics LVE limits. T=-10°C, f=1 Hz.

Mastic	$G^*_{max}$ (Pa)	$0.95G^*_{max}$ (Pa)	$\tau_{limit}$ (Pa)	$\tau_{governing}$ (Pa)	$\tau_{chosen}$ (Pa)
40/60_WG60K_Fresh	546490000.0	519165500.0	398050.0		
40/60_WG_Fresh	432040000.0	410438000.0	398050.0		
40/60_BD_Fresh	463620000.0	440439000.0	501000.0		
40/60_GR_Fresh	434680000.0	412946000.0	316180.0		
40/60_QZ_Fresh	448350000.0	425932500.0	500990.0		
40/60_BE_Fresh	486010000.0	461709500.0	316180.0		
40/60_WG60K_Aged	570820000.0	542279000.0	501010.0	316180	150000
40/60_WG_Aged	515120000.0	489364000.0	794210.0		
40/60_BD_Aged	526600000.0	500270000.0	501010.0		
40/60_GR_Aged	505820000.0	480529000.0	794210.0		
40/60_QZ_Aged	517240000.0	491378000.0	316180.0		
40/60_BE_Aged	521440000.0	495368000.0	794210.0		

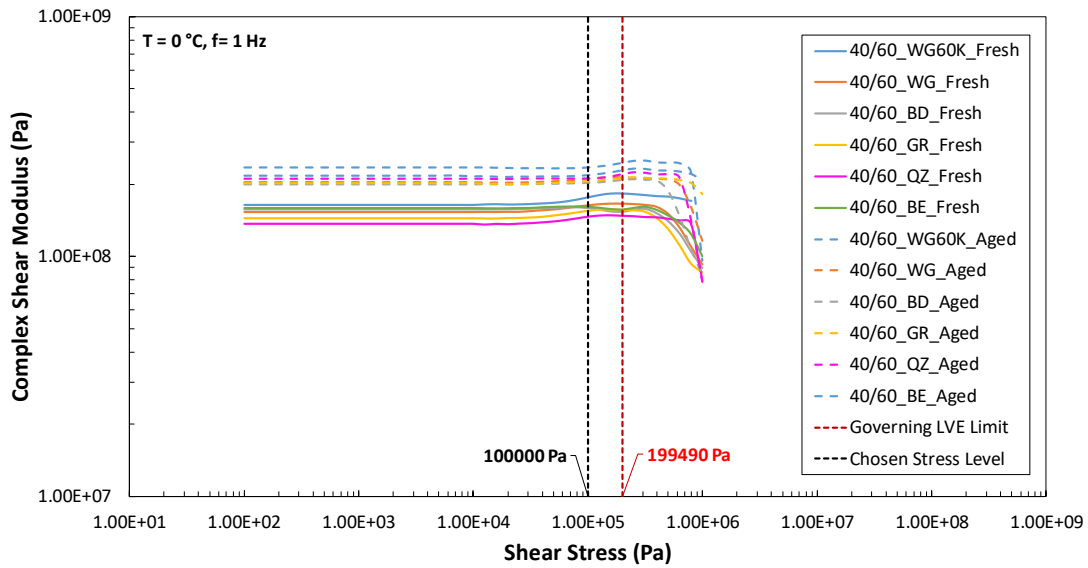


Figure B.2: Mastics amplitude sweep test results. T=0°C, f=1 Hz.

Table B.2: Mastics LVE limits. T=0°C, f=1 Hz.

Mastic	$G^*_{max}$ (Pa)	$0.95G^*_{max}$ (Pa)	$\tau_{limit}$ (Pa)	$\tau_{governing}$ (Pa)	$\tau_{chosen}$ (Pa)
40/60_WG60K_Fresh	183740000.0	174553000.0	630840.0		
40/60_WG_Fresh	165730000.0	157443500.0	398030.0		
40/60_BD_Fresh	160900000.0	152855000.0	199490.0		
40/60_GR_Fresh	157280000.0	149416000.0	316170.0		
40/60_QZ_Fresh	148310000.0	140894500.0	630840.0		
40/60_BE_Fresh	161570000.0	153491500.0	398030.0		
40/60_WG60K_Aged	251730000.0	239143500.0	630850.0	199490	100000
40/60_WG_Aged	213810000.0	203119500.0	501100.0		
40/60_BD_Aged	209480000.0	199006000.0	398030.0		
40/60_GR_Aged	214070000.0	203366500.0	794170.0		
40/60_QZ_Aged	225150000.0	213892500.0	630840.0		
40/60_BE_Aged	232490000.0	220865500.0	794180.0		

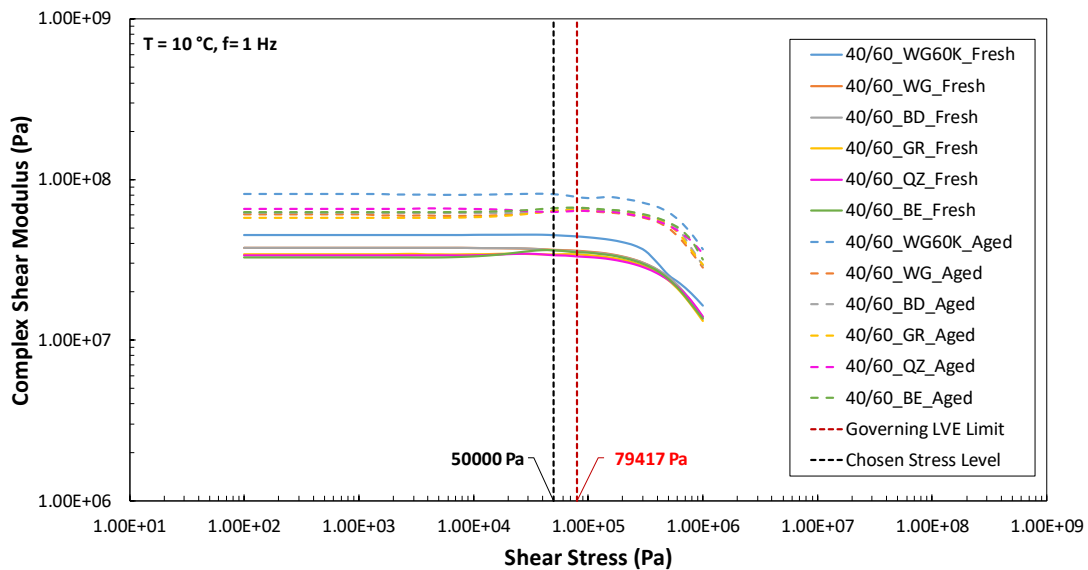


Figure B.3: Mastics amplitude sweep test results. T=10°C, f=1 Hz.

Table B.3: Mastics LVE limits. T=10°C, f=1 Hz.

Mastic	$G^*_{max}$ (Pa)	$0.95G^*_{max}$ (Pa)	$\tau_{limit}$ (Pa)	$\tau_{governing}$ (Pa)	$\tau_{chosen}$ (Pa)
40/60_WG60K_Fresh	45196000.0	42936200.0	99975.0		
40/60_WG_Fresh	37646000.0	35763700.0	79419.0		
40/60_BD_Fresh	37430000.0	35558500.0	79417.0		
40/60_GR_Fresh	34523000.0	32796850.0	125870.0		
40/60_QZ_Fresh	34552000.0	32824400.0	99990.0		
40/60_BE_Fresh	36143000.0	34335850.0	99990.0		
40/60_WG60K_Aged	81445000.0	77372750.0	158460.0	79417	50000
40/60_WG_Aged	63951000.0	60753450.0	199480.0		
40/60_BD_Aged	65973000.0	62674350.0	199480.0		
40/60_GR_Aged	64996000.0	61746200.0	199480.0		
40/60_QZ_Aged	66049000.0	62746550.0	158460.0		
40/60_BE_Aged	66838000.0	63496100.0	199480.0		

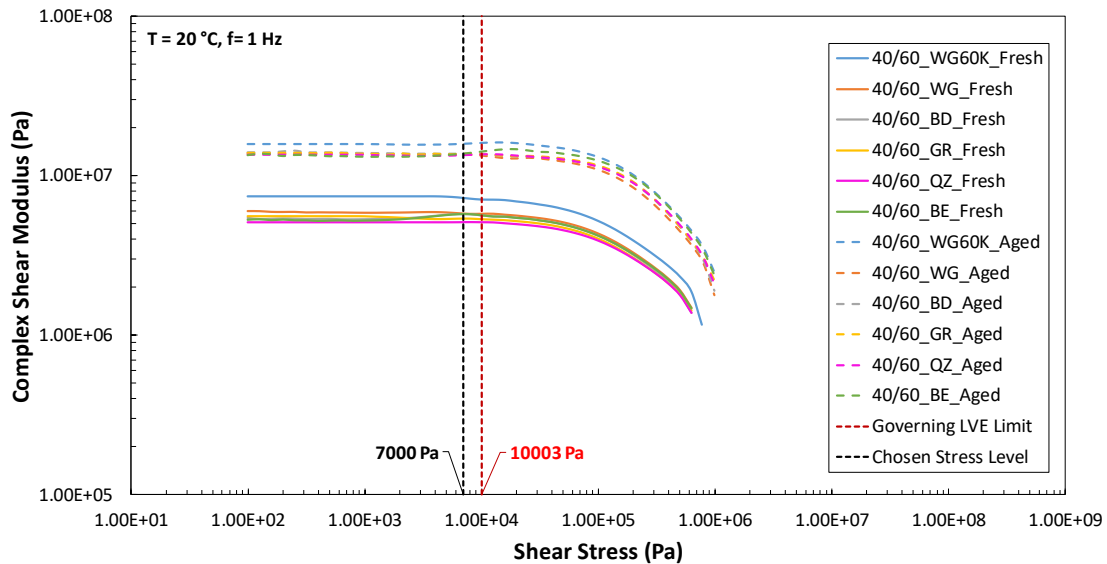


Figure B.4: Mastics amplitude sweep test results. T=20°C, f=1 Hz.

Table B.4: Mastics LVE limits. T=20°C, f=1 Hz.

Mastic	$G^*_{max}$ (Pa)	$0.95G^*_{max}$ (Pa)	$\tau_{limit}$ (Pa)	$\tau_{governing}$ (Pa)	$\tau_{chosen}$ (Pa)
40/60_WG60K_Fresh	7417600.0	7046720.0	12606.0		
40/60_WG_Fresh	6020500.0	5719475.0	12610.0		
40/60_BD_Fresh	5750900.0	5463355.0	15875.0		
40/60_GR_Fresh	5609200.0	5328740.0	12611.0		
40/60_QZ_Fresh	5112700.0	4857065.0	25165.0		
40/60_BE_Fresh	5772500.0	5483875.0	15876.0		
40/60_WG60K_Aged	16260000.0	15447000.0	31628.0	10003	7000
40/60_WG_Aged	13793000.0	13103350.0	12591.0		
40/60_BD_Aged	14360000.0	13642000.0	10003.0		
40/60_GR_Aged	14030000.0	13328500.0	31628.0		
40/60_QZ_Aged	13643000.0	12960850.0	31627.0		
40/60_BE_Aged	14750000.0	14012500.0	39819.0		



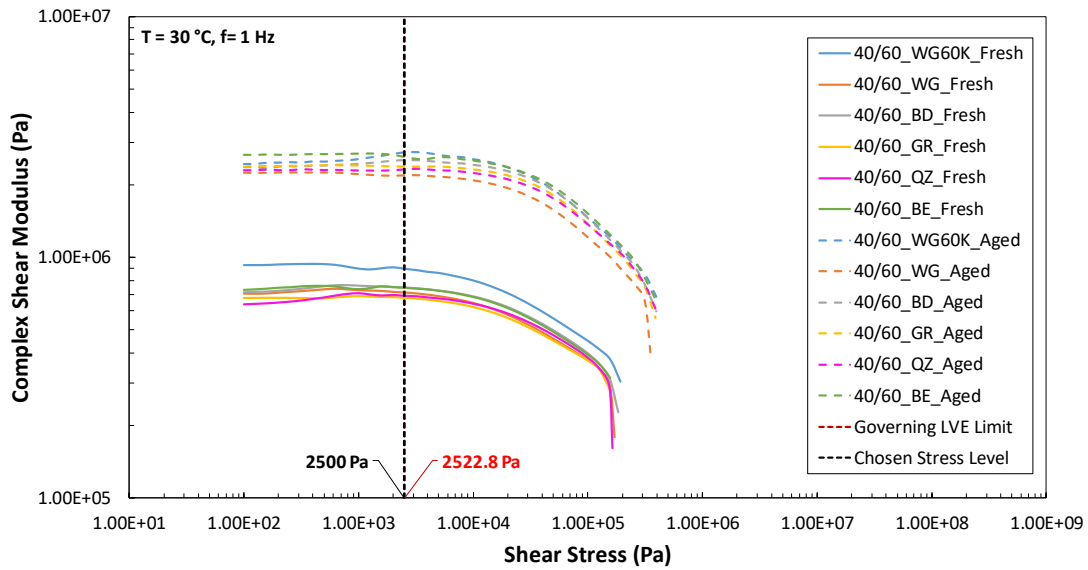


Figure B.5: Mastics amplitude sweep test results. T=30°C, f=1 Hz.

Table B.5: Mastics LVE limits. T=30°C, f=1 Hz.

Mastic	$G^*_{max}$ (Pa)	$0.95G^*_{max}$ (Pa)	$\tau_{limit}$ (Pa)	$\tau_{governing}$ (Pa)	$\tau_{chosen}$ (Pa)
40/60_WG60K_Fresh	938730.0	891793.5	2522.8		
40/60_WG_Fresh	737920.0	701024.0	3177.7		
40/60_BD_Fresh	761990.0	723890.5	5035.2		
40/60_GR_Fresh	689330.0	654863.5	5036.0		
40/60_QZ_Fresh	709370.0	673901.5	5036.5		
40/60_BE_Fresh	761550.0	723472.5	5035.0		
40/60_WG60K_Aged	2728200.0	2591790.0	7972.2	2522.8	2500
40/60_WG_Aged	2249900.0	2137405.0	6334.8		
40/60_BD_Aged	2523500.0	2397325.0	10031.0		
40/60_GR_Aged	2413000.0	2292350.0	10033.0		
40/60_QZ_Aged	2334500.0	2217775.0	10034.0		
40/60_BE_Aged	2684600.0	2550370.0	6330.7		

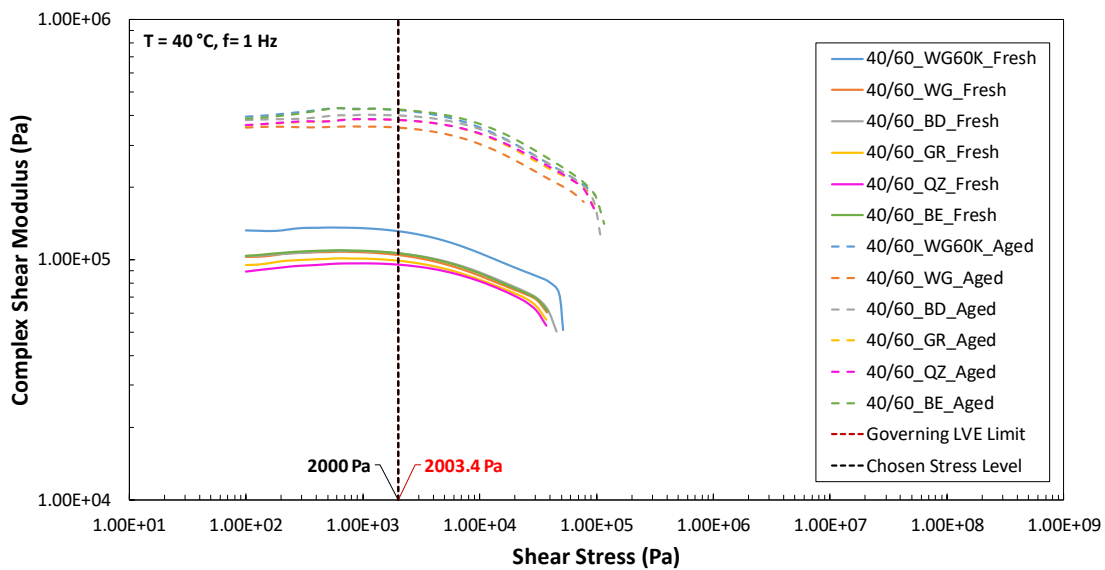


Figure B.6: Mastics amplitude sweep test results. T=40°C, f=1 Hz.

**Table B.6:** Mastics LVE limits. T=40°C, f=1 Hz.

Mastic	$G^*_{max}$ (Pa)	$0.95G^*_{max}$ (Pa)	$\tau_{limit}$ (Pa)	$\tau_{governing}$ (Pa)	$\tau_{chosen}$ (Pa)
40/60_WG60K_Fresh	136340.0	129523.0	2003.4		
40/60_WG_Fresh	108190.0	102780.5	2516.6		
40/60_BD_Fresh	109110.0	103654.5	3166.9		
40/60_GR_Fresh	101450.0	96377.5	2517.9		
40/60_QZ_Fresh	96482.0	91657.9	3168.3		
40/60_BE_Fresh	109960.0	104462.0	2517.5	2003.4	2000
40/60_WG60K_Aged	428080.0	406676.0	3178.1		
40/60_WG_Aged	360590.0	342560.5	3998.2		
40/60_BD_Aged	401150.0	381092.5	5031.8		
40/60_GR_Aged	385050.0	365797.5	3999.0		
40/60_QZ_Aged	385240.0	365978.0	3999.2		
40/60_BE_Aged	429680.0	408196.0	3999.3		

*Bitumen LVE limits*

In Fig. A.7 to A.12 the stress sweep test results for the neat bitumen at each testing temperature are presented. On the graphs, the governing LVE limit as well as the chosen stress level for each case are also highlighted. In Tables A.7 to A.12 the determination of the materials' LVE limits, the governing LVE limit and the chosen stress level for the corresponding test temperature are summarized.

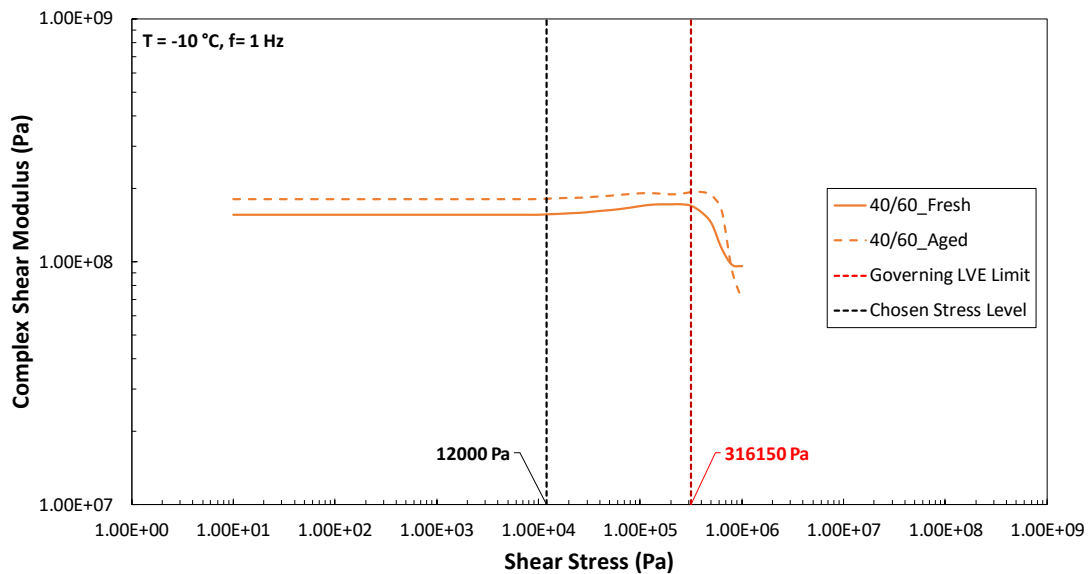


**Figure B.7:** Bitumen amplitude sweep test results. T=-10°C, f=1 Hz.

**Table B.7:** Bitumen LVE limits. T=-10°C, f=1 Hz.

Bitumen	$G^*_{max}$ (Pa)	$0.95G^*_{max}$ (Pa)	$\tau_{limit}$ (Pa)	$\tau_{governing}$ (Pa)	$\tau_{chosen}$ (Pa)
40/60_Fresh	173240000.0	164578000.0	316150.0	316150	12000
40/60_Aged	193430000.0	183758500.0	501060.0	316150	12000

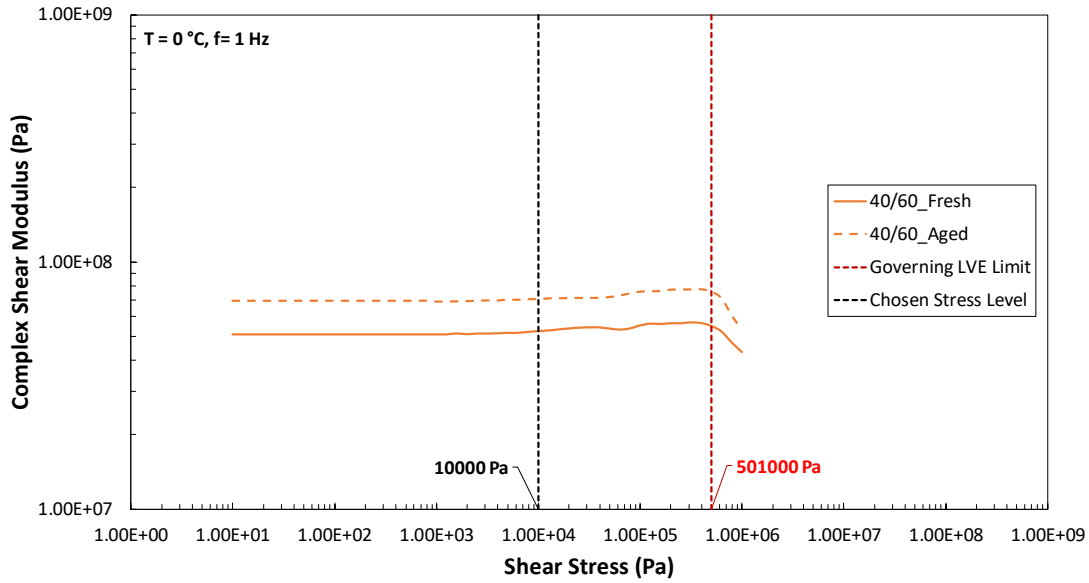


Figure B.8: Bitumen amplitude sweep test results. T=0°C, f=1 Hz.

Table B.8: Bitumen LVE limits. T=0°C, f=1 Hz.

Bitumen	$G^*_{max}$ (Pa)	$0.95G^*_{max}$ (Pa)	$\tau_{limit}$ (Pa)	$\tau_{governing}$ (Pa)	$\tau_{chosen}$ (Pa)
40/60_Fresh	56878000.0	54034100.0	501020.0	501000	10000
40/60_Aged	77643000.0	73760850.0	501000.0	501000	10000

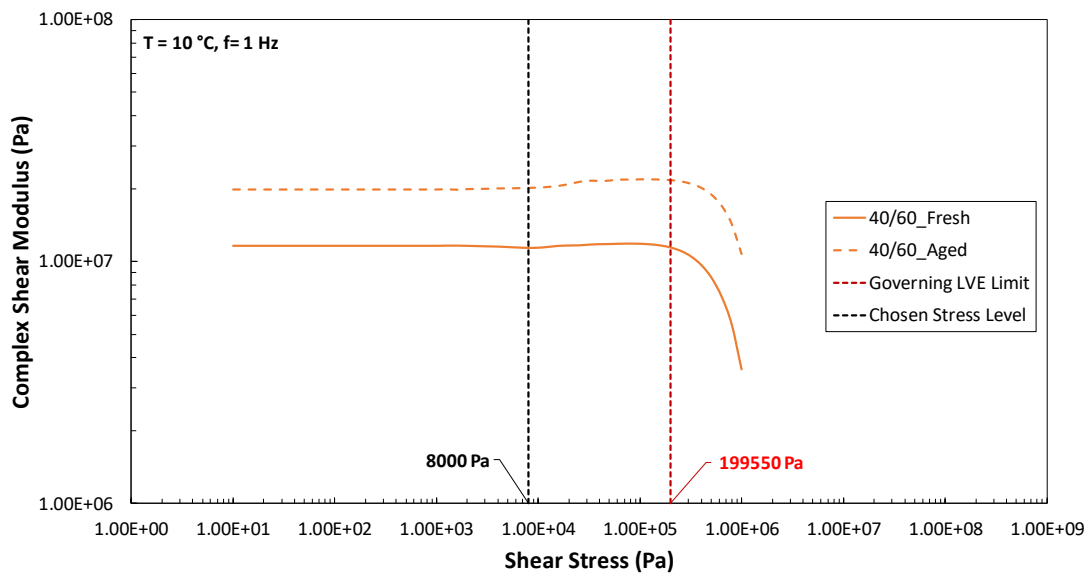


Figure B.9: Bitumen amplitude sweep test results. T=10°C, f=1 Hz.

Table B.9: Bitumen LVE limits. T=10°C, f=1 Hz.

Bitumen	$G^*_{max}$ (Pa)	$0.95G^*_{max}$ (Pa)	$\tau_{limit}$ (Pa)	$\tau_{governing}$ (Pa)	$\tau_{chosen}$ (Pa)
40/60_Fresh	11836000.0	11244200.0	199550.0	199550	8000
40/60_Aged	21868000.0	20774600.0	316060.0	199550	8000

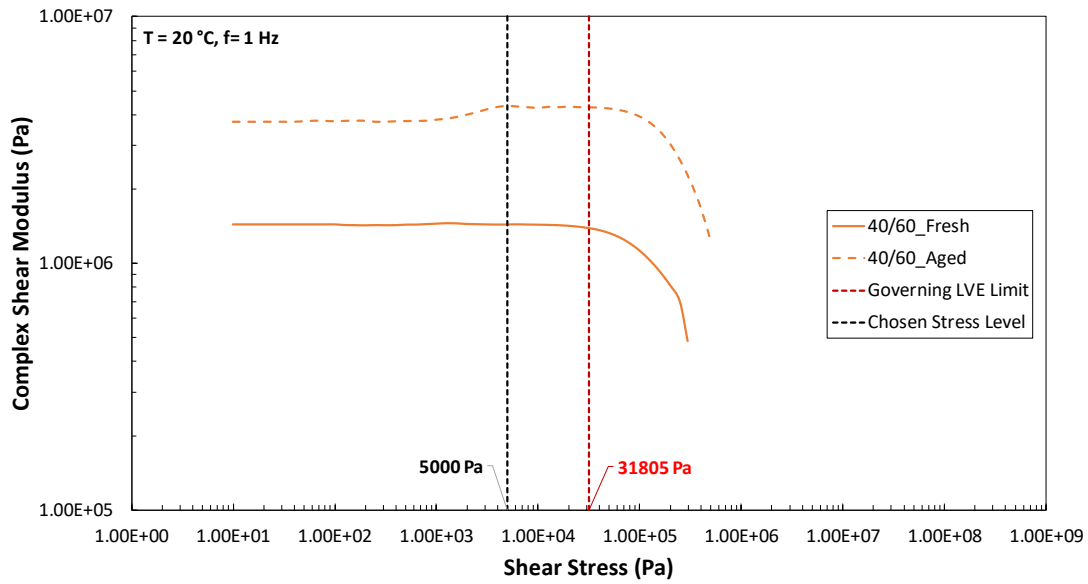


Figure B.10: Bitumen amplitude sweep test results. T=20°C, f=1 Hz.

Table B.10: Bitumen LVE limits. T=20°C, f=1 Hz.

Bitumen	$G^*_{max}$ (Pa)	$0.95G^*_{max}$ (Pa)	$\tau_{limit}$ (Pa)	$\tau_{governing}$ (Pa)	$\tau_{chosen}$ (Pa)
40/60_Fresh	1450900.0	1378355.0	31805.0	31805	5000
40/60_Aged	4337500.0	4120625.0	63121.0	31805	5000

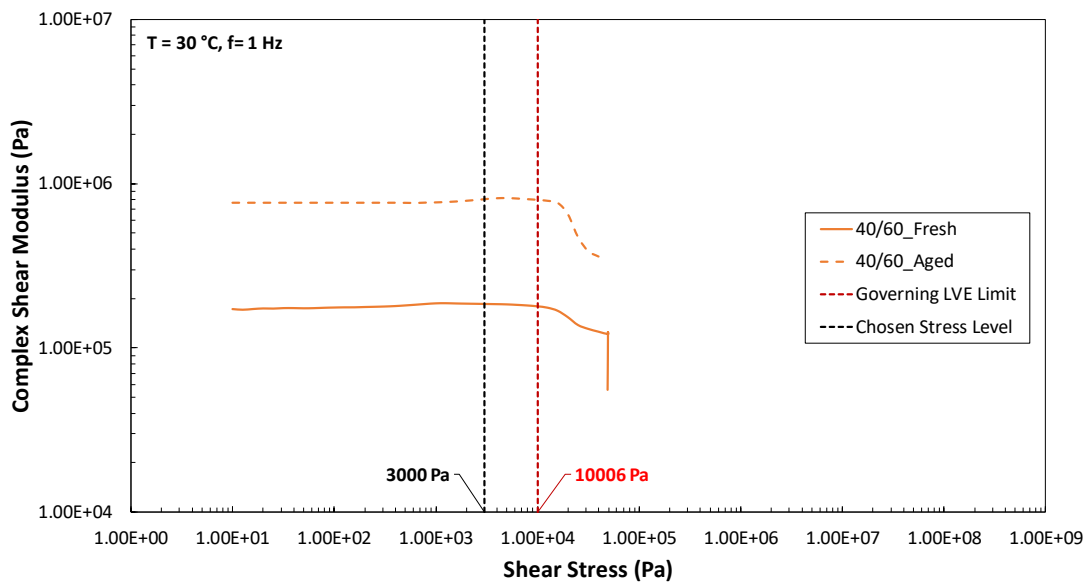


Figure B.11: Bitumen amplitude sweep test results. T=30°C, f=1 Hz.

Table B.11: Bitumen LVE limits. T=30°C, f=1 Hz.

Bitumen	$G^*_{max}$ (Pa)	$0.95G^*_{max}$ (Pa)	$\tau_{limit}$ (Pa)	$\tau_{governing}$ (Pa)	$\tau_{chosen}$ (Pa)
40/60_Fresh	186820.0	177479.0	10006.0	10006	3000
40/60_Aged	815590.0	774810.5	15849.0	10006	3000

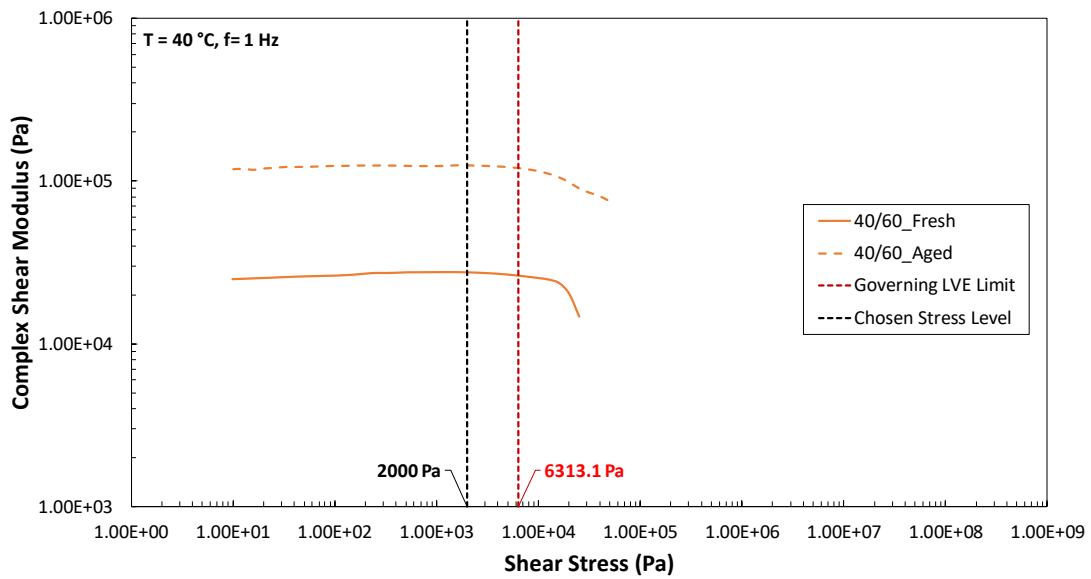


Figure B.12: Bitumen amplitude sweep test results. T=40°C, f=1 Hz.

Table B.12: Bitumen LVE limits. T=40°C, f=1 Hz.

Bitumen	$G^*_{max}$ (Pa)	$0.95G^*_{max}$ (Pa)	$\tau_{limit}$ (Pa)	$\tau_{governing}$ (Pa)	$\tau_{chosen}$ (Pa)
40/60_Fresh	27541.0	26164.0	6333.2	6313.1	2000
40/60_Aged	124940.0	118693.0	6313.1		



# **Appendix C**

WLF master-curves

Mastics master-curves

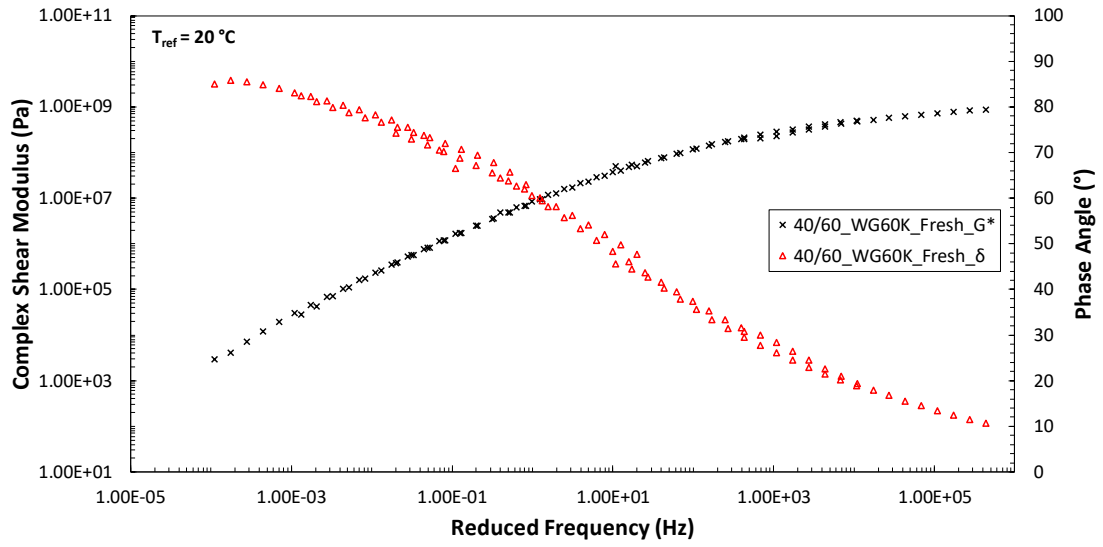


Figure C.1: WLF master-curves. 40/60\_WG60K\_Fresh.

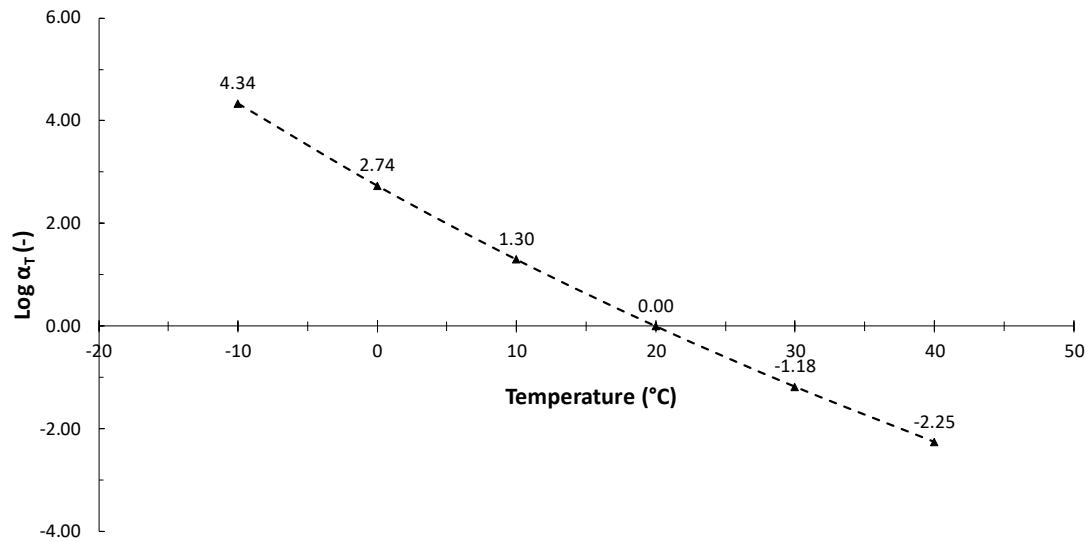


Figure C.2: WLF shift factors. 40/60\_WG60K\_Fresh.

Table C.1: WLF constants. 40/60\_WG60K\_Fresh.

Mastic	WLF Coefficients (-)	
	C <sub>1</sub>	C <sub>2</sub>
40/60_WG60K_Fresh	25.439	205.834



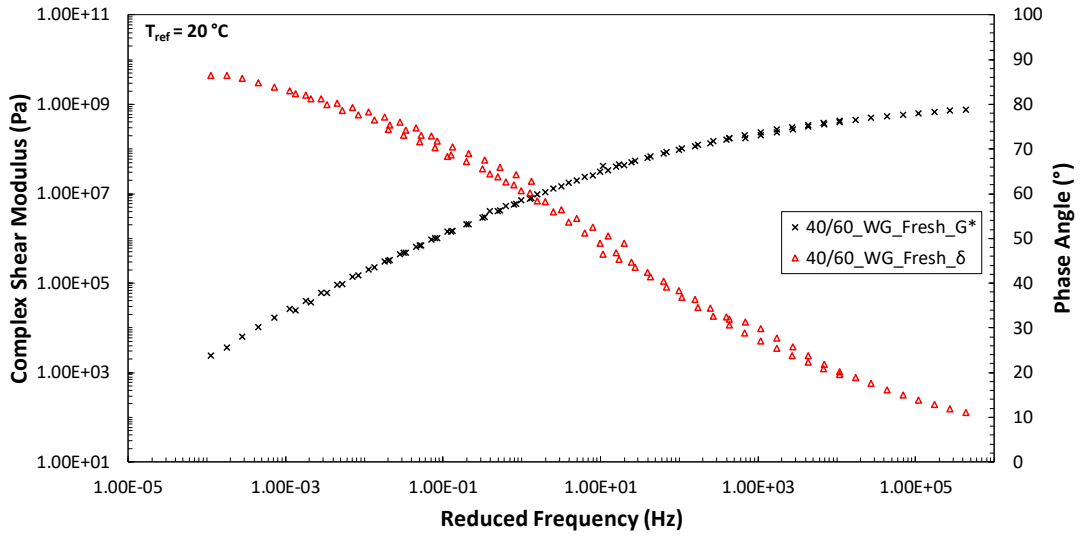


Figure C.3: WLF master-curves. 40/60\_WG\_Fresh.

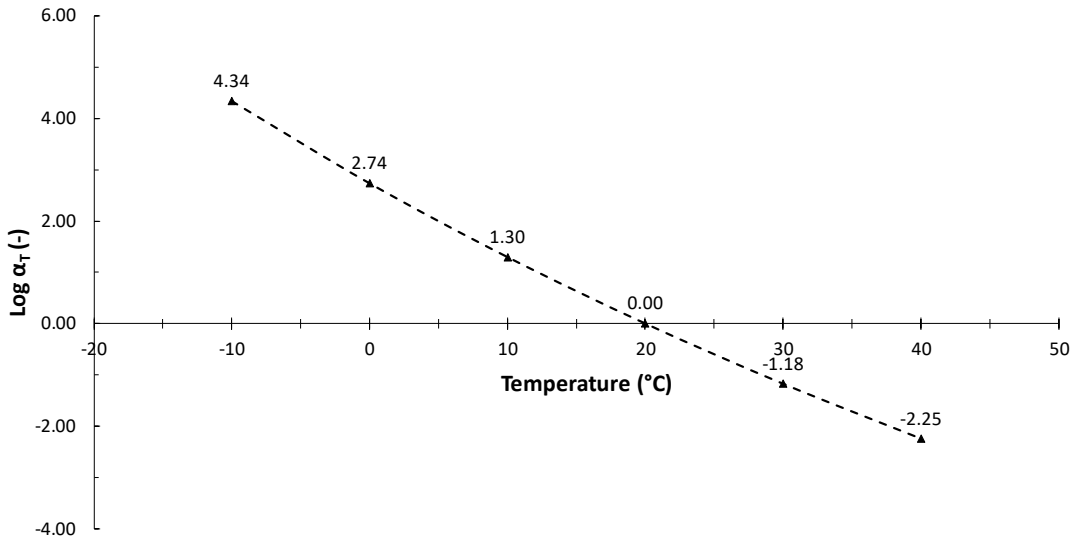


Figure C.4: WLF shift factors. 40/60\_WG\_Fresh.

Table C.2: WLF constants. 40/60\_WG\_Fresh.

Mastic	WLF Coefficients (-)	
	C <sub>1</sub>	C <sub>2</sub>
40/60_WG_Fresh	25.115	203.652

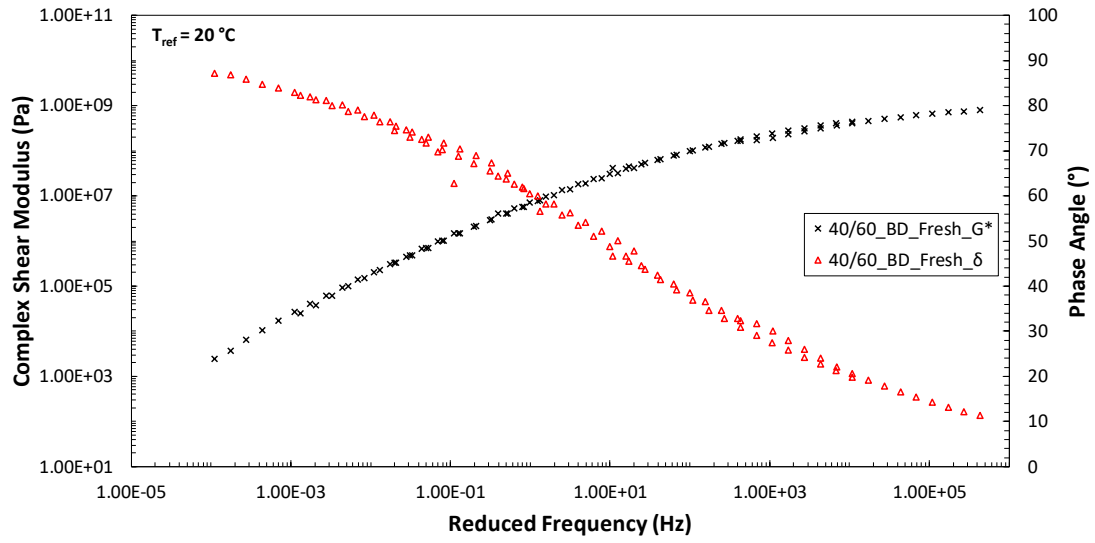


Figure C.5: WLF master-curves. 40/60\_BD\_Fresh.

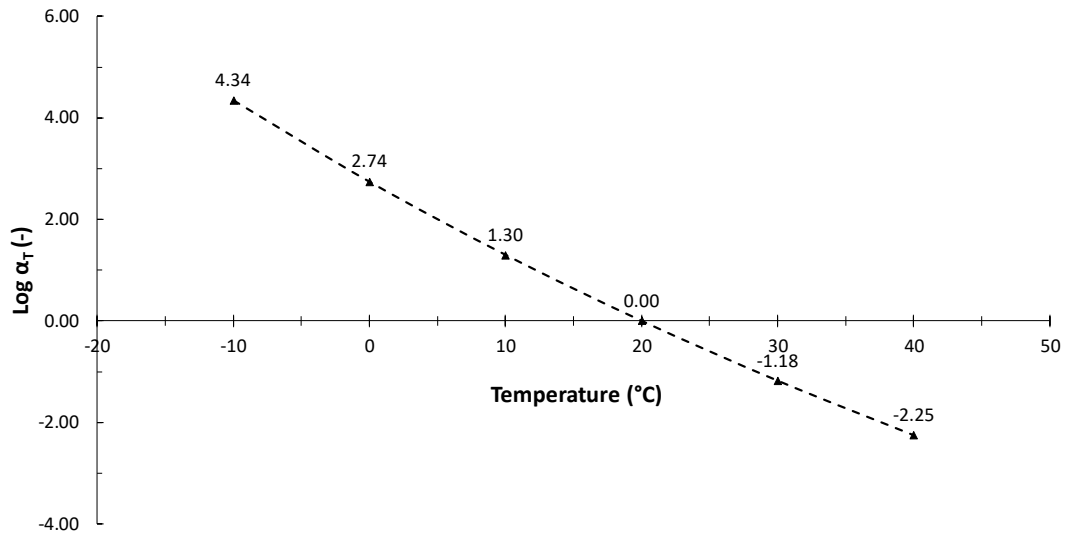


Figure C.6: WLF shift factors. 40/60\_BD\_Fresh.

Table C.3: WLF constants. 40/60\_BD\_Fresh.

Mastic	WLF Coefficients (-)	
	C <sub>1</sub>	C <sub>2</sub>
40/60_BD_Fresh	25.439	205.834

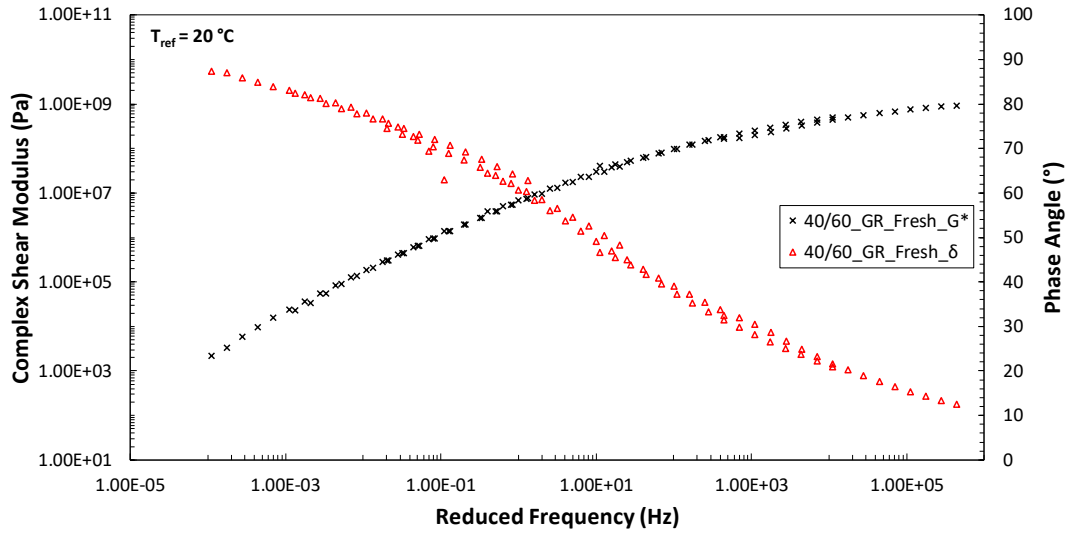


Figure C.7: WLF master-curves. 40/60\_GR\_Fresh.

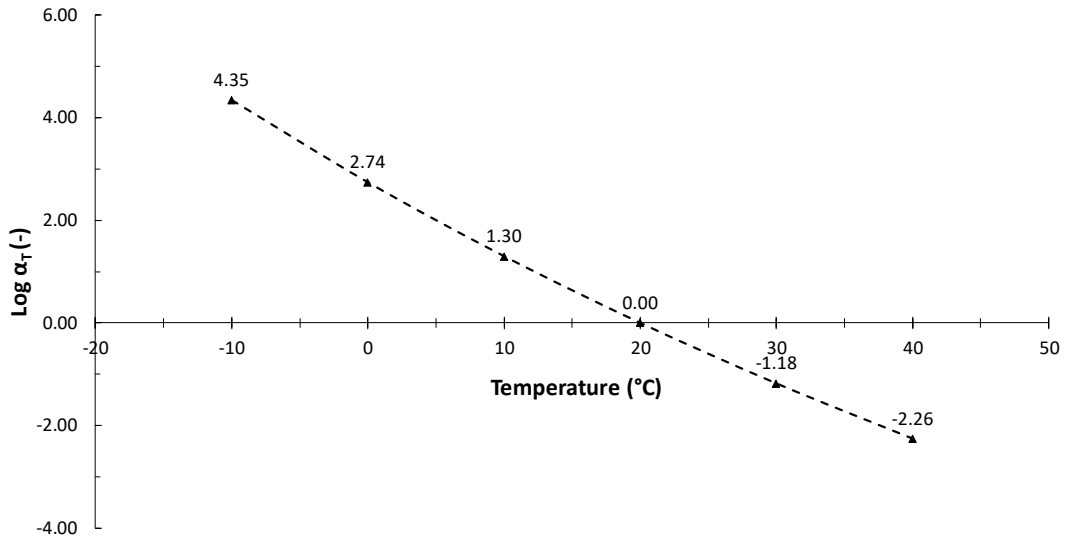


Figure C.8: WLF shift factors. 40/60\_GR\_Fresh.

Table C.4: WLF constants. 40/60\_GR\_Fresh.

Mastic	WLF Coefficients (-)	
	C <sub>1</sub>	C <sub>2</sub>
40/60_GR_Fresh	25.544	206.369

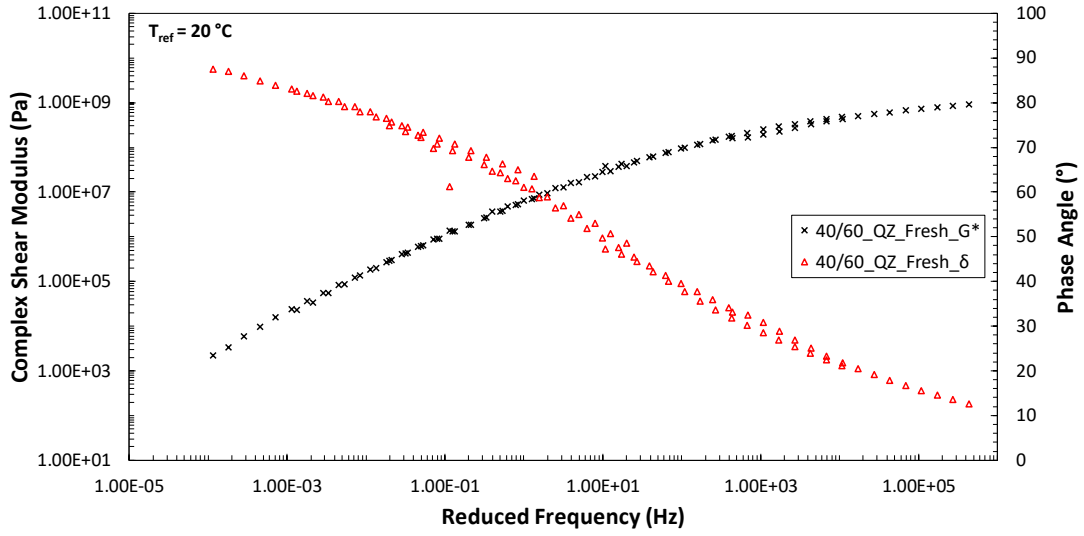


Figure C.9: WLF master-curves. 40/60\_QZ\_Fresh.

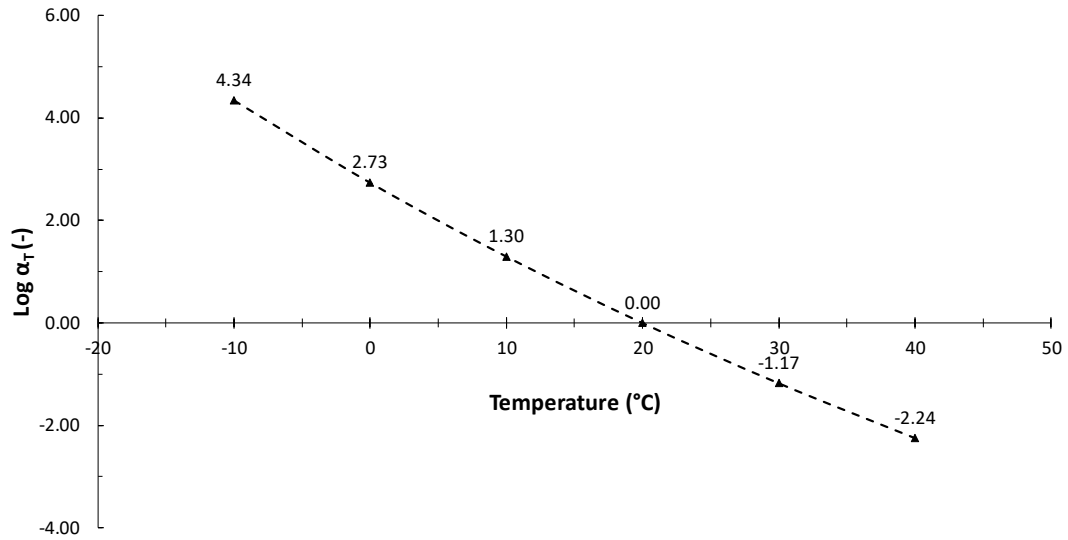


Figure C.10: WLF shift factors. 40/60\_QZ\_Fresh.

Table C.5: WLF constants. 40/60\_QZ\_Fresh.

Mastic	WLF Coefficients (-)	
	C <sub>1</sub>	C <sub>2</sub>
40/60_QZ_Fresh	24.933	202.377

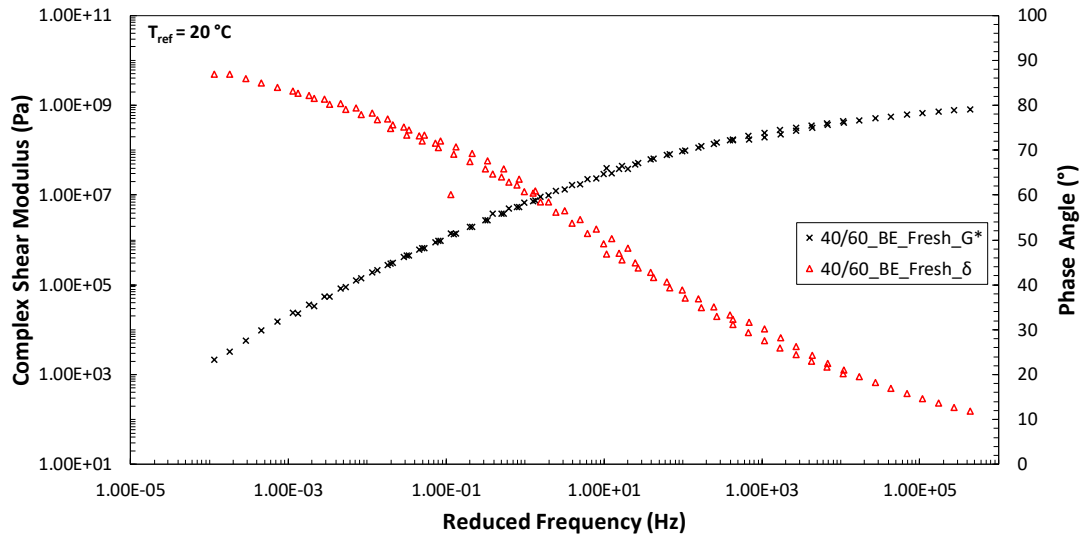


Figure C.11: WLF master-curves. 40/60\_BE\_Fresh.

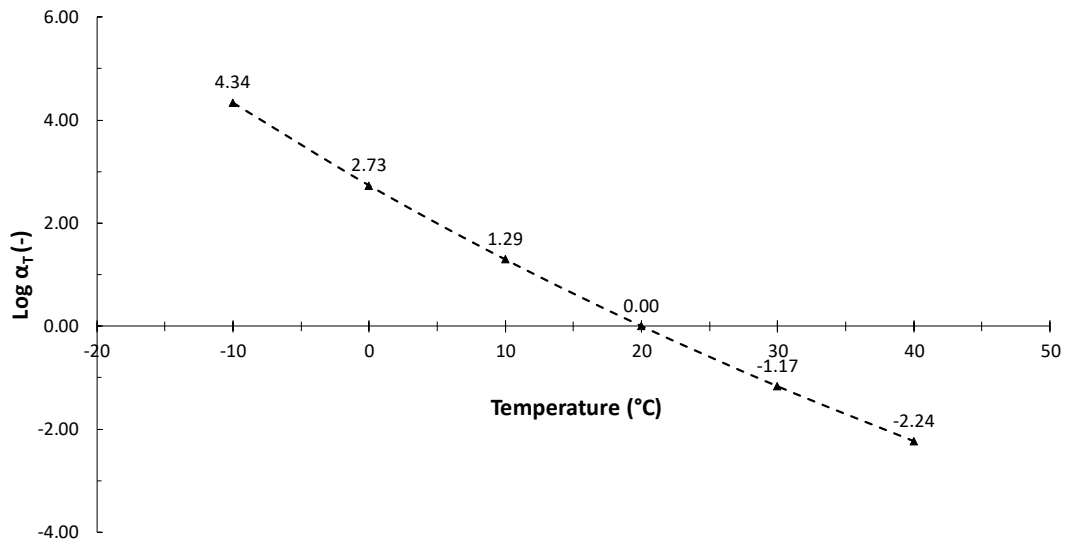


Figure C.12: WLF shift factors. 40/60\_BE\_Fresh.

Table C.6: WLF constants. 40/60\_BE\_Fresh.

Mastic	WLF Coefficients (-)	
	C <sub>1</sub>	C <sub>2</sub>
40/60_BE_Fresh	24.653	200.433

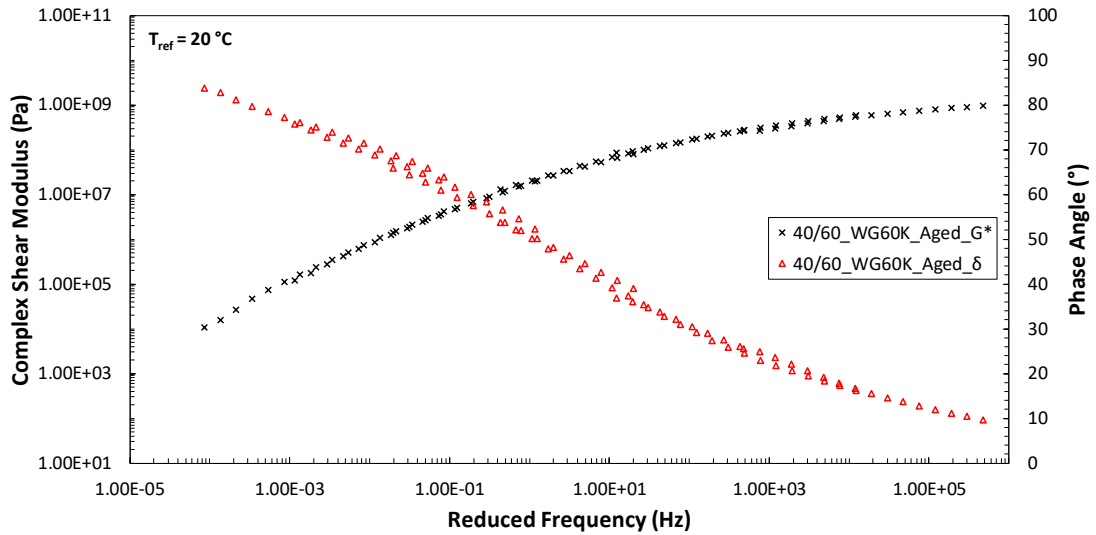


Figure C.13: WLF master-curves. 40/60\_WG60K\_Aged.

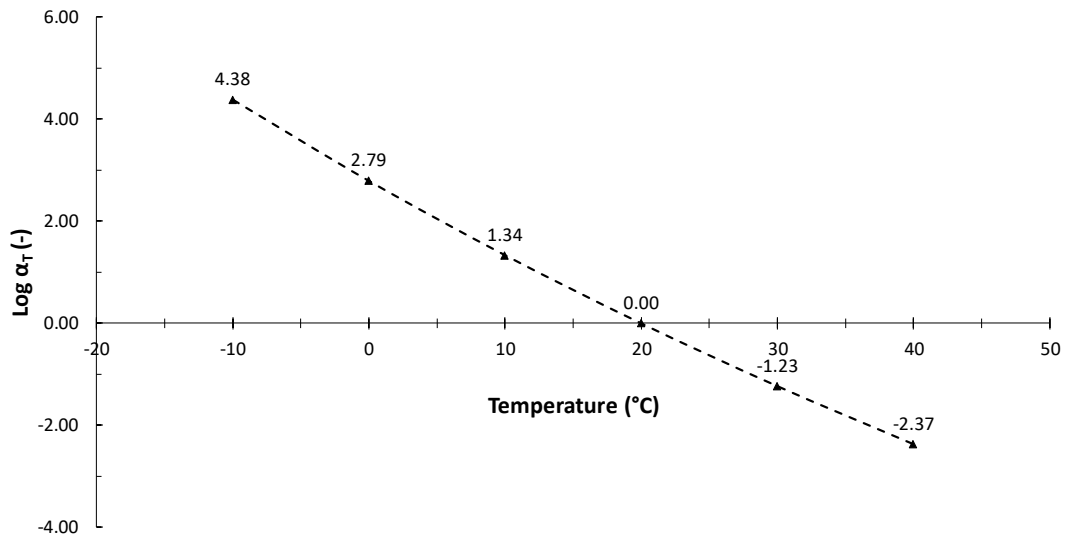


Figure C.14: WLF shift factors. 40/60\_WG60K\_Aged.

Table C.7: WLF constants. 40/60\_WG60K\_Aged.

Mastic	WLF Coefficients (-)	
	C <sub>1</sub>	C <sub>2</sub>
40/60_WG60K_Aged	31.138	243.173

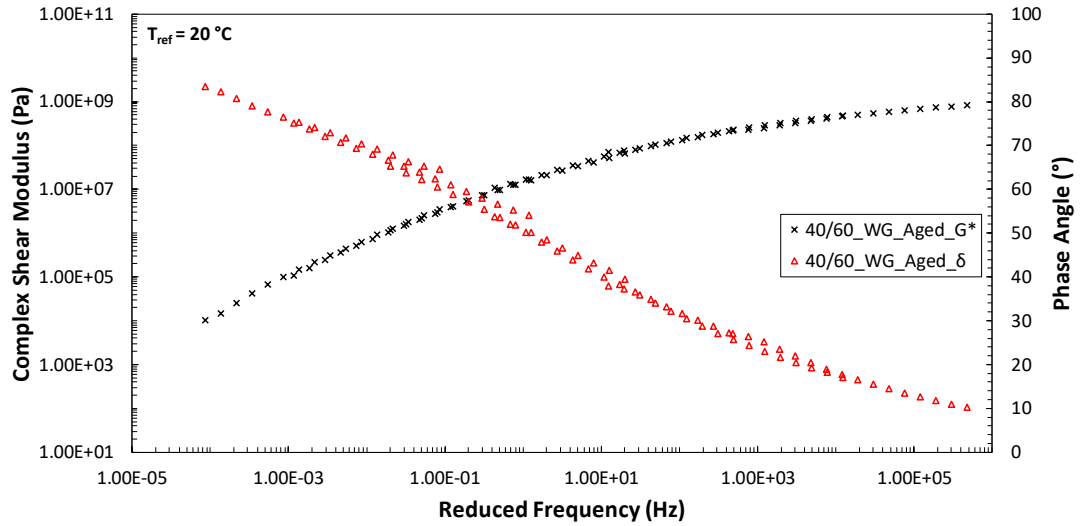


Figure C.15: WLF master-curves. 40/60\_WG\_Aged.

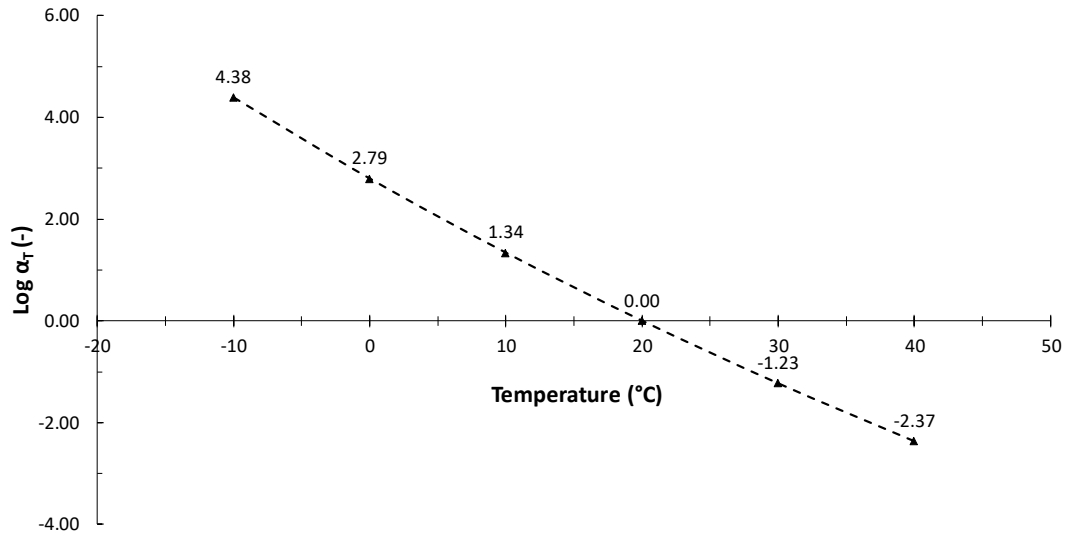


Figure C.16: WLF shift factors. 40/60\_WG\_Aged.

Table C.8: WLF constants. 40/60\_WG\_Aged.

Mastic	WLF Coefficients (-)	
	C <sub>1</sub>	C <sub>2</sub>
40/60_WG_Aged	31.138	243.173

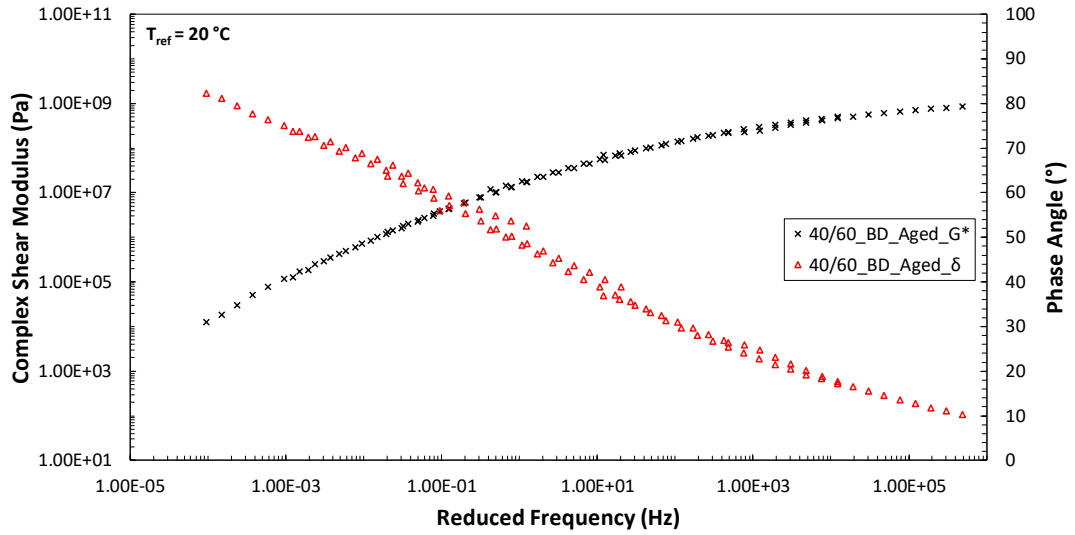


Figure C.17: WLF master-curves. 40/60\_BD\_Aged.

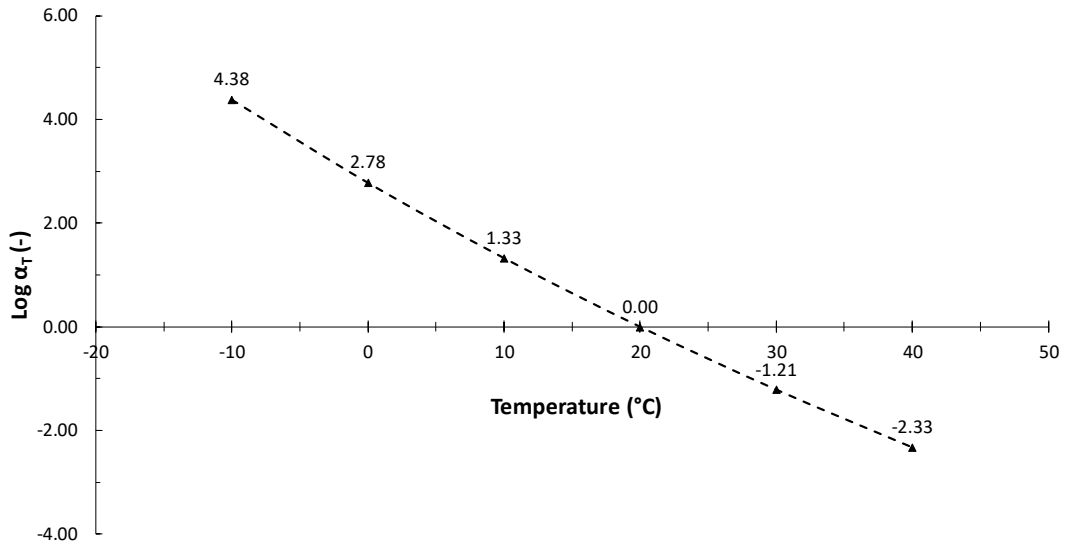


Figure C.18: WLF shift factors. 40/60\_BD\_Aged.

Table C.9: WLF constants. 40/60\_BD\_Aged.

Mastic	WLF Coefficients (-)	
	C <sub>1</sub>	C <sub>2</sub>
40/60_BD_Aged	28.655	226.161



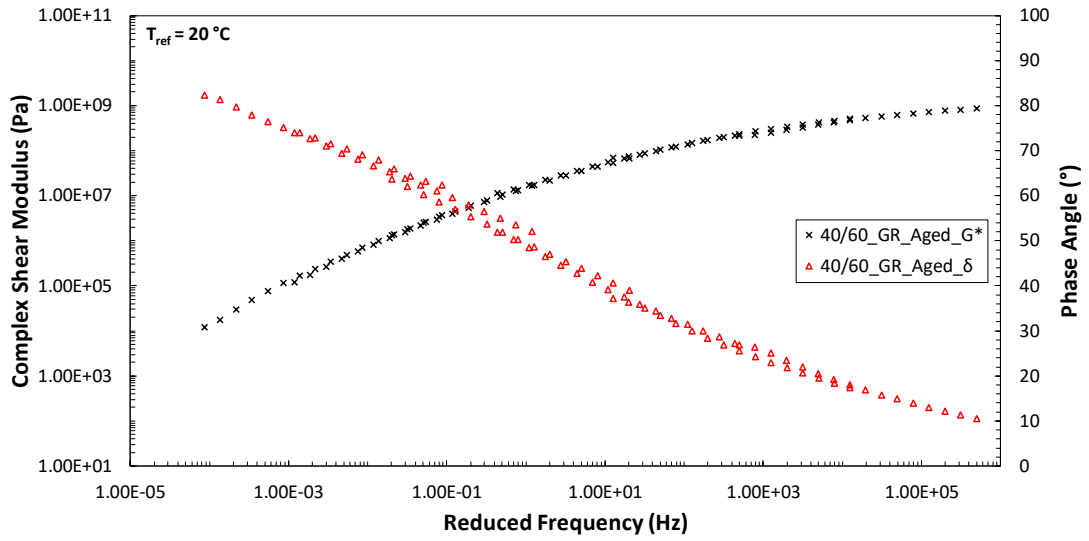


Figure C.19: WLF master-curves. 40/60\_GR\_Aged.

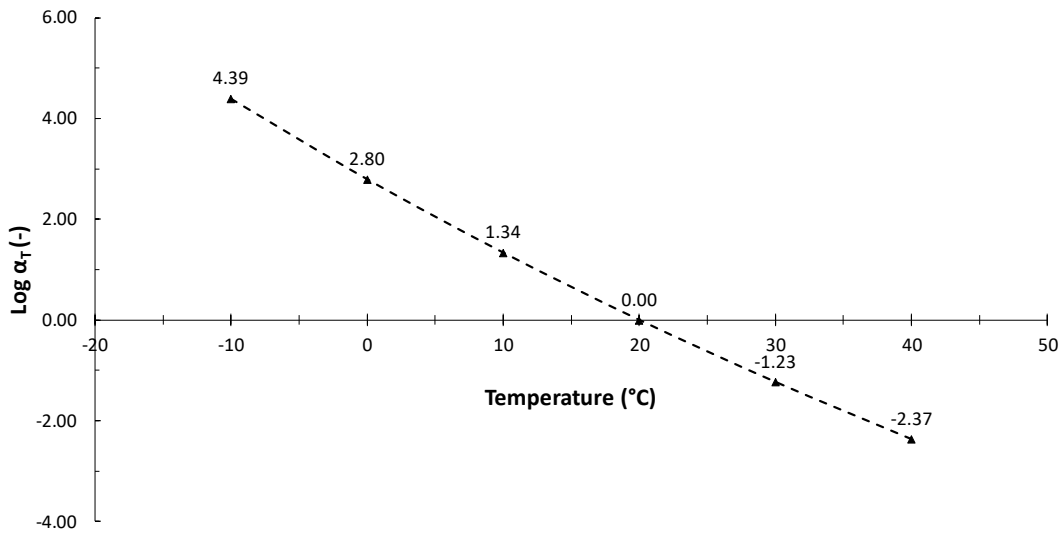


Figure C.20: WLF shift factors. 40/60\_GR\_Aged.

Table C.10: WLF constants. 40/60\_GR\_Aged.

Mastic	WLF Coefficients (-)	
	C <sub>1</sub>	C <sub>2</sub>
40/60_GR_Aged	31.003	241.828

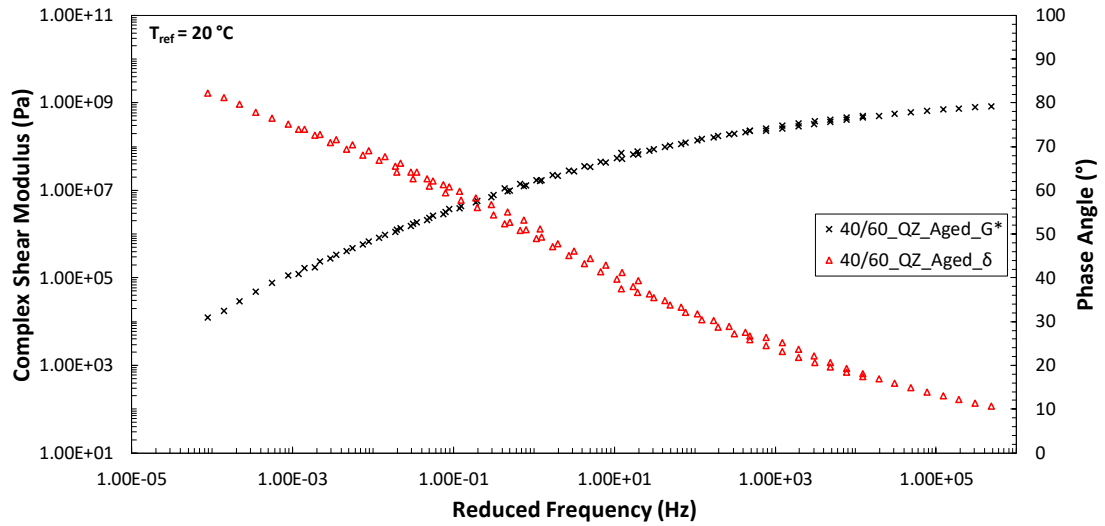


Figure C.21: WLF master-curves. 40/60\_QZ\_Aged.

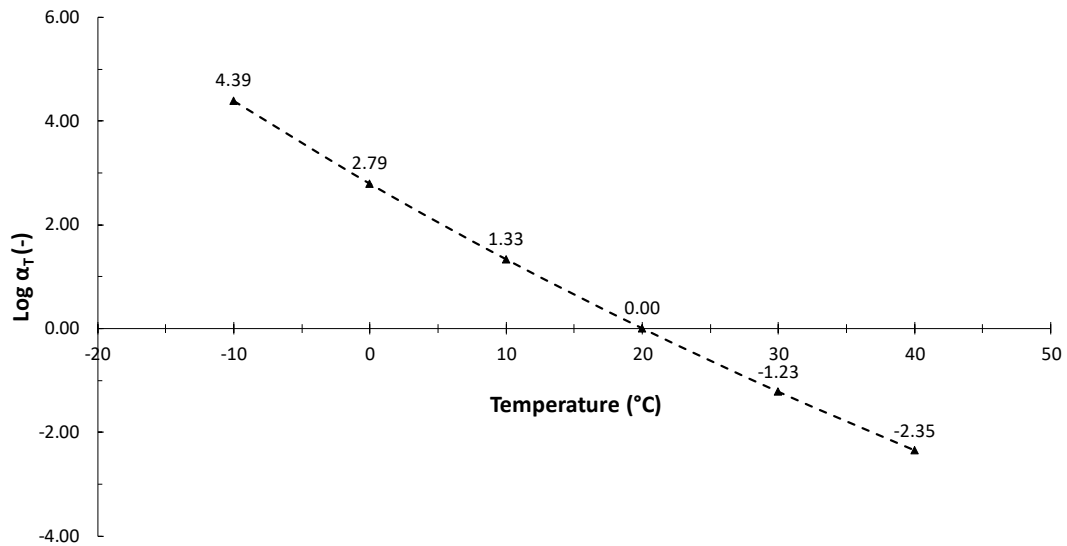


Figure C.22: WLF shift factors. 40/60\_QZ\_Aged.

Table C.11: WLF constants. 40/60\_QZ\_Aged.

Mastic	WLF Coefficients (-)	
	C <sub>1</sub>	C <sub>2</sub>
40/60_QZ_Aged	30.154	236.123

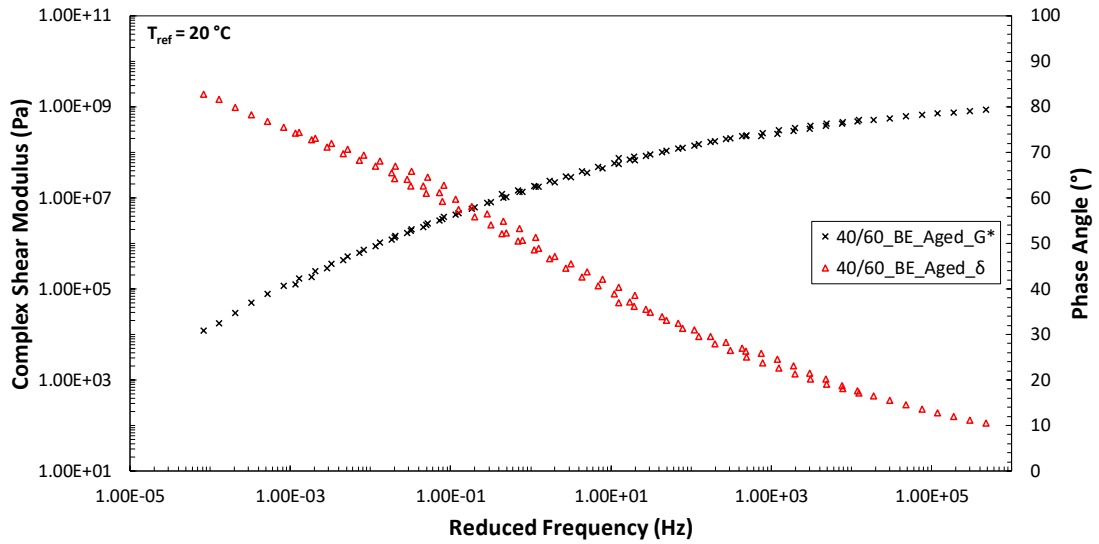


Figure C.23: WLF master-curves. 40/60\_BE\_Aged.

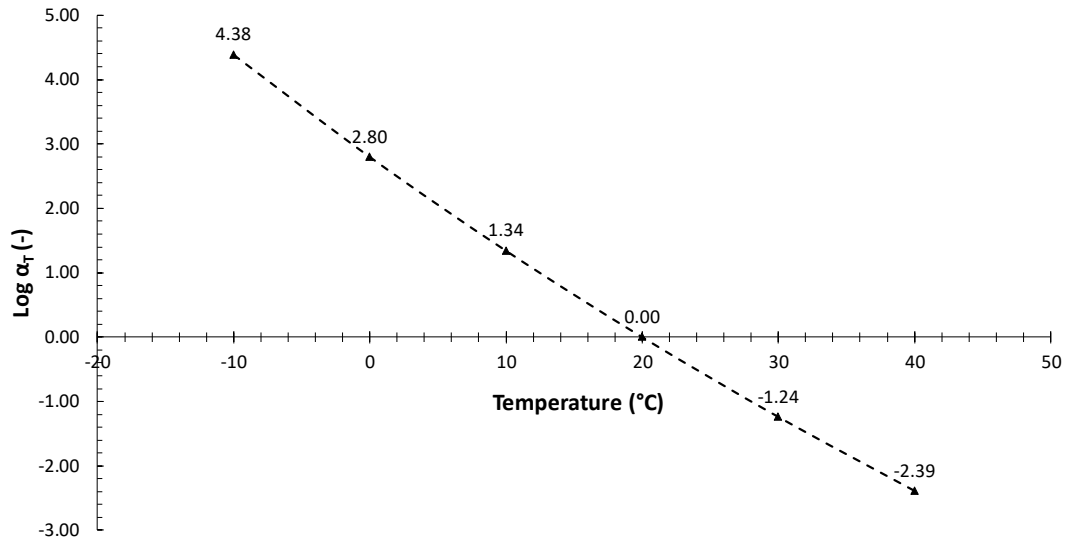


Figure C.24: WLF shift factors. 40/60\_BE\_Aged.

Table C.12: WLF constants. 40/60\_BE\_Aged.

Mastic	WLF Coefficients (-)	
	C <sub>1</sub>	C <sub>2</sub>
40/60_BE_Aged	32.529	252.767

Bitumen master-curves

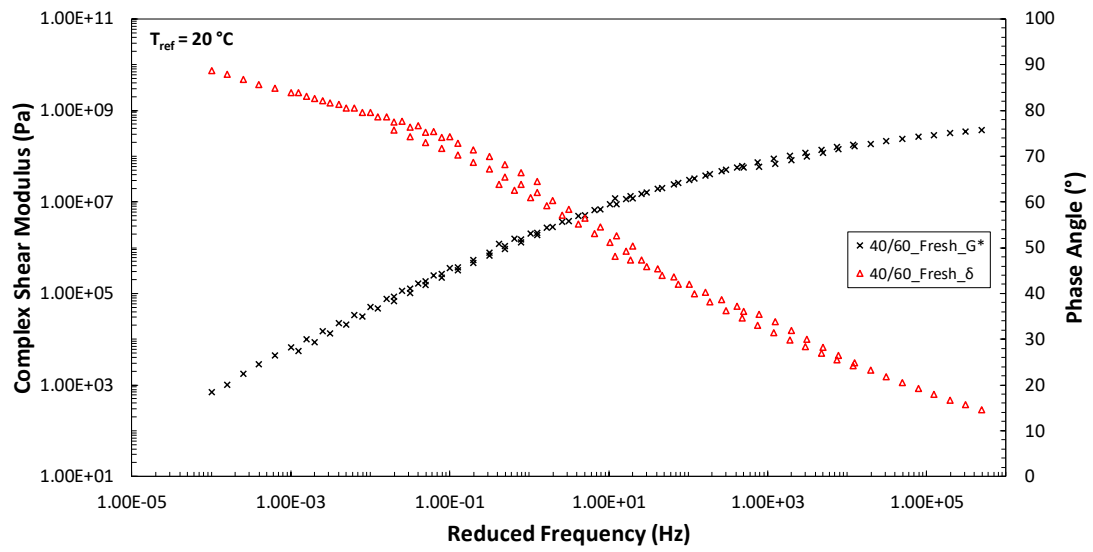


Figure C.25: WLF master-curves. 40/60\_Fresh.

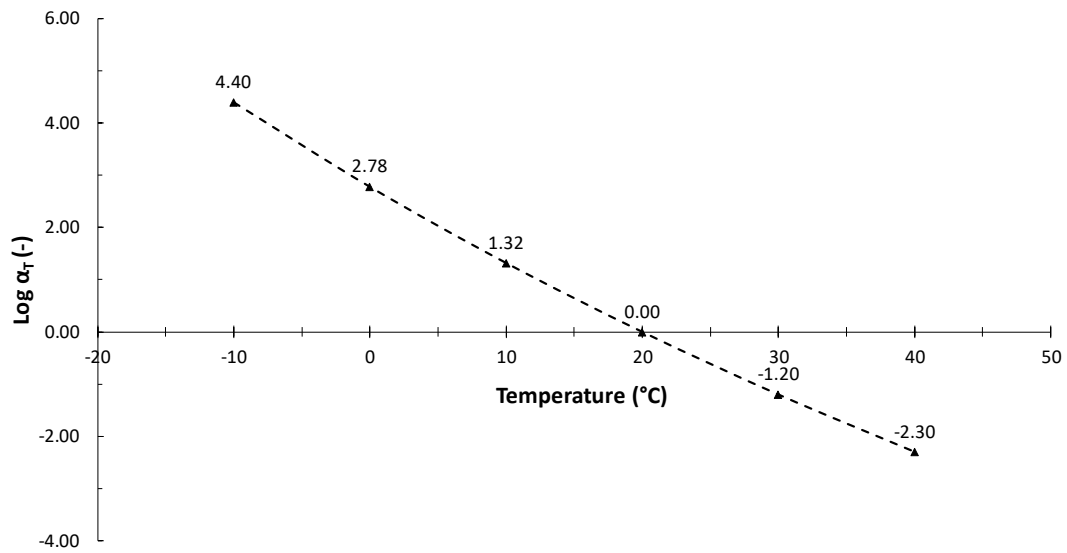


Figure C.26: WLF shift factors. 40/60\_Fresh.

Table C.13: WLF constants. 40/60\_Fresh.

Bitumen	WLF Coefficients (-)	
	C <sub>1</sub>	C <sub>2</sub>
40/60_Fresh	26.594	211.485

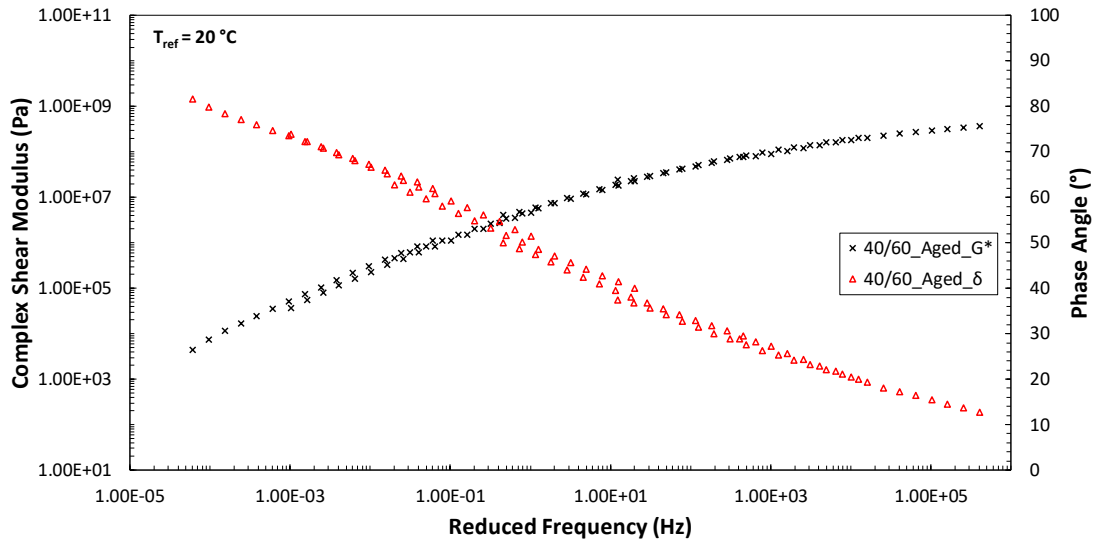


Figure C.27: WLF master-curves. 40/60\_Aged.

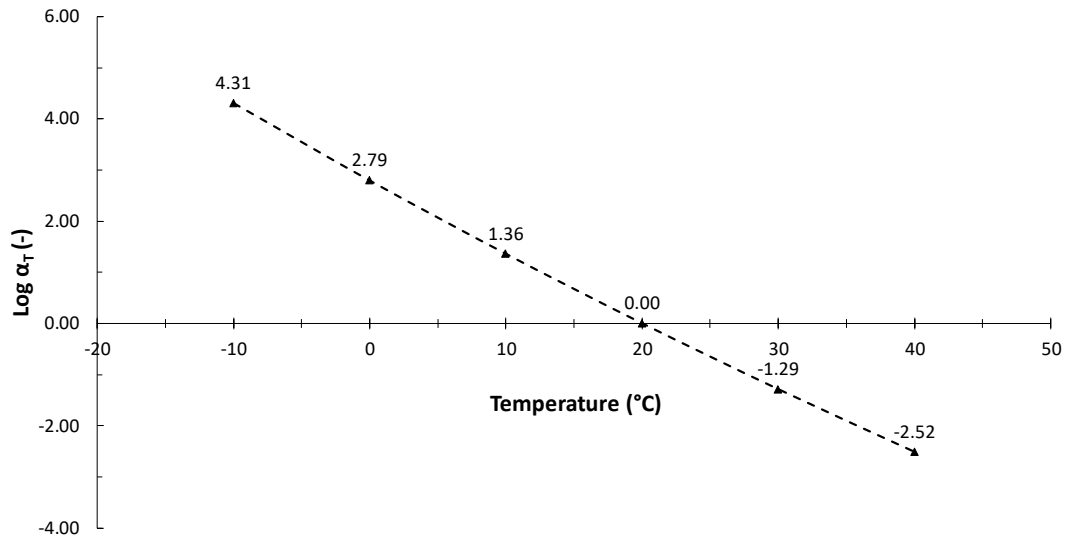


Figure C.28: WLF shift factors. 40/60\_Aged.

Table C.14: WLF constants. 40/60\_Aged.

Bitumen	WLF Coefficients (-)	
	C <sub>1</sub>	C <sub>2</sub>
40/60_Aged	50.627	382.405

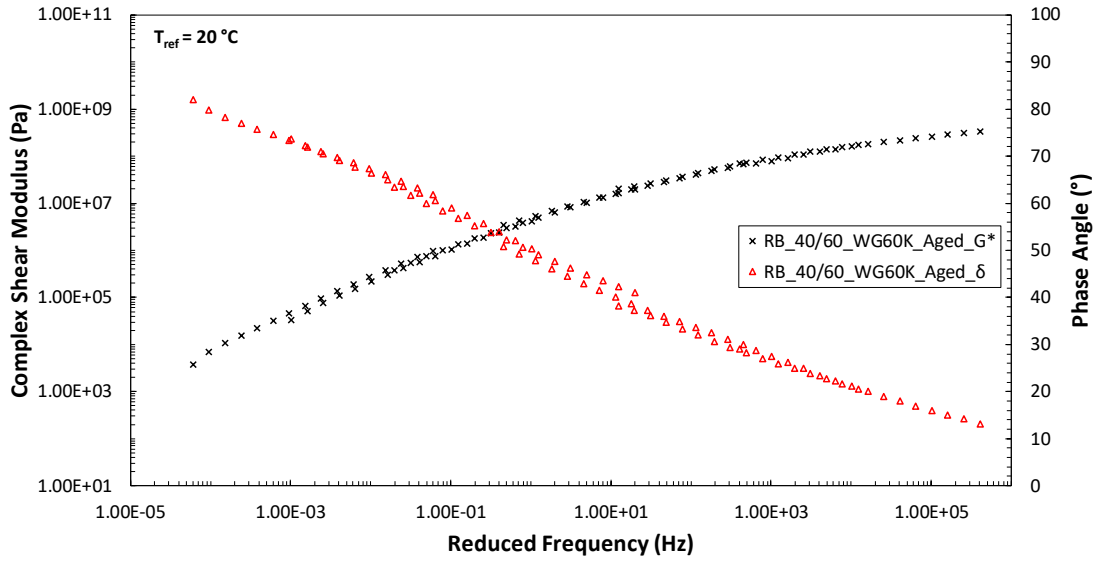


Figure C.29: WLF master-curves. RB\_40/60\_WG60K\_Aged.

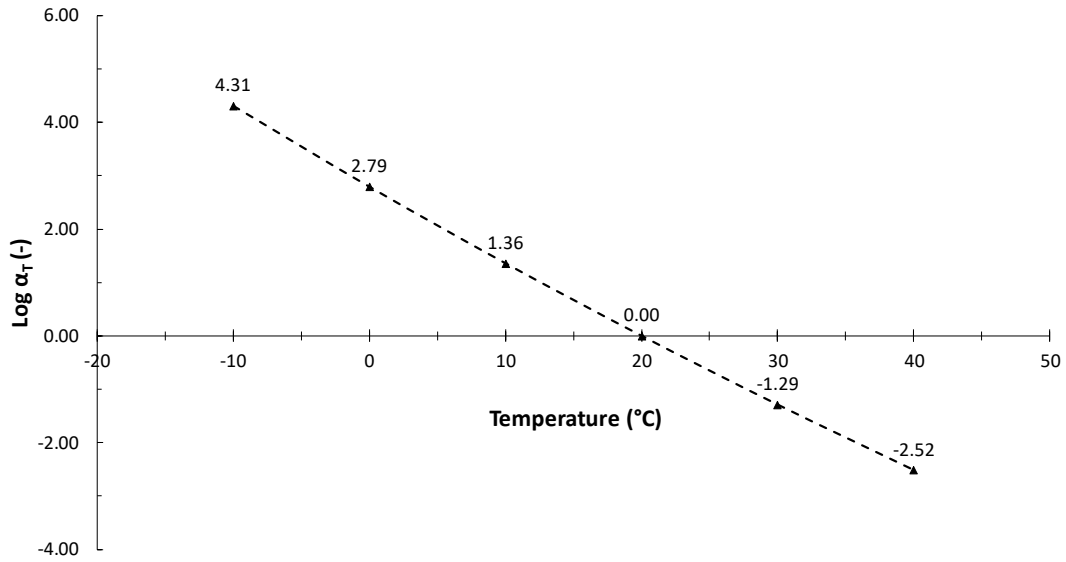


Figure C.30: WLF shift factors. RB\_40/60\_WG60K\_Aged.

Table C.15: WLF constants. RB\_40/60\_WG60K\_Aged.

Bitumen	WLF Coefficients (-)	
	C <sub>1</sub>	C <sub>2</sub>
RB_40/60_WG60K_Aged	50.627	382.405

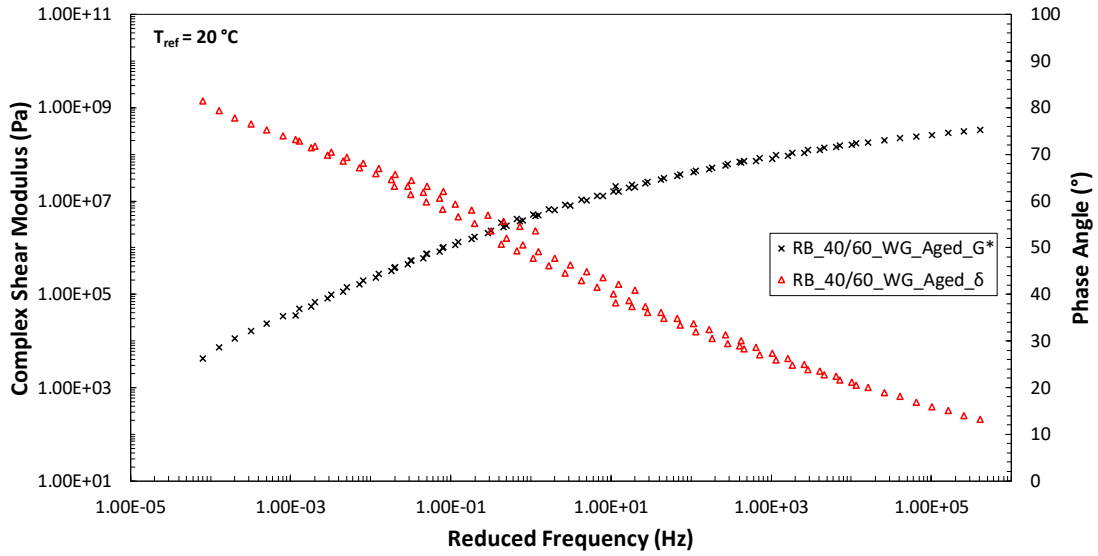


Figure C.31: WLF master-curves. RB\_40/60\_WG\_Aged.

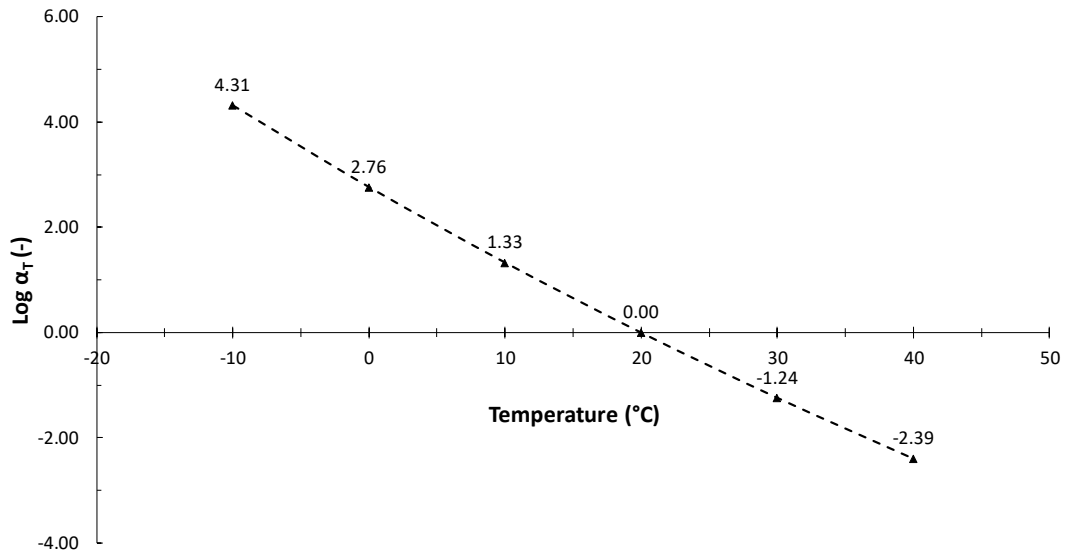


Figure C.32: WLF shift factors. RB\_40/60\_WG\_Aged.

Table C.16: WLF constants. RB\_40/60\_WG\_Aged.

Bitumen	WLF Coefficients (-)	
	C <sub>1</sub>	C <sub>2</sub>
RB_40/60_WG_Aged	35.582	277.446

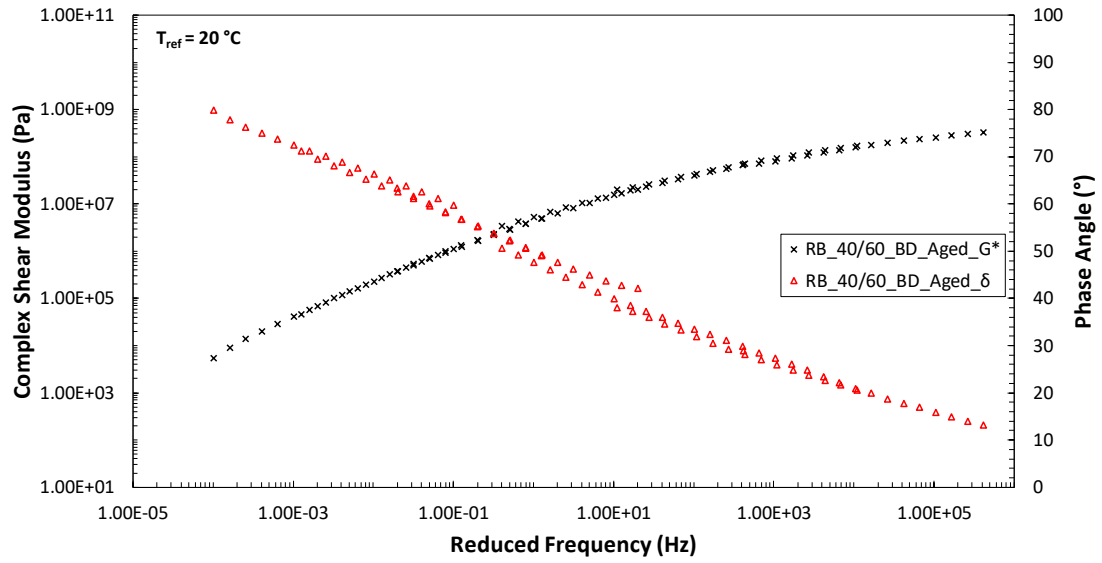


Figure C.33: WLF master-curves. RB\_40/60\_BD\_Aged.

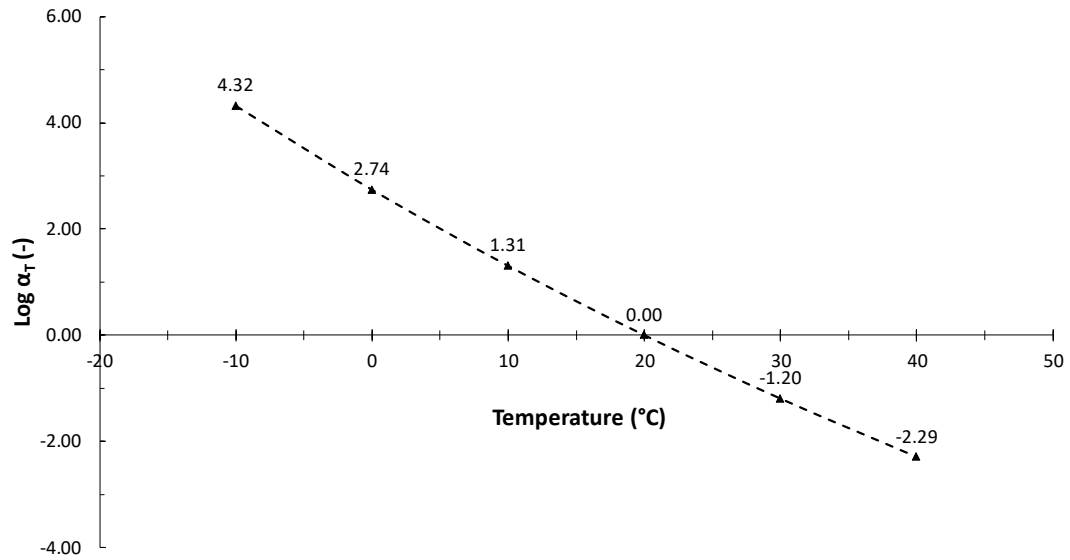


Figure C.34: WLF shift factors. RB\_40/60\_BD\_Aged.

Table C.17: WLF constants. RB\_40/60\_BD\_Aged.

Bitumen	WLF Coefficients (-)	
	C <sub>1</sub>	C <sub>2</sub>
RB_40/60_BD_Aged	28.177	225.701



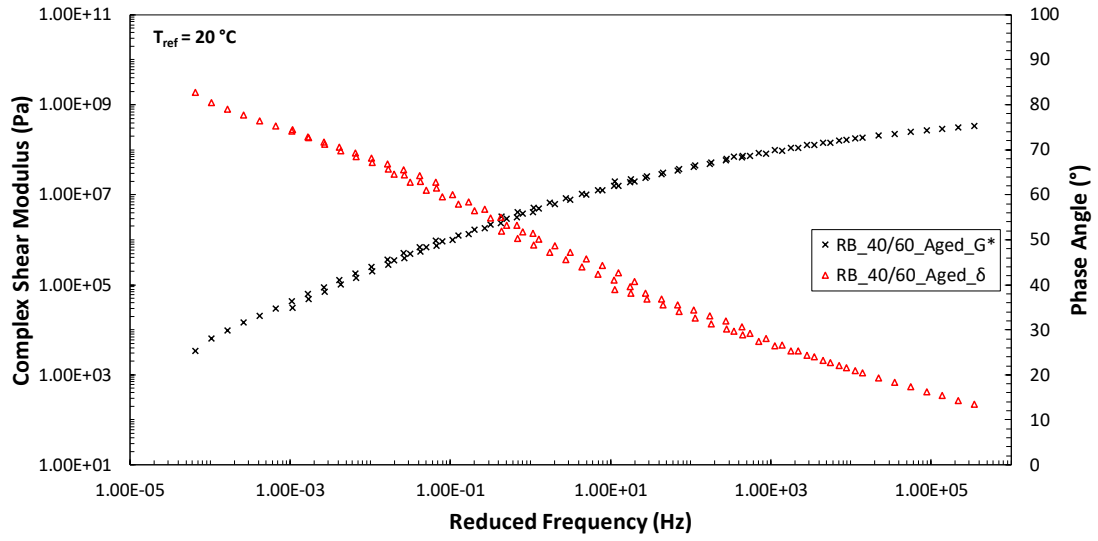


Figure C.35: WLF master-curves. RB\_40/60\_GR\_Aged.

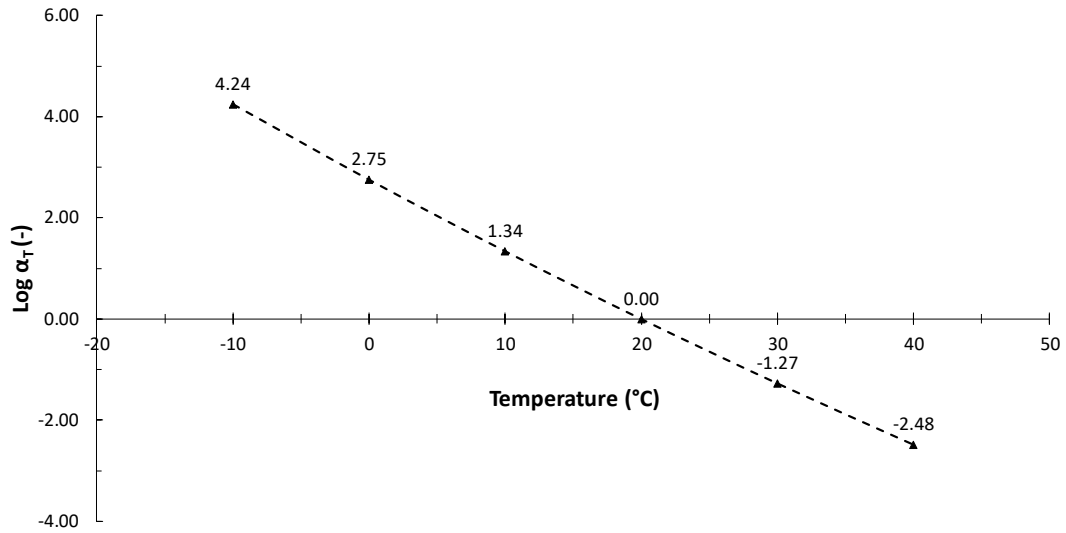


Figure C.36: WLF shift factors. RB\_40/60\_GR\_Aged.

Table C.18: WLF constants. RB\_40/60\_GR\_Aged.

Bitumen	WLF Coefficients (-)	
	C <sub>1</sub>	C <sub>2</sub>
RB_40/60_GR_Aged	50.616	387.799

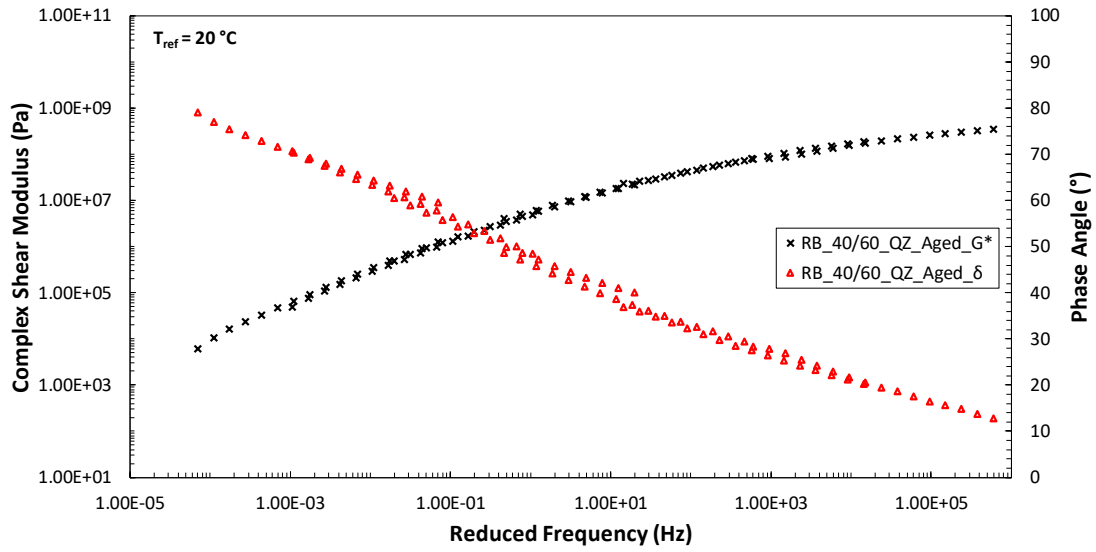


Figure C.37: WLF master-curves. RB\_40/60\_QZ\_Aged.

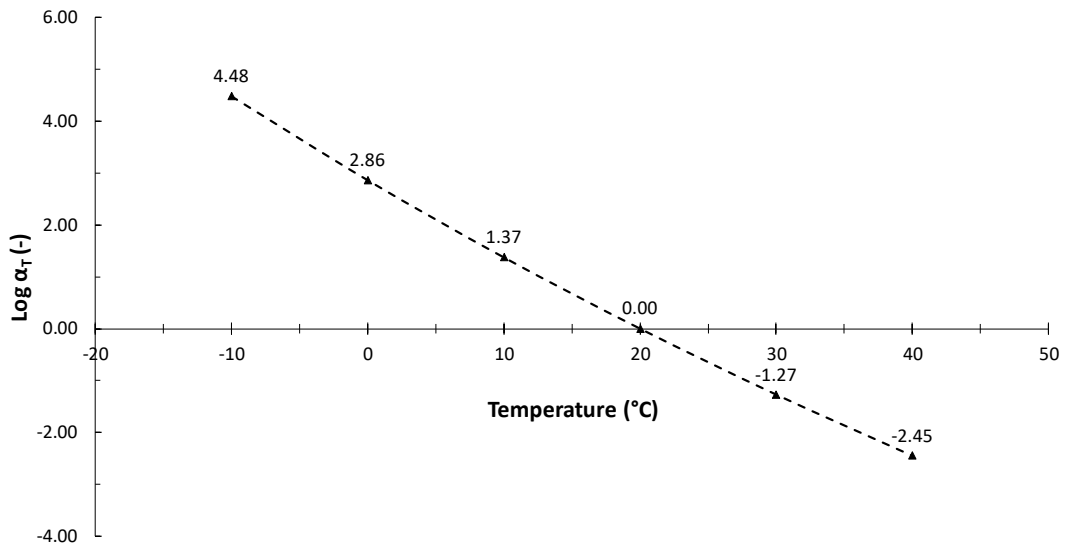


Figure C.38: WLF shift factors. RB\_40/60\_QZ\_Aged.

Table C.19: WLF constants. RB\_40/60\_QZ\_Aged.

Bitumen	WLF Coefficients (-)	
	C <sub>1</sub>	C <sub>2</sub>
RB_40/60_QZ_Aged	34.287	259.481

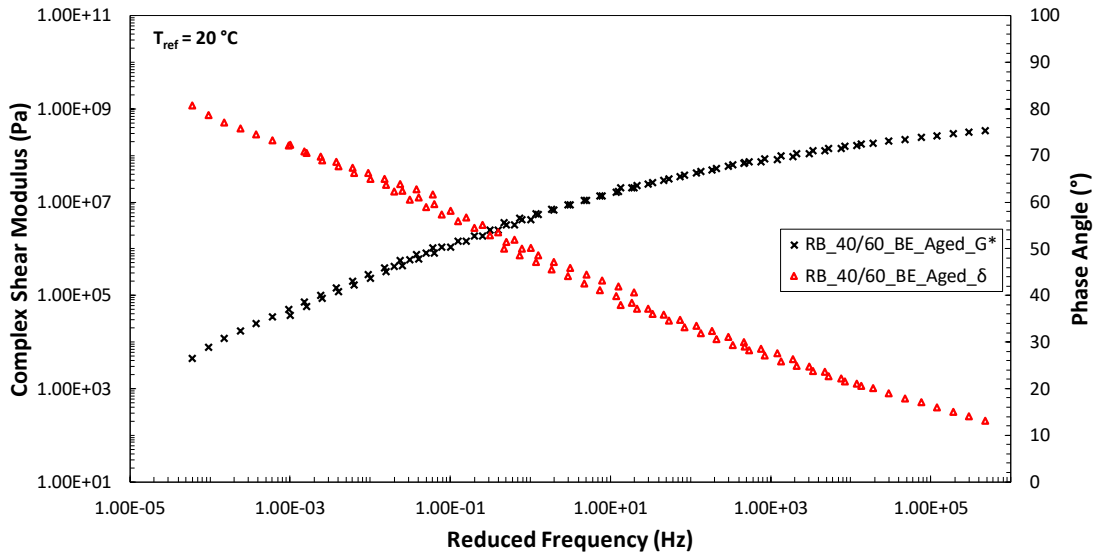


Figure C.39: WLF master-curves. RB\_40/60\_BE\_Aged.

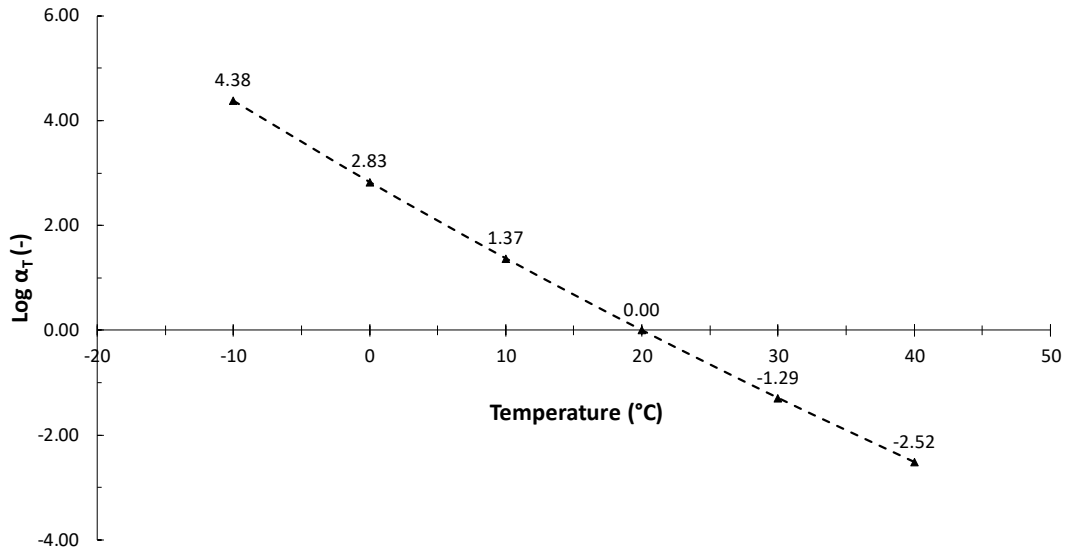


Figure C.40: WLF shift factors. RB\_40/60\_BE\_Aged.

Table C.20: WLF constants. RB\_40/60\_BE\_Aged.

Bitumen	WLF Coefficients (-)	
	C <sub>1</sub>	C <sub>2</sub>
RB_40/60_BE_Aged	45.620	342.280

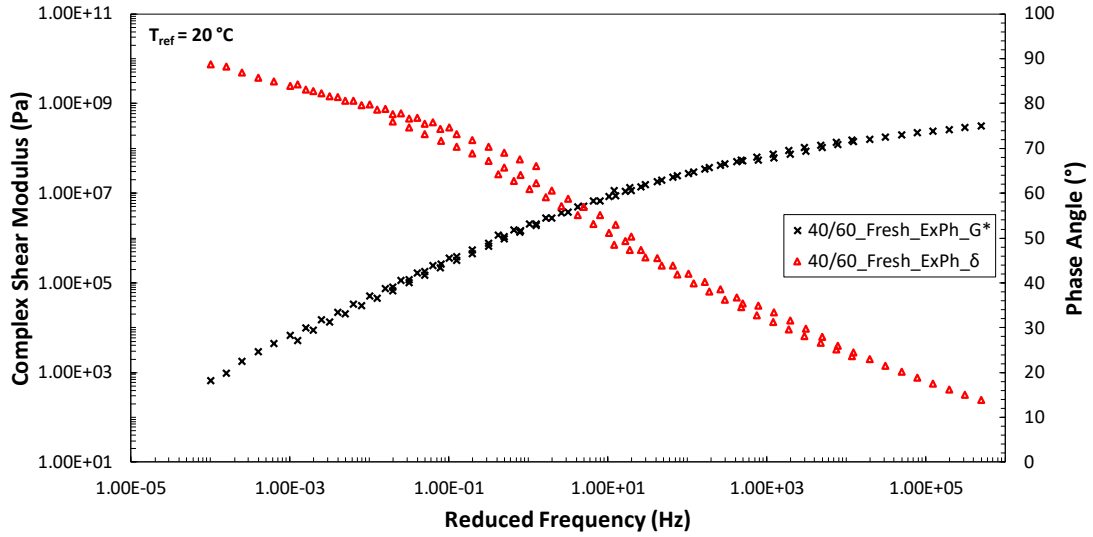


Figure C.41: WLF master-curves. 40/60\_Fresh\_ExPh.

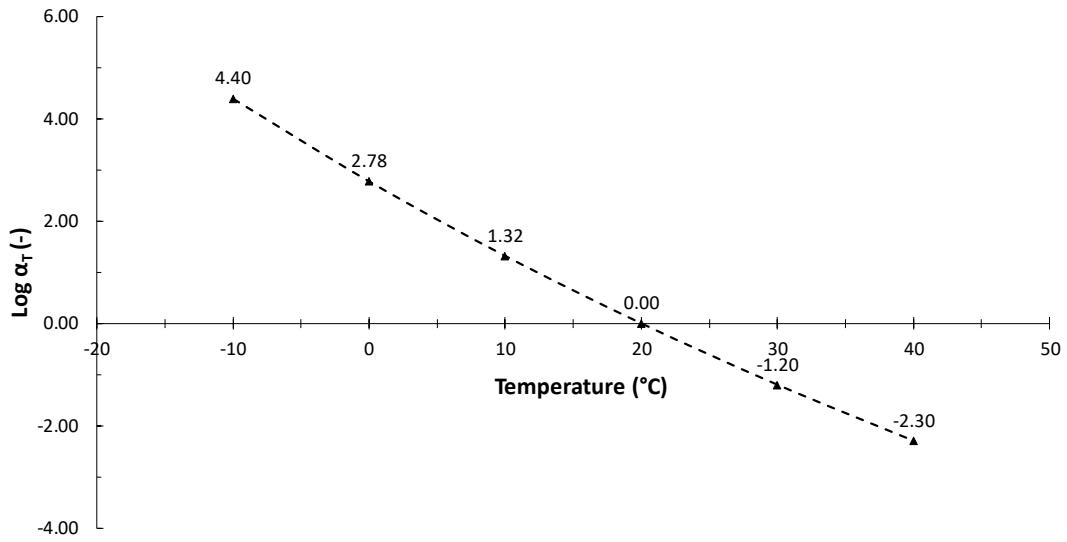


Figure C.42: WLF shift factors. 40/60\_Fresh\_ExPh.

Table C.21: WLF constants. 40/60\_Fresh\_ExPh.

Bitumen	WLF Coefficients (-)	
	C <sub>1</sub>	C <sub>2</sub>
40/60_Fresh_ExPh	26.594	211.485

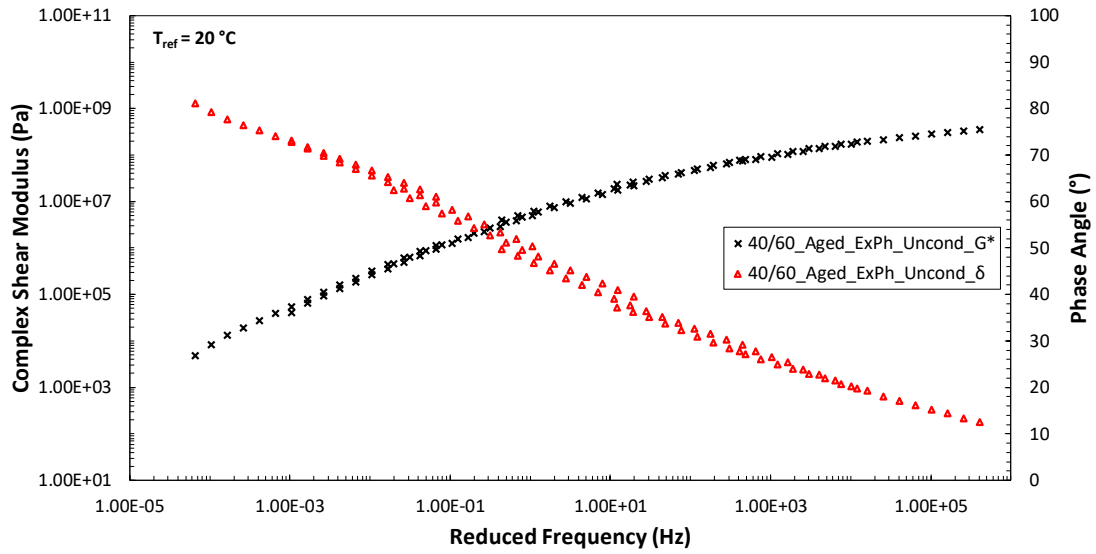


Figure C.43: WLF master-curves. 40/60\_Aged\_ExPh\_Uncond.

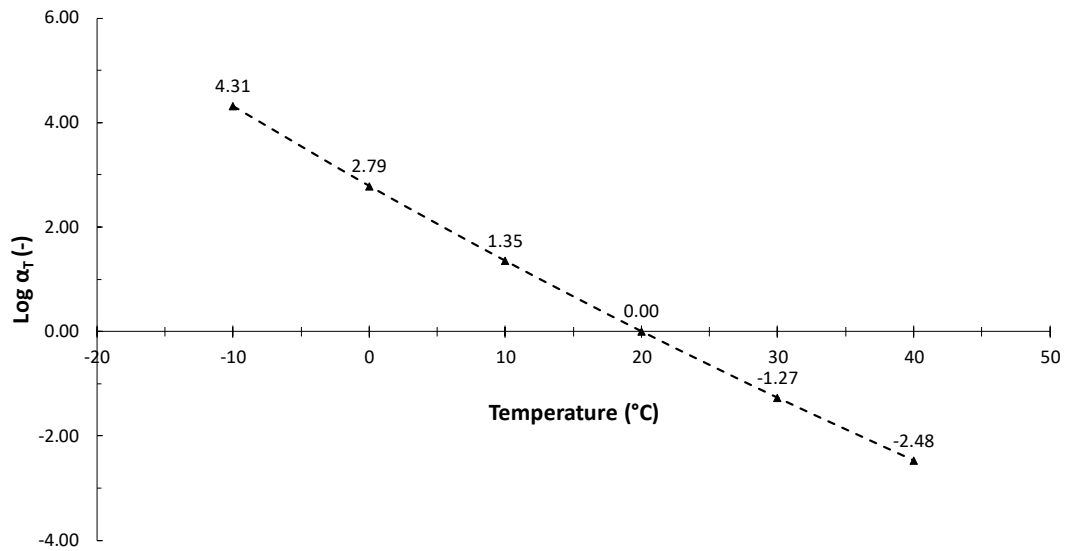


Figure C.44: WLF shift factors. 40/60\_Aged\_ExPh\_Uncond.

Table C.22: WLF constants. 40/60\_Aged\_ExPh\_Uncond.

Bitumen	WLF Coefficients (-)	
	C <sub>1</sub>	C <sub>2</sub>
40/60_Aged_ExPh_Uncond	44.427	338.955

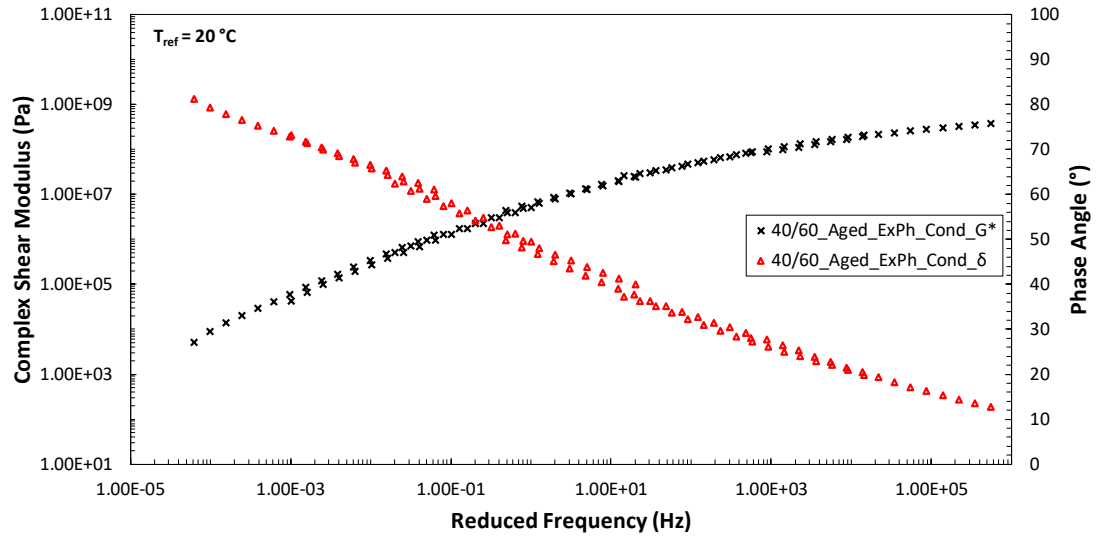


Figure C.45: WLF master-curves. 40/60\_Aged\_ExPh\_Cond.

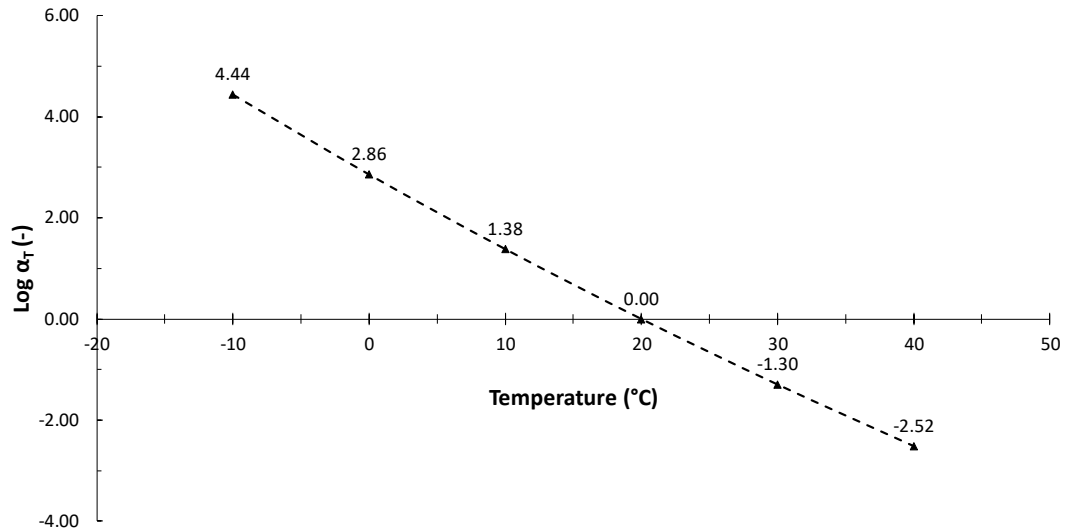


Figure C.46: WLF shift factors. 40/60\_Aged\_ExPh\_Cond.

Table B.23: WLF constants. 40/60\_Aged\_ExPh\_Cond.

Bitumen	WLF Coefficients (-)	
	C <sub>1</sub>	C <sub>2</sub>
40/60_Aged_ExPh_Cond	41.918	313.308

# **Appendix D**

Modified CAM model fitting parameters

**Table D.1:** Modified CAM model fitting parameters.

<b>Material</b>	<b><math>G_e^*</math> (GPa)</b>	<b><math>G_g^*</math> (GPa)</b>	<b><math>f_c</math> (Hz)</b>	<b><math>\delta_e</math> (<math>^\circ</math>)</b>	<b><math>\delta_g</math> (<math>^\circ</math>)</b>	<b><math>f_d</math> (Hz)</b>	<b><math>k</math> (-)</b>	<b><math>m</math> (-)</b>
40/60_WG60K_Fresh	0	2.32	3.500	86.50	0	7.5E-05	0.175	1.22
40/60_WG_Fresh	0	2.04	3.344	87.50	0	5.4E-05	0.173	1.22
40/60_BD_Fresh	0	2.01	2.737	88.00	0	3.1E-05	0.169	1.23
40/60_GR_Fresh	0	2.85	2.855	89.00	0	9.6E-06	0.160	1.25
40/60_QZ_Fresh	0	2.76	3.294	89.00	0	1.1E-05	0.160	1.24
40/60_BE_Fresh	0	2.22	2.622	88.00	0	2.2E-05	0.166	1.25
40/60_WG60K_Aged	0	2.23	0.158	87.50	0	4.5E-07	0.154	1.31
40/60_WG_Aged	0	2.00	0.162	87.50	0	2.9E-07	0.149	1.29
40/60_BD_Aged	0	2.25	0.078	87.50	0	5.5E-08	0.143	1.34
40/60_GR_Aged	0	234	0.082	87.50	0	4.9E-08	0.142	1.33
40/60_QZ_Aged	0	2.21	0.116	87.50	0	8.4E-08	0.143	1.30
40/60_BE_Aged	0	2.24	0.100	87.50	0	8.4E-08	0.144	1.31
40/60_Fresh	0	1.51	3.470	90.00	0	2.5E-06	0.147	1.26
40/60_Aged	0	1.61	0.211	89.00	0	3.8E-09	0.126	1.21
RB_40/60_WG60K_Aged	0	1.67	0.119	90.00	0	1.1E-09	0.122	1.26
RB_40/60_WG_Aged	0	1.49	0.056	90.00	0	7.6E-10	0.123	1.34
RB_40/60_BD_Aged	0	1.70	0.089	89.00	0	8.6E-10	0.122	1.30
RB_40/60_GR_Aged	0	1.67	0.203	90.00	0	2.9E-09	0.125	1.24
RB_40/60_QZ_Aged	0	1.79	0.024	90.00	0	6.1E-11	0.115	1.33
RB_40/60_BE_Aged	0	1.73	0.094	89.00	0	6.2E-10	0.120	1.25
40/60_Fresh_ExPh	0	0.99	1.067	90.00	0	2.8E-06	0.152	1.38
40/60_Aged_ExPh_Uncond	0	1.56	0.185	90.00	0	2.3E-09	0.125	1.20
40/60_Aged_ExPh_Cond	0	1.23	0.106	90.00	0	9.7E-10	0.122	1.23